Title

Structure and Speciation in Molten Fluoride Salts and Knowing and Being as a Nuclear Engineer

ISBN

9798276025827

Author

Williams, Haley

Publication Date

2025-12-06

Peer reviewed|Thesis/dissertation

Structure and Speciation in Molten Fluoride Salts and Knowing and Being as a Nuclear Engineer

By

Haley Williams

A dissertation submitted in partial satisfaction of the

requirements for the degree of

Doctor of Philosophy

in

Engineering - Nuclear Engineering

in the

Graduate Division

of the

University of California, Berkeley

Committee in charge:

Prof. Raluca O. Scarlat, Chair
Prof. Mark Asta
Prof. Rebecca Abergel
Prof. Cathryn Carson

Fall 2025

Abstract

Structure and Speciation in Molten Fluoride Salts
and Knowing and Being as a Nuclear Engineer

by
Haley Williams

Doctor of Philosophy in Nuclear Engineering

University of California, Berkeley

Professor Raluca O. Scarlat, Chair

This work describes the structure of molten mixtures of lithium fluoride and beryllium fluoride for their relevance to fission reactors and fusion machines, as well as the speciation of chromium in molten fluoride salts more broadly. In an operating molten salt system, a multitude of possible chemical species exist including solvent ions, oxidants from moisture, corrosion products, fission products, and activation products. Describing speciation in the salt entails identification of the possible species (their oxidation states, molecular structures of solvation and corresponding coordination numbers) in which an ion or molecule might exist in the melt. Understanding both solvation structure (first-nearest neighbors, and intermediate-range ordering in the melt) and speciation (oxidation states) is relevant to describing the interaction between the melt and its solutes. In addressing both the structure of LiF-BeF_2 solvents (in Chapter 2) and chromium solute speciation (in Chapter 3), this work presents fundamental studies of solvent and solute behavior which are relevant to chemistry control in molten fluoride salt systems, providing novel refinements of the concept of fluoroacidity and broad structural interpretation across temperature and composition.

In an attempt to make apparent the understandings of knowledge and engineering held by myself and more broadly in the nuclear engineering community, in the final chapter, I introduce the themes of knowing and being as a nuclear engineer, referring to the nature of engineering knowledge (epistemology) and the core identity of nuclear engineers. This reflexive thinking is made manifest in an embedded-values analysis of core nuclear engineering textbooks. Starting with the premise that epistemological norms affect the practice of engineering, I identify my own understanding of the nature of knowledge as well as trace statements in core textbooks about the role and responsibilities of the nuclear engineer. By reflecting on the conceptualizations of knowledge and identity within the field of nuclear engineering, this chapter presents foundational thought on pioneering the philosophy of nuclear engineering.

Through and for Mary

TABLE OF CONTENTS

LIST OF FIGURES

LIST OF TABLES

TERMINOLOGY & ABBREVIATIONS

Terminology is described here according to what terms refer to within the contexts of this work. Abbreviations are defined.

Acid (fluoroacid)	An electron-pair (fluoride) acceptor
AIMD	Ab Initio Molecular Dynamics
ARE	Aircraft Reactor Experiment
Base (fluorodonor)	An electron-pair (fluoride) donor
brF	Bridging F^-
brF_{ex}	Number of bridging F^- in excess of that required to maintain a given coordination number, given the stoichiometrically available F^-
brF_{min}	Minimum number of bridging F^- required to maintain a given coordination number, given the stoichiometrically available F-
brF_{tot}	Total number of bridging F^- (brF_{min} + brF_{ex})
ChE	Chemical engineering
Chemistry control	The active monitoring and adjustment of the salt's chemical environment, including its redox potential, solute (oxide, metals, sulfur) levels, fluoroacidity, and solute speciation, with the goal of maintaining materials compatibility, performance, and safety during operation
CN	Coordination number
Complex (complex ion)	Ions which interact to the extent that they are considered as a singular entity within the dynamic system; defined by Volkov as "the collectivization of the electron pairs and [atoms] of the reaction components provided that the number of collectivized electron pairs and particles exceeds the formal oxidation state of the central complexing atom" [1]
Corrosion product	A solute which results from corrosion. Often Cr^{2+}/Cr^{3+}, Fe^{2+}/Fe^{3+}
CV	Cyclic voltammogram/voltammetry
Disproportionation	Reaction in which a single element in one oxidation state is simultaneously oxidized and reduced, forming two species with different oxidation states; e.g., $3Cr^{2+} = 2Cr^{3+} + Cr^0$
dsF	Dissociated F^-
Embedded values (in NE education)	Refers to the underlying beliefs, assumptions, and worldviews that are subtly integrated into educational content and teaching methods, which shape how students perceive their roles as engineers and the nature of the knowledge they acquire
Epistemology	The study of the nature of knowledge
EPSR	Empirical Potential Structure Refinement
FLiBe	$2LiF\text{-}BeF_2$; referred to as $33.3BeF_2$ in Chapter 2
FLiNaK	46.5LiF-11.5NaF-42KF
Fluorine potential	The redox potential measured with respect to the $F_{2(g)}/F^-$ couple; describes if the salt is more or less oxidizing than the $F_{2(g)}/F^-$ reference couple

FNN	First nearest neighbor
g(r)	Pair distribution function. More detail in Section 1.2
Intermediate-range order	Refers to ionic ordering beyond the FNN, including second-nearest neighbors and the organization of molecular associates into oligomers
LANL	Los Alamos National Laboratory
Long-range order	Typically refers to translational symmetry
Monomer	A single, discrete complex ion with terminal fluorides only (no bridging); Would be a unit of the repeating polymeric structure (e.g., BeF_4^{2-} in LiF-BeF_2 systems)
MSRE	Molten Salt Reactor Experiment
NE	Nuclear engineering
NNMD	Neural Network Molecular Dynamics
NSLS-II	National Synchrotron Light Source II
OCP	Open circuit potential
Oligomer	A chain or cluster of a finite number of repeating units (typically 2 to 10 units); sometimes described by the number of units (equivalent to the number of cation centers), e.g., dimer, trimer
ORNL	Oak Ridge National Laboratory
Oxidant	A species which causes oxidation/corrosion and in the process is reduced; an oxidizing species
Oxyfluoride	Complex ion which contains oxide (O^{2-}) and fluoride (F^-); often complexed with an acidic cation
PDF	Pair distribution function. More detail in Section
pF	Fluoroacidity, $pF = -\log(aF^-)$ where aF^- is the activity of dissociated F^-
Polymer	A large-scale extended structure which leads to a system-spanning network
QRE	Quasi-reference electrode
Redox potential	Describes the ratio between the high and low valence states of every ion in the melt, in equilibrium with all other redox couples in the melt
S(Q)	Structure factor (also called structure function). More detail in Section
Salt	A chemical compound composed of positively and negatively charged ions. Refers to the solvent salt + all dissolved species. In the molten state, this describes the complete high-temperature ionic liquid.
Short-range order	Also known as local structure, refers to the first nearest neighbor environment; length scale approximately that of an atomic bond distance (about 2-5 Å)
SNN	Second nearest neighbor
SNS	Spallation Neutron Source (located at ORNL)
Solute	Dissolved species in the solvent; typically introduced to the salt intentionally for experimental studies; or undesired dissolved

	species which exist in minor quantities relative to the bulk solvent; may exist as a dissolved species or as a fluoride constituent (e.g., O^{2-}, Cr^{2+})
Solvent	Refers to the salt mixture which we define as our "pure" composition; the primary composition of fluorides in which other species are dissolved; e.g.: FLiBe.
Speciation	The identity, oxidation state, and (by relation) the chemical coordination of a component of the liquid
Strong associate	Ions interacting in a manner which is reversible and transient, on the timescale of tens of picoseconds
Structure	The dynamic ordering of ions from short- to intermediate-range
SWV	Square wave voltammogram/voltammetry
totF	Stoichiometric number of F^-
TRE	Thermodynamic reference electrode
trF	Terminal F^-
uCC	Under-coordinated cation
Weak associate	Ions interacting in a manner which is reversible and transient, on the timescale of < 1 picosecond

ACKNOWLEDGMENTS

I am deeply grateful and humbled to have worked on such enriching projects with the help and support of so many people.

Thank you, Professor Scarlat, for your continued support and commitment as an educator. Your zeal for educating students is inspiring, and I offer my sincere thanks for the ways in which you have shaped me as a researcher and academic. Thank you to Professor Karl van Bibber for your mentorship and generosity—I see how your abundant hope and charity have uplifted so many in the NE department and I am truly grateful to call you a mentor. Thank you to Professor Abergel for your support and example, and many thanks to you, Meltem Erol, and Amanda Gill for your kindness and efforts in helping me cross the finish line. Thank you to Professor Carson for your guidance and thoughtfulness in helping me imagine and develop an interdisciplinary dissertation—your contributions to the boundary work of nuclear engineering are inspiring. Thank you to Professor Asta for your kindness, sincerity, and example as a researcher. Thank you to Dr. Judith Vidal and Dr. Youyang Zhao for serving as sponsors in my grad school pursuits, and thank you to Prof. Todd Otanicar for encouraging me to look beyond the boundaries of my research. You all showed me what it means to earn a Ph.D. and how it might be possible for me, and I thank you for helping me arrive here. And thank you to the Berkeley Chancellor's Fellowship, FUTURE EFRC, Speciation of Light Elements at High Temperatures NEUP, France Berkeley Fund, Ron and Gail Gester and the Gester Global Solutions Fellowship in Nuclear Engineering, the Lydia Castelino Memorial Fellowship Fund, and the Jennifer J. Moriarta & Chao Chen Family which funded my studies and research.

Thank you to the SALT Group, for building and maintaining together a lab where we could eke out a degree and have some fun in the meantime. Lorenzo Vergari, Christian Sclafani, Tony Consiglio, Ryan Hayes, Sasha Kennedy, Michael Borrello, Nathanael Gardner, Timothy Pickarski, Nicole Johnson, Sarah Heagy, Sara Mastromarino, Randall Chiu, Sander Ratso, Qiye Hu, Christian Sclafani, Maksim Pecherskiy, and Zachary Falkowski—thank you for the countless hours troubleshooting gloveboxes, cleaning all horizontal surfaces in the lab, and deliberating in lab meetings. I've learned from each and every one of you, and I'm so grateful for and impressed by you all.

Thank you to all students I've had the opportunity to work alongside and learn from: William Heriot, Ruben Cho, Kirthi Kumar, Reese Carlson, Nigel Mesta, Nicolas Albiani, Colton Bruni, as well as my many E125 students. You all make the university one of my favorite places to be. Thank you to my collaborators, including Nicholas Winner, Shivani Shrivastava, Andrea Hwang, Sean Fayfar, Boris Khaykovich, and Sven Vogel—it's been a joy and honor to learn from and with you, and I look forward to the collaborations to come. And thank you to the people who helped me and the SALT Group to do safe research, including Alan Bolind, David Scrimger, and Jeremy Hamilton. Your work is so valuable, and it did not go unnoticed.

Thank you to my fellow nuclear contextualizers, Dr. Denia Djokić, and Dr. Samuel Dotson, for the conversation and mutual encouragement. Denia, your insight and support mean so much to me and have helped me keep going when the path forward is unclear; I am so thankful for your mentorship. Thank you also to Professor Bruno Coppi and Professor Jack Wisdom for welcoming me to MIT and helping me find a place here. Your encouragement, kindness, and

wisdom are so appreciated.

To Jess, Christina & Yaya, Angus & Harbor friends, Anne, Julia & Kristen, Brianna, Stephanie & Lina, and Richdale friends—you have all reminded me of the bigger questions in life and have brought joy and comfort whenever it's needed. Thank you! Friar Bernard Joseph, my sincerest thanks for your sustaining prayers. To Cousin John, thank you for your grandfatherly wisdom and welcoming me to your garden and vineyard.

And my deepest, most heartfelt, and resounding thanks to those who have accompanied me and carried me throughout my life. Mom and Dad, I don't know how to express the extent of my thanks. Thank you for showing me unending love and teaching me how to love. I wouldn't be here without you in more ways than one. Lucie, Ilya, Tim, Micaela, Colin, Joe, and now Lainey and Ottilie, you are my favorite people, and I thank God for you every day. Thank you for always being there. And Karol, thank you for being my truest, Aleredian friend in every possible way. I'm so grateful to share everything with you. Nie lękajcie się—Otwórzcie na oścież drzwi Chrystusowi.

1 INTRODUCTION

To introduce the topic of **structure and speciation in molten salts**, I wish to address:

1) What has generally been said and studied before about the topic and how we understand structure and speciation,
2) And what relevance the topic has to the field of nuclear engineering.

Structure in molten salts refers to the varied degree of order and disorder of the arrangement of ions in the high temperature melt beyond their first-nearest-neighbor (FNN) coordinates. *Speciation* refers to the identity, oxidation state, and corresponding FNN coordination of a component of the liquid. Together, these concepts address the interaction between a molten salt and its solutes, which are fundamental to chemistry control in molten fluoride salt systems.

In addition, I will introduce the notion of **reflexive thinking** in (nuclear) engineering practice, including discussion of:

3) The "world making" dimensions of engineering research.
4) The drawing of disciplinary boundaries and conceptions of a field.

This framing, in which we consider the creative and definitive elements of the field, paves the way for discussion of how one might think about the field of nuclear engineering, considering both engineering knowledge and identity.

1.1 The study of molten fluoride salts

A molten salt is what its name implies: an ionic compound consisting of cations and anions in its liquid state. "Molten salt" generally refers to the category of ionic liquids which are molten at high temperatures (typically above 400°C), since some salts (primarily organics composed of complex ions with delocalized charge) [2] can form "*room temperature* ionic liquids", which are used in the chemical industry as solvents and process aids [3]. Figure 1.1 shows 2LiF-BeF_2 (FLiBe) with added LiH as a solid at room temperature and as a liquid when it was heated to 700°C. Solid salts are defined by their ionic character—they are typically crystalline solids, but depending on their composition, they may be glass-formers. The likelihood of glass formation can often be explained by Zachariasen's rules [4]. At high temperatures, the ions in a salt dissociate, giving rise to a varied degree of order and disorder which comprise the structure of the liquid.

Figure 1.1. FLiBe + 0.8 mol% LiH at room temperature (left) and at 700°C (right).

Molten salts are known to have been a subject of formal research since the late-19th century for their ability as solvents. The first breakthrough for the study and application of molten salts was the development of the Hall-Héroult process in 1886 for large-scale production of aluminum metal [5] via electrolysis in molten 3NaF-AlF_3. Due to their ability to remain molten with low vapor pressure at high temperatures, to solvate fission products, and to moderate neutrons with low absorption cross-sections, molten fluoride salts were first proposed for use in nuclear reactors during the Aircraft Reactor Experiment in the U.S. in 1954, which, after several design iterations, was developed to use a circulating liquid fuel composed of NaF, ZrF_4, and UF_4 [6]. Fluoroberyllate salts were first used for nuclear energy applications in the Molten Salt Reactor Experiment (MSRE) at Oak Ridge National Laboratory (ORNL) in the 1960s [7]. Fluoroberyllates are continually favored in nuclear applications due to their neutronic behavior, ability to breed tritium (at high Li-6 enrichment) [8], modest congruent melting point, and thermal properties that enable passive and inherent safety features and high-temperature operation [9], [10]. Presently, molten $2LiF{-}BeF_2$ (FLiBe) is a candidate salt for use as a coolant in the fluoride salt-cooled high temperature reactor (FHR) currently being commercialized by Kairos Power [11], [12]. In addition, FLiBe is a candidate salt for the tritium breeding blanket of fusion systems [13], [14].

1.2 Characterizing molten salt structure

As stated, molten salt *structure* refers to the dynamic ordering of ions from short- to intermediate-range. Different salts display different degrees of ionic ordering. Here I explain core concepts used to describe molten salt structure.

Short-range or **local structure** refers to the FNN environment, with a length scale approximately that of an atomic bond distance (about 2-5 Å). Short-range structure results from the competition of *overlap-repulsion* (where the filled electron shells of nearby ions repel each other to avoid violation of the Pauli principle) and *Coulombic interactions* between the ions. The balance of these forces dictates the distance of closest approach between ions and the alternating ordering of the charged species [15]. Molten salts often display prominent short-range order because of the coordination of unlike and like ions via charge alternation [16]. This ordering is

indicated by a prominent first peak in the radial distribution function (see definition below), with a strong minimum (meaning there is a sharply defined bond length for the correlation of a cation-anion pair). Some concepts used to describe short-range ordering include:

- **Coordination number (CN):** calculated by integration from $r_{initial}$ to r_{min} (spanning the peak of the PDF representing a given ion pair) of $r^2g(r)$ with respect to r, multiplied by 4π times the average number density of ions [17]. The first coordination shell, composed of FNN of a particular species, is defined by ions whose separation distance is less than the first minimum, r_{min} (sometimes referred to as the *cutoff* distance) in the g(r) [18]. "Coordinates" refers to the species which comprise the coordination shell, which could be a first shell of FNN or second shell of second nearest neighbors (SNN).

- **Associates**: generally describes an interaction between ions which is reversible and transient (which is generally relevant given the dynamic structure of high temperature molten salts). Associates may be classified by the lifetime of their local environments. Be^{2+}—F^- coordinates are considered long-lived or strong associates, with a cage correlation time around 25 ps [19]. Conversely, Li_+—F^- coordinates are short-lived or weak associates, with a cage correlation time less than 1 ps [19].

- **Bond angle distribution**: A "bond" in this case refers to the vector connecting coordinated ions, not necessarily a description of a chemical bond between them [1]. The bond angle distribution is the quantification of the average angles defined by the two vectors determined by a common ion and two of its coordinates. When the anion has a relatively low dipole polarizability (e.g. F^- in BeF_2), the Be-F-Be angles within BeF_4^{2-} tetrahedra remain obtuse (> 140°) to minimize Be-Be repulsion, leading to the predominance of corner-sharing over edge-sharing [20].

- **Bond length**: Typically refers to the nearest neighbor distance, or the most probable length at which an ion is found from its FNN, indicated by the location of the maximum of the pair distribution function (PDF, defined below).

Intermediate-range ordering refers to ionic ordering beyond the FNN, including SNN and the organization of molecular associates into oligomers. It describes the way that the building blocks of monomers or oligomers arrange themselves with respect to each other. These may be referred to as "clusters". McGreevy and Pusztai emphasize that the first and second coordination shells generally have a "considerable" degree of inter-penetration, and therefore, considering also the degree of disorder in molten salt systems, descriptions of their structure should be considered an *approximation* of the dominant local structure [18]. Some concepts used to describe ionic ordering include:

- **Common neighbor connections (CNCs):** describes how an ion is correlated with SNN by indicating how coordination polyhedra connect with each other. The number of connections is categorized as vertex sharing (1 shared ion), edge sharing (2 shared ions), or face sharing (3-4 shared ions). [21]

- **Complex ion formation or "complexes"**: ions which interact to the extent that they are considered as a singular entity within the dynamic system. Complexation is defined by Volkov as "the collectivization of the electron pairs and [atoms] of the reaction components provided that the number of collectivized electron pairs and particles exceeds the formal oxidation state of the central complexing atom" [1]. For example, BeF_4^{2-} is a fluoroberyllate complex with an overall oxidation state of 2-, consisting of 5 particles.

- **Oligomer distribution**: describes the fraction of species which exist as monomers (species with a single central complexing ion, which forms an isolated polyhedron with its coordinates) and oligomers (species with several inter-connected coordination units, typically counted by their central cations). Oligomers are typically distinguished as dimers, trimers, or small chains of n_{X+}, the number of cation centers (n approx. < 5). Longer oligomers may form chains or clusters. Instances of long-range connectivity are described as polymers.

- **Cluster**: Generally describes the geometric grouping of ions. Oligomers which are branched are sometimes called clusters.

Long-range order typically refers to translational symmetry over large length scales. Truly "long-range" order is absent from molten salts—no sharp Bragg peaks are formed upon diffraction since they are liquids. But network-forming salts may form rings which would lead to structural features at longer length scales (beyond 10 Å). Note that some films of room temperature ionic liquids are known to demonstrate ordering over micrometer length scales [22].

Volkov classifies all chemical reactions in molten salts as (1) acid-base reactions, (2) redox reactions, or (3) solvation reactions. Acid-base type reactions are said to include complexation reactions, and redox reactions are said to include disproportionation reactions. In real systems, chemical reactions typically include features of several of these reaction types [1]. Acid-base reactions follow from the Lewis definition, where acids as electron pair receptors and bases are electron pair donors. These reactions involve the redistribution of electron density, without a net transfer of electrons that would change the formal oxidation state of the participating elements [1], [23]. This distinguishes acid-base reactions from redox reactions which involve formal electron transfer and changes in oxidation state. Since complexation reactions, such as the formation of BeF_4^{2-}, are acid-base type reactions, the concepts of Lewis acidity and basicity (fluoroacidity, see Section 3.1) can provide insight into the structure of molten salt systems. In molten fluorides, the components can be categorized as [19]:

- Acidic species, including:
  - **Under-coordinated cations (uCC)**: a cation center with a lower CN than nominal, which can receive an electron-donating coordinate (fluoride)
  - **Bridging fluorides (brF)**: shared fluorides which form bridges between cation centers in complex ions. Bridges may be broken to produce two separate terminal fluorides, meaning they may be receptors of electron-pair donating fluorides.

- Basic species, including:
  - **Dissociated fluorides, (dsF):** fluorides which are not coordinated; sometimes referred to as "free" fluorides [24]
  - **Terminal fluorides, (trF):** fluorides which are coordinated with only one cation center such they are not bridging but available to serve as brF.

The component salts of a molten salt system are sometimes distinguished by their behavior as network-formers or as network-modifier salts. **Network-forming salts** are those which have a significant degree of intermediate-range or long-range ordering. This type of behavior is typically observed in salts with higher-oxidation state cations, such as halides of Be^{2+} or Y^{3+}. Cross-linking of cations, or bridging between long oligomers [25], is characteristic of network formation. Some network-forming salts are glass-formers in the solid state. **Modifier salts** either decrease the number of bridges or increase the CN of species because of charge compensation. Emerson et al. refer to lower-oxidation state modifier salts which alternately coordinate with higher-oxidation state networked salts as **"spacer salts"**. They determine that the spacing between networked ions caused by spacer salts is the source of the low-Q peak ("pre-peak") that appears in the X-ray S(Q ~ 1 $Å^{-1}$) when NaCl is added to $LaCl_3$ at 900°C (100°C above the melting point of NaCl) [26]. The structure factor S(Q) is defined on the following page.

In binary systems of network-former and modifier salts, there are typically two major regimes. At low concentrations of the network-former, the network-former cations typically exist in their coordination environment as monomers or oligomers [27]. At higher concentrations, the higher degree of cross-linking of the oligomers (Be-Be correlations, for example) produces a networked structure and the viscosity sharply increases [27]. Corradini et al. suggest that the individual links between monomers become more stable and rigid as the network becomes more extended, evidenced by the correlation of the Be-F cage time and the timescale of oligomer link breakage at low BeF_2 concentrations and the increased timescale of oligomer link breakage at higher BeF_2 concentrations [27].

Experimental techniques for studying liquid salt structure include neutron and X-ray scattering [28], [29], [30], Nuclear Magnetic Resonance (NMR) [24], [31], [32], [33], and Raman and Infrared spectroscopy [34], [35], [36], [37], [38]. The structural information provided by neutron and X-ray scattering is provided by the:

- **Structure factor (S(Q))** which is a function of the measured scattering intensity (Q, scattering vector magnitude or momentum transfer) and describes the reciprocal-space correlations of the liquid. Measured neutron scattering intensity is proportional to the differential scattering cross-section, which in turn reflects the total structure factor or 'structure function', S(Q) [39]. The first sharp diffraction peak (FSDP) in S(Q) can provide insight into charge alternation, anion-anion correlations, or intermediate-range structure in molten salts [20], [26]. We use "structure factor" to refer to the total structure factor for all components of the system. Partial structure factors are the structure factors of particular ion pairs and will be referred to explicitly as "partial".

- **Pair distribution function (g(r), or PDF)** which is generated from a Fourier transform of the structure factor (Fourier transform of the total S(Q) provides the total g(r), with other inputs being Q_{max}, the maximum Q of the instrument, and ρ, the average number density of the sample). The PDF provides the number density of atoms at a distance *r* from a central atom.
    - There are various forms of the PDF which vary in units, normalization, and functionality. When the origin atom is undefined, the PDF can be referred to as a **radial distribution function (RDF)** [39]. Radial PDFs can be generated from X-ray and neutron diffraction, where the function is often weighted by the scattering power of atoms, depending on the type of incident radiation (e.g., X-ray form factors for X-rays and atomic scattering lengths for neutrons) [39].
    - In this work, we use "g(r)" or "PDF" to refer to the function which is the radial distribution function normalized by the volume of a shell centered at *r* and scaled by the average number density.
    - **Partial PDF** describes the correlations between particular ion pairs in multicomponent mixtures (mixtures with more than two types of ions). The partial PDFs, weighted for their scattering power, sum to produce the PDF. Partial PDFs cannot be directly measured for multicomponent systems, so the partial contributions must be isolated using differences in isotopics or modeling. The partial PDF unweighted by scattering weights may also be called the RDF [39].
    - Note also that X-ray form factors are dependent on Q which requires corrections during normalization. For neutrons, atomic scattering lengths are not dependent on Q, so this does not apply. Equations for the calculation of g(r) from S(Q) can be found in [29]. Peterson et al.'s work provides a list of equations for the conversion of these functions among other formalisms [39]. A table summarizing the neutron scattering lengths relevant to the studies presented in this work can be found in the Appendix in Table 6.4.

The difference between neutron and X-ray scattering lies in the interaction between the incident radiation and the target material. Neutrons interact with atomic nuclei (and therefore their scattering depends on an element's isotopic composition). The relationship between neutron scattering and isotopic composition depends partially on the scattering cross section of the material, which is an inherent property. This means neutrons are isotope-sensitive and do not have a straightforward trend in their interactions with matter. As electromagnetic radiation, X-rays scatter from the electron clouds of the target materials, thus their scattering intensity increases with the atomic number of the element. This means X-rays are more sensitive to F than to Li or Be, which are less distinguishable because of their ionic size.

To emphasize the pertinence of structural studies, we note that structure is relevant to engineering applications of molten salts in the following ways:

- The short-range and intermediate-range ordering within the liquid are related to macroscopic properties such as viscosity [40], [25], [41], [42].
- Complexation can lead to nonideal mixing in binary and ternary molten salt systems, and

thus, better understanding of complexation, short-range ordering, and deviations from idealities aids in the formation of better models to predict changes in thermophysical properties, such as density, with changes in composition [43], [44].
- Solvation is dependent on salt structure, and understanding the structure of molten salts helps us to better understand and predict changes in solubility as a function of composition [45].
- Fluoroacidity, a function of composition, has been identified as relevant to the corrosivity of a molten salt [46, p. 98], and thus, structure, in addition to and following from chemical composition, is fundamentally related to corrosion in the melt.

1.3 Characterizing speciation in molten salts

We defined *speciation* as the identity, oxidation state, and (by relation) the chemical coordination environment of a component. For example, most simply we can state that chromium speciates at Cr^{2+} and Cr^{3+} in molten FLiNaK [47], [48], [49]. But the predominant oxidation state depends on the redox potential of the salt as well as the identity (chemical composition) of the solvent. There is also more to be known about the mechanisms of dissolution and diffusion, for example, which could be related to the formation of complex ions such as CrF_6^{3-}. To describe speciation in greater detail, we must understand the local environment of a species.

Solutes in the molten salt systems of fission reactors or fusion machines may be existing impurities, introduced during salt purification, fission products, corrosion products, activation products, introduced by air ingress, or introduced by other reactor components. Some solutes relevant to molten salt systems for nuclear applications are:
- Hydrogen (tritium, and other activation products)
- Beryllium
- Carbon
- Oxygen
- Sulfur
- Chromium (and other transition metal corrosion products)
- Lanthanides (and other fission products)
- Actinides - Uranium, thorium, plutonium (fuel salts)

To emphasize the pertinence of speciation studies, we note that speciation is relevant to the engineering applications of molten salts in the following ways:
- The speciation of a solute is related to its stability in the melt, which is relevant to safety and operation of molten salt systems. For example, it is relevant to know if radioactive fission products will stay dissolved in the salt or bubble out into the cover gas.

- Some techniques for monitoring salt chemistry are dependent on the speciation of the element. For example, electrochemical techniques for oxide quantification typically measure the oxidation reaction of O^{2-}. If oxide is found not just on its own but as a part of a complex species, the technique may not quantify it correctly absent additional information or appropriate calibration corrections [50], [51].

- Speciation most basically implies oxidation state, and the oxidation state of constituent species is indicative of the redox potential of the salt. Redox potential (discussed in Section 3.1) must be controlled in molten salt systems to avoid corrosion and undesired deposition (see Table 1.1).

1.4 Looking to chemistry control

What is needed to safely and effectively employ a molten salt system? When thinking about chemistry control for molten salt systems, it is helpful to first address what comprises the "chemistry" of molten salt chemistry. "Salt chemistry" is a vague term that, in application to engineering systems, generally encompasses the **composition** of the solvent salt, the inventory of **solutes** or trace contaminants and their solubilities (e.g. oxide, sulfur), the overall **redox** potential and chemical activities, and relevant radiochemical features of the salt (fuel salt depending on the fuel cycle, **tritium** management, etc.) [52], [53]. "Salt chemistry" can also refer to the details of thermodynamic properties of molten salts (including electrochemical behavior), interactions of molten salts with materials, and modeling of salt systems and salt properties [54], [55], [56], [57], [58].

Secondly, for chemistry control we must consider the target operating limits and how they should be determined and measured for safe and effective operation. We need to be able to know if the system is within these limits, so the ability to quantify relevant aspects of salt chemistry is imperative. Analytical techniques for monitoring salt chemistry include electrochemical techniques, spectroscopic techniques, analytical tests via chemical reactivity, and techniques for measuring radioactivity. A summary of some of these techniques is provided in Table 1.1.

Table 1.1. Some techniques for monitoring molten fluoride "salt chemistry".

Technique	**Used to measure:**	**Strengths**	**Challenges**
Electrochemical probes	Redox, oxide content, tritium	May be online. Variety of techniques (open circuit potential, cyclic voltammetry, potentiometry). May be used for multiple solute measurements.	Materials compatibility. Stability of reference electrodes [59]. May require precise and robust design (electrode immersion depth, etc.). Mostly relevant to measurement of soluble species.
Optical spectroscopy (IR, UV-Vis)	Composition	Sensitive to speciation.	Requires transparent, high temperature, chemically compatible optical cell [60].

ICP-OES/MS (Inductively coupled plasma – optical emission spectroscopy/mass spectroscopy)	Composition	High sensitivity elemental analysis.	Offline, occurs after quenching. Representative and repeatable sampling is necessary. Dependent on the dissolution of salt sample in aqueous solution.
GC-MS (Gas chromatography – mass spectroscopy)	Tritium [61]	Measures HT or T_2 in cover gas.	May be difficult to separate HT and T_2 if they co-elute. High-resolution MS needed.
Gas sparging (H2/HF) and off-gas analysis	Oxide content	Capabilities may already be in place for salt purification. Provides total oxide content including precipitates. [62]	Differences in reactivity of different oxide species with H_2. Must minimize atmospheric contamination.
IC (Ion chromatography)	Sulfur, oxide, phosphate, nitrate content	Differentiates between species.	Used in conjunction with carbothermal reduction (inert gas fusion) which provides total oxide content.
LSC (Liquid scintillation counting)	Tritium [61]	Well-established technique for measuring T.	Requires water-trapping. Several steps removed from salt system.

Lastly, control entails maintaining and modifying salt chemical conditions. Depending on the chemical condition being controlled, this can be done via several techniques including additions of salt or redox control agents, gas sparging, filtering, or via engineered systems. As an example, we can consider strategies for redox control in several molten salt nuclear systems [63]:

- In salt-fueled (fission) reactors, redox is typically controlled by the ratio of oxidation states of fuel. For example, decreasing the ratio of the mole fraction of UF_4 to UF_3 to below the oxidation potential of structural metals means that UF_3 would be oxidized by any oxidant present, avoiding corrosion of the structural metals [60]. The target ratio was determined to be $[UF_4]/[UF_3] < 100$ for the MSRE, which would maintain the CrF_2 mole fraction to be < ~0.0001 at 700°C. The ratio was also given a lower limit of 10 to avoid the further reduction and precipitation of UF_3 to uranium carbides [58].

- Beryllium metal redox control has also been studied for use in fusion blankets within the JUPITER-II program [64], [65]. Beryllium redox control is also planned for use in the LIBRA (Liquid Immersion Blanket: Robust Accountancy) experiment [66].

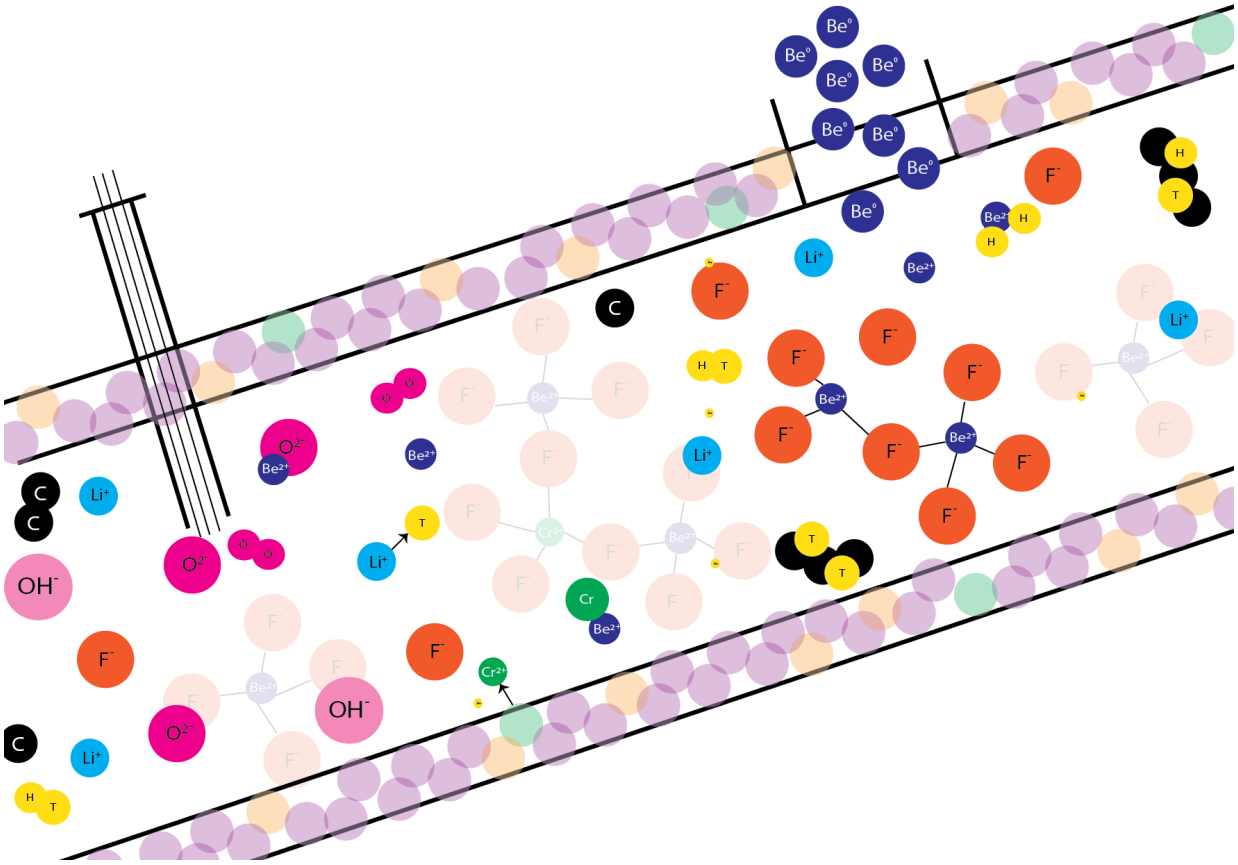

Figure 1.2. Imagining the species present in FLiBe. Non-equilibrium depiction of FLiBe with H, T, Be, C, O, and Cr solutes within Hastelloy N piping.

Figure 1.2 gives us an idea of the elements of "salt chemistry" of relevance to a FLiBe system in a salt-cooled fission reactor. We see a depiction of the FLiBe solvent, consisting of Be_xF_y complexes and dissociated F^- [29]. In the background, we can see Cr^{2+} solvated within one of these complexes [19]. The solvation shells of other solutes are not depicted, but we can see the diversity of their speciation. Chromium (green) is oxidizing from Hastelloy N (composed of mostly nickel (purple), some molybdenum (orange), little chromium (green), and very little iron (not depicted)) as Cr^{2+}, and we see Cr^0 directly bonding with Be^{2+} [19]. We see tritium as HT, T_2, and TF (produced by the transmutation of Li^+), some of which is adsorbed onto carbon species, introduced by the presence of graphite in the reactor [67]. Thermally unstable intermediate BeH_2 is depicted, as well [68]. In the top right, we see Be metal being added for redox control [60], [69]. On the left, we see an electrochemical probe oxidizing O^{2-} to O_2—a technique used to quantify oxide in a melt [50]. Oxygen is also seen speciating as hydroxide. Overall, this graphic gives a sense of the multi-element equilibrium of a molten salt system. Variation in salt composition, temperature, and irradiation flux leads to dynamic changes in the redox potential and fluoroacidity (3.1) of the system which together describe the evolving chemical equilibrium among dissolved species.

1.5 Thinking about the field of nuclear engineering

"As we 'make things work', what kind of world *are we making?"* Langdon Winner.

Research in engineering and the sciences involves a great deal of "making things work". The scales of the "making work" vary. My own research experience has involved making gloveboxes work, making molten salt electrochemical cells work, and making lab operations work. These practices support the larger engineering goals of making molten salt sensors work and making molten salt chemistry control systems work. The higher order objective is to make nuclear reactors work, or, from the perspective of academic research, to examine the conditions and seek deeper understanding of the underlying chemistry in which such systems might work. Regardless of the scale of our understanding or the scope of our perceived impact, we engineers are building artifacts—apparatuses and processes, understandings and methodologies—which sustain and develop the field and all that it embodies. Political scientist Langdon Winner emphasizes the great responsibility of this role and elaborates on what makes up the "worlds" of our creation:

> This suggests that we pay attention not only to the making of physical instruments and processes, although that certainly remains important, but also to the **production of psychological, social, and political conditions as a part of any significant technical change**. Are we going to design and build circumstances that enlarge possibilities for growth in human freedom, sociability, intelligence, creativity, and self-government? Or are we headed in an altogether different direction? [70] (emphasis added)

The psychological, social, and political conditions of our work might be more visible at the larger scales of "making work". In the field of nuclear engineering, we have grotesque examples of the psychological and political impacts of our technologies [71], [72], [73]. I believe it is Winner's suggestion that this attention to both social and technical conditions ought to be applied to even the smaller scales of "world making". That is, we can think about molten salt sensors and even electrochemical cells as physical embodiments of our social and political realities, and thus, we should also think critically about their design and functionality. This means first asking what social and political realities we wish to embody, which involves reflection on our contexts and role as engineers as well as meta-cognition about our epistemic assumptions.

Reflection is the process by which we remember and contemplate our methods and ways of previous understanding, whereas reflexivity is the practice of critical analysis of foundational knowledge and the cultivation of the self-awareness which results from our reflection. Reflexivity is actively forward-thinking, anticipatory, and continually evolving; it involves understanding the assumptions, frameworks, and perspectives of our work, and not just looking at the outcomes and their significance. In this way, reflexivity encompasses the goal of the reflection and meta-cognition prompted by Winner. Several educators have promoted and examined reflexive practices in engineering education [74], [75]. These reflexive practices are often suggested as a response to the need to change and contest "traditional" views of engineering, however, in Section 4.2.2 I point out that narratives of engineering are not always self-consistent. In an attempt to consider the social and political aspects of nuclear engineering work, I find it valuable to go back to the foundational conceptualization of the field. Who is a nuclear engineer? What does it mean to be a nuclear engineer? How do engineers know? What

values are most fundamental to engineering? Starting with the engineering identity allows us to examine alignment or misalignment of foundational values with engineering outcomes.

Reflexive practices are not confined to the artifacts we are making but also apply to critically examining the field or discipline in which our work is contained. When we think about what it means to be a nuclear engineer or how engineers know, it might be understood that there are certain traits that are *not* the traits of an engineer, or ways of knowing which are *not engineering ways* of knowing. In the contexts of the relatively modern and multidisciplinary field of nuclear engineering, these boundaries of what is and is not engineering are particularly interesting. Boundaries carry significance in the establishment of identity and the maintenance of a community of practice. At the same time, boundaries offer an enrichment of our identity and help us to understand our relationship to the natural world. Poet and philosopher Édouard Glissant's interprets the significance of borders as both formative of identities and conducive to encounter and evolution, saying:

> We are drawn to borders, not because they are signs or elements of the impossible but because they are places of passage and transformation. Relationship depends on the mutual influence of identities, be they individual or collective, and requires each identity to be distinct and independent. Relationship does not mean confusion or dilution. I can change by exchanging with the Other and still not lose or distort myself. That is why we need borders, not as places to stop at, but as the point at which we may exercise the right of free passage from the same to the Other; savour the wonder of here and there [76].

Reflexive thinking on how a field is defined (the boundaries of a field) is called for when thinking about the foundations of the nuclear engineering identity and profession. Understanding the mutual influence of identities of engineers and society can help us address the conflicting narratives of engineering. In exploring the foundations and the borders of nuclear engineering, we can better examine the "worlds" we are making through engineering.

1.6 Organization of the dissertation

In this dissertation, I present studies of the structure of molten fluoride salts and the speciation of chromium solutes in molten fluoride salts, both of which are part of larger research collaborations with co-authors acknowledged. These results and analyses are arranged into two primary technical chapters:

- Chapter 2 describes structural studies of molten LiF-BeF_2 mixtures. Mixtures varied from 33 to 100 mol% BeF_2 and were studied using neutron and X-ray scattering, with analysis supported by structures generated by Reverse Monte Carlo techniques. This chapter addresses the research questions:
    - How can we describe the structure of LiF-BeF_2 mixtures and the effects of composition and temperature?
    - What is the relationship between fluoroacidity (as affected by the ratio of LiF to BeF_2) and salt structure in LiF-BeF_2 mixtures?

- Chapter 3 describes studies of chromium speciation in various molten fluorides and examines how solute behavior is related to the fluoroacidity of each of the melts. Chromium is of relevance as a corrosion product in molten fluoride systems. We examine thermodynamic and kinetic indicators of fluoroacidity as well as the electrochemical behavior of chromium solutes in each melt. This chapter addresses the research question:
    - Do acidic solvent species necessarily compete with chromium containing solutes for dissociated F^-?

The final content chapter focuses on social-philosophical aspects of nuclear engineering. This includes a textbook analysis which was a collaborative work, as well as an introductory discussion of the philosophy of nuclear engineering which consists of a literature review and my own interpretation. More specifically:

- Chapter 4 discusses what it means to identify and know as a nuclear engineer, introducing concepts related to the philosophy of nuclear engineering. In this chapter, I express that engineering in its fullest expression is that which is reflexive and participates in both affective and rational reflection on network actors, including the self. The chapter includes an analysis of embedded values in some core nuclear engineering textbooks. "Values" is used to refer to attitudes and understandings related to the nature of engineering knowledge and the identity of the nuclear engineer. The textbook review addresses the research question:
    - What beliefs about knowledge and the role of the engineer are embedded in core nuclear engineering textbooks?

To practice reflexive work through definition of a subfield, an analysis of how the field of nuclear engineering emerged is included in a the Appendix Section 6.2. We particularly examine the relationship between chemical engineering and nuclear engineering and present a current definition of nuclear chemical engineering within the contexts of reactors which employ molten salts. To conclude, I synthesize the key findings of each chapter and present a reflection the field of nuclear engineering.

2 STRUCTURAL STUDIES OF HIGH TEMPERATURE LiF:BeF_2 MIXTURES

In this chapter, I aim to **characterize the structure of molten LiF-BeF_2 mixtures, specifically analyzing *changes in* and *drivers for network formation across temperature and composition***. Through neutron and X-ray scattering experiments of LiF-BeF_2 mixtures coupled with validation of neural-network molecular dynamics (NNMD) models of the same compositions performed by collaborators at the University of Massachusetts – Lowell (similar to [77], details forthcoming), the structural understanding of LiF-BeF_2 salt mixtures is refined. Experimental results are further analyzed via Reverse Monte Carlo modelling, specifically Empirical Potential Structural Refinement (EPSR) [78] performed by collaborators at Lawrence Berkeley National Laboratory (details forthcoming). In this chapter, I describe the oligomer distribution, the effect of composition and temperature on structure, and thermodynamic contributors to salt structure to further serve refinement of salt chemical models and provide a baseline model for future investigations of solvation in fluoroberyllate melts. In describing the structure of these fluoride salts, I address the question:

- How can we describe the structure of LiF-BeF_2 mixtures and the effects of composition and temperature?

2.1 Background

The composition of the salt in a fusion or fission system can change as a consequence of production of fission products [79], [80], [81], neutron activation of the salt [82], air or steam ingress, corrosion of structural materials in contact with the salt [60], or introduction of redox control agents [69]. These compositional changes depend on the reactor operating conditions (starting isotopic composition, neutron flux, redox control techniques, etc.).

As a point of reference, it is estimated that about 4 kg Be/yr would be needed for redox control in the tritium breeding and heat transfer blanket of the Affordable, Robust, Compact (ARC) fusion machine [13] due to the oxidizing effect of activation reactions [82]. If LiF was not replenished to account for the shift from the stoichiometric ratio of FLiBe caused by 4 kg of Be addition, the FLiBe composition would change by 0.02 mol% BeF_2 per year [82]. Additionally, the Li-6 for tritium production may need to be replenished by LiF additions, depending on the enrichment of the lithium supply. To operate at 90% Li-6 enrichment, 14.5 kg LiF (95.4% Li-6 enrichment) would need to be added each year to account for the components consumed by activation. This fraction of LiF in the 958-tonne inventory of FLiBe [13] would be a change of 0.02 mol% LiF. At 700˚C (the temperature examined in highest resolution in this study and the approximate operating temperature of the FHR [83]), LiF-BeF_2 mixtures with 20 mol% BeF_2 or more are in liquid solution, and mixtures with lower BeF_2 content form a two phase solid/liquid mixture [84] (see Figure 2.1). As such, phase changes are not anticipated due to fluctuations in composition resulting from neutron activation. However, compositional changes may have an effect on the solubility of solutes (e.g., oxides, corrosion or fission products), related to changes in fluoroacidity, or the activity of dissociated fluoride in the melt [23]. Further, a liquid-liquid immiscibility gap in mixtures around 80 mol% BeF_2 has been calculated but not experimentally examined [85], [86], [87]. In this study, by investigating the LiF-BeF_2 composition space (from

33 mol% to 100 mol% BeF_2), we can characterize solvent structure representative of a range of fluoroacidities, including those at high BeF_2 concentrations.

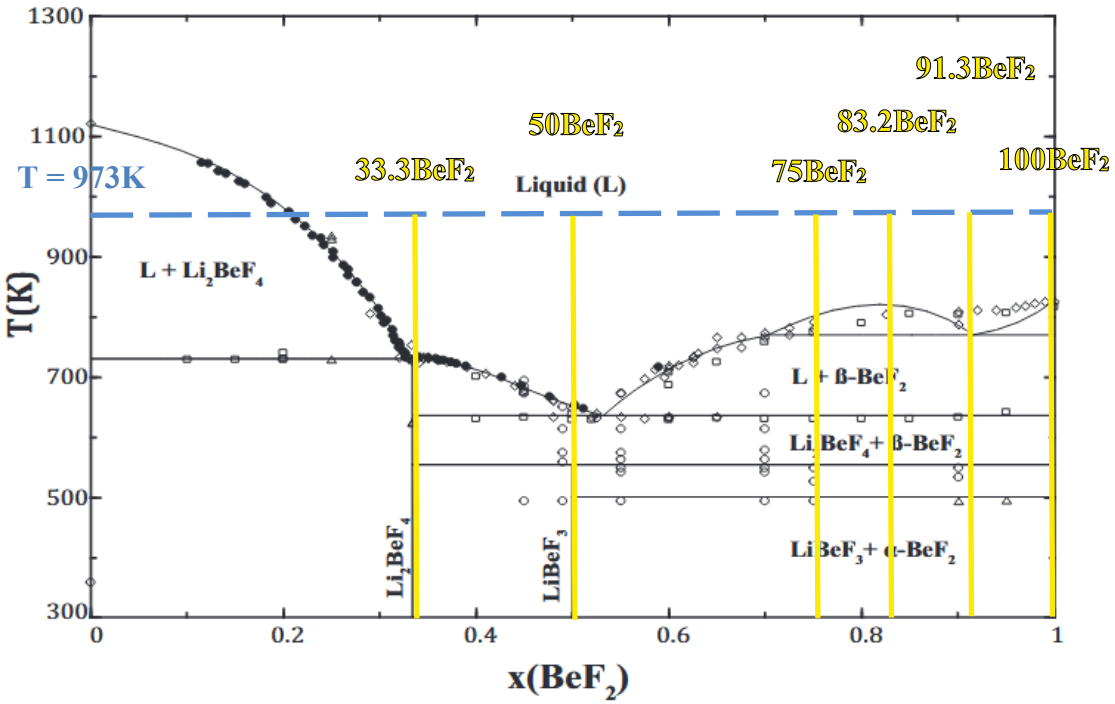

Figure 2.1. Calculated LiF-BeF_2 phase diagram reproduced from Smith et al. 2020 (https://doi.org/10.1016/j.molliq.2019.112165) licensed under CC by 4.0 [87]. Data points represent experiments data from [88], [89], [90], [91], [87]. Dashed blue line indicates temperature of neutron data presented in this chapter, and solid yellow lines indicate the compositions studied.

The first published model of LiF-BeF_2 mixtures to our knowledge is a geometric polymer model developed by C.F. Baes in 1970 [25]. Baes describes LiF-BeF_2 mixtures as consisting of primarily corner-sharing BeF_4^{2-} tetrahedra with bridging anions occasionally disrupted by the presence of basic (electron pair donating) LiF. The thermodynamic fitting parameters for the model are the energy of polymerization of fluoroberyllate anions, the interaction energy among non-bridging F^-, and the energy of ring-formation. These parameters were fit to the activity coefficient of BeF_2, which had been measured electrochemically [92], as a function of composition.

Baes' model defined the polymeric network of BeF_2 by constraining cations to have four coordinates based on the nominal coordination assumed for the solid state of glassy BeF_2 (by analogy to SiO_2 and GeO_2) and validated by X-ray diffraction [25], [93]. An outcome of Baes' thermodynamic model fitting was calculation of the volume fraction of each polymer species Be_aF_{3a+1} (corner sharing tetrahedra) and Be_aF_{2a+2} (edge sharing tetrahedra). Baes calculated that a mixture of 33.3 mol% BeF_2 (33.3BeF_2) consists of ~60 vol% BeF_4^{2-} monomers, ~20 vol% dissociated F- (dsF), and the remainder polymers of $a \geq 2$ of the corner-sharing type (Be_aF_{3a+1}). An increase in edge-sharing species was observed at compositions around 50BeF_2. Edge-sharing

F- for all oligomers was observed to dominate over corner-sharing for $x_{BeF_2} = 0.6\ to\ 0.8$. In Baes' polymer thermodynamic model, edge-sharing and CN=3 are stoichiometrically equivalent.

A 2021 work by Winner et al. compares Baes' oligomer distribution of 33.3BeF_2 to an ab-initio molecular dynamics (AIMD) model which allows for a Be-F CN of 3 in addition to 4. Where Baes found 54 mol% of F were present in BeF_4^{2-} monomers, Winner found 29±13 mol% of F in CN=4 monomers and 5±2 mol% of F in CN=3 monomers (BeF_3^{1-}) [19]. Baes did not calculate any oligomers with $n_{Be} > 4$, but Winner calculated that ~ 9 mol% of F are a part of CN=4 and CN=3 polymers with 5 or more Be [19].

The structure of LiF-BeF_2 mixtures has been further characterized through X-ray diffraction studies [28] and complementary AIMD simulations [94]. Vaslow's 1972 study led to the first measurements of the coordination numbers (CN) of Be and Li by F in their primary fluoride melt (4.0±0.3 at 700˚C and 3±1 at 880˚C, respectively). The high uncertainty of the Li-F CN supported the interpretation that the local environment of Li was "grossly distorted from average tetrahedrality" [28]. Measurements of *mixtures* of LiF and BeF_2 led to the conclusion that a higher concentration of LiF generated more deviation from tetrahedrality in local structure of Li-F, while Be^{2+} maintained its tetrahedral coordination [28]. The dynamic structure of Li in FLiBe has been further confirmed via AIMD simulations which indicate that the cage correlation time of Li by F is an order of magnitude less than that of Be by F (0.4±0.1 ps vs 24.6±0.8 ps, respectively) [19].

To date, other experimental studies of LiF-BeF_2 structure include Raman spectroscopy [34], [35], [36], IR spectroscopy [95], and high-temperature NMR studies [32] (other HT-NMR studies contain NaF in addition to LiF and BeF_2 [96], [97]). Spectroscopic studies have not indicated edge sharing or cluster formation, however, caveats were presented in one study that moisture might have affected the melt [95] and in another study that band overlap in the spectra and multiple possible contributors to vibrational modes could render peak differentiation impossible [35]. NMR studies suggested the formation of a new coordination structure (distinguished from what had been attributed to the dynamics of monomeric BeF_4^{2-} units) at concentrations of BeF_2 greater than 25 mol%, suggesting polymerization of the melt with chains containing $n_{Be} \geq 3$, with the fraction of monomers and dimers decreasing as BeF_2 increased above 25 mol% [32]. Additionally, ^7Li NMR indicated that Li^+ are not purely dissociated, but rather are dynamically coordinated by dissociated fluorides (dsF), BeF_4^{2-}, and the polymeric Be-F network [32].

Most recently, Fayfar et al. performed measurements of the structure factor of FLiBe at 700˚C by neutron and X-ray scattering and supporting neural-network-based modeling [29]. Fayfar et al. demonstrated the fittingness of neural-network interatomic potential (NNIP)-based molecular dynamics (NNMD) over AIMD for capturing the structural behavior of FLiBe and examined structure beyond the first nearest neighbor. At 700°C, NNMD showed chains varying in length from $n_{Be} \geq 2$ to $n_{Be} \geq 7$, with ~13 mol% of Be existing in dimers and ~8 mol% of Be existing in chains with $n_{Be} \geq 3$.

Other AIMD models of FLiBe systems have been developed with the goals of predicting thermophysical properties [98], [99], studying tritium transport [100], [101], and examining

chromium speciation [19], [102]. More recent thermodynamic and quasi-chemical models of $LiF\text{-}BeF_2$ systems include those by Romero-Serrano et al. in 2009 [86] and Smith et al. in 2020 [84].

Romero-Serrano et al.'s model is built upon the free energy change of the depolymerization of BeF_2 upon addition of LiF (the formation of two terminal Fs (trF) from a bridging F (brF) and dsF), with the Be-F CN restricted to 4 [86]. They found the fraction of moles of monomers per moles of solution to be approximately 15% (assuming all monomers contain 4 F, with it being unclear how they define moles of solution). They compare their results to the AIMD model of Salanne et al. [103] who found FLiBe to be predominantly composed of monomers (with 35% of F^- composing BeF_4^{2-} tetrahedra) which are nearly exclusively corner-sharing. For comparison, they convert Salanne et al.'s results to their own metric (per moles of solution), the value of which is approximately 12 mol-soln% monomers in FLiBe. Thus, 35% of F in monomers is equivalent to 12% of moles as monomers by their metric. Romero-Serrano et al. additionally found that Li^+ move independently from the fluoroberyllate network such that their motion is decoupled from the viscosity of the $LiF\text{-}BeF_2$ mixture (the mixtures they modeled ranged from 33.3 to 50 mol% BeF_2) [103].

Smith et al.'s work was based on the polarizable ion model which then informed a CALPHAD thermodynamic model. For a structural interpretation, it was assumed that the $LiF\text{-}BeF_2$ mixtures consisted of dsF, Li^+, monomers, dimers, and trimers (with any higher n_{Be} polymers being categorized as networked trimers). At 627°C, Smith et al. found that approximately 36% of F composed BeF_4^{2-} tetrahedra, similar to Salanne et al. The key difference between Smith et al. and Salanne et al. (except for a slight temperature difference: 627°C and 600°C, respectively) is that Smith et al. investigated more compositions which were able to show that monomer fraction is even higher at lower BeF_2 mole fractions (50% of F in monomers in 20 mol% BeF_2). Smith et al. show that the fraction of F in monomers drops to zero around a composition of 55 mol% BeF_2, and at the same point, the liquid is composed nearly exclusively of polymers of $n_{Be} \geq 5$.

In our structural analysis, we examine the effect of temperature on Be-F and F-F bond lengths in the various compositions. These bond lengths have been measured in the solid [104] and are estimated in the liquid based on the peak position of the PDF. As such, "bond length" refers to the most probable bond (highest atom number density) length for a given pair of atoms. The shrinkage of U-Cl bonds upon melting in UCl_3 has been reported in Maltsev et al. [105]. Their analysis showed that in the liquid there exist short, transient, U-Cl bonds with greater participation of U (5f orbitals) compared to the solid state. That is, short U-Cl bonds with a higher degree of covalency are observed in the liquid. Walz and Van Der Spoel used molecular dynamics to calculate the change in first nearest neighbor (FNN) and second nearest neighbor (SNN) distances between the experimental melting point and m.p. + 100°C for several alkali halides [106]. For both of their models (polarizable and non-polarizable), the FNN distance *decreased* on average 0.14-0.35% with a 100°C increase in temperature, and SNN distance *increased* 0.73-0.78%. They explain this behavior by describing that FNN interactions (cation-anion) strengthen as SNN shielding (like-like) decreases, and they make note of an accompanying decrease in CN with increasing temperature, with a greater decrease in the second coordination shell CN [106]. A neutron diffraction study of CsCl has indicated no change in bond length with temperature, however; over a 300°C range in the liquid, the authors reported no

change in the first sharp diffraction peak (FSDP) position, claiming consistency with Raman scattering studies in indicating no structural changes with temperature [107].

In the existing literature, studies examining the structure of $33.3BeF_2$ have reported the Be-F and F-F bond length at various temperatures, although they have not looked explicitly at trends in temperature. Experimental and modeled $33.3BeF_2$ Be-F and F-F bond lengths from literature are shown in Figure 2.2. The scatter of the data indicates no substantial trend in bond length with temperature.

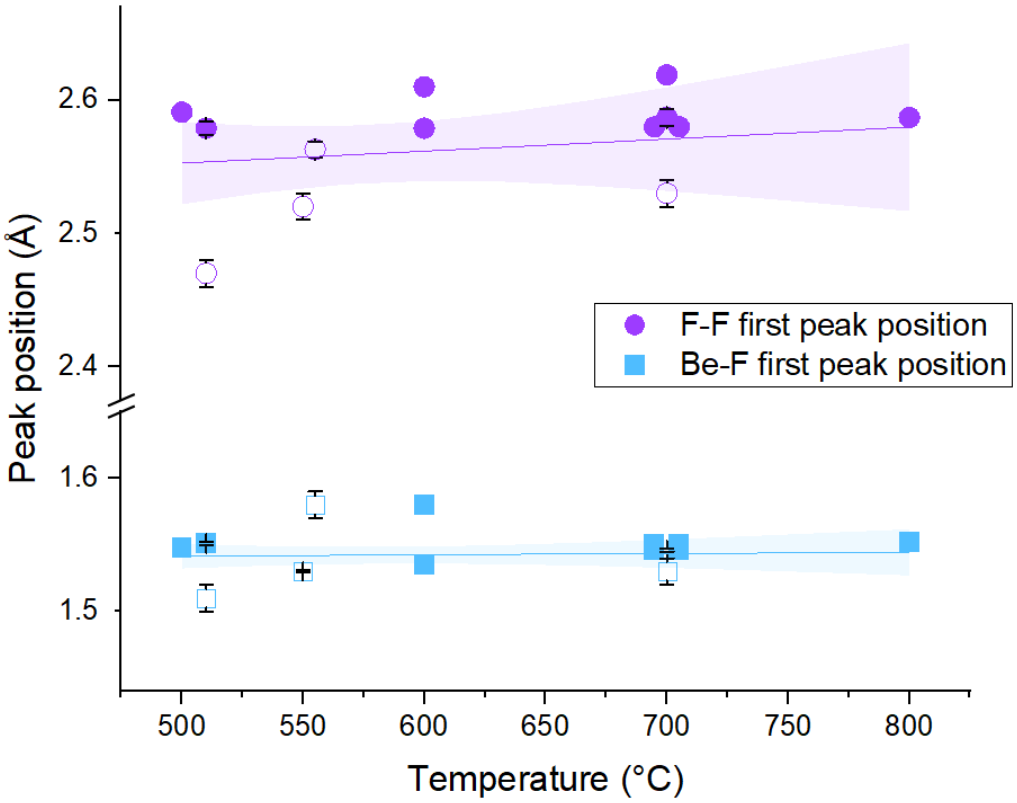

Figure 2.2. Be-F and F-F peak position in $33.3BeF_2$ as measured experimentally via neutron [29] and X-ray diffraction [28] (open data points) and as calculated from FPMD/AIMD [19], [102], [103], [108], and NNMD [29] (closed data points). Linear fits shown across all data, with 95% confidence interval shown.

Overall, prior studies provide a picture of $LiF\text{-}BeF_2$ liquid structure in which Be^{2+} exist primarily in BeF_4^{2-} tetrahedra as isolated monomers or in corner-sharing oligomers, with the fraction of monomers decreasing as BeF_2 fraction increases. In these systems, Li^+ is weakly coordinated, with its coordinate species depending on the composition of the mixture. Broadly, the existing structural understanding for $LiF\text{-}BeF_2$, particularly the role of CN = 3 species and quantitative oligomer distribution, has been seen to vary depending on the system model. Further, there exist little data in the prior literature on the sensitivity of structural features to temperature and

composition. In light of the current understanding of liquid LiF-BeF_2 structure presented here, this chapter focuses on how the structure of molten LiF-BeF_2 evolves with composition and temperature, exploring which structural descriptors best capture and explain the nature of network formation in fluoroberyllate melts.

2.2 Methods

The structure of FLiBe and LiF-BeF_2 mixtures has been analyzed using neutron scattering, X-ray scattering, and molecular dynamics. Neutron scattering samples were prepared at UCB and work was done to ensure the compatibility and safety of the sample can design. Work done by UCB and outcomes of safety discussions between UCB and ORNL are detailed below. In this work, we present neutron scattering data on LiF-BeF_2 mixtures ranging from 33.3 mol% BeF_2 to 100% BeF_2, referring to each mixture by its molar percentage of BeF_2—e.g. FLiBe is 33.3BeF_2.

2.2.1 Sample can design, sample preparation, & beryllium safety

Samples for the (2023) neutron scattering experiments as well as the BeF_2 X-ray experiment were prepared at the University of California - Berkeley using natural isotopic beryllium fluoride (BeF_2, Materion, 97.55% purity) and lithium-7 enriched lithium fluoride (LiF, Sigma Aldrich CAS 17409-87-9, 99% chemical purity, 99.00 atom% Li-7). Sample names and descriptions are located in Table 2.1. All sample preparation took place inside of an LC Technology argon glovebox with monitored oxygen and moisture levels (< 5 ppm O_2, < 1 ppm H_2O). To prepare the samples, first, a bulk batch of 33.3BeF_2 was created using by using a Phoenix GH-252 analytical balance to weigh out the necessary amounts of LiF and BeF_2 powder. This powder was then added to a tapered glassy carbon crucible and heated in a Watlow full cylinder ceramic fiber furnace to 800°C until fully molten. After cooling inside the furnace, the resolidified salt was removed and pulverized into powder using a stainless-steel mortar and pestle.

Using a plastic funnel, the 33.3BeF_2 powder was added to the vanadium PAC cans. Then using the analytical balance, BeF_2 powder was added to dilute the samples to the compositions listed in Table 2.1. The unsealed vanadium cans were then heated to 800°C for around 1 hour to ensure that the powder inside became molten. The cans containing the samples were allowed to cool inside the furnace. The cans, each now containing a homogeneous chunk of resolidified powder, were then sealed using a graphite gasket made of 1/32-inch-thick McMaster-Carr high-temperature high-pressure graphite gasket material and screwing on the perforated titanium lid.

Vanadium cans were used as sample containers because of their transparency to neutrons. To test the compatibility of vanadium with the samples, the vanadium cans were leak tested at ORNL prior to experiments in 2022. A vanadium can filled with FLiBe was heated up to 750°C for 12 hours under vacuum (6.3E-6 Torr), sealed prior to heating in a sample containment test performed by ORNL researchers. The sample was swiped before and after heating under vacuum. The sample showed 0.17 µg/100cm^2 beryllium after heating (with an undetectable level (<0.025 µg) before heating) according to analysis at the ORNL Industrial Hygiene Analytical Laboratory on February 21st, 2022. No further leak testing took place prior to the 2023 experiments, under the assumption that an equivalent sample

can design would be used and with missed communication about modification of the cap design.

Figure 2.3. FLiBe in vanadium PAC can with graphite gasket and Ti lid prior to heat testing under vacuum in preparation of the NOMAD 2022 experiment. Photos by ORNL staff researchers.

Table 2.1. Compositions of samples in this study. (n) indicates the sample was prepared for neutron scattering studies, and (X) indicates the sample was prepared for X-ray scattering studies. For neutron scattering studies, Li in LiF was 99.00 at% Li-7. Densities are estimated from experimental values in the literature, interpolating across experimental densities at the nearest temperature and compositions.

Sample ID	Mole percent BeF_2	Weight percent BeF_2	Estimated density at 700°C (g/cm^3)	Estimated melting point (°C) [9], [10]	Atomic number density (atoms/$Å^3$)	Heating Rate (°C/min)
(n) 33.3BeF_2	33.3	47.5	1.948[109]	458	0.0827	2
(X) 33.3BeF_2	33.3	47.5	1.948[109]	458	0.0827	2
(n) 50BeF_2	50.0	64.4	1.927[110]	380	0.0801	4
(n) 75BeF_2	75.0	84.4	1.925[41]	519	0.0774	10
(n) 83.2BeF_2	83.2	90.0	1.929[41]	532	0.0767	10
(n) 91.3BeF_2	91.3	95.0	1.936[41], [111]	498	0.0760	4
(n) 100BeF_2	100	100	1.959[111]	554	0.0753	2
(X) 100BeF_2	100	100	1.959[111]	554	0.0753	2

Sample cans were cleaned inside the glovebox by repeated wiping with Ghost Wipes (deionized-water-wetted wipes) with repeated glove changes. Samples were then swiped with Ghost Wipes to survey for remaining beryllium contamination according to OHSA ID-125G. The neutron scattering samples were further cleaned by wiping in a fume hood at ORNL to attempt to reach a surface level contamination below the free release limit of 0.2 μg/100cm^2.

After running the samples, the beamline furnace showed levels of beryllium contamination ranging from 0.03-4.3 μg/100 cm^2 in various areas throughout the furnace which had not been in contact with the sample. Since this was above the DOE housekeeping limit of 3 μg/100cm^2, an incident safety review by ORNL beamline scientists, EH&S staff, and UC Berkeley researchers was performed. The cause of the contamination was traced to the failure of the graphite gaskets in the high-temperature vacuum furnace. The PAC can design used had two small holes in the sample lid—one on the top and one on the side of the lid. For the 33.3BeF_2 and 91.3BeF_2 samples, post-mortem analysis showed that the graphite gasket had ruptured (see Figure 2.4). We note that a change in PAC can lid design was made between experiments that took place in 2022 in the study by [29] and this experiment which took place in 2023.

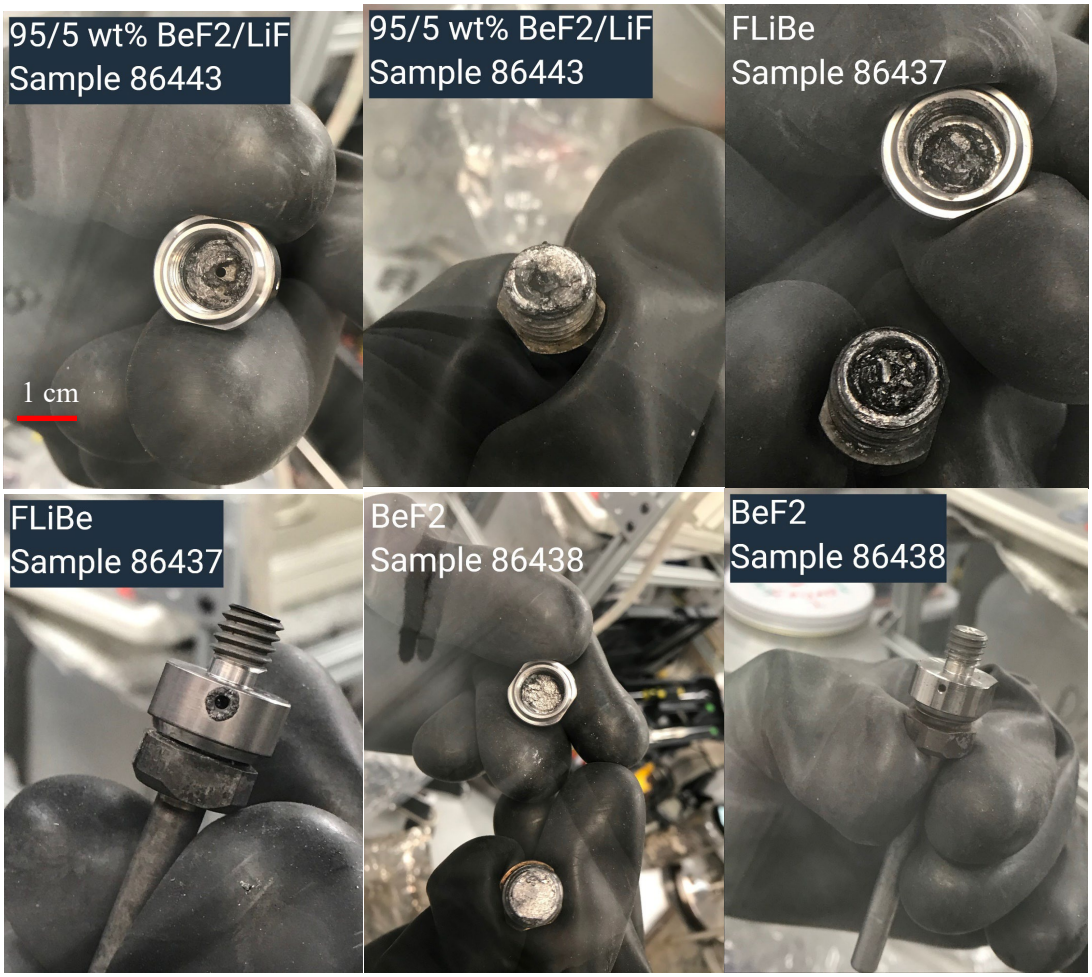

Figure 2.4. 33.3BeF_2, 91.3BeF_2, 100BeF_2 samples after running on the NOMAD beamline.

We make note of the following recommendations to ensure the safety of high-temperature beryllium-containing experiments at user facilities. The details of the incident analysis, communicated to ORNL, can be found in the report located in the Appendix Section 6.3.2.

- **A safety review should be performed by the user prior to all experiments.**

Receipt of sample canisters should take place well in advance of scheduled beamtime to allow for leak testing. Enhanced communication of expectations to demonstrate safety and iteration on safety review should take place well in advance of scheduled beamtime. Confirmation that samples are below free-release standards should be communicated prior to shipment to the beamline.

- **Sample cans should be qualified whenever a new can design is used for beryllium-containing samples, including changes to gaskets or lids.**

Changes in can design and results of the can qualification should be communicated to users. Leak testing should be conducted with a new sample container design. An alternative to graphite is needed if can lids with holes are to be used.

- **Beryllium survey swipes of the beamline furnace should be consistently collected.**

Identification of key areas to swipe should take place prior to experiments/beamtime. Consistent swiping before and after experiments should take place so that contamination sources can be systematically traced.

The 100BeF_2 sample for X-ray study was prepared at the University of California – Berkeley in a manner similar to that detailed in [112]. The sample was placed in a graphite container (high purity, highly oriented pyrolytic graphite rod (SPI Supplies) machined with a 2 mm diameter hollow) held in a quartz capillary (NMR capillary, Wilmad-LabGlass, 3 mm diameter) with quartz wool to hold the graphite in place in the capillary. After being capped in an inert Ar glovebox, the capillary was melt-sealed in a fume hood using an oxygen/MAPP torch by D. Nathanael Gardner and Michael Borrello. The samples analyzed via X-ray scattering were successfully decontaminated from surface beryllium contamination in a fume hood at UC Berkeley to levels below OSHA free release.

2.2.2 Neutron and X-ray scattering measurements

Neutron diffraction experiments were conducted on the Nanoscale-Ordered Materials Diffractometer (NOMAD) beamline at the Spallation Neutron Source (SNS) at Oak Ridge National Laboratory by D. Nathanael Gardner and Sean Fayfar with beamline scientist Jörg C. Neuefeind as described in [29]. Background measurement of an empty vanadium can was completed prior to sample can loading. Measurements were collected with a five-minute exposure time upon heating from room temperature to the experiment temperature of 700°C. Data was collected during the temperature ramp to observe the solid structure and for comparison to prior literature. Ramp rates ranged from 2 to 10°C/min. The samples were then measured for five hours each at 700°C. Conversion of the raw neutron scattering intensity to total S(Q) was completed on-site at the beamline using ADvanced DIffraction Environment

(ADDIE) [113]. Details of how total structure factor S(Q), the pair distribution function g(r), and coordination numbers (CN) were calculated are the same as that provided in [29]. Notably, NOMAD's Q range extends to 50 $Å^{-1}$, but a shorter Q_{max} was used for calculating S(Q) and subsequent data to ensure high resolution of the data presented, following the reasoning of [114], which found consistency in PDF measurements up to approximately 20 Å for the NOMAD instrument.

X-ray diffraction experiments were performed on beamline 28-ID-1 (Pair Distribution Function (PDF) beamline) at the National Synchrotron Light Source II (NSLS-II) at Brookhaven National Laboratory by Sean Fayfar, David Sprouster, and Dan Olds. Background measurement of an empty graphite/quartz capillary was completed prior to sample loading and later subtracted from the sample measurement. The sample was heated to 715°C using a hot-air blower at a heating rate of ~3°C/min. Sample temperature was later verified by referencing the calibrated temperature dependency of the Q = (002) graphite peak [115] as described in [112]. Once at temperature, the sample measurement was collected with an exposure time of approximately 5 minutes. Raw detector images were corrected similarly to the methods described in [29]. PDFgetX3 was used to convert scattering intensities into total structure factor S(Q) [116].

A benchmarking comparison of neutron diffraction experimental total structure factors and pair distribution functions at 700°C of the 33.3 mol% BeF_2 sample measured in 2022 [29] and again in 2023 are shown in Figure 2.5 and Figure 2.6. Structure factor peak positions and intensities show negligible difference between the 2022 and 2023 data as seen by the near-zero residual, with a difference of peak intensity of approximately 0.018 for the peak at 2.0 $Å^{-1}$. Similarly, peak positions are similar for the g(r)s, and the largest difference between peak intensities is that of the first pronounced peak at about 1.5 Å, with a difference of ~0.5.

This benchmark demonstrates repeatability and provides validation of NOMAD 2023 sample preparation methods and data analysis. Unless otherwise specified, 33.3BeF_2 refers to the 2023 experiment. In some cases, the data from the 2022 experiment described in [29] are shown as a point of comparison and are labeled as such in the results and discussion.

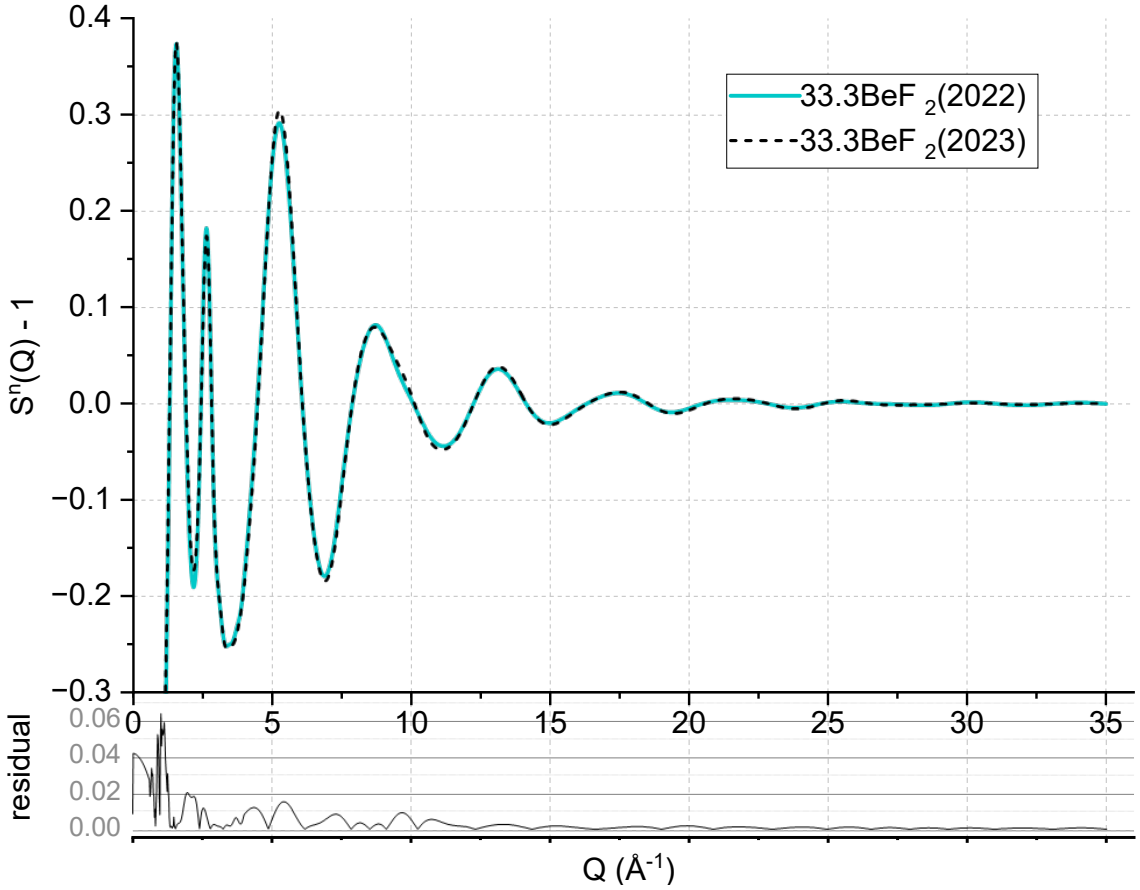

Figure 2.5. Structure factor benchmarked against 2022 data from a similar experiment (Fayfar 2024). Residual shows the absolute value of the difference between the 2022 and 2023 data. The 2022 sample was prepared from isotopically enriched ^{7}LiF from ORNL (unknown enrichment) and BeF_2 from Materion.

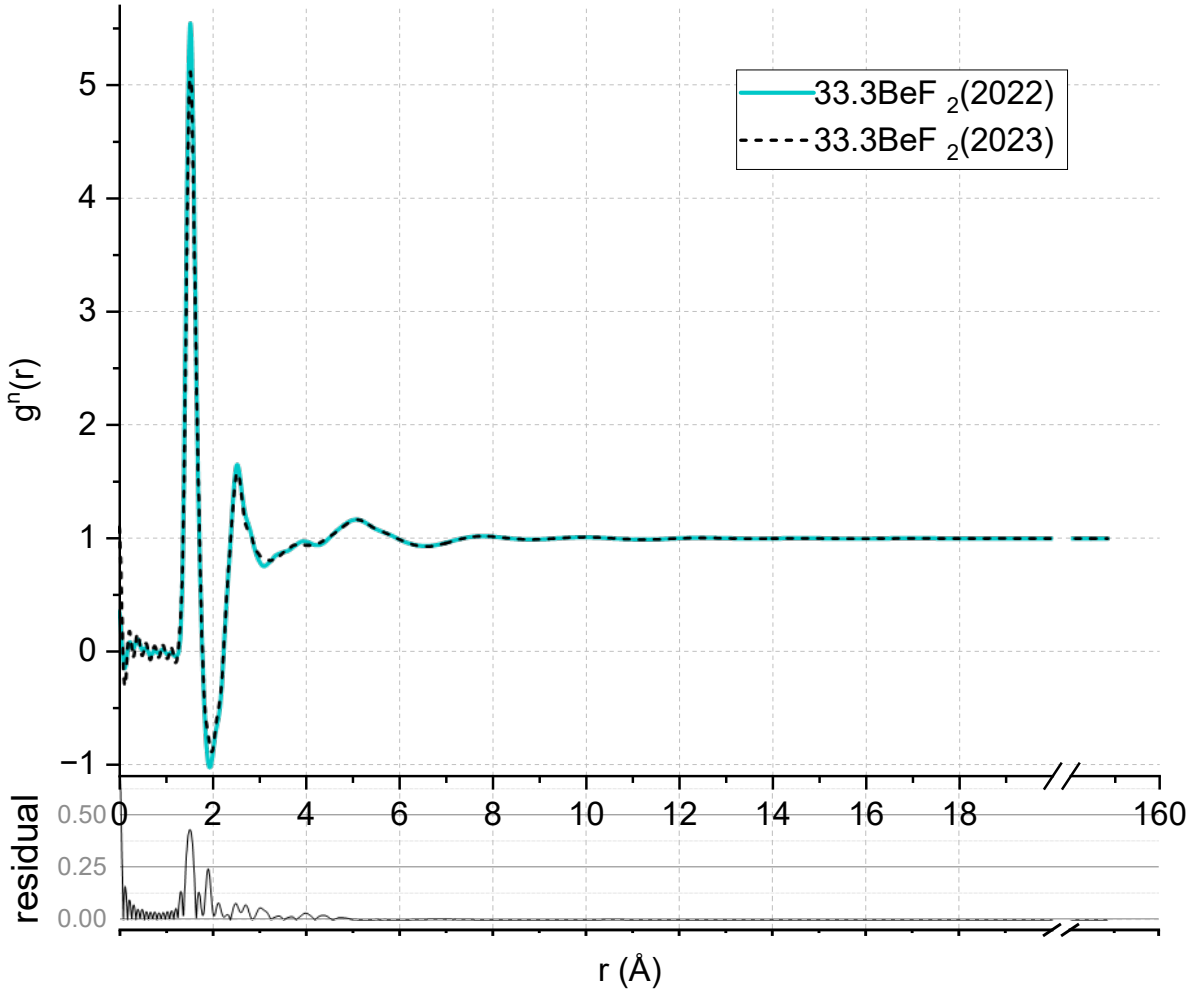

Figure 2.6. Pair distribution function benchmarked against 2022 data from a similar experiment (Fayfar 2024). Residual shows the absolute value of the difference between the 2022 and 2023 data. The 2022 sample was prepared from isotopically enriched ^{7}LiF from ORNL (unknown enrichment) and BeF_2 from Materion.

2.2.3 Empirical Potential Structure Refinement

Empirical Potential Structure Refinement (EPSR) is a reverse Monte Carlo technique for fitting structural models to experimental data. To allow for further analysis of the experimental neutron and X-ray data, EPSR was performed by Bora Kalkan at Lawrence Berkeley National Laboratory. Upon receiving the xyz plots, I used the Open Visualization Tool (OVITO [117]) to visualize the structure, analyze cluster formation, calculate the F balance (Section 2.4.1). EPSR outputs including S(Q)s (total, partial, weighted, and unweighted), PDFs (total, partial, weighted, and unweighted), bond angle distributions, angular variance, and quadratic elongation, were further analyzed for peaks and trends and were compared to NNMD and total neutron scattering data using OriginPro.

EPSR starts with Lennard-Jones and Coulomb inter-atomic potentials for estimation of an initial configuration, constrained by minimum approach distances for each atom pair and mass density (Table 2.1). EPSR then refines the configuration to match experimentally measured structure factor. EPSR has been used for the refinement of the structure of other high-temperature molten salts, namely $ZnCl_2$ and sulfate glasses [118], [119]. Prior to the introduction of EPSR, reverse Monte Carlo techniques have been used to fit experimental data for neutron diffraction studies of molten LiCl [120]. Note that EPSR produces only a possible atomistic configuration of each composition based on experimental data. To our knowledge, this study is the first to perform EPSR on molten fluoride salts.

Table 2.2. Number of atoms used for EPSR simulations, Lennard-Jones parameters, Coulomb charges for the studied systems. Parameters defining the interatomic potentials were taken from [121], [122].

Element	Number of atoms in studied systems						Ɛ (kJ/ mol)	σ (Å)	q (C)
	$33BeF_2$	$50BeF_2$	$75BeF_2$	$83.2BeF_2$	$91.3BeF_2$	$100BeF_2$			
Li	400	300	200	100	87	0	0.69	1.50	+1
Be	200	300	600	495	913	600	0.39	1.60	+2
F	800	900	1400	1090	1913	1200	0.30	2.00	-1

Table 2.3. Ion pair cut-off distances used in EPSR simulations, calculated using atomic radii or taken from [29].

Pairs	Minimum approach (Cut-off) distances (Neutron) (Å)	Minimum approach (Cut-off) distances (X-ray) (Å)
Li-Li	2.0	2.13
Li-Be	2.0	1.91
Li-F	1.45	1.59
Be-Be	2.10	2.02
Be-F	1.34	1.35
F-F	2.00	2.10

2.2.4 Neural Network Molecular Dynamics

As a point of comparison and to evaluate the accuracy of existing molecular models of LiF-BeF_2 molten salts, I present neural-network-based molecular dynamic (NNMD) simulations of the sample compositions listed in Table 2.1, performed by Shubhojit Banarjee and Prof. Stephen Lam at the University of Massachusetts – Lowell. I note some relevant details about the NNMD simulations below.

- AIMD data were used to train the neural network interatomic potentials. The compositions used for the training data were: 100BeF_2 at experimental volume and 15% expanded volume at 850°C, 100LiF at experimental volume and 5% expanded volume at 1027°C, 33.3BeF_2 at experimental volume and 5% and 10% expanded volume at 700°C, and 75BeF_2 at experimental volume at 700°C.

- For encoding the local environment of each atom to a per-atom energy, a smooth cutoff at 2 Å and a hard cutoff at 8 Å were chosen, meaning a weighting function is used for calculating the energies of atoms between 2 and 8 Å, and after 8 Å, energy contributions are considered zero.
- Densities were estimated from MSTDB-TP [123]. The densities of 83BeF_2 and 91BeF_2 were estimated by interpolation of experimental data at the nearest compositions and temperatures, as listed in Table 2.4.

Table 2.4. NNMD simulation details for compositions modeled. Temperature for all systems is 973 K (700°C).

mol% BeF2	Density (g/cm^3)	Box length (Å)	# Be	# Li	# F
33	1.935176	20.57	104	208	208
50	1.937448	29.14	400	400	1200
75	1.927453	24.31	300	100	700
83	1.929*	18.13	495	100	1090
91	1.9368*	33.83	913	87	1919
100	1.985405	38.9230184	1500	0	3000

*Densities estimated by linear interpolation of experimental data of density and temperature at the nearest compositions and temperatures.

2.3 Results

Below are neutron scattering data (structure factors, pair distribution functions) and the same structural data from EPSR and NNMD, along with partial structure factors and partial pair distribution functions from these models. The superscripts “n” refer to the S(Q) or PDF measured via neutron scattering or based on neutron scattering data. The superscripts “EPSR” and “NNMD” refer to the technique used to generate the partial PDFs. Figure captions specify if the plots display structure factors or PDFs weighted with neutron scattering lengths or X-ray atomic form factors (“weighted”) or not (“unweighted”). Additionally, bond angle distributions for all ion groupings from EPSR, coordination number calculations from neutron scattering, EPSR, and NNMD, and trends in peak position with temperature from the neutron PDFs are presented.

2.3.1 Structure factors

The predominant difference between the structure factors of the different LiF-BeF_2 mixtures is the shape of the peak around 2.7 $Å^{-1}$. According to the partial S(Q)s from NNMD (see Figure 2.9), all pairs contribute to this peak. The Be-Li, F-F, Li-Li, and Be-Be peaks in this region are positive, and the Li-F and Be-F peaks are negative such that in mixtures with more Be, the total peak is more positive. In 33.3BeF_2, the F-F and Be-F peaks are centered roughly at 2.7 $Å^{-1}$, but in 100BeF_2, they are located at a slightly higher Q value. In 33.3BeF_2, peaks which include Li are at slightly lower Qs than 2.7 $Å^{-1}$. As such, Li contributions mean that the peak is slightly left-shifted relative to compositions which contain little Li. The asymmetry in the negative peaks at 2.7 $Å^{-1}$ in the samples with BeF_2 content greater than 83mol% is caused by the slight offset of the Be-Be, F-F, and Be-F peaks.

The first peak at 1.5 $Å^{-1}$ is generally higher for the lower BeF_2 concentration mixtures (33.3BeF_2 and 50BeF_2) but is lowest for the 83.3BeF_2 sample; that is, the 1.5 $Å^{-1}$ peak does not follow a consistent trend with composition. Conversely, the peak at 5.2 $Å^{-1}$ increases in intensity with an increase in BeF_2 content. For all compositions, it appears that the ratio of the 1.5 $Å^{-1}$ peak to the 5.2 $Å^{-1}$ peak decreases with increasing BeF_2 content. That is, for the low BeF_2 samples (33.3BeF_2 and 50BeF_2), the 1.5 $Å^{-1}$ peak is at a higher intensity than the 5.2 $Å^{-1}$ peak, for 75BeF_2 the peak intensities are nearly equivalent, and at the high BeF_2 samples (83-100BeF_2), the 1.5 $Å^{-1}$ peak is at a lower intensity than the 5.2 $Å^{-1}$ peak. The peak intensity order of all other peaks/valleys continues in the trend of the 5.2 $Å^{-1}$ peak, where samples with more BeF_2 having a higher intensity peak and less BeF_2 having a lower intensity peak. An anomaly to this pattern is seen in the 100BeF_2 sample at around 6.5 $Å^{-1}$. At that position, the peak flattens to a slightly positive slope. A similar but less pronounced feature is seen in the same location for the 91.3BeF_2 sample. Looking at the partial S(Q)s from NNMD, the Be-Be contribution to the 6.5 $Å^{-1}$ region is negligible for 33.3BeF_2, but there is a visible Be-Be peak around 7 $Å^{-1}$ in 100BeF_2.

The fits of NNMD and EPSR models to the experimental S(Q) for each composition are shown in Figure 2.8. Upon visual inspection, EPSR better fits the experimental data, particularly at low Q values (< 2.5 $Å^{-1}$). Specifically, NNMD failed to capture some features of the peak around 2.7 $Å^{-1}$, especially for 75BeF_2 where the peak seems absent. In addition, the 5.2 $Å^{-1}$ peak for the NNMD modeled data are consistently shifted to 10% lower Q than the measured value. This shift in the 5.2 $Å^{-1}$ peak is also observed for some of the EPSR compositions (50BeF_2, 75BeF_2, 100BeF_2) but is not consistently observed.

The NNMD models fit the smooth regions of the experimental data, whereas EPSR models occasionally introduce minor fluctuations in what would otherwise be smooth regions of the structure factor. For example, some minor fluctuations appear in the EPSR model at Q > 2.6 $Å^{-1}$ for 91.3BeF_2 and 75BeF_2. Looking more closely at the unweighted S(Q) partials from EPSR and NNMD (Figure 2.10), we see the Li-Li partial oscillate up to an amplitude of 2 at Q values < 2 $Å^{-1}$ for NNMD. For EPSR, the Li-Li partial for 91.3BeF_2 increases asymptotically as Q goes to 0 $Å^{-1}$.

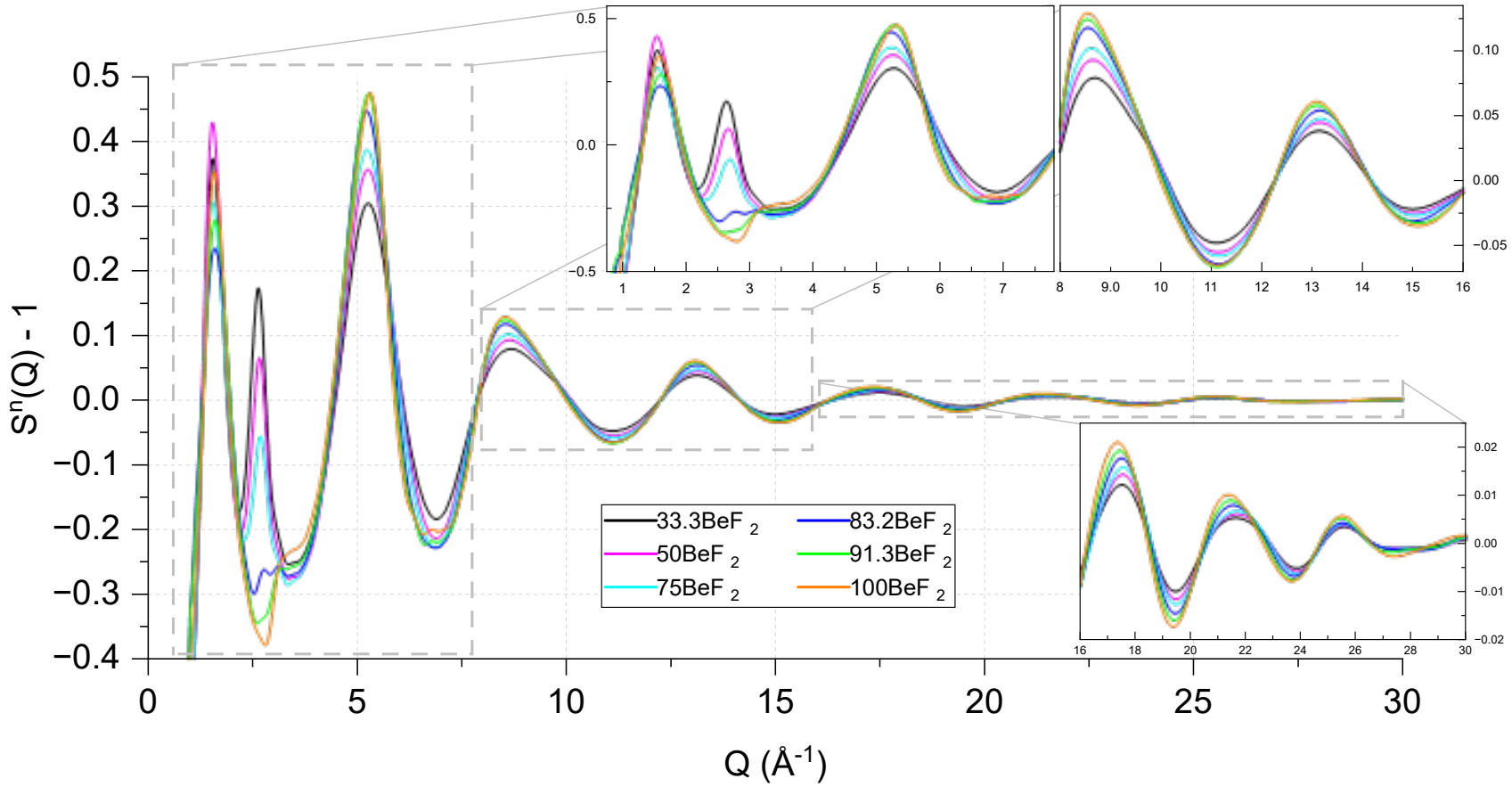

Figure 2.7. Total structure factor measured by neutron scattering at 700°C.

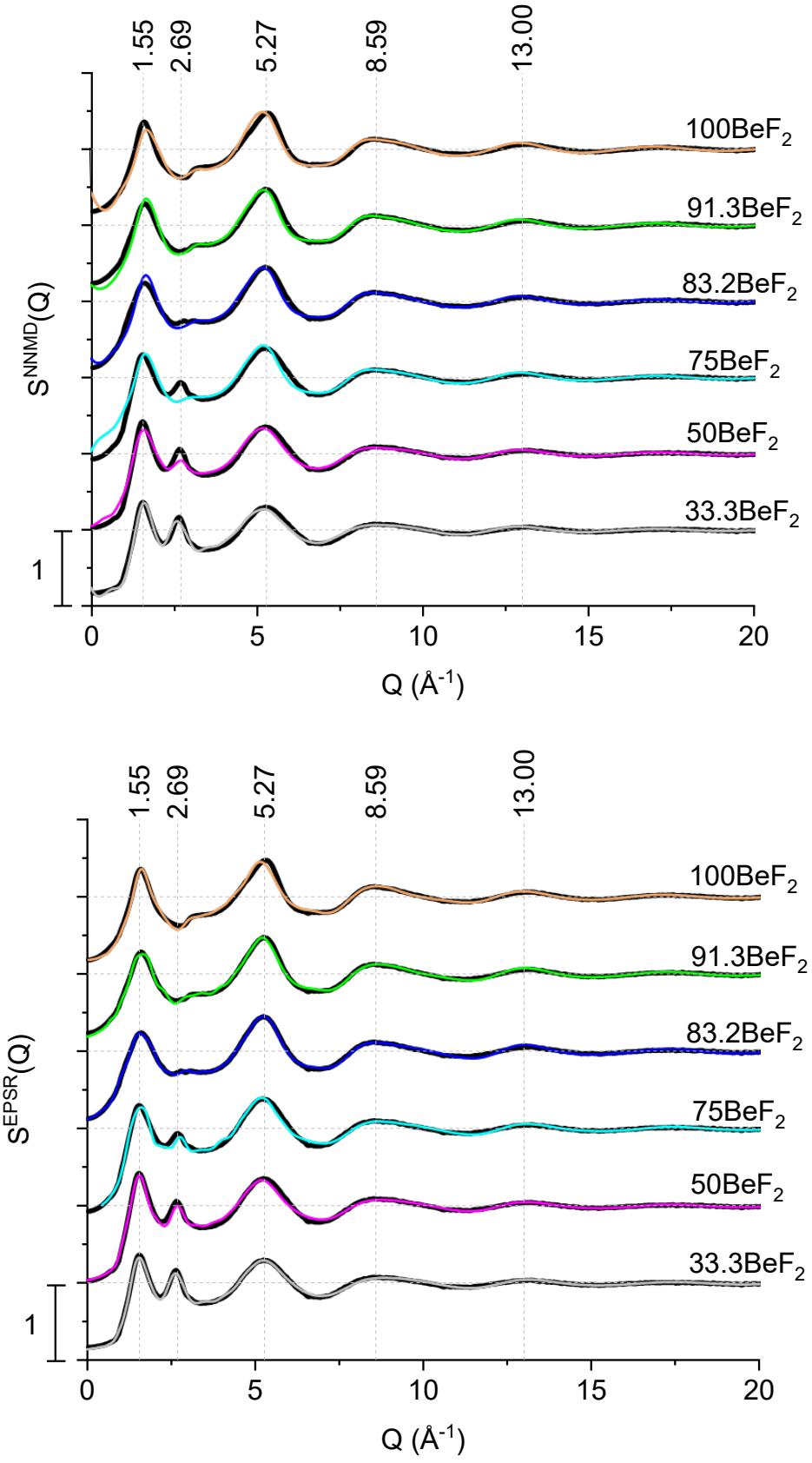

Figure 2.8. Total structure factor from neutron scattering (black lines) NNMD (color lines, top) and EPSR (color lines, bottom) at 700°C. Data offset for clarity.

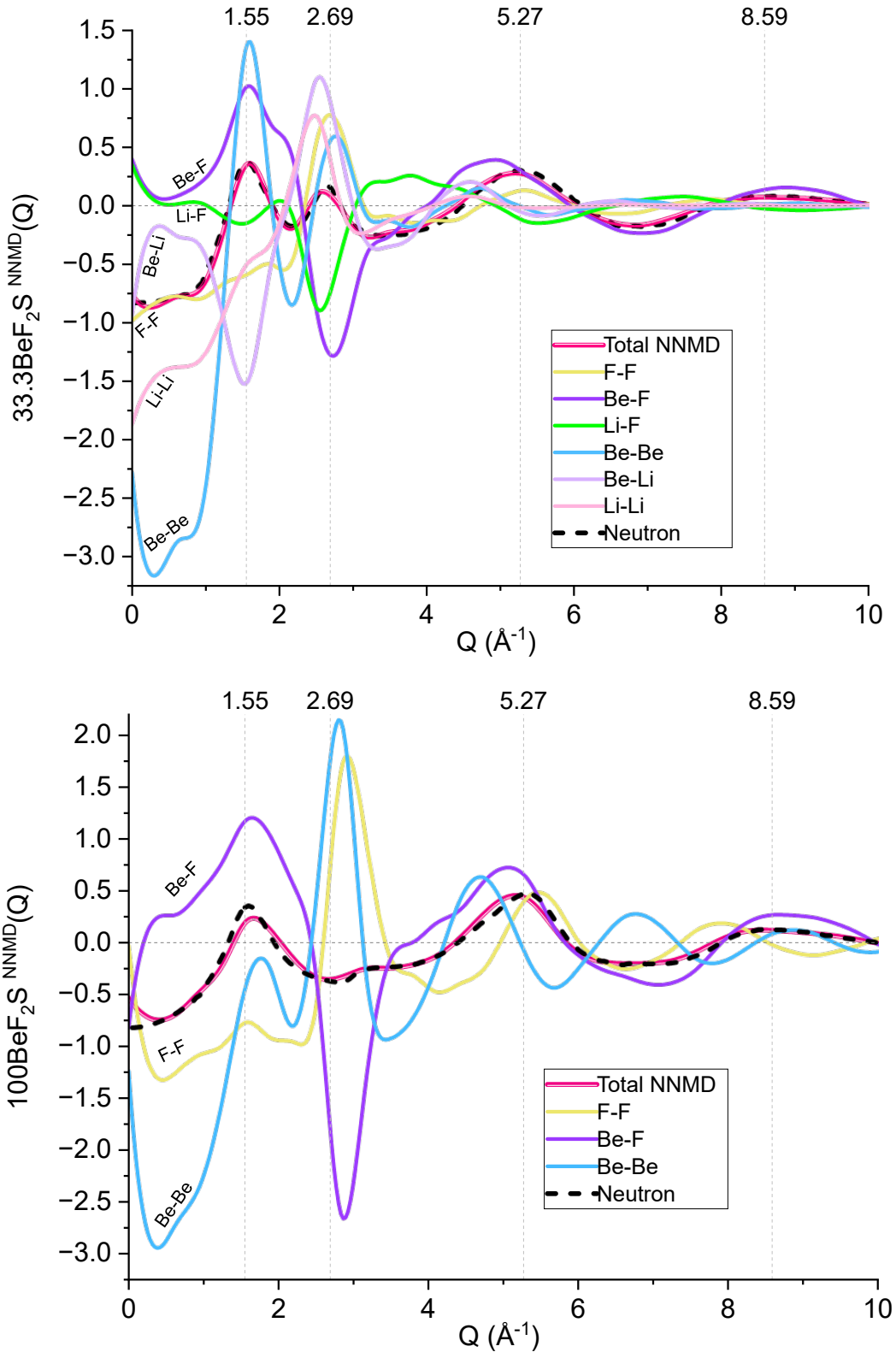

Figure 2.9. Weighted partial structure factors and total structure factor from NNMD and S(Q) from neutron experiments for 33.3BeF_2 (top) and 100BeF_2 (bottom). All data at 700°C. Other compositions in the Appendix Section 6.3.

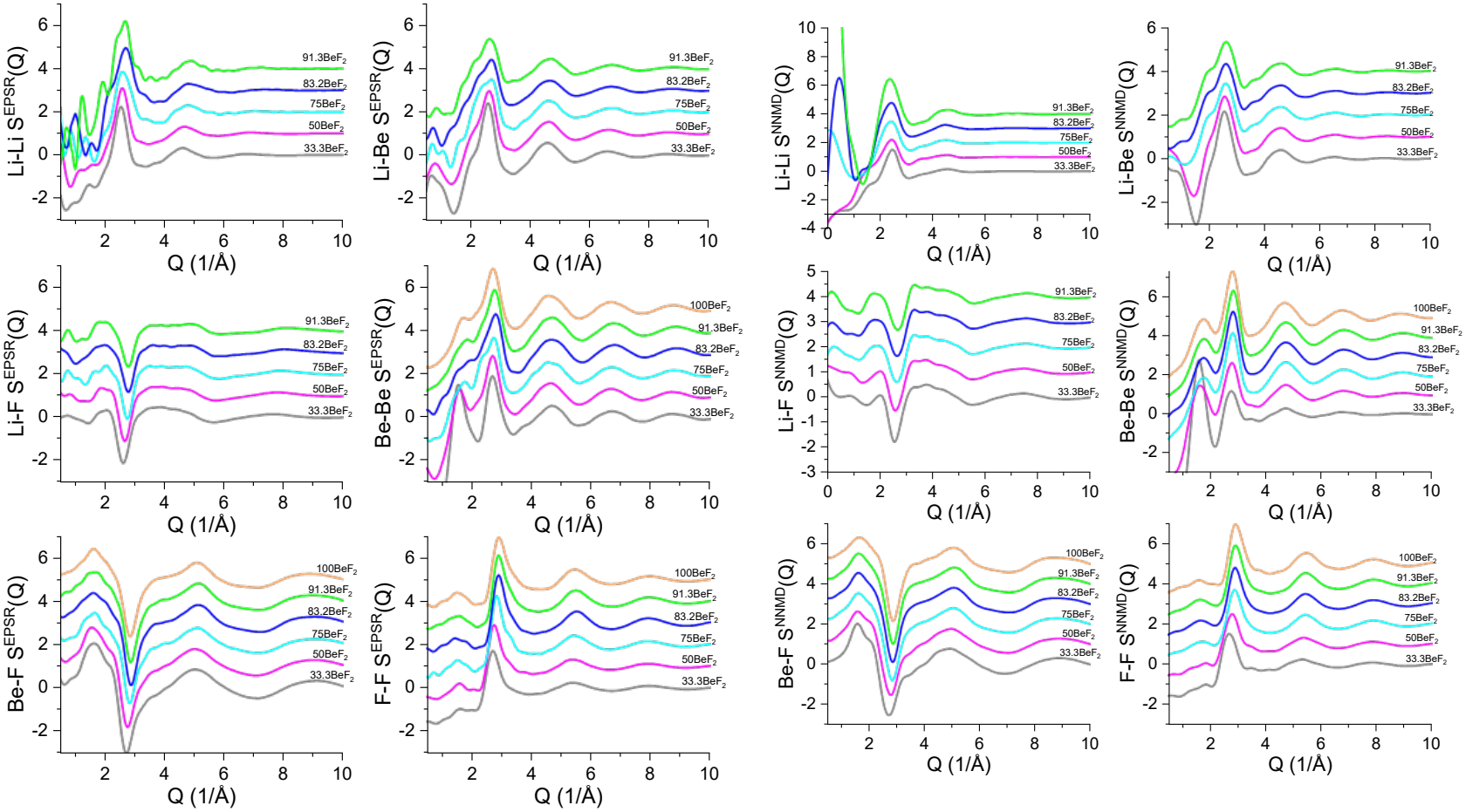

Figure 2.10. Unweighted S(Q) partials from EPSR (left) and NNMD (right) at 700°C.

2.3.2 Pair distribution functions

The PDFs of all samples examined by neutron scattering are shown in Figure 2.11. The first pronounced diffraction peak at around 1.5 Å generally increases in intensity with decreasing fraction of BeF_2 with the exception of $75BeF_2$ which has the lowest intensity of all the compositions studied. From partial pair distribution functions from NNMD and EPSR (Figure 2.12 and Figure 2.13), it is known that the primary contributor to this peak is the Be-F pair. Peak intensity is relevant only insofar as it contributes to the overall peak area which is integrated in the calculation of the Be-F coordination number. Since the pair distribution function is a number density comparing measured atomic density a distance *r* from a central atom relative to the bulk density, the 1.5 Å peak position is an indicator of the most probable Be-F distance. The Be-F distance in $33.3BeF_2$ and $50BeF_2$ is approximately the same, with the Be-F distance increasing slightly at compositions with higher molar fractions of BeF_2 (except for $75BeF_2$).

The trend of the negative peak around 2.0 Å follows the composition of the samples, increasing in amplitude with decreasing fraction of BeF_2. It is known that the primary contributor of this peak is the Li-F pair, making the peak negative due to the negative neutron scattering length of Li. The -0.05 intensity negative peak in $100BeF_2$, then, is likely an artifact of data processing. It can be seen in Figure 2.12 that the total PDF from NNMD goes to zero in this region, showing no negative peak. The same is true for the total PDF from EPSR shown in Figure 2.13. The inflection point in the negative peak around 2.05 Å can be attributed to the location where the overlapping contribution of the Be-F peak becomes zero. Both EPSR and NNMD fail to capture the full intensity and features of the experimentally observed negative peak, at all compositions (Figure 2.12, Figure 2.13).

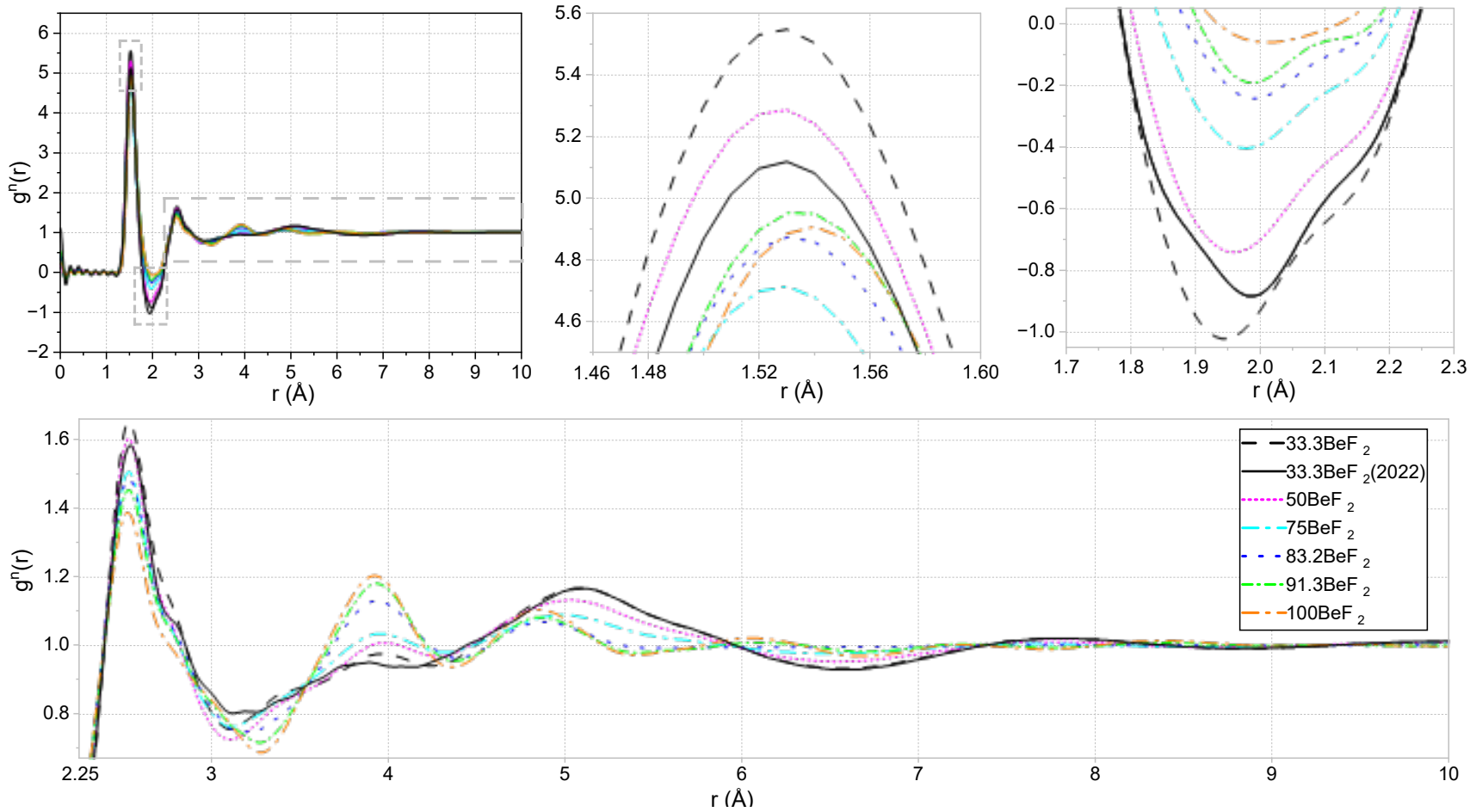

Figure 2.11. Pair distribution functions measured by neutron scattering at 700°C.

From the partial PDFs from both EPSR and NNMD (Figure 2.12 and Figure 2.13), we see two more peaks for the F-F pair—the first at ~2.5 Å and the second at ~5 Å. These F-F peaks are the primary contributors to the overall PDF at those *r* values. As such, the experimental peak locations in these regions can be analyzed to indicate F-F bond length changes across temperature and composition, which will be discussed in Section 2.3.6.

Similarly, the peak at ~4 Å is primarily indicative of the Be-F pair, although this peak is somewhat hidden by F-F and Li-F contributions at low BeF_2 concentrations. Partial PDFs from EPSR and NNMD show that this Be-F peak is asymmetric, with a higher number density of Be-F pairs at lengths slightly shorter than 4 Å.

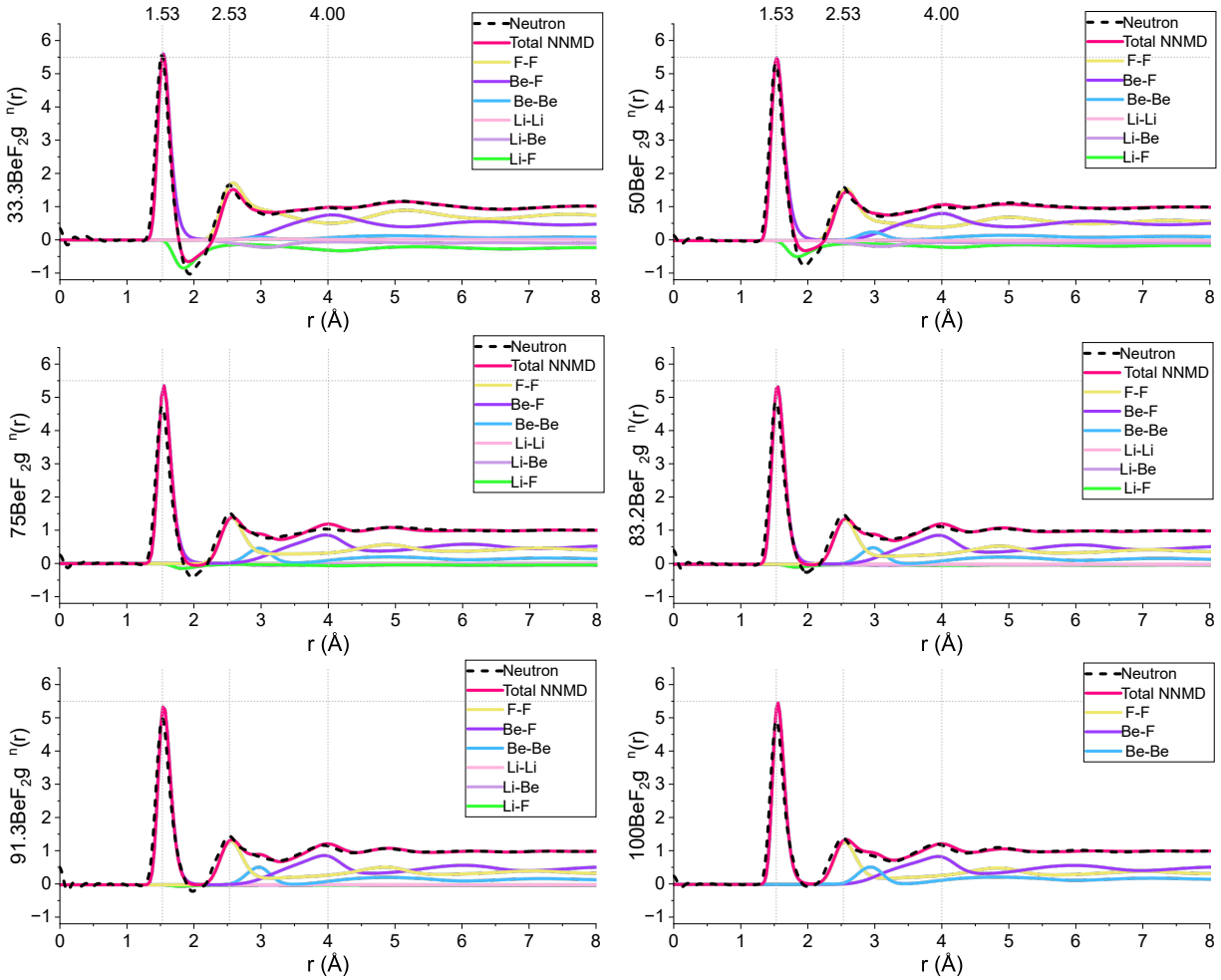

Figure 2.12. Pair distribution function for each sample composition from neutron scattering and NNMD, with partials from NNMD shown. All data at 700°C.

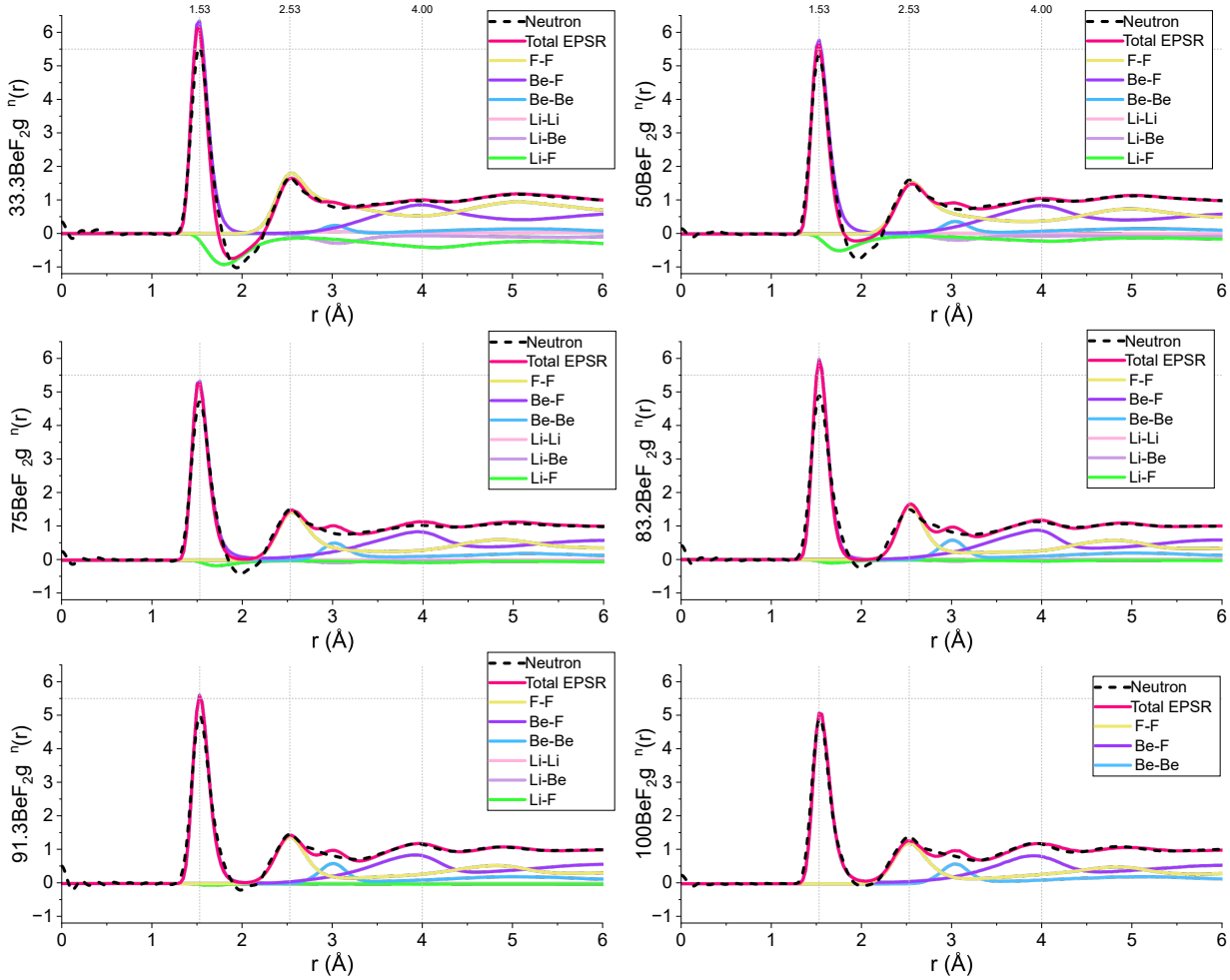

Figure 2.13. Pair distribution function for each sample composition from neutron scattering and EPSR, with partials from EPSR shown. All data at 700°C.

From Figure 2.12 and Figure 2.13, we see that both NNMD and EPSR reproduce the main features of the total g(r), with alignment of peak positions for the first peak around 1.5 Å. However for all compositions, EPSR and NNMD both generally over-estimate the intensity of the first peak at 1.5 Å. The second peak around 2.3-2.5 Å varies in intensity and shape, depending on the composition due to contributions by the F-F and Li-F ion pairs. At higher concentrations of BeF_2, NNMD calculates more sharply defined F-F peaks (around 2.5 Å). Li-F contributions are also different for EPSR and NNMD, with the Li-F peak approximately 0.1 Å further left for EPSR (noticeable for 33.3BeF_2 and 50BeF_2).

From Figure 2.13, it appears that EPSR is over-calculating the contribution of the Be-Be pair at around 3 Å. The EPSR-calculated total PDF has a higher peak at 3 Å compared to what was experimentally measured. The Be-Be peak at 3 Å calculated by NNMD is broader and less intense compared to the EPSR Be-Be peak, and thus, NNMD better captures the PDF character around 3 Å (although it slightly under-estimates the peak intensity).

Figure 2.14 gives greater insight into the differences between EPSR and NNMD across compositions by showing the unweighted partial PDFs. Comparing the Be-Be partials between EPSR and NNMD, we see the first peak around 2.5 Å is less sharply defined for NNMD

compared to EPSR (make note of the difference of scale of the EPSR and NNMD plots).

Li-Li partials for NNMD are broader and shifted to higher *r* values by about 0.1 Å, particularly at higher fractions of BeF_2. Li-Be partials for NNMD and EPSR are better aligned than the Li-Li partials, but EPSR generally has sharper, higher intensity peaks than NNMD for Li-Be. Trends in the Li-F peaks when comparing NNMD to EPSR are similar to those of Li-Be—EPSR has greater peak amplitude, with higher peaks and lower local minima. F-F and Be-F partials are similar for NNMD and EPSR. The F-F peak around 5 Å has minor variation between the two methods for the $50BeF_2$, $75BeF_2$, and $83.2BeF_2$ compositions.

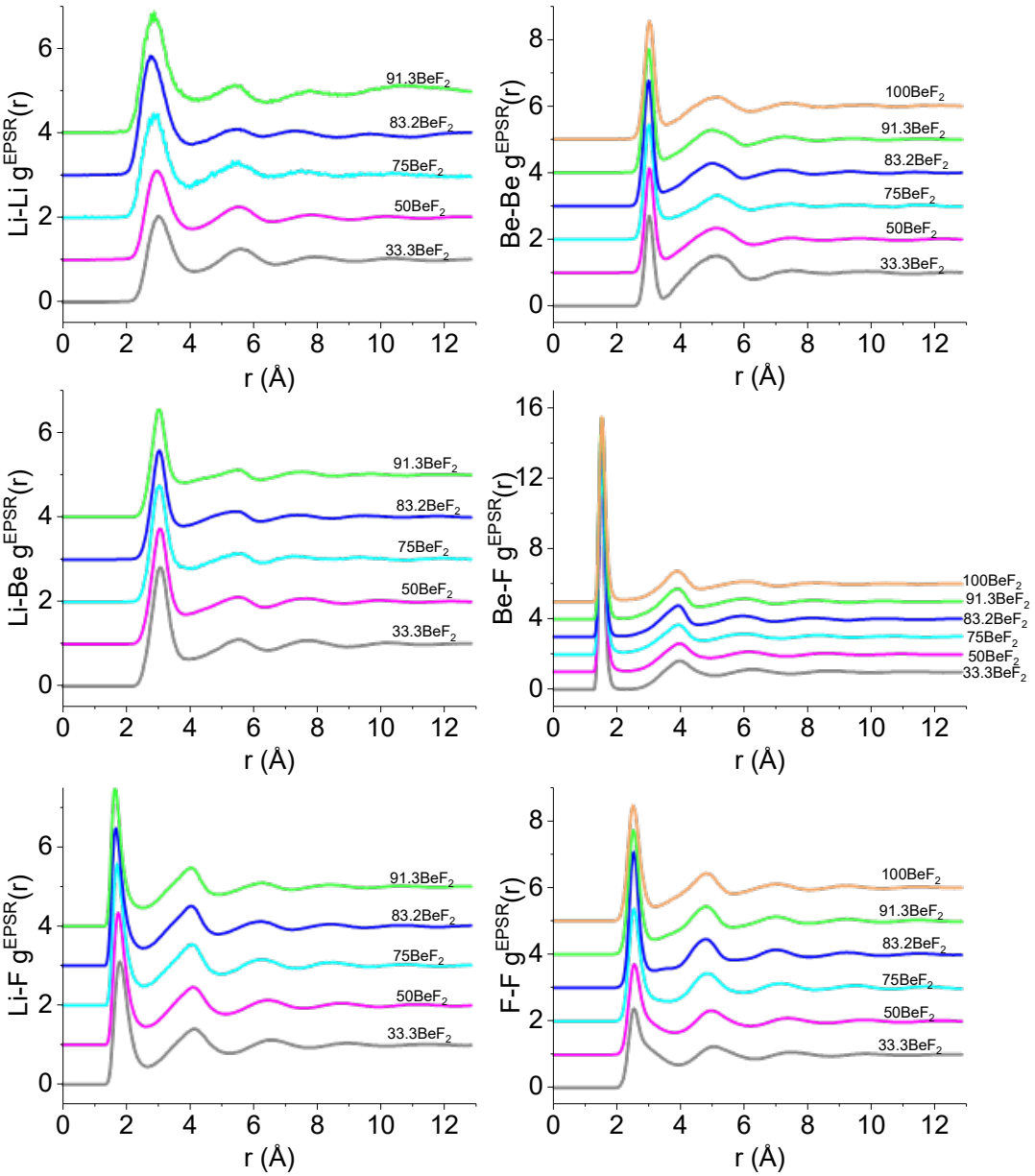

Figure 2.14. Unweighted partial radial distribution function) from EPSR fit to neutrons at 700°C.

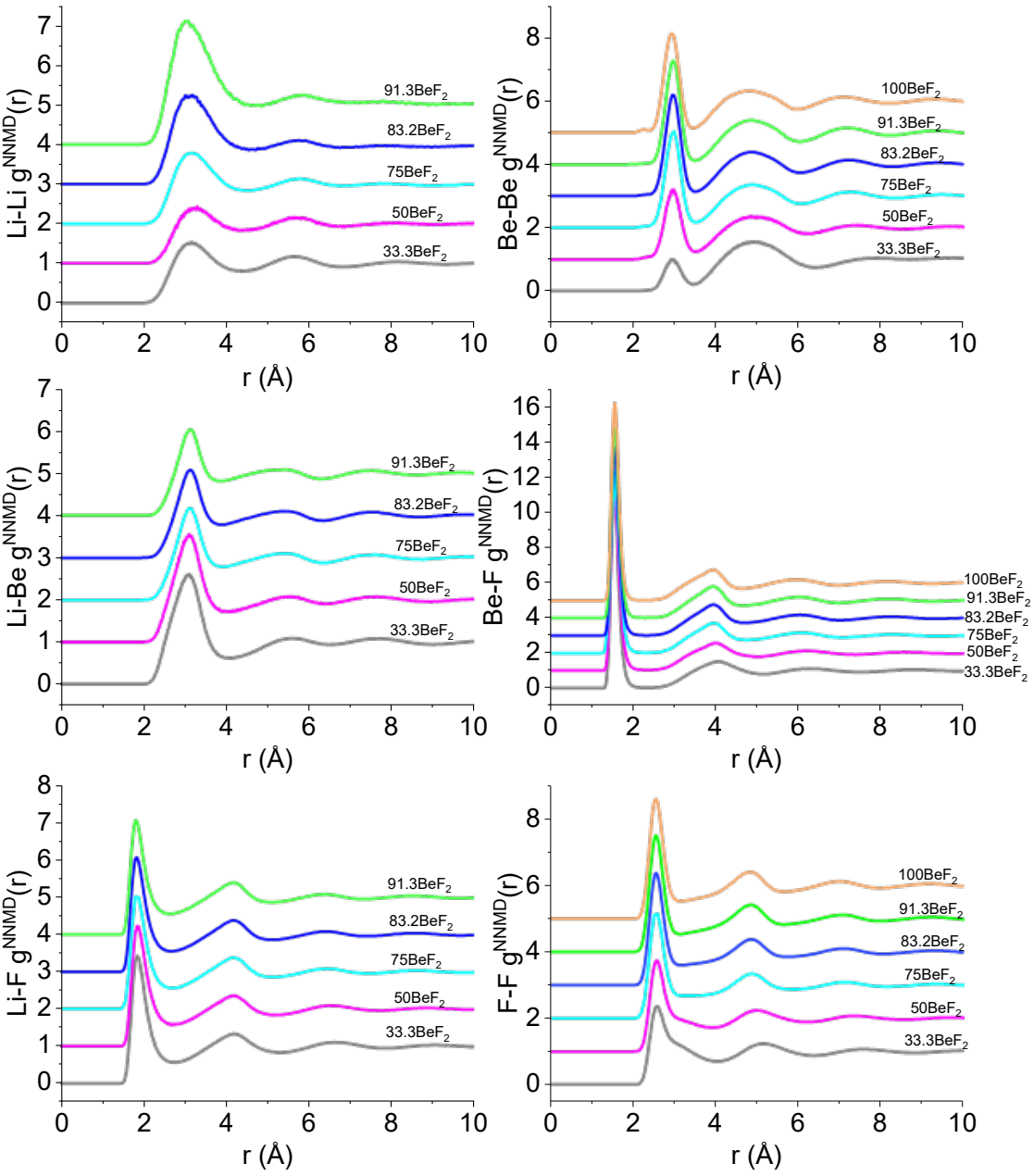

Figure 2.15. Unweighted partial PDFs (radial distribution functions) from NNMD at 700°C

2.3.3 Atomic snapshots

The following snapshots were generated using OVITO (Figure 2.16) [117] and Mercury (Figure 2.17) [124]. The number of atoms for each composition are listed in Table 2.2, and box size dimensions and total atom counts for each composition are listed below in Table 2.5. Note that the number of atoms varies from composition to composition (from 1400 atoms for 33BeF_2 to 2913 for 91.3BeF_2). The snapshots of the EPSR simulation cells show just Be and F atoms (not to relative scale) and also display bars for Be-F with a separation ≤ 2.1 Å.

Table 2.5. Simulation box dimensions from EPSR and total atom counts.

Sample	Box dimension X (Å)	Box dimension Y (Å)	Box dimension Z (Å)	Total atom count
33BeF_2(n)	25.640	25.659	25.664	1400
33BeF_2(X)	25.647	25.674	25.660	1400
50BeF_2	26.506	26.540	26.519	1500
75BeF_2	30.497	30.510	30.478	2200
83.2BeF_2	27.998	27.997	27.952	1685
91.3BeF_2	33.681	33.698	33.716	2913
100BeF_2	28.792	28.800	28.781	1800

In Figure 2.16, an increase in the fluoroberyllate density is observed as the mole fraction of BeF_2 increases, but at the same time, the number of atoms per cell increases with BeF_2 content. From what is visible around the perimeter of the cell, there are fewer dissociated F (dsF) in the mixtures with a higher fraction of BeF_2. The exact quantities of dsF for each mixture are presented in Table 2.8. Note that Be-F bonds are visualized in Figure 2.16 for any Be and F within 2.1 Å from each other. This distance was chosen since it is the cutoff distance used for calculating Be-F CN in Winner et al., where the Be-F partial PDF has nearly decayed to zero [19].

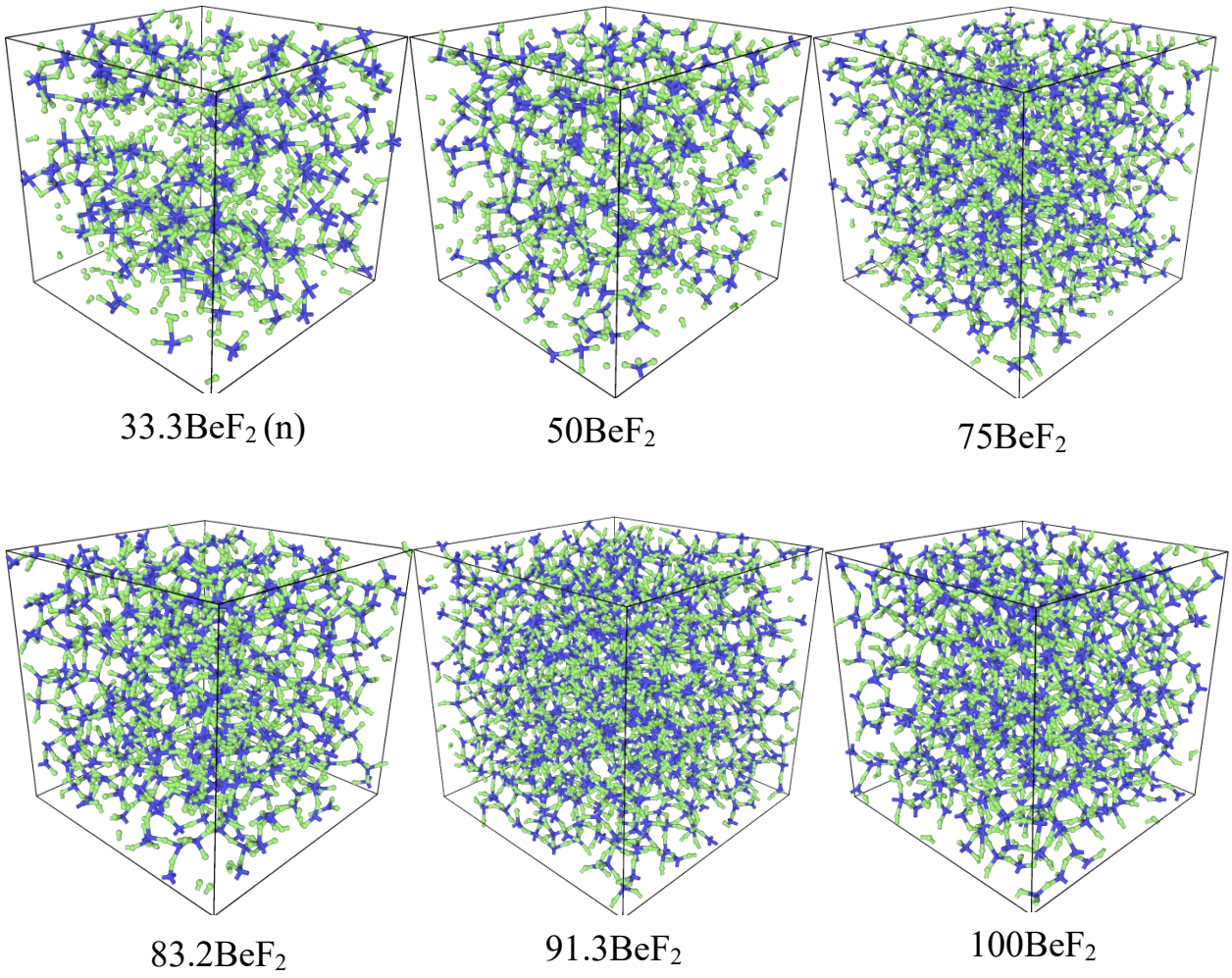

Figure 2.16. Snapshot of atom configurations at 700°C generated from experimental data using EPSR. Li^+ not shown. Be^{2+} = blue, F^- = green. Ionic radii not to scale. Be-F bonds are displayed for Be-F with a cutoff length of 2.1 Å.

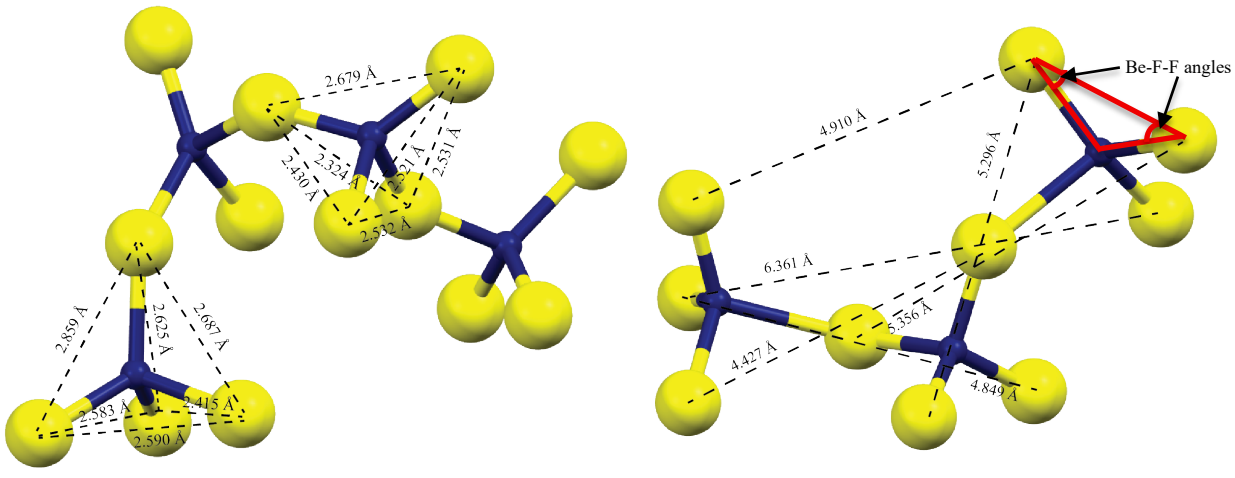

Figure 2.17. Snapshots of Be-F clusters from NNMD (clusters generated by Rajni Chahal [29] and labeled figure generated by D. Nathanael Gardner using Mercury 4.0 [124]) with F-F distances labeled. Be^{2+} = blue, F^- = yellow. Ion sizes not proportional.

2.3.4 Bond angle distribution

Figure 2.18 shows the bond angle distribution from EPSR for all ion triplets across compositions, with Be-F-F and Be-Be-Be shown just for $100BeF_2$. Some plots are at lower resolution for others due to differences in the number of iterations required to converge for EPSR.

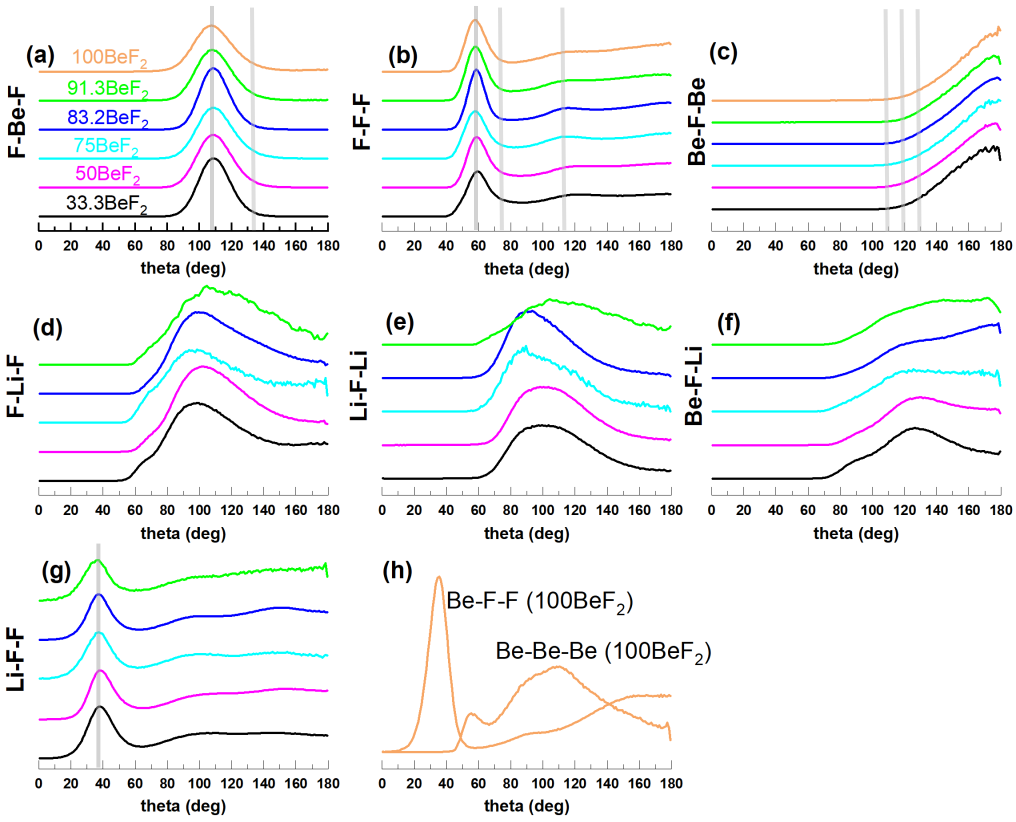

Figure 2.18. Bond angle distributions from EPSR. Vertical gray reference lines added in panels (a), (b), (c), and (g).

The degree of distortion for LiF_4^{3-} and BeF_4^{2-} tetrahedra is quantified in terms of quadratic elongation (QE) and angle variance (AV). QE indicates the degree of distortion in bond lengths from that of ideal polyhedron, in which all lengths would be equal. AV indicates the degree of distortion of bond angles from their ideal values from that of an ideal polyhedron. QE and AV are defined by [125] (applied to solid tetrahedral structure) as:

$$QE = \sum_{i=1}^{4} \frac{\left(\frac{d_i}{d_0}\right)^2}{4} \qquad (Eqn.\,2.1)$$

$$AV = \sum_{i=1}^{6} (\theta_i - \theta_0)^2/(6-1) \qquad (Eqn.\,2.2)$$

where d_0 is the distance between center and vertex (Be-F distance for BeF_4^{2-}, and Li-F distance for LiF_4^{3-}) of a regular tetrahedron of the same volume as the strained tetrahedron defined by the measured lengths and angles, d_i represents the i-th individual bond length in the strained

tetrahedron, θ_0 is the ideal bond angle within a regular tetrahedron (109.47°) and θ_i represents the i-th individual bond angle in the strained tetrahedron. The values of QE and AV for an ideal tetrahedron are unity and zero, respectively. The results are depicted in Figure 2.19.

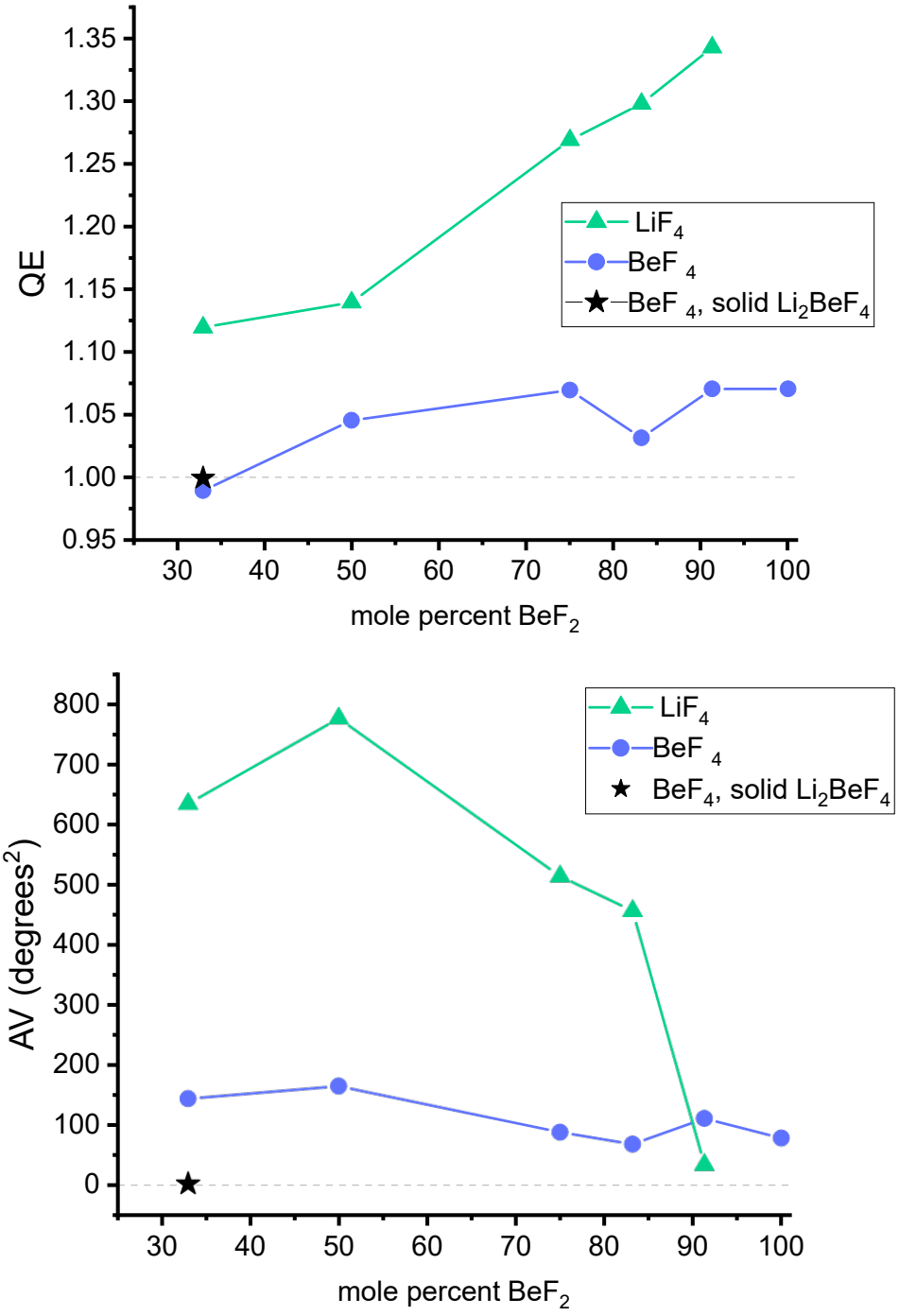

Figure 2.19. Quadratic elongation (QE, top) and angle variance (AV, bottom) of LiF_4 and BeF_4 tetrahedron as a function of mole fraction BeF_2. QE values have been calculated using the average Be-F and Li-F bond-lengths within the BeF_4 and LiF_4 tetrahedral units, and AV have been calculated using the F-Be-F (intra- BeF_4 tetrahedral) and F-Li-F (intra- LiF_4 tetrahedral) bond angle distributions. Values for solid Li2BeF4 calculated using data from [104], [126], [127].

QE results showing values close to one suggest the presence and thus stability of regular BeF_4^{2-} tetrahedral units. As the amount of BeF_2 content increases, the degree of distortion increases for LiF_4^{3-} tetrahedral units (increasing by about 0.25 QE units across the studied compositions), but QE values for BeF_4^{2-} tetrahedral units change by only ~0.05 QE units across compositions.

Considering both QE and AV, LiF_4^{3-} tetrahedra show a higher degree of distortion (with higher QE values and with an average AV of ~480) compared to BeF_4^{2-} tetrahedra over the studied compositional range. AV of LiF_4^{3-} tetrahedra show a continuous decrease starting at $50BeF_2$, reaching a minimum at the highest concentration BeF_2 mixture studied ($91.3BeF_2$). The LiF_4^{3-} AV at $91.3BeF_2$ is around the same degree of distortion as BeF_4^{2-} tetrahedral units at that composition. That is, LiF_4^{3-} tetrahedra have maximally elongated Li-F bonds but minimally distorted F-Li-F bond angles in $91.3BeF_2$, whereas BeF_4^{2-} tetrahedra are consistently less distorted (than LiF_4^{3-}) across all compositions, with a local minimum degree of tetrahedral distortion in $83.2BeF_2$. Figure 2.20 shows AV vs QE for both LiF_4^{3-} and BeF_4^{2-}, with LiF_4^{3-} angular vs bond deformation showing a roughly linear correlation ($R^2 = 0.731$), with QE decreasing as AV increases. Robinson et al. calculated the opposite trend, observing a linear increase in QE vs AV for solid tetrahedra in silicates and aluminosilicates [125]. BeF_4^{2-} deformation shows no discernable trend in angular vs bond deformation in the EPSR models of the compositions (Figure 2.20).

Figure 2.19 includes the QE and AV of Be-F bond lengths and F-Be-F bond angles for the BeF_4 tetrahedra in solid Li_2BeF_4. Data were taken from three different studies: Seiler 1993 (-192°C, QE = 1.000, AV = 2.26) [104], Burns & Gordon 1966 (20°C, QE = 1.000, AV = 2.62) [126], and Collins et al. 1983 (20°C, QE = 1.000, AV = 2.31) [127]. Solid data show minimal angular variance compared to the liquid, but both solid and liquid show near-unity QE for BeF_4 tetrahedra. Specifically, for BeF_4^{2-} tetrahedra in liquid $33.3BeF_2$, QE = 0.99 and AV = 143.87.

Panel (a) of the bond angle distribution Figure 2.18 shows a peak near 109.5° for the F-Be-F angle for all compositions indicating generally regular tetrahedral units. At $100BeF_2$, the peak is centered around 107.5°, but as BeF_2 fraction decreases, the peak shifts toward 109° and is more sharply defined, with less of a tail (less broad). This indicates more consistently structured tetrahedra at lower BeF_2 concentrations. In addition, QE is lower at lower BeF_2 concentrations, but AV is not. We note that AV is calculated using static bond angles, and a closer comparison would require calculation of the error in AV and QE values from fluctuations in the dynamic structure.

The AV calculated from the F-Be-F angle (Figure 2.19) shows slightly higher variation from regular tetrahedrality (109.5° angles) at lower BeF_2 concentrations. Thus, the monomers are more uniform (more sharply defined F-Be-F angle distribution) but are not perfect tetrahedra if their F-Be-F angles are considered. These small distortions might be due to the presence of Li coordinates. The broader F-Be-F angle distribution at high BeF_2 fractions suggests geometric strain across inter-connected tetrahedra.

Looking at the F-F-F angle distribution panel (b) in Figure 2.18, we see two primary features: a peak around 60° and a shoulder around 110-115°. As BeF_2 content decreases, the peak at 60° shifts to about 62° at $33.3BeF_2$ and the peak becomes less defined.

Most bonds containing Li (panels (d), (e), and (f) in Figure 2.18) are broad and increase in prominence with increasing LiF content. The broad peaks are consistent with the understanding that Li is not strongly coordinated. In panel (g), the Li-F-F angle (around 38°) shows a clear peak which increases as the fraction of BeF_2 decreases, increasing from about 36.5° to 38.5° from $95BeF_2$ to $33.3BeF_2$. The Li-F-F angle depends on the Li coordination by F as well as how constrained the available fluorine is by surrounding Be-F coordinates. The availability of more F at lower BeF_2 concentrations (as seen by the higher Li-F CN at lower BeF_2 concentrations in Figure 2.21) supports the picture of more open Li-F-F angles.

The Be-F-F angle distribution is shown for $100BeF_2$ in panel (h) of Figure 2.18. It shows three features: a peak around 35°, a shoulder around 90°, and a broad plateau around 150°-180°. The sharpest and strongest peak at the acute angle of 35° would be indicative of a Be-F-F within a tetrahedron. The F-Be-F angle is around 109.5°, and thus in an isosceles triangle defined by F-Be-F, the Be-F-F angles would be 35.25°. The sharply defined peak suggests that this is a consistent and repeating unit within the structure. Corner sharing of tetrahedra would mean more Be-F-F angles of 35°, normalized to the number of F in the system. The sharpness of the peak could be indicative of more structural regularity, enforced by the presence of corner-sharing tetrahedra. We can examine the symmetry of the 35° peak to further explore indication of corner-sharing. Where a symmetric peak would indicate homogeneous connectivity or individual tetrahedra, a skewed left peak might suggest tighter angles due to edge-sharing or ring formation, and a skewed right peak might suggest more non-bridging fluorides and greater disorder. The skewness of the peak is calculated to be approximately +1.3 (skewed right, quantified in Figure 6.7), meaning the peak rises quickly at lower angles and tapers with a tail stretching toward higher angles (i.e., there are more lower angles than high angles, but with a longer tail of high angles). This is consistent with the lack of low Be-F-Be angles, discussed in Section 2.4.1.

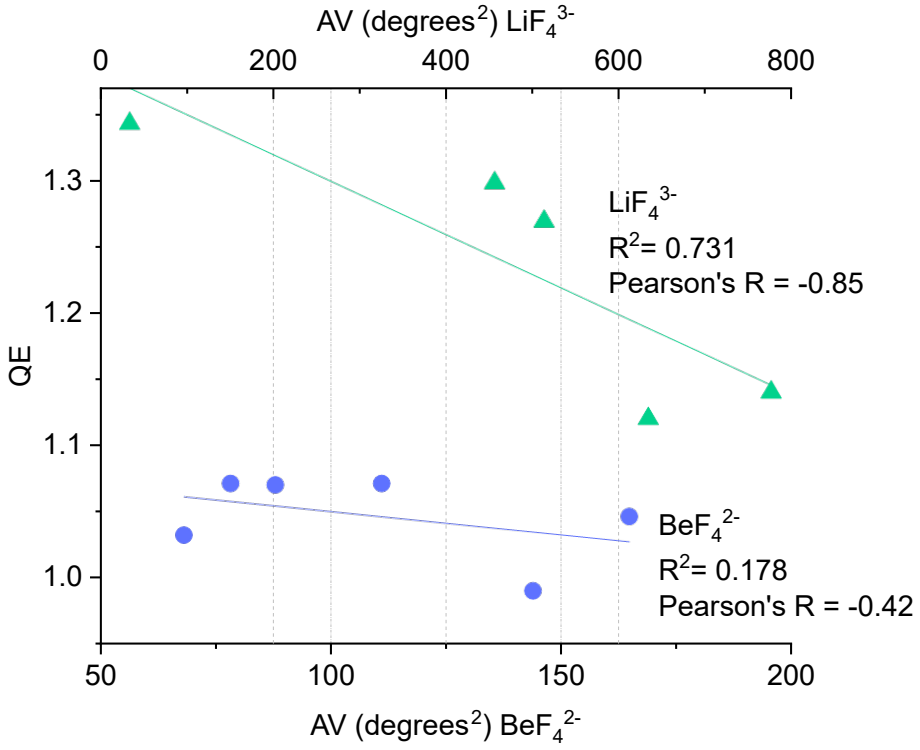

Figure 2.20. QE vs AV for LiF_4^{3-} and BeF_4^{2-}, from EPSR model generated from neutron data. Linear fits shown for each, labeled with R^2 and Pearson's R.

2.3.5 Coordination number

The nominal CN of Be by F is four, given its regular tetrahedrality and coordination environment in the solid state [99], [104], [126], [128], [129]. Vaslow "least squares" method entails fitting a function to the scattering intensity which is a summation for all ion pairs and includes a parameter equivalent to the coordination number of the ion pair.

To estimate Be-F CN from neutron scattering data, a skewed Gaussian was fit to the first peak (which is nearly exclusively representative of Be-F according to modelling) which is then unweighted for neutron scattering lengths and integrated, following the methods described in [29]. To compare across models and experiments, skewed Gaussians were also fit to EPSR and NNMD partial pair distribution functions (g(r)) to provide the CNs for Be-F, Li-F, and F-F, presented in Table 2.6.

Trends show that the Be-F CN is around 3.8-4.0, largely independently of temperature and composition, although this is discussed further in Section 2.4. The Li-F CN is more variable, ranging from around 3.8 to almost 5. At 700°C, the Li-F CN generally decreases with increasing BeF_2 content. This suggests greater F^- availability at lower BeF_2 fractions, consistent with the understanding of less network formation. F-F coordination shows wider scatter than Be-F and Li-F CN across both temperature and composition. At 700°C, F-F CN is generally highest at intermediate BeF_2 concentrations (50-75 mol%), where CNs approach 12. Note however, that it is difficult to directly compare across compositions because of the differences in technique for calculating CN and modelling the salt, thus, conclusions drawn from these trends are tentative. Ab initio and classical simulations tend to report higher CNs for F-F compared to experimental techniques.

Table 2.6. Coordination number of Be by F, Li by F, and F by F in LiF-BeF_2 mixtures. For modeling techniques, CN is calculated by integration of the first peak of the Be-F partial PDF. For experimental techniques, the methods for calculating CN are discussed in [29]. n/a means not available or existent. r_{min} is the cutoff distance for the peak integration in the calculation of the CN, where relevant.

Composition	Study	Technique	Temp (˚C)	r_{min} (Å) Be-F	Be-F CN	r_{min} (Å) Li-F	Li-F CN	r_{min} (Å) F-F	F-F CN
33.3BeF_2	Winner 2021	AIMD	700	1.92	3.9	g(r) min	4.4	g(r) min	12
33.3BeF_2	Winner 2021	AIMD	700	2.14	4.0	n/a	n/a	n/a	n/a
33.3BeF_2	Nam 2014	FPMD	700	g(r) min	4.0	g(r) min	4.7	g(r) min	12
33.3BeF_2	Vaslow 1973	X-ray	555	Least sq	4.0(3)	Least sq	4(1)	Least sq	8(2)
33.3BeF_2	Vaslow 1973	X-ray	750	Least sq	4.0(5)	Least sq	4(1)	Least sq	8(2)
33.3BeF_2	Salanne 2006	PIM	600	g(r) min	4.0(1)	g(r) min	4.0(7)	g(r) min	11.3
33.3BeF_2	Baral 2021	AIMD	727	1.80	3.79	2.80	4.10	n/a	n/a
33.3BeF_2	Baral 2021	AIMD	577	1.80	3.94	2.80	4.30	n/a	n/a
33.3BeF_2	Baral 2021	AIMD	727	2.40	3.90	3.40	4.96	n/a	n/a
33.3BeF_2	Dai 2016	AIMD	600	2.1	4	n/a	n/a	n/a	n/a
33.3BeF_2	Wang 2022	AIMD	500	g(r) min	4.0	g(r) min	4.4	g(r) min	12.2
33.3BeF_2	Wang 2022	AIMD	600	g(r) min	4.0	g(r) min	4.4	g(r) min	12.3
33.3BeF_2	Wang 2022	AIMD	700	g(r) min	4.0	g(r) min	4.4	g(r) min	12.4
33.3BeF_2	Wang 2022	AIMD	800	g(r) min	4.0	g(r) min	4.3	g(r) min	12.1
33.3BeF_2	Fayfar 2024	AIMD	700	2.35	3.99(5)	2.75	4.52(8)	n/a	n/a
33.3BeF_2	Fayfar 2024	NNMD	700	2.35	3.97(5)	2.75	4.50(8)	n/a	n/a
33.3BeF_2	Fayfar 2024	Neutron	700	2.35	3.67(15)	n/a	n/a	n/a	n/a
33.3BeF_2	Fayfar 2024	Neutron	550	2.35	3.73(15)	n/a	n/a	n/a	n/a
33.3BeF_2	Fayfar 2024	AIMD	510	2.35	4.00(5)	2.75	4.63(8)	n/a	n/a
33.3BeF_2	Fayfar 2024	NNMD	510	2.35	4.00(5)	2.75	4.66(8)	n/a	n/a
33.3BeF_2	This study	Neutron	700	2.35	3.56	n/a	n/a	n/a	n/a
33.3BeF_2	This study	NNMD	700	2.35	3.977	2.75	4.495	4.0	11.748

46

$33.3BeF_2$	This study	EPSR (n)	700	2.35	4.004	2.75	4.221	4.0	11.269
$33.3BeF_2$	This study	EPSR (X)	510	2.35	3.991	2.75	4.555	4.0	11.391
$46BeF_2$	Salanne 2006	PIM	600	g(r) min	4.0(1)	g(r) min	4.0(7)	n/a	n/a
$50BeF_2$	Salanne 2006	PIM	600	g(r) min	4.0(1)	g(r) min	4.0(7)	n/a	n/a
$50BeF_2$	Vaslow 1973	X-ray	400	Least sq	4.0(3)	Least sq	4(1)	Least sq	8(2)
$50BeF_2$	This study	Neutron	700	2.35	3.610	n/a	n/a	n/a	n/a
$50BeF_2$	This study	EPSR	700	2.35	3.964	2.75	4.165	4.0	11.130
$50BeF_2$	This study	NNMD	700	2.35	3.958	2.75	4.440	4.0	11.587
$75BeF_2$	This study	Neutron	700	2.35	3.570	n/a	n/a	n/a	n/a
$75BeF_2$	This study	EPSR (n)	700	2.35	3.907	2.75	4.226	4.0	11.212
$75BeF_2$	This study	NNMD	700	2.35	3.968	2.75	4.044	4.0	10.409
$83.2BeF_2$	This study	Neutron	700	2.35	3.880	n/a	n/a	n/a	n/a
$83.2BeF_2$	This study	EPSR (n)	700	2.35	3.939	2.75	3.949	4.0	10.773
$83.2BeF_2$	This study	NNMD	700	2.35	3.980	2.75	4.033	4.0	10.900
$91.3BeF_2$	This study	Neutron	700	2.35	3.990	n/a	n/a	n/a	n/a
$91.3BeF_2$	This study	EPSR (n)	700	2.35	3.989	2.75	3.786	4.0	10.803
$91.3BeF_2$	This study	NNMD	700	2.35	3.947	2.75	3.940	4.0	10.907
$100BeF_2$	Vaslow 1973	X-ray	700	Least sq	4.0(3)	n/a	n/a	Least sq	6.0(3)
$100BeF_2$	This study	Neutron	700	2.35	3.930	n/a	n/a	n/a	n/a
$100BeF_2$	This study	EPSR (n)	700	2.35	4.024	n/a	n/a	4.0	10.856
$100BeF_2$	This study	NNMD	700	2.35	3.992	n/a	n/a	4.0	11.257

47

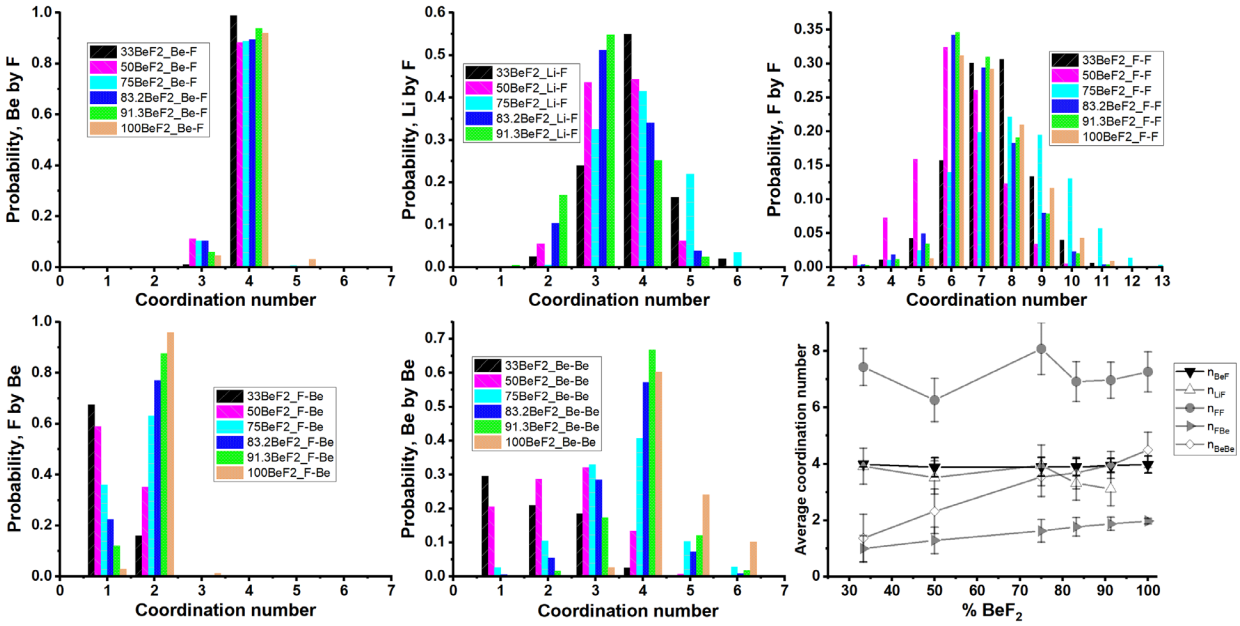

Figure 2.21. Distributions of coordination number for Be, Li, and F atoms in the studied systems. The average coordination numbers around Be, Li and F are shown in the bottom right inset.

Distributions of coordination numbers from EPSR indicate that the values presented in Table 2.6 are experimentally measured or computationally derived *averages*. For example, Be-F coordination is seen to vary from 3 to 5 for the mixtures studied (top left of Figure 2.21). The Be-F CN has a strong peak at 4, indicating that Be is predominantly tetrahedrally coordinated by F. Mixtures with less BeF_2 (e.g. $50BeF_2$) show some lower coordination (CN = 3), with the fraction of CN = 3 decreasing as BeF_2 concentration increases. Overall, the average coordination shown in the bottom right inset shows that the Be-F CN remains approximately 4 across all compositions.

Lithium is coordinated predominantly by 3 to 4 F ions for most compositions. At a higher fraction of BeF_2 ($91.3BeF_2$), the distribution skews toward lower coordination (CN = 3), whereas lower BeF_2 concentration ($33BeF_2$) has higher coordination (CN = 4 to 5). Thus, when more BeF_2 is present, Li has a lower degree of coordination.

The distribution of F-F coordination is broad, ranging primarily from 4 to 11 coordinates, peaking at 6 to 8 depending on the composition. Peak F-F CN does not strictly follow a trend with composition. In $100BeF_2$, there is a sharper cutoff of the distribution; CN < 6 is nearly absent, whereas for the other compositions, there is more of a normal distribution of F-F coordinates. At $x_{BeF2} > 83.2BeF_2$, the F-F CN stabilizes around 7, suggesting that the F network becomes more consistently ordered.

The coordination of F by Be tells us about the formation of Be-F bridges. At lower concentrations of BeF_2, F are more often bonded to one Be. At higher concentrations of BeF_2, it is more probable that F is coordinated by two Be, indicating that more bridges are formed by Be-F-Be linkages. This trend tracks clearly with composition. The bottom right inset shows how F-

Be CN increases roughly linearly from CN = 1 to CN = 2 across the compositions studied.

Be-Be coordination shows an increase in coordination with an increase in BeF_2 concentration. In 33.3BeF_2, a Be typically has a single neighboring Be. In 100BeF_2, a Be has 4 to 5 Be neighbors. This increasing Be-Be coordination suggests growing Be-F-Be network connectivity with increasing BeF_2 concentration. Looking at the slope of this increase, we observe a steep rise in Be-Be CN up to 75BeF_2 (slope of 0.05 CN/mol%), a plateau with less of a slope (0.3 CN/mol%), and then a continued increase (slope of 0.06 CN/mol%). Since Be-Be coordinates are limited by the number of F available to bridge them, once roughly all F are participating in bridging, an increase in the concentration of BeF_2 will not necessarily increase the Be-Be CN.

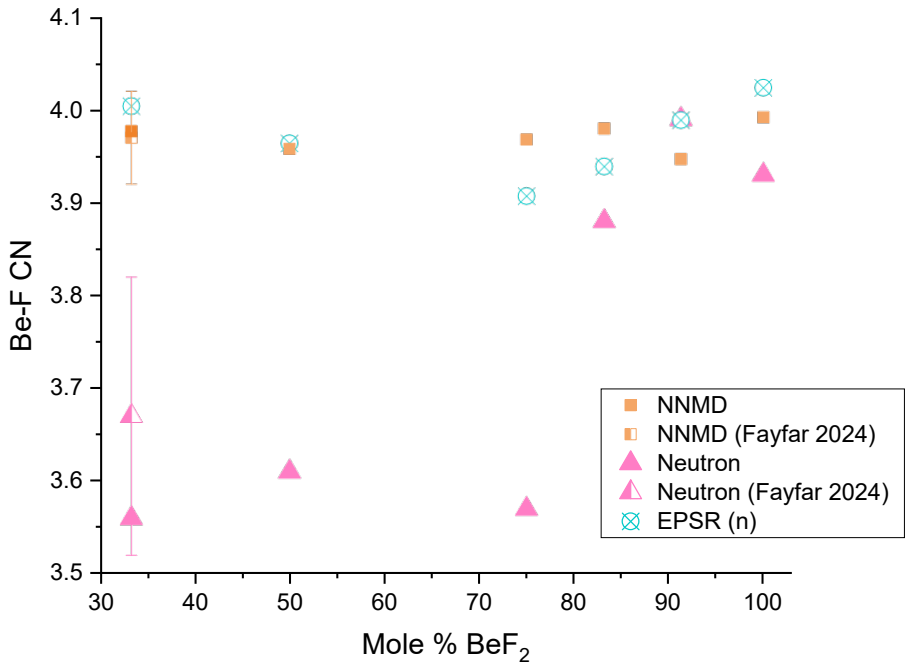

Figure 2.22. Be-F coordination number with composition from NNMD, Neutron scattering, and EPSR of the neutron data, all at 700°C.

Figure 2.22 shows the CN of Be by F from NNMD, neutron scattering data, and EPSR of neutron scattering as a function of composition. The CN for 33.3BeF_2 from Fayfar et al. are shown as a point of comparison, with error bars calculated from the fitting of a skewed Gaussian to the first diffraction peak in the total g(r) [29]. In Figure 2.12 and Figure 2.13 we see that NNMD and EPSR over-calculate the first diffraction peak (the first Be-F peak) which correlates with the higher values for CN reported by NNMD and EPSR compared to neutron data.

2.3.6 Temperature effects

To verify trends in peak position with temperature, we examine the scatter in peak position measurements. At repeated measurements at 700˚C, the range of the data is 0.008 Å on average for Be-F and 0.04 Å on average for F-F (seen in Figure 2.23), but the temperature trends in are generally larger than this scatter. Because of the scatter and variation in number of data points

for each composition (ranging from 25 to 93), the R^2 for each of the linear fits is low. We rely then on Pearson's R to give a sense of the strength of positive or negative correlation of the data. Note also that the scatter in measurements at the same temperature shown in Figure 2.23 is random, not directional, giving greater confidence that trends with temperature are real.

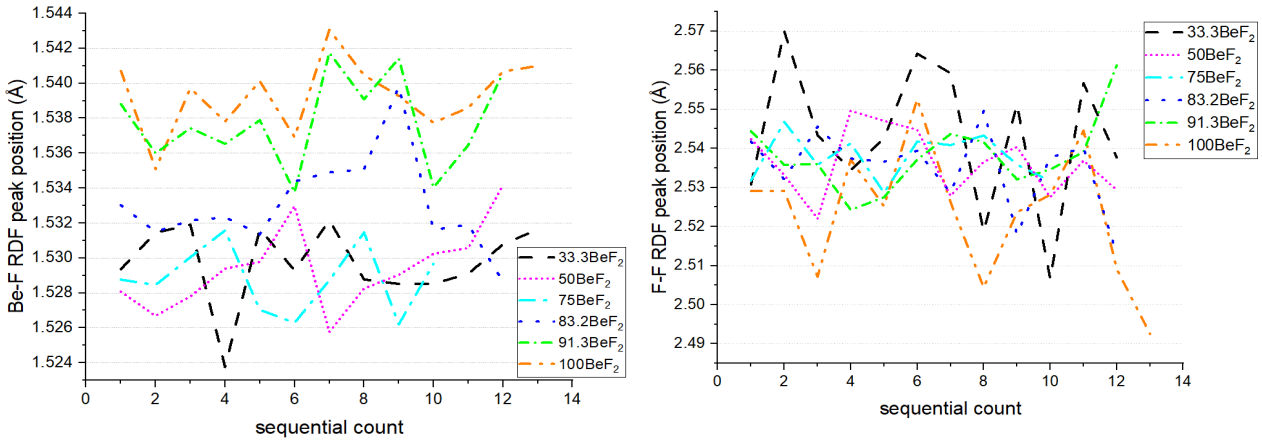

Figure 2.23. Variation across sequential measurements of peak position for Be-F and F-F, extracted from neutron g(r) at 700˚C.

The samples were measured with a 5-minute exposure time at ramp rates ranging from 2-10 °C/min as shown in Table 2.1. Because of this, temperature ranges for each peak position measured during heating range from 10 to 50 °C. This variation in the number of data points for each peak position adds uncertainty to the calculated Pearson's R and slopes of the samples in the liquid and solid states. For future neutron diffraction studies, we suggest selecting a standard heating rate to minimize the variation in temperature ranges represented by each peak position given the measurement (sample exposure) time.

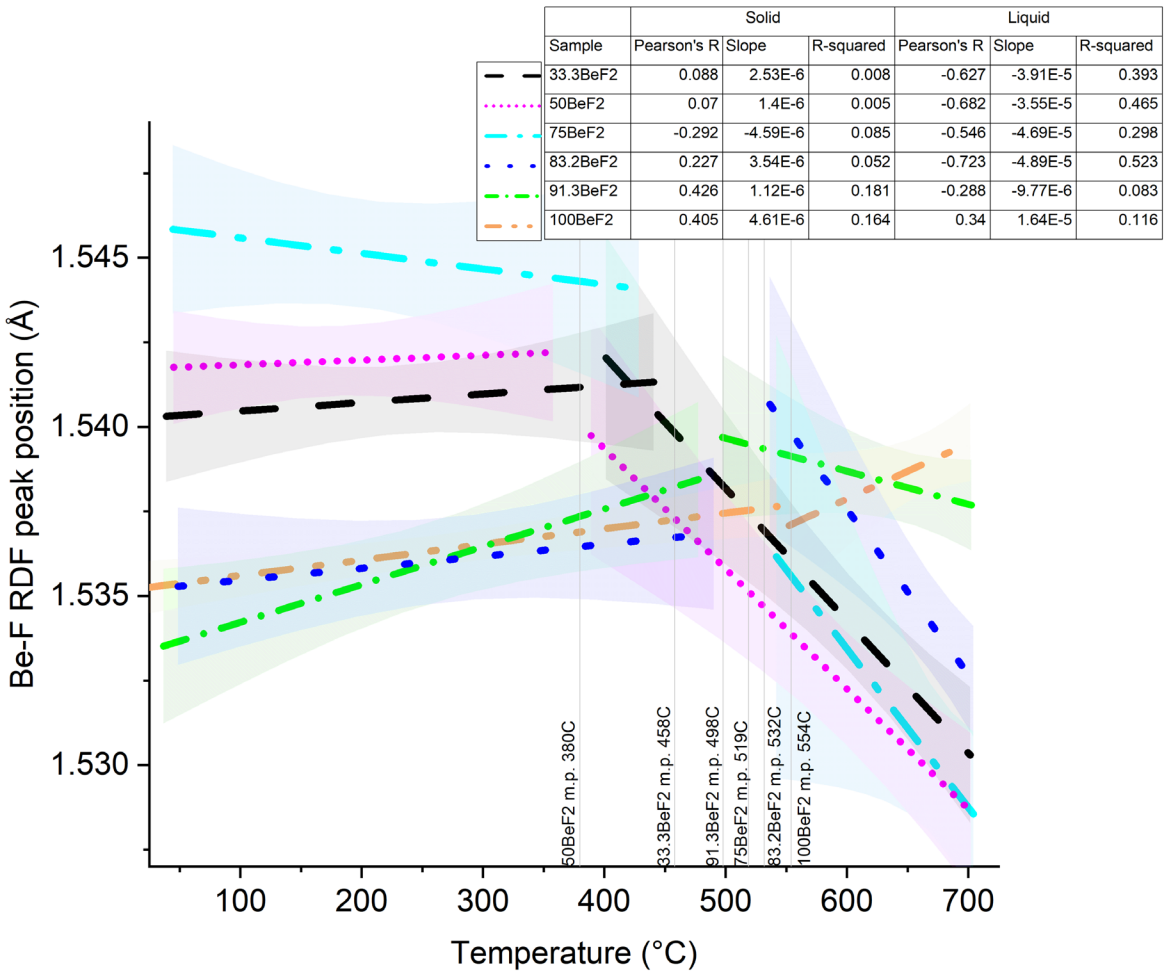

Figure 2.24. Linear fits of first diffraction peak from neutron scattering (Be-F peak position) as a function of temperature. 33.3BeF_2 includes heating and cooling, all other compositions are from heating. 95% confidence interval bands are shown. Melting points are indicated by vertical reference lines (estimated from MSTDB-TC [9], [10].)

Figure 2.24 shows the linear correlation for the Be-F peak position from room temperature to 700˚C. Linear fits were done separately for data below and above the melting point liquidus temperature of each mixture. The first Be-F peak is identified as the first diffraction peak in the experimental PDF around 1.5 Å. From the partial PDF, we know that the primary contributor to this peak is Be-F. At the lower mole percentages of BeF_2 (33%, 50%, 75%) there is a strong negative correlation between peak position and temperature in the liquid; that is, as temperature increases, Be-F distance decreases. At higher mole percentages of BeF_2 (91.3%) the decrease in Be-F distance with temperature is less (Pearson's R of -0.288 compared to an average of -0.650 at the lower BeF_2 compositions). At the highest percentage of BeF_2 (100%), the trend is reversed—Be-F distance slightly increases with increasing temperature.

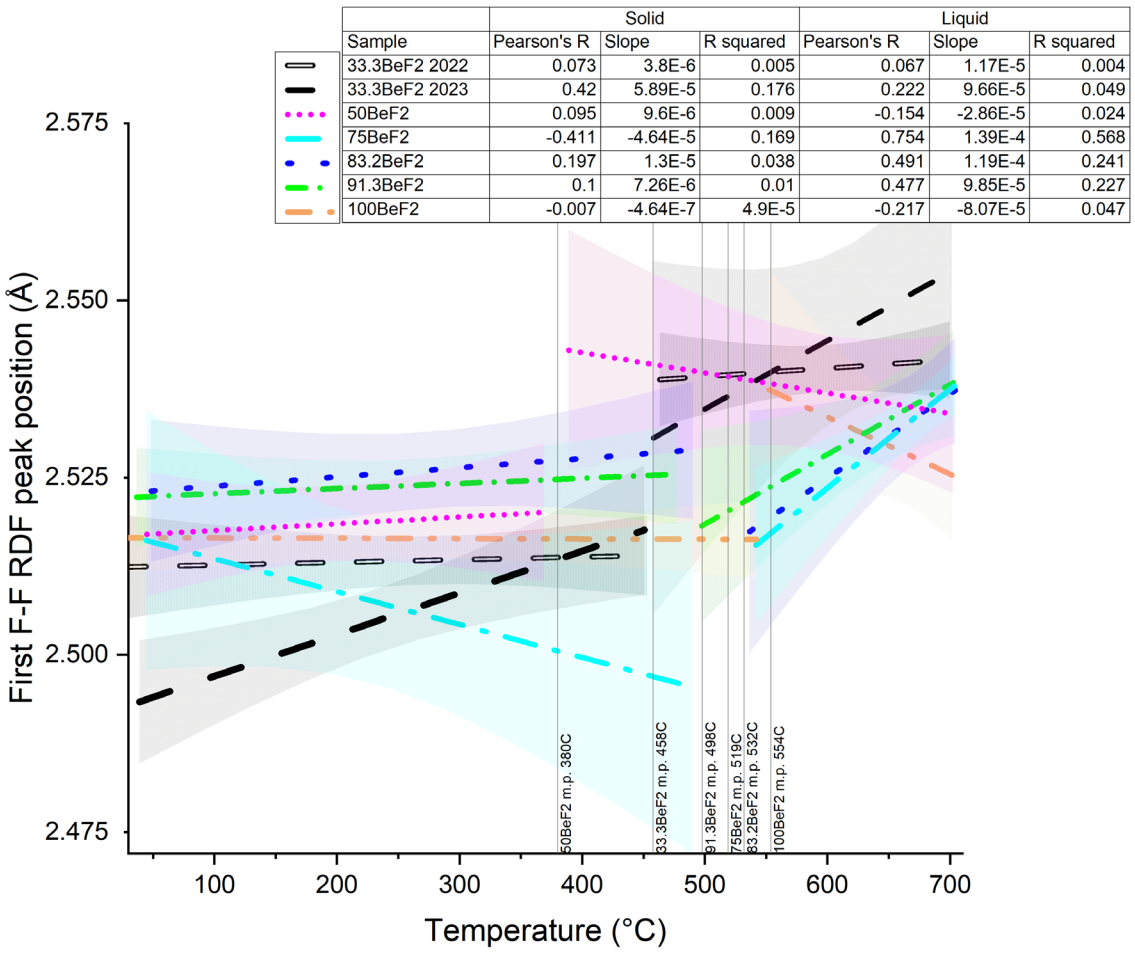

Figure 2.25. Linear fits of second major positive diffraction peak from neutron scattering (first F-F peak) as a function of temperature. 33.3BeF_2 includes heating and cooling, all other compositions are from heating. 95% confidence interval bands are shown. Melting points are indicated by vertical reference lines and are estimated from MSTDB-TC [9], [10].

Similar plots for the first and second F-F peak are shown in Figure 2.25 and Figure 2.26. We call these the F-F peaks because the primary contributor to the experimental peak in the PDF is the F-F pair according to the partial PDFs from NNMD and EPSR. The peak position corresponds to the second major positive diffraction peak in the neutron scattering data, located around 2.5 Å. However, for the first F-F peak, the partial PDFs indicate that there are other contributors to this peak, namely negative Li-F and Be-Li peaks.

In Figure 2.25 in the solid, this peak position is generally constant (near-zero Pearson's R for most compositions), indicating a constant bond length. In the liquid, the F-F peak position increases with temperature with slopes generally an order of magnitude higher than in the solid. This peak position increase is contrary to the first Be-F peak behavior. Potential distances illustrated by this F-F expansion are illustrated in the diagram of a snapshot of a NNMD LiF-BeF_2 cluster in Figure 2.17.

Temperature trends in the peak at ~ 5 Å, also attributed primarily to F-F and called the "second F-F peak", generally increase with temperature in the solid phase according to the Pearson's R but

demonstrate a drop in bond length upon the transition from solid to liquid. In the liquid phase, the behavior varies with higher BeF_2 melts (91.3BeF_2 and 100BeF_2) showing positive trends and mixtures with lower BeF_2 contents showing negative trends. As illustrated in the molten cluster snapshot in Figure 2.17, the F-F distances represented by the second F-F peak around ~ 5 Å can range from being fluorine atoms bonded to adjoining berylliums, fluorine atoms further down an oligomer with certain Be-F angles, and fluorine atoms in adjacent oligomers.

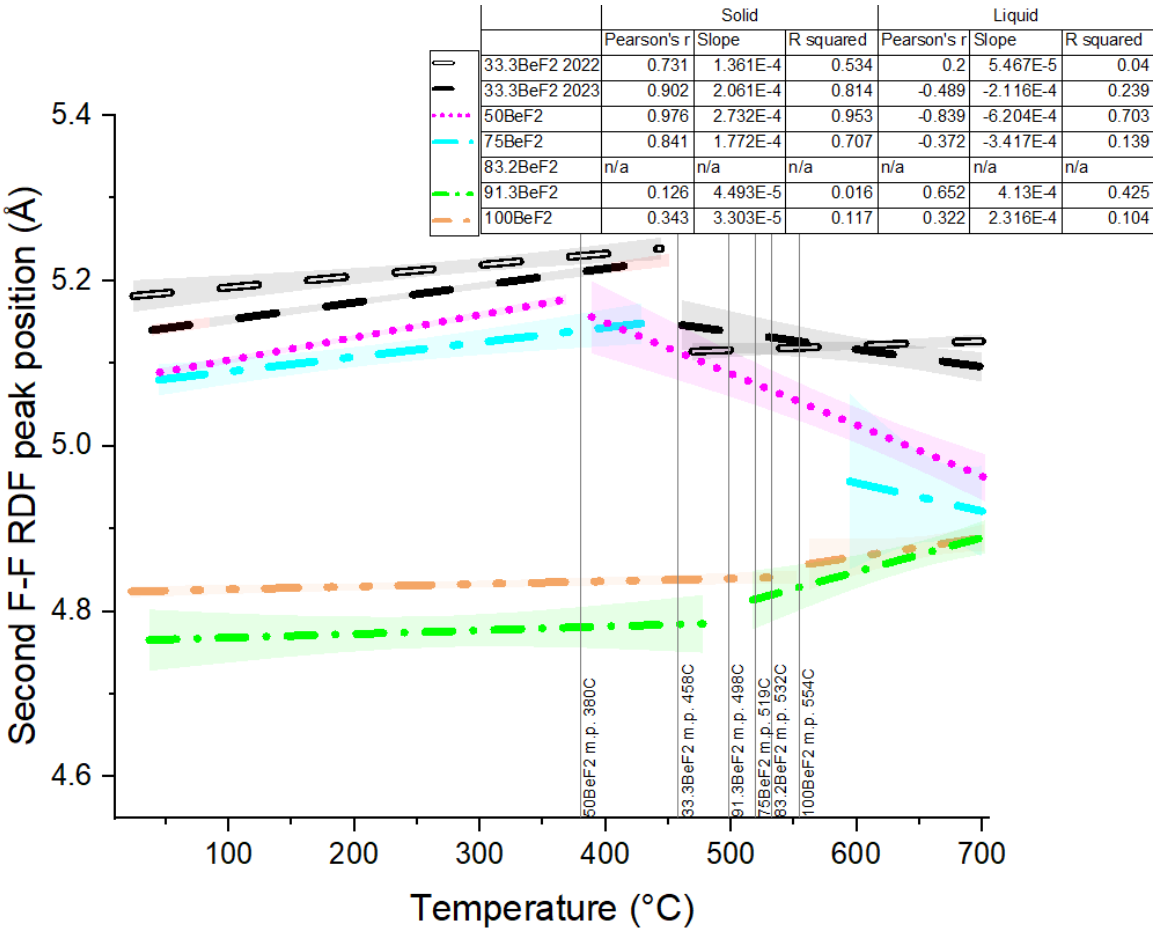

Figure 2.26. Linear fits of diffraction peak around 5 Å from neutron scattering (second F-F peak) as a function of temperature. 33.3BeF_2 includes heating and cooling, all other compositions are from heating. 95% confidence interval bands are shown. Melting points are indicated by vertical reference lines and are estimated from MSTDB-TC [9], [10]. Due to the high ramp rate and difficulties with peak fitting, data for 83.2BeF_2 not shown.

2.3.7 X-ray scattering data

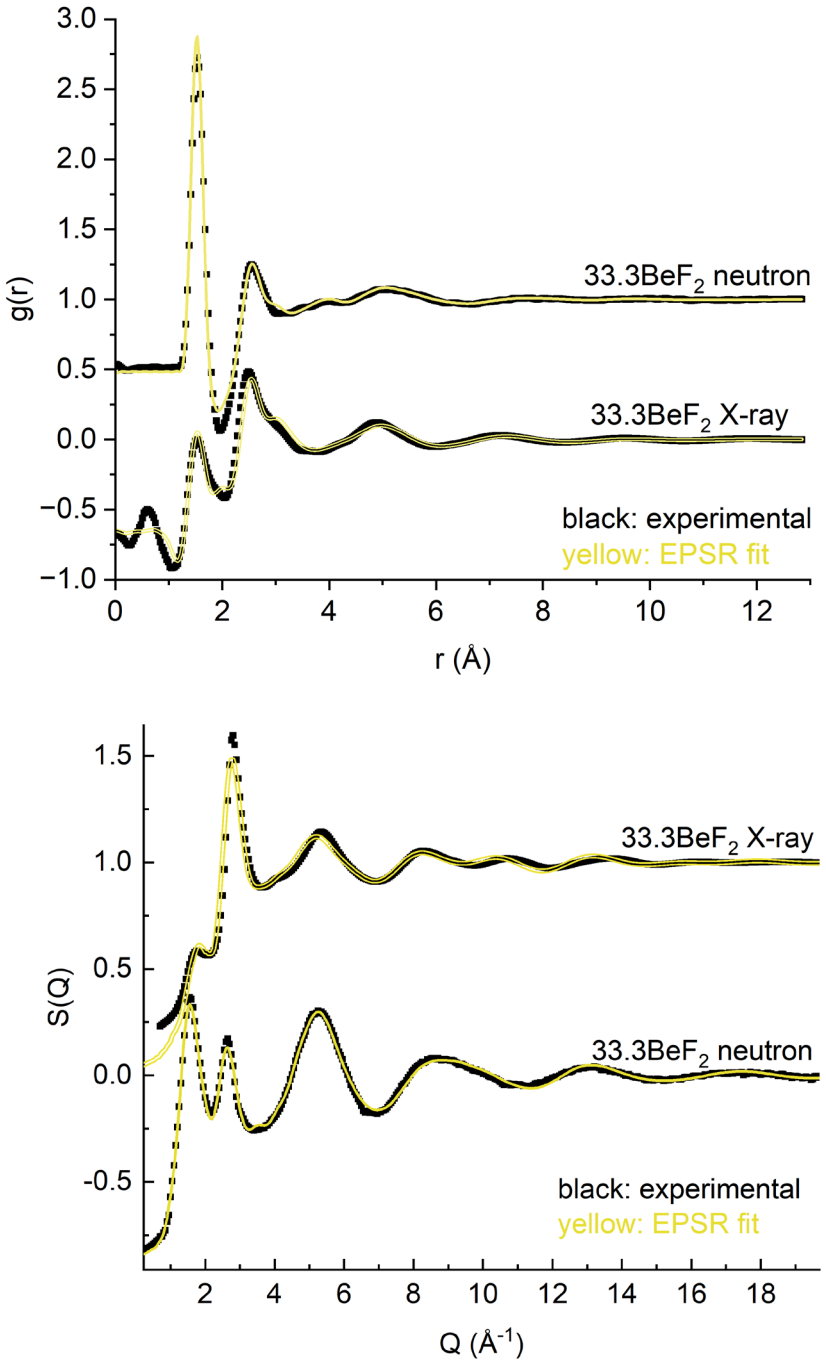

Figure 2.27. Experimental data (black) and EPSR fit (yellow) for neutron and X-ray scattering experiments of 33.3BeF₂. Top: PDF. Bottom: Structure factor. Neutron data at 700°C and X-ray data at 510°C.

Figure 2.27 shows the pair distribution function g(r) and structure factor S(Q) for 33.3BeF₂ using both X-rays and neutrons, offset for clarity. For the PDFs, neutrons have a strong, sharp peak at ~1.5 Å, whereas X-rays show a broader peak of less intensity with a wider shoulder. Neutrons are more sensitive to the dominant contributor to short range order (Be-F). The peak around 2.4-

2.5 Å has a larger shoulder in the X-ray data, likely due to X-rays' higher sensitivity to F. The narrow peaks from the neutron g(r) provide more precise information about bond lengths, particularly for Be-F.

The FSDP around a Q of 2 $Å^{-1}$ is a pronounced positive peak in the neutron data and less intense peak in the S(Q) which does not go above 1. At Q > 10 $Å^{-1}$, X-rays show more frequent, small oscillations, whereas neutrons show roughly two broad peaks from oscillations out to Q = 19 $Å^{-1}$. The more defined oscillations in the X-ray data show greater sensitivity to short- and intermediate-range periodicity, likely from F contributions.

Table 2.7 provides a summary of the first peak positions for each ion pair from the partial PDFs of 33.3BeF_2 calculated from both neutron and X-ray data using EPSR. The peak positions reflect differences in weighting between neutron and X-ray scattering. The differences between Be-F, F-Be, and F-F distances is ≤ -0.02 Å. This gives confidence that EPSR is consistently capturing the Be-F structure of 33.3BeF_2. Li-F, Li-Li, and Li-Be peaks appear at longer distances in the X-ray data (with up to 0.13 Å difference between the techniques). Since Li is light, X-ray scattering is less sensitive to it. In addition, it is understood that Li coordinates are weaker and more disordered due to its lower charge density, further contributing to the possible variation in distances calculated by EPSR.

Table 2.7. Peak position from partial PDFs (generated by EPSR) for 33.3BeF_2(n) at 700°C and 33.3BeF_2(X) at 510°C.

Pair	Neutron peak position (Å)	X-ray peak position (Å)
Li-Li	3.00	3.06
Li-Be	3.06	3.18
Li-F	1.80	1.93
Be-Be	3.02	3.05
Be-F	1.53	1.51
F-F (first)	2.55	2.52
F-F (second)	5.04	5.07
F-Be	1.53	1.51

2.4 Discussion

2.4.1 Excess bridging, energy contributions, and CNCs

By fixing the coordination number to the values calculated experimentally, we can calculate the minimum number of fluoride anions which must participate in bridging (brF_{min}) by the following equation for compositions for which the CN is greater than the total number of F^- available stoichiometrically (totF) (which we refer to as Regime I).

$$Regime\ I: CN - totF = brF_{min} \qquad (Eqn.\ 2.3)$$

Since F may exist as a bridging species, as a terminal F^- (trF) within a monomer or oligomer, or as a dissociated species (dsF), we can express totF as the sum of all possible F^- species. We further distinguish between minimum brF, defined as those which are stoichiometrically dictated by the coordination number of Be (Eqn. 2.3), and excess brF (brF_{ex}), defined as those bridges

which are observed to form despite stoichiometric necessity. The overall F balance is then:

$$totF = dsF + trF + brF_{min} + brF_{ex} \quad (Eqn.\ 2.4)$$

As such, total bridging F^- (brF_{tot}) is defined as:

$$brF_{tot} = brF_{min} + brF_{ex} \quad (Eqn.\ 2.5)$$

From EPSR, we have calculated the Be-F CN and know the fraction of dsF. Additionally, totF is known based on the stoichiometry of each composition. Since any excess bridging frees an F^- which is not required for coordination, the quantity of **brF_{ex} is equivalent to dsF_{ex}**. Similarly, by substituting Eqn. 2.5 into Eqns. 2.3 and 2.4, we can solve for brF_{ex} to find this equivalence. The quantity of trF can be found from the overall F balance (Eqn. 2.4).

For $33.3BeF_2$, the Be-F CN is less than totF, therefore the difference between the two indicates the minimum quantity of dsF (dsF_{min}) rather than the minimum quantity of bridging F^-. We refer to this as Regime II.

$$Regime\ II: CN - totF = dsF_{min} \quad (Eqn.\ 2.6)$$

In Regime II, any brF are always in excess since they are not required to maintain the CN of ~4, therefore $brF_{tot} = brF_{ex}$. Eqn. 2.4 can then be used to find trF. The results of this F balance are presented in Table 2.8.

Table 2.8. F^- balance if Be-F CN from EPSR fit to neutron data is maintained, normalized to beryllium count (i.e., values for F- counts are per Be).

	Sample	totF	CN from EPSR (r_{min} = 2.35 Å)	brF_{min}	dsF_{min}	dsF from EPSR (r_{min} = 1.92 Å)	dsF_{ex}	brF_{ex}	brF_{tot}	trF
II	$33.3BeF_2$	4.00	3.99	0	0.01	0.60	0.59	0.59	0.59	2.82
I	$50BeF_2$	3.00	3.88	0.88	0	0.08	0.08	0.08	0.96	1.97
I	$75BeF_2$	2.33	3.90	1.57	0	0.03	0.03	0.03	1.60	0.69
I	$83.2BeF_2$	2.20	3.89	1.69	0	0.02	0.02	0.02	1.71	0.46
I	$91.3BeF_2$	2.10	3.94	1.84	0	0.13	0.13	0.13	1.97	0.00
I	$100BeF_2$	2.00	3.98	1.98	0	0.04	0.04	0.04	2.02	-0.05
						Adjusted dsF				
I	$91.3BeF_2$	2.10	3.94	1.84	0	0.03	0.03	0.03	1.87	0.20
I	$100BeF_2$	2.00	3.98	1.98	0	0.01	0.01	0.01	1.99	0.00

The F balance results in a zero or small negative number (-0.05) of trF for $91.3BeF_2$ and $100BeF_2$, which is unphysical and indicates an error in the F balance. The difference likely reflects the manner in which bond cutoffs are defined. The Be-F CN from EPSR assume a cutoff distance of 2.35 Å, where the Be-F partial g(r) has decayed to zero. The dsF from EPSR is counted from the average representative structure with Be-F bond lengths set to 1.92 Å. Entities which are not bound are then taken to be dsF, with the count normalized to the number of Be per ESPR cell (which varies from 200 to 913, Table 2.2). It is notable that the $91.3BeF_2$ composition has the largest atom count (2913 atoms) and a slightly larger box size (Table 2.5), as well as a relatively high number of dsF. It is plausible that the dsF count is off because of the defined bond

cutoff length relative to the box size. If the dsF count is adjusted to lower values (0.03 dsF per Be and 0.01 dsF per Be) which might be expected for high BeF2 concentrations, the trF values would be 0.20 F per Be for 91.3BeF_2 and 0.00 F per Be for 100BeF_2 (bottom two rows of Table 2.8).

From the F balance, we see that bridging is not stoichiometrically required in 33.3BeF_2 and yet each Be is connected to approximately 1 Be-F-Be linkage (0.59 brF_{tot} per Be means 1.18 Be-F-Be linkages). Excess bridging is also observed in the 50BeF_2 mixture, although only slightly more than the stoichiometric requirement (brF_{ex} = 0.08 F per Be). All compositions demonstrate bridging in excess of that which is stoichiometrically required to maintain the EPSR CN (brF_{ex} > 0), with excess bridging generally decreasing as BeF_2 concentration increases but total bridging increasing with BeF_2 concentration. From analysis of the CN distribution in Figure 2.21, it seems that the structural threshold where network formation begins to dominate occurs around 75BeF_2, where the Be-Be CN increases to over 3.5 and F-Be to over 1.6 (closer to two than to one).

Bridging decreases the degrees of freedom locally (decreasing configurational entropy), but at a larger scale, bridging enables a greater variety of ionic arrangements (chains, rings, diverse branching structures). In this way, configurational entropy might be increased even when local ordering within oligomers exists. Figure 2.28 shows that the entropy of mixing and configurational entropy calculated by Smith et al. [84] are positive for all mixtures of LiF and BeF_2, with two maxima in configurational entropy at the 33.3BeF_2 and 75BeF_2 compositions. This reasoning explains how we might observe maximal configurational entropy in a moderately networked system (or possibly one with intermediate-range ordering), which we know to exist in 33.3BeF_2 and 75BeF_2.

To elaborate, configurational entropy (calculated by Smith et al. from the mole fractions of LiF, BeF_2, Be_2F_4, and Be_3F_6 species [84]) has two maxima, the first around 33BeF_2 and the second around 75BeF_2 (Figure 2.28). We might expect the first maximum to result from maximal network disruption, with many possible arrangements for monomers or short oligomers. The presence of Li allows for shielding and disordered solvation. At lower fractions of BeF_2, the presence of dissociated species purely would mean lower configurational entropy. The second maximum might be caused by a continuous network of diverse structures. 75BeF_2 is the composition at which we have seen first indication of a nearly continuous network. Between 33BeF_2 and 75BeF_2 we would have a partially polymerized melt, with a high degree of entropy, but not yet a maximum because of the fewer distinct ionic arrangements due to a lesser degree of polymerization. Beyond 75BeF_2, the increasing polymerization would mean less possible structural features and more uniform, long chains, and thus, a decrease in configurational entropy. In an ideal system, the maximum entropy of mixing would occur at the equal molar composition. The maximum is slightly above this point (in a mixture with approximately 55 mol% BeF_2). This is consistent with the understanding that non-idealities in mixing are introduced by complexation caused by BeF_2.

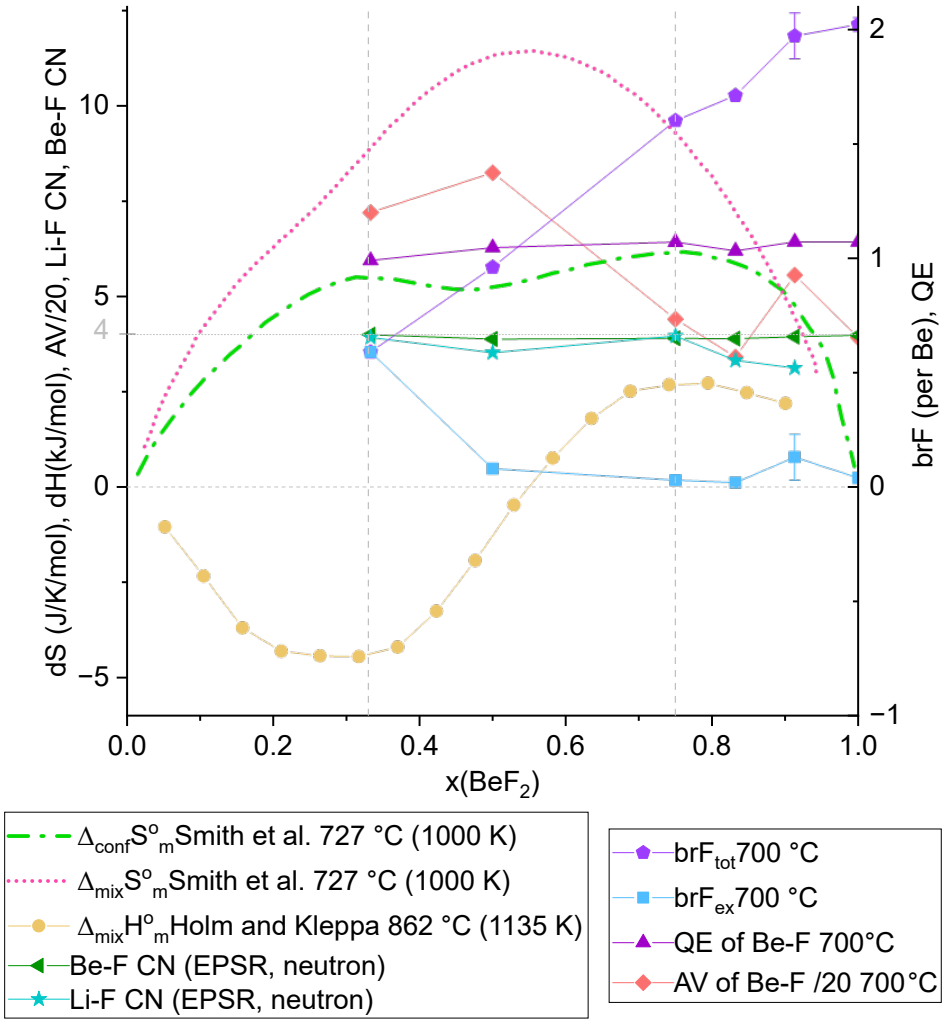

Figure 2.28. Calculated entropy of mixing and configurational entropy from Smith et al. Enthalpy of mixing from Holm and Kleppa. Total and excess bridging from F balance based on EPSR CN and dsF. Quadratic elongation and angle variance of Be-F from EPSR fit to neutron data, provided in Figure 2.19. Reference lines at x(BeF_2) = 0.33 and 0.75.

The enthalpy of mixing measured by Holm and Kleppa [130] is ploted also in Figure 2.28, along with the number of excess and total brF per Be and the quadradic elongation of Be-F from perfect tetrahedral length (all from EPSR). The minimum enthalpy of mixing occurs in mixtures with slightly less BeF_2 than 33BeF_2. The structures formed at this ratio of LiF to BeF_2 must have low strain to provide the most enthalpically stable composition, possibly due to the ability to form a network with minimal Be-Be competing effects. The excess bridging we see in the 33BeF_2 mixture then does not seem to have an enthalpic cost—rather we might guess that enthalpic contributions might also favor the formation of bridges. From Baes' polymer model, the free energy of formation of two separate species from a brF in 33.3BeF_2 at 700°C was calculated to be -18,000 J/mol [25]. The entropy change from the formation of two trF from one brF and one dsF would be expected to be negative, so the enthalpy of breaking a bridge would be even more negative, however. Excess bridging may be driven by the greater degree of electronic stability provided by F bridges by distributing electron density across multiple cations. Or perhaps shared Fs allow for more perfect BeF_4^{2-} tetrahedra with less Be-F bond strain. We observe the degree of total bridging to increase with BeF_2 content but with no appreciable

change in the quadratic elongation of tetrahedra (Figure 2.19), which is consistent with the picture of consistently minimally strained tetrahedra even at compositions with a high degree of complexation. In fact, the angular variation of tetrahedra from the nominal 109.5° F-Be-F angle is lowest at compositions with 75 and greater mol% BeF_2, although it is non-zero for all compositions, indicating tetrahedral distortion (Figure 2.28).

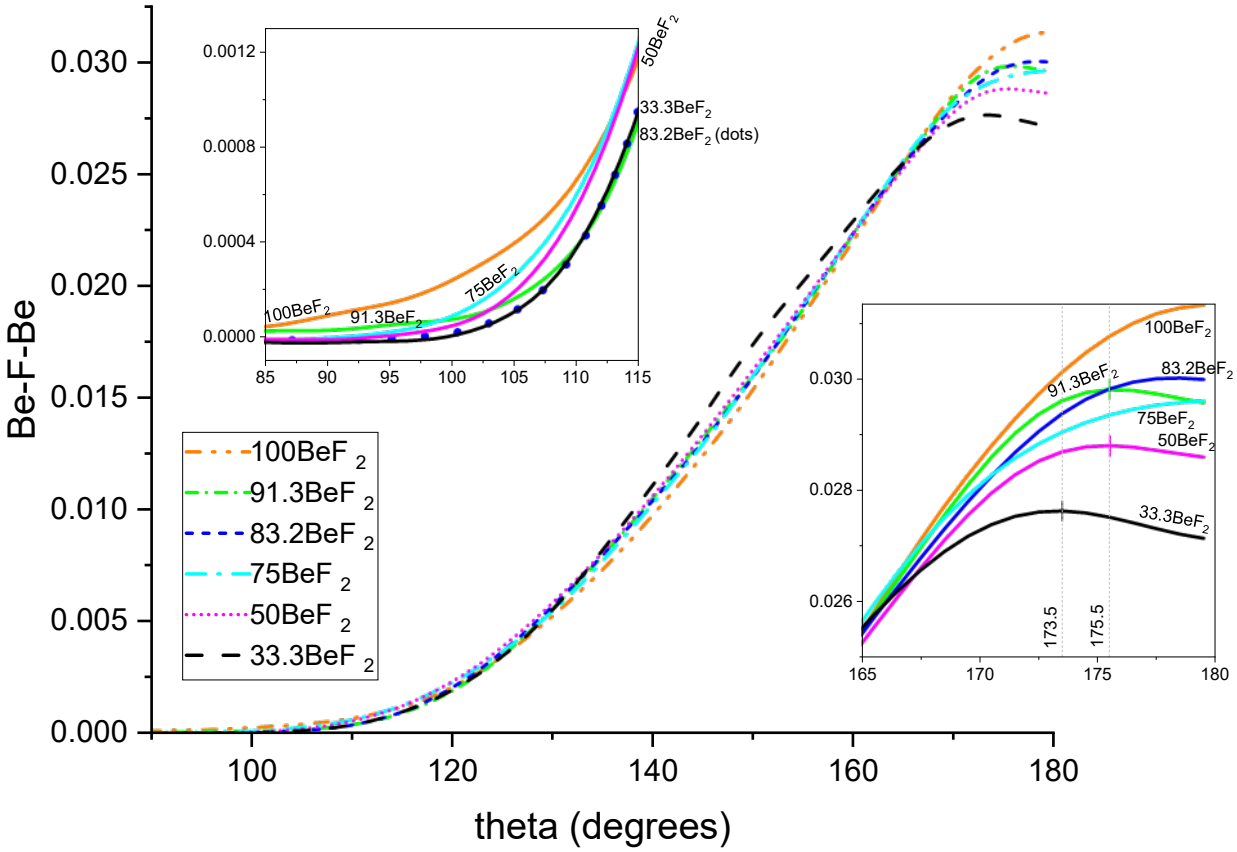

Figure 2.29. Be-F-Be bond angle distribution from EPSR fit to neutron data. Smoothing by FFT (cutoff frequency = 0.1).

Looking at the Be-F-Be bond angle distribution (Figure 2.29), we see that all compositions have a maximum around 173.5° to 180° which suggests that tetrahedra are primarily corner-sharing. $100BeF_2$ has the highest fraction of angles in the 165° to 180° range, as well as the highest fraction of angles in the 85° to 115° range, as seen in the inset figures. Conversely, $33.3BeF_2$ has the lowest distribution of high (165°-180°) and low (85°-115°) angles, and its distribution is higher than the other compositions at mid-range angles (from 140° to 160°). Lower Be-F-Be angles would likely be indicative of edge-sharing tetrahedra (which share two Fs).

Winner et al. found that Be-F-Be was purely corner sharing (CNC = 1) in $33.3BeF_2$ at 700°C [19]. From their simulated bond angle distribution, they saw a broad peak in the Be-F-Be angle around 30° and a primary peak around 125° [19]. The Be-F-Be distributions from AIMD and NNMD in Fayfar et al. are also noticeably different compared to the distribution of EPSR (Figure 2.30). The EPSR angle distributions continuously increase to a maximum around 180°, whereas the AIMD/NNMD distributions go to zero at 180°. NNMD has a slightly higher fraction

of higher bond angles (140°-180°) compared to AIMD, and NNMD also shows a larger tail of low-angle bonds (70°-100°) compared to AIMD. Both AIMD and NNMD show a small fraction of low angles (80°-105°), whereas EPSR indicates nearly no angles in this region.

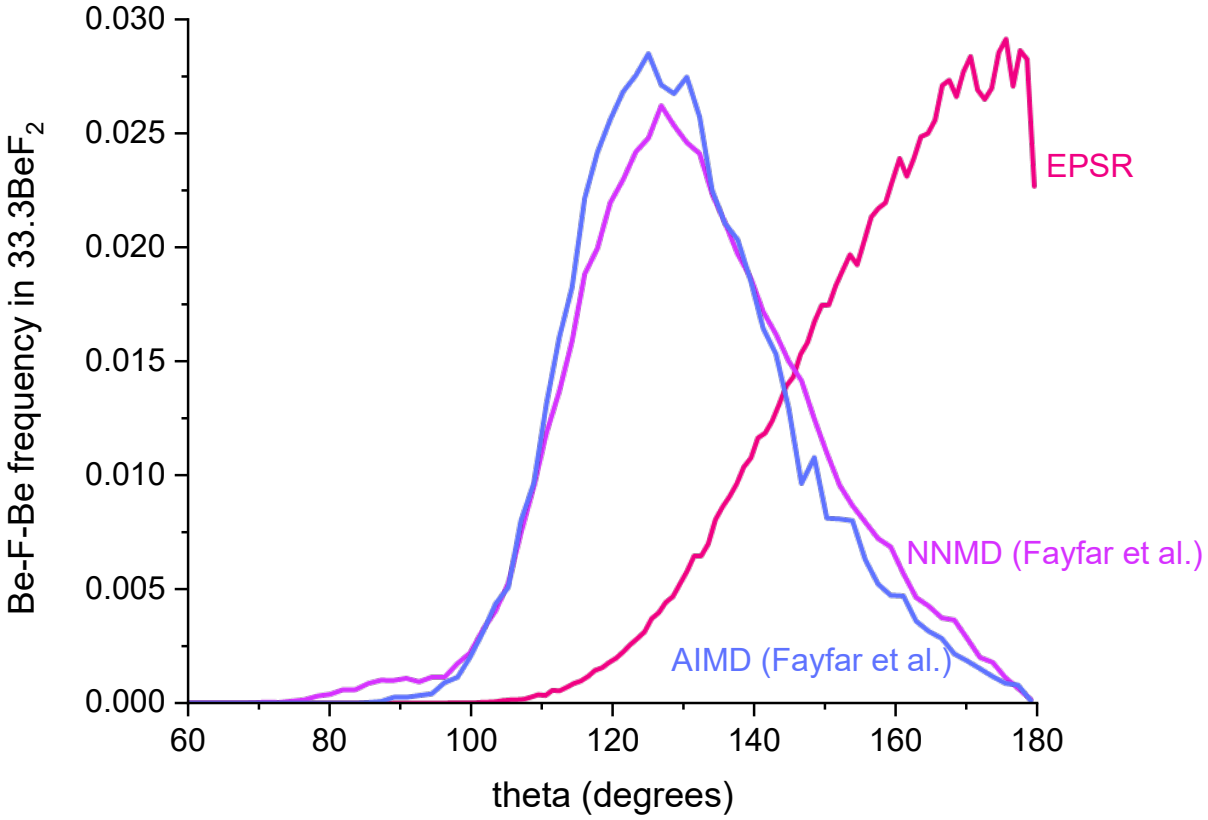

Figure 2.30. Be-F-Be bond angle distribution for 33.3BeF_2 at 700°C from AIMD and NNMD (Fayfar et al. 2024) and EPSR (fit to neutron data). Normalized such that all distributions integrate to one.

Overall, the MD simulations indicate that the Be-F-Be angles are approximately normally distributed around 125°. This suggests that the angles between corner-sharing tetrahedra fluctuate slightly around a nominal bond angle of 125°, with fluctuations likely due to the temperature of the system. The empirical distribution contains a plateaued tail from 70° to 100°. This angle range might be representative of edge-sharing tetrahedra or more complicated oligomeric structures. EPSR indicates that Be-F-Be angles are predominantly ~180°, meaning that the Be centers of adjoining tetrahedra are linear with their bridging F. The nominal Be-F-Be angles of 125° (MD) or 180° (EPSR) are both representative of corner-sharing tetrahedra. An example of a Be-F-Be angle in a corner-sharing $Be_2F_7^{3-}$ dimer generated by NNMD is shown in Figure 2.31. We can envision small fluctuations around the 110° angle at high temperature, without the possibility of large fluctuations or smaller corner-sharing Be-F-Be angles due to steric hindrances. For the BeF_4^{2-} tetrahedra to be edge-sharing (for two CNCs), the Be-F-Be angles would have to be acute. EPSR calculates nearly no Be-F-Be angles below 90°, but the fraction of angles < 90° is generally higher in the BeF_2-rich mixtures (91.3 and 100BeF_2), as seen in Figure 2.29.

In order for $100BeF_2$ to maintain a Be-F CN of 4, a fully networked Be-F system is required. That is, all F must be shared. Pure corner-sharing is stoichiometrically possible as long as all F are shared, but this is complicated by boundary effects, the degree of cross-linking, and the distribution of CNs. From Table 2.8, to maintain the CN from EPSR for $100BeF_2$, 3.96 Be-F-Be links per tetrahedron are required. That is, nearly all F are shared by two Be, with the remainder of available F (0.01 to 0.04/Be) existing as dissociated species. Baes' geometric model suggests that corner-sharing networks may not provide enough bridging to accommodate the fixed Be-F CN of 4 and includes edge sharing in high-BeF_2 mixtures due to the constraints of finite, linear Be-F chains [25]. Baes calculated an increase in edge-sharing species around $50BeF_2$. Edge-sharing was observed to dominate over corner-sharing for oligomers of nBe > 1 in mixtures with 60-$80BeF_2$.

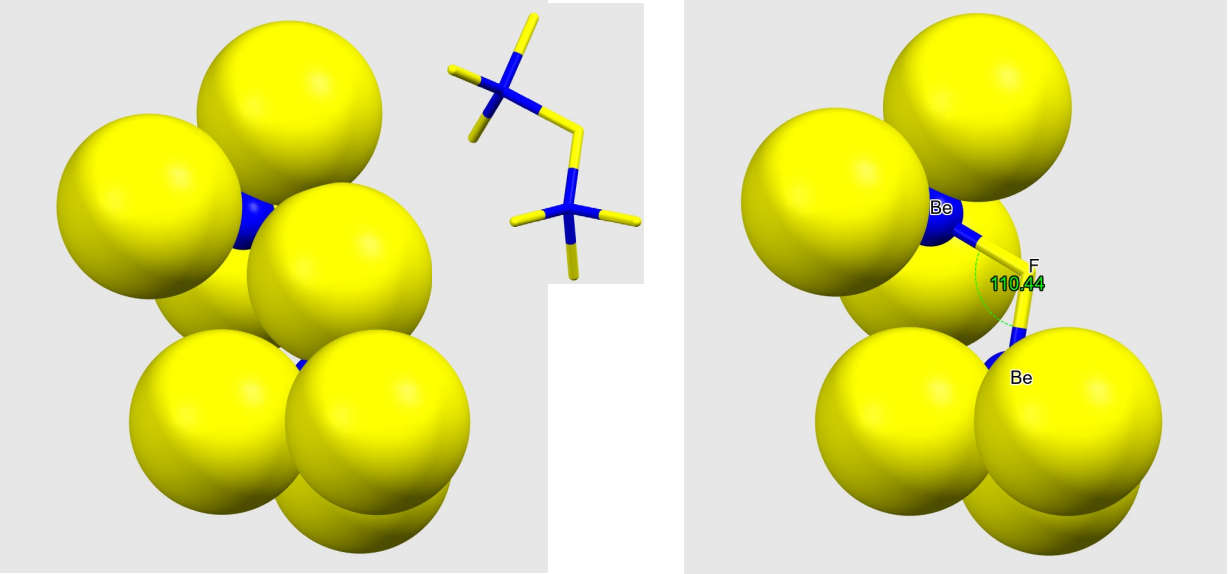

Figure 2.31. $Be_2F_7^{3-}$ dimer from NNMD [29] with Be^{2+} and F^- scaled by their ionic radii. Be^{2+} (blue, CN = 4) radius = 0.27 Å. F^- (yellow, CN = 2) radius = 1.285 Å. Center inset shows wire frame model. Right structure has the brF hidden to show Be-F-Be bond angle of 110.44°. Visualization using Mercury 4.0 [124] and scaling of ionic radii from [131], [132].

The differences in the Be-F-Be bond angle distributions give greater insight into the differences in the structures produced by EPSR and NNMD. Figure 2.32 shows snapshots of visualizations of Be-F bonds with a cutoff of 2.35 Å (no particles displayed). As a reference in comparing the cell volumes and particle counts, there are 12.11 $Å^3$/particle for the NNMD cell (728 particles with cell of 8818 $Å^3$ volume) and 12.06 $Å^3$/particle for the EPSR cell (1400 particles with cell of 16884 $Å^3$ volume). Overall, MD models and EPSR, despite showing structural similarities in the PDFs for each composition (Figure 2.12 and Figure 2.13), display differences in CNCs and CN distribution. Table 2.9 compares the structural features related to bridging and CNC in the two models.

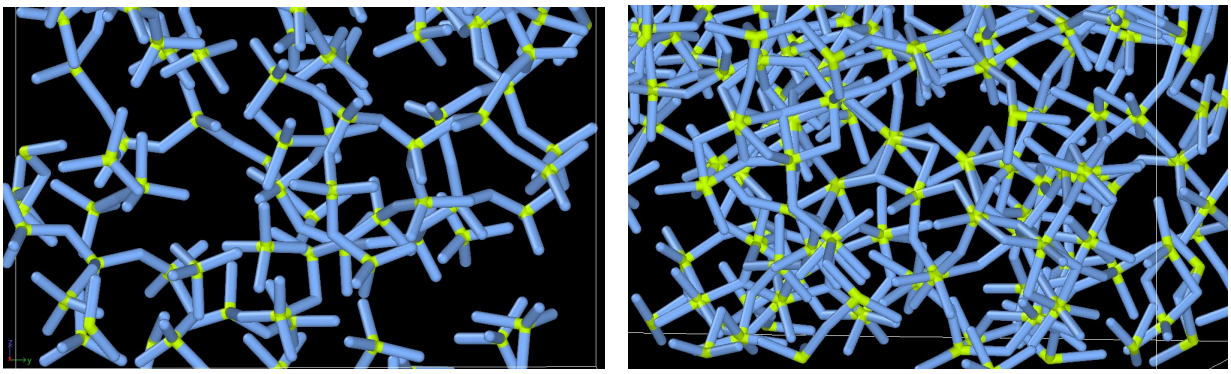

Figure 2.32. Snapshots of Be-F bonds in 33.3BeF_2 from NNMD (left) and EPSR fit to neutron data (right). Bonds are defined by a cutoff distance of 2.35 Å. Both systems at 700°C.

Table 2.9. Comparing bridging and CNC in NNMD and EPSR models.

NNMD	EPSR
Be-F CN more consistently near 4 for the compositions studied, particularly for higher BeF_2 compositions (Table 2.6)	Distribution of Be-F CN (from 3 to 5) (Figure 2.21Figure 2.18), with wider range of average Be-F CNs across the compositional space and some average Be-F CN values > 4 (Table 2.6)
Some acute Be-F-Be angles (Figure 2.18, Figure 2.30)	All Be-F-Be angles > 90°, suggesting a purely corner-sharing network (Figure 2.18, Figure 2.30)
Poor fit in the 2.5 Å region of the total PDF, possibly due to the primary F-F distance being too large (left side of the 2.5 Å peak is undercalculated) (Figure 2.12)	Poor fit in the 3 Å region of the total PDF, possibly due to the primary Be-Be distance being too large (region just before the 3 Å peak is undercalculated) (Figure 2.13)

Looking at the F-F CN in Table 2.6, MD simulations consistently calculate a higher F-F CN (average of 12.20 across all compositions for the 12 entries) than EPSR (average of 11.13). This suggests that the simulations include more distant F-F neighbors, represented by broader tails in the F-F g(r).

As discussed, Be-F-Be angles from EPSR are approximately linear (180°), and thus the length between Be cation centers in a linear Be-F-Be chain would be 3.11 Å given their Shannon ionic radii [131]. To give a sense of the variation of the Be-Be distance with Be-F-Be angle, if the Be-F-Be angle was 160°, the length between the Be cation centers would be 3.06 Å. If the Be-F-Be angle was 90°, the length between the Be cation centers would be 2.20 Å. The Be-Be peak at 3 Å in the EPSR models suggests closely packed tetrahedra in which Be-F-Be are nearly linear. Further, the lack of 70-100° angles in the EPSR Be-F-Be angle distribution would imply the complete absence of edge sharing or tightly bent (corner sharing) oligomers. However, these are present in the NNMD model, which also better captures the experimental peak around 3 Å by presenting shorter Be-Be bond lengths (Figure 2.12). Since the Be-Be peak is either over-predicted or overly lengthened by EPSR, the linear alignment of tetrahedra, and thus, possibly the preference for ~180° Be-F-Be angles, is not as significant in the experimental system as in

the EPSR model. As such, the lack of low-angle Be-F-Be bonds indicated by EPSR may be inaccurate.

2.4.2 Lithium contributions, screening, and F^- polarization

Looking more closely at the bond angle distribution (Figure 2.18) and partial PDFs for each composition (Figure 2.12 and Figure 2.13) we see that the evolution of F-F shoulder around 3.0-3.2 Å can be correlated with change in angular variance across composition (Figure 2.19). These figures are summarized in Figure 2.33. For $33.3BeF_2$ and $50BeF_2$, the F-F shoulder is clearly visible, then becomes less intensive with decreasing LiF content, and then almost absent in $95BeF_2$and $100BeF_2$. At the same time, $33.3BeF_2$ and $50BeF_2$ show a high degree distortion of F-Li-F bond angle, with a decrease as BeF_2 content decreases, reaching a minimum distortion of F-Li-F bond angle for $95BeF_2$ and $100BeF_2$. The bond angle distribution shows that in lower-BeF_2 mixtures, there is a higher proportion of lower F-Li-F angles (in the range from 60° to 90°).

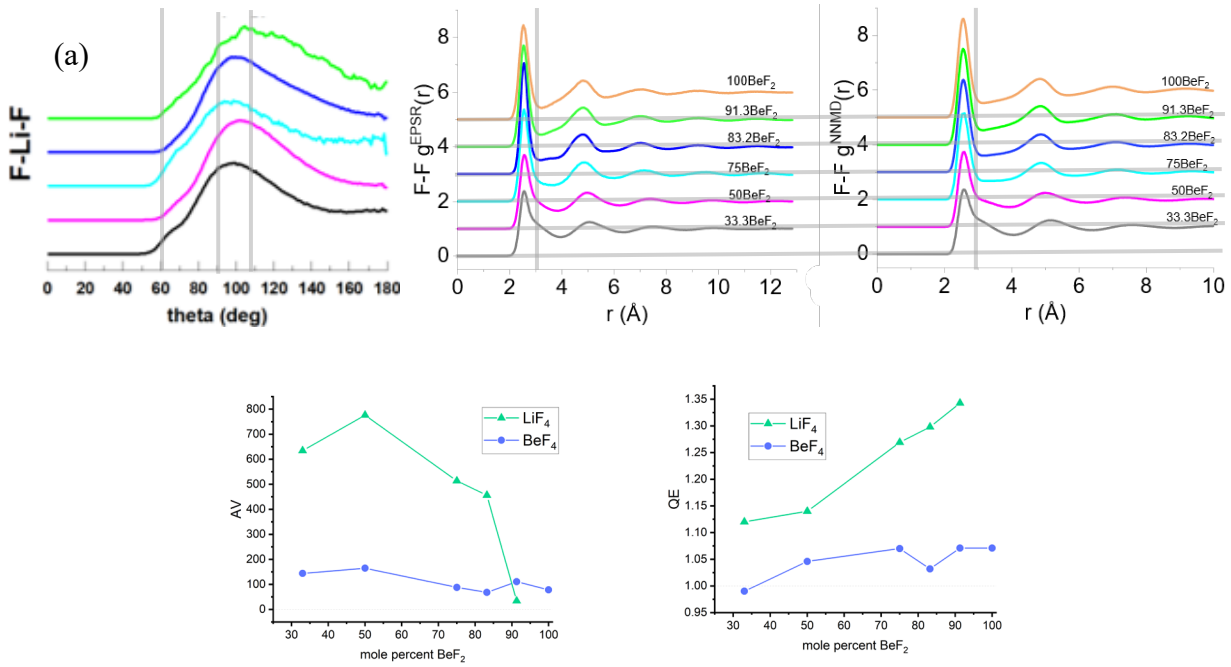

Figure 2.33. Examining the shoulder in the F-F partial PDF alongside the F-Li-F bond angle distribution from EPSR fit to neutron data and angle variance and quadratic elongation of LiF_4 tetrahedra from EPSR.

Figure 2.17 shows that the distance between F within a BeF_4^{2-} tetrahedron is around 2.5 Å, which is approximately the location of the F-F peak from the partial g(r) which has a broad shoulder around 3 Å. From the peak location of the Li-F partial g(r), the Li-F bond length is approximately 1.8 Å. For an F-Li-F angle of approximately 100° (Figure 2.33), the F-F distance within an LiF_4^{3-} tetrahedron would be 2.76 Å. In a more perfect tetrahedron with an F-Li-F angle of 109.5°, the F-F distance would be 2.94 Å. The 3 Å shoulder then, given also its appearance at lower concentrations of BeF_2, likely reflects correlations between fluorides coordinated to the same Li. Additionally, we observe differences in the distribution of the Li-F CN across composition. For $33.3BeF_2$, the Li-F CN is distributed between 2 and 6 (with 4 as the predominant CN). $50BeF_2$ almost has an equivalent fraction of 3- and 4-coordinated Li by F

(Figure 2.21). For 83.2BeF_2 and 91.3BeF_2, the Li-F CN is predominantly 3, with a distribution between 2 and 5. Together, this structural information paints the picture of lower-BeF_2 mixtures (33.3-50BeF_2) having more trF and higher, more distorted Li coordination (with a substantial population of LiF_5, LiF_6, and skewed LiF_4). In the BeF_2-rich systems (83.2-91.3BeF_2), Li exists in more regular, lower CN (primarily 3) environments as F are tied up in the Be_xF_y network.

We note that also in the 3 Å region of the partial PDFs, the first Be-Be peak appears, which we previously identified as increasing in intensity with BeF_2 concentration and as being over-calculated by EPSR compared to experimental results (Figure 2.13). Given this, the shoulder located at 3 Å could be caused by either F-F coordinated to the same Li or by Be-Be separations. Lithium has a small neutron scattering length and is thus susceptible to being under-constrained—that is, without appropriate constraints, the optimization performed by EPSR would likely adjust parameters like Be-Be correlations more significantly since Be's weighting causes it to have a higher effect on the structural data. Given the observed over-calculation of the Be-Be peak in EPSR, we suspect that the model is under-constrained such that part of the signal at 3 Å is misattributed to Be-Be rather than F-F (within LiF_x). This should be verified by classifying F in the F-F partial by trF, brF, and dsF and comparing the shoulders, or by artificially removing Li from the model and examining the altered F-F PDF for a drop in the 3 Å shoulder.

Similarly, it was noted in the results that both EPSR and NNMD fail to capture the full intensity and features of the experimentally-observed negative peak (caused by Li-F contributions), at all compositions (Figure 2.12, Figure 2.13). This is likely also due to the under-constrained systems which diminish Li contributions. In addition, it was mentioned that the Li-F peak is approximately 0.1 Å further left (shorter bond length) for EPSR compared to NNMD (noticeable for 33.3BeF_2 and 50BeF_2). By the same reasoning, since EPSR is optimizing fit with respect to *total* scattering data (specifically the S(Q)), the weakly-weighted Li-F partials are not prioritized to fit. Since the S(Q) is fit, it is possible that EPSR could truncate short-range pairs to achieve better alignment of high-Q oscillations. In addition, NNMD is sensitive to error in the assumed density of the melt, which could affect NN distances [133]. It is important, therefore, to constrain the models such that Li contributions are not neglected.

The existing structural understanding has emphasized that Li is a network modifier [84], disrupting or causing "breakdown" of the network formation of BeF_2 [130] and "depolymerization" [86]. It is important to note that this "breaking" is not mechanical, but rather has to do with electrostatics, leading to a reversible shift in the equilibrium network. The presence of Li *screens* and *stabilizes* trF, which leads to less brF. If F is terminal, F forms a strong dipole which is aligned in the direction of the Be-F bond, but if F is bridging, the dipole is slightly weaker and is less aligned, with a slight orientation along the Be-F-Be angle bisector [134]. Nearby Li^+ reduces the polarization strength of Be^{2+}, moderating the dipole, and stabilizing trF. Thus, it is relevant to know if Li are located near brF or trF to understand their role in screening charge. A relevant next question would be to investigate experimentally (and via EPSR) if Li tends to be located near trF, indicating its role in decreasing the strength of the F dipole. High-temperature-NMR has indicated two ^7Li signals in samples of 22BeF_2 and 25BeF_2 [32]. The separation of peaks in the ^7Li NMR spectra was suggested to be caused by the reduction in the exchange rate of Li coordinated with BeF_4^{2-} monomers and Li coordinated with the larger Be-F network brought on by the formation of an extended Be-F network at those

compositions [32]. As such, there is evidence that Li exists in detectibly different coordination environments in LiF-BeF_2 mixtures, and its role in the structure of mixtures with BeF_2 might be further investigated.

In addition to looking at the changes in the number of brF across compositions, we can similarly look for evidence of Li screening in lower-BeF_2 mixtures. From our current analysis of the data, we observe that at higher concentrations of BeF_2 (meaning fewer trF (Table 2.8)), the Li-F CN decreases (Figure 2.21). We see this visualized in Figure 2.28 as the BeF_2 content increases, the number of brF increases and the Li-F CN decreases. In addition, at higher fractions of BeF_2, the spread of F-Li-F angles decreases (Figure 2.18), consistent with the growth of a Be-F network. Similarly, F-Li-F angular variance decreases with BeF_2 fraction, consistent with Li leaving trF sites as the F become brF. These trends are summarized in Figure 2.34 where brF_{tot} decreases with Li-F CN (Pearson's R of -0.625) and AV increases with Li-F CN (Pearson's R of 0.629).

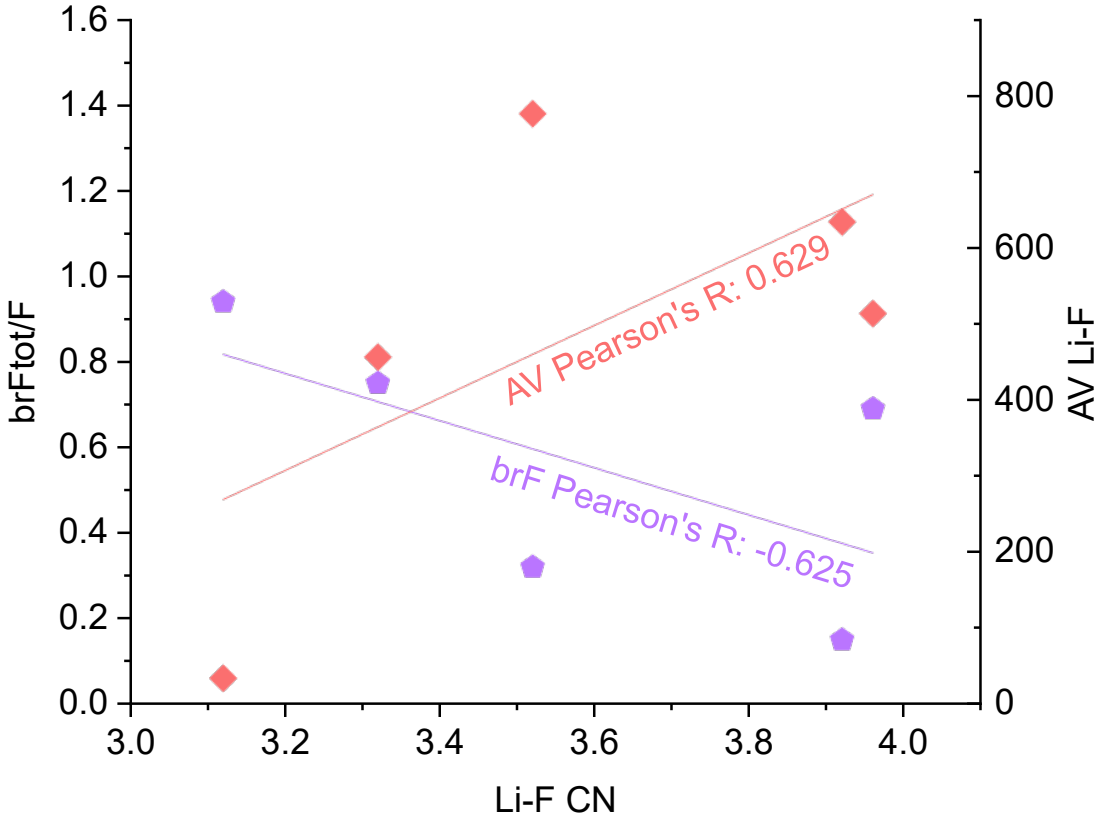

Figure 2.34. Change in brF_{tot} (normalized per total F) and angular variance of F-Li-F with Li-F CN, calculated from EPSR fit to neutron data.

Be-F bonds are known to be ionic-covalent due to F^- polarization by Be^{2+} and hybridization, and anion polarization effects are known to be important to accurately modeling halide melts [135], [134], [136]. Molten covalent systems can have strong directional bonds carrying significant electron density between the atomic centers [137]. Since Li reduces F polarization, this may affect the degree of covalent bonding of Be-F bonds, causing its role in de-polymerization. Salanne and Madden further explain that the F^- dipole (itself screened by the presence of Li^+) screens cation-cation (Be-Be) repulsion and lowers the total energy, meaning that the angles of Be-F-Be can be bent, affecting the shape of the Be-F network [134]. This is consistent with the broad distribution of Be-F-Be angles from 110° to 180° observed across the compositions by

EPSR. In Figure 2.29, we see that the compositions with the most LiF (33.3 and 50BeF_2) have a peak Be-F-Be angle around 173°-175°, whereas most of the higher-BeF_2 compositions continuously increase. This could be due to angling of the F^- dipole caused by the adjacent, stabilizing Li in more LiF-rich compositions.

Førland suggests that the greater deformation caused by polarization of F^- upon mixing leads to a lower energy of the mixed system [138]. Upon mixing of LiF and BeF_2, it is possible for Be cations to come into contact with more F^- anions in order to reach a nominal Be-F coordination number of 4. The F^- ions originally coordinated with Li^+, upon mixing, come to coordinate Be^{2+}, a higher charged cation which generates a higher degree of polarization of F^- [139]. Combining this understanding with the role of Li as a charge screener, we summarize two competing effects:

(A) Upon the addition of BeF_2 to LiF, more F can move into the more polarizing Be environments. The local energy change is negative as F^-'s electric field grows, stabilizing the system.

(B) Upon the addition of LiF to BeF_2, Li^+ acts to stabilize trF by screening the electric field locally, shifting equilibrium away from the formation of bridges. The lack of bridges means less stabilization for the network; the energy cost is positive as bridges are disrupted/prevented.

The total enthalpy of mixing includes the balancing of these stabilizing and de-stabilizing changes. Enthalpy is minimized when strongly polarized Be-F bonds displace the weaker Li-F interactions (A). This occurs approximately when all Be have reached their nominal CN of 4, which is around 33BeF_2 (Figure 2.28). At compositions with an intermediate fraction of BeF_2, Be are already 4-fold coordinated, so Li^+ stabilize trF and cause the breaking of bridges (B), such that ΔH_{mix} increases (Figure 2.28).

2.4.3 Effect of temperature on structure

A summary of diffraction peak (bond length) trends with temperature (and composition) are shown in Table 2.10. Looking at the Be-F bond length in the solid, the slight increase at higher fractions of BeF_2 is representative of low thermal expansion of the Be-F bond within a constrained solid framework. (From room temperature to melting the lattice parameters *a* and *c* in 33.3BeF_2 increase by 0.06-0.08 Å [128]). In compositions of higher-BeF_2, where the Be-F network is pervasive, we observe slightly more expansion. In the liquid, we might hypothesize that Be-trF bonds would be slightly shorter than Be-brF bonds on average, since the F^- in Be-trF is unshared and the strongly polarizing Be^{2+} cation has less competition in pulling a greater fraction of the F^- electron density. In mixtures with more LiF, the stabilization of trF by Li along with the depolymerization (breaking of brF) means that the shorter Be-trF bonds can become more populous at higher temperatures. In 100BeF_2, no Li is present to stabilize trF, so we can observe thermal expansion of Be-F.

Table 2.10. Trends in diffraction peaks attributed to Be-F and F-F with temperature and composition. Low $xBeF_2$ in the solid and liquid refers to 33, 50, and 75BeF_2. High $xBeF_2$ in the liquid refers to 83.2 and 91.3BeF_2, and high $xBeF_2$ in the solid refers to 83.2, 91.3, and 100BeF_2.

Diffraction peak position in g(r)	Bond	As temperature increases				
		In the solid at low x_{BeF2}	In the solid at high x_{BeF2}	In the liquid at low x_{BeF2}	In the liquid at high x_{BeF2}	In the liquid at 100BeF_2
~1.5 Å	Be-F (within tetrahedron)	No change (~1.540-1.545 Å)	Slight increase (~1.535 Å)	Decreases (including 83.2BeF_2)	Decreases less (slope ~OM[1] less)	Increases
~2.5 Å	F-F ("first peak", within tetrahedron)	No change/slight increase*	No change /slight increase*	Increases** (slope ~OM[1] higher than in solid)	Increases (slope ~OM[1] higher than in solid)	Decreases
~5 Å	F-F ("second peak", on adjoining Be, within same oligomer, within adjacent oligomers)	Increase	Increase	Decreases	Increases	Increases

* excluding 75BeF_2 which has high uncertainty
** excluding 50BeF_2 which has high uncertainty
[1]OM = order of magnitude

The F-F bond length within BeF_4^{2-} tetrahedra is geometrically related to the Be-F bond length (r_{Be-F}) and the F-Be-F angle (θ_{FBeF}):

$$r_{F-F} = \sqrt{2r_{Be-F}^2(1 - cos(\theta_{FBeF}))} \qquad (Eqn.\ 2.7)$$

Therefore, we can see that the F-F bond length is affected by stretches in the tetrahedra (described by Be-F QE) and bending of the F-Be-F bonds (described by F-Be-F AV). For the r_{Be-F} seen in the solid at high BeF_2 (1.535 Å), r_{F-F} for θ_{FBeF} = 109.5° would be 2.51 Å. For the r_{Be-F} seen in the solid at low BeF_2 (1.540-1.545 Å), r_{F-F} for θ_{FBeF} = 109.5° would be 2.52 Å. The nearly zero or slightly positive change in F-F distance with temperature at all compositions is consistent with minor growth in r_{Be-F} and a constant θ_{FBeF}. In the liquid, F-F distance increases with temperature in all compositions containing LiF. If r_{Be-F} is decreasing and r_{F-F} is increasing, then θ_{FBeF} must be increasing. In 100BeF_2, the opposite occurs; r_{Be-F} increases and r_{F-F} decreases, implying a decrease in θ_{FBeF}. Despite this, we calculate a low AV for BeF_4^{2-} in 100BeF_2 (Figure 2.19). Note that AV is calculated from an averaged variation from 109.5° of the six F-Be-F angles within a single tetrahedron [125]. Looking directly at the bond angle distribution for F-

Be-F (Figure 2.35), we see that $100BeF_2$ has the widest distribution, with the largest tails in the 70°-90° and 135°-155° regions. $100BeF_2$ also has its F-Be-F peak at one of the lowest angles relative to all other compositions, supporting the understanding that BeF_2's slightly smaller tetrahedral angles are the response to a thermally expanding r_{Be-F} in order to maintain the Be-F network.

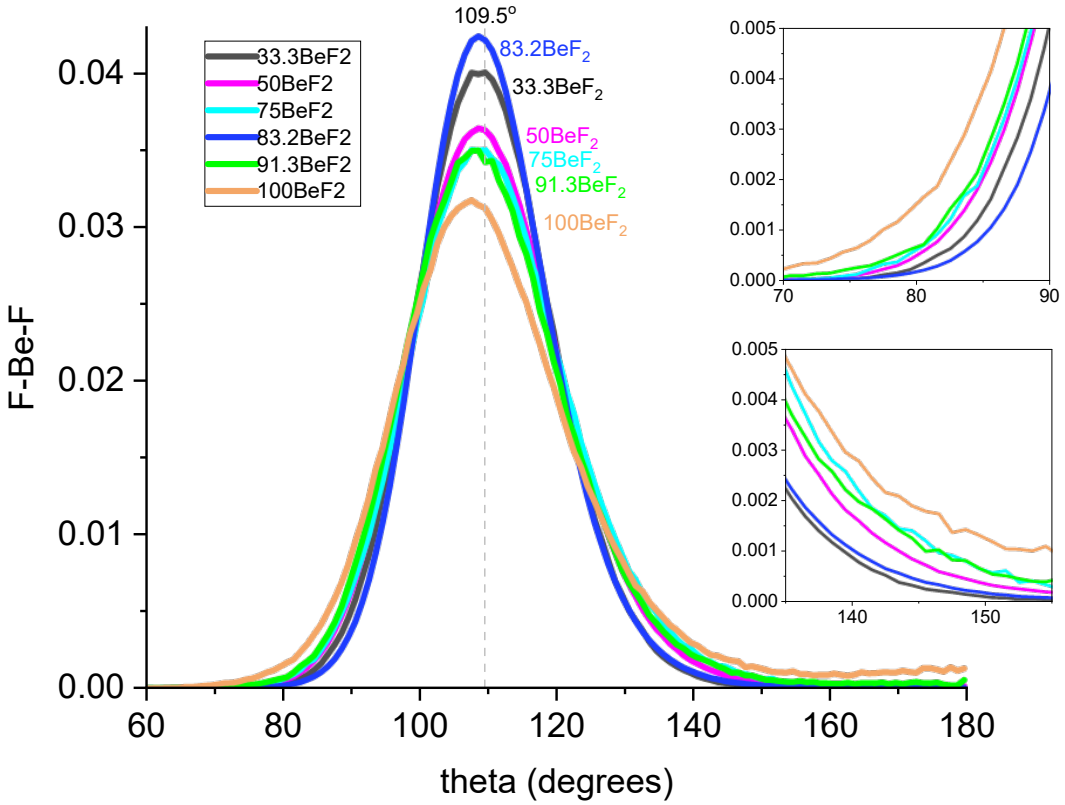

Figure 2.35. F-Be-F bond angle distribution from ESPR fit to neutron data, with compositions plotted together for comparison.

For the peak at 5 Å, peak position in the solid at all compositions (and thus we interpret F-F inter-tetrahedral spacing) increases with temperature, indicative of thermal expansion of the lattice [128]. In the liquid at low-x_{BeF2}, inter-tetrahedral F-F decreases with increasing temperature. In these mixtures, decreased Be-F-Be connectivity due to stabilization of trF by Li means that medium range structure collapses as Li supports the depolymerization of Be-F networks.

The temperature dependence of bond length changes offers further confirmation of the role that Li plays in charge-screening, leading to network modification. To reiterate, r_{Be-F} decreases with temperature only when Li is abundant and can serve as a stabilizer of monomers. At the same time, in low-BeF_2 mixtures, the first F-F peak increases with temperature, implying that F-Be-F bond bending (the opening of angles) dominates over bond stretching (since r_{Be-F} shortens). The second F-F peak in the low-BeF_2 mixtures shortens with temperature, providing further evidence of loss of medium-range structure supported by the stabilizing charge-screening of Li.

2.5 Conclusion

In this chapter, I present a structural interpretation of LiF-BeF_2 mixtures ranging from 33.3 to 100 mol% BeF_2 using neutron scattering data, EPSR models, and NNMD simulations. The structure of LiF-BeF_2 mixtures has been generally interpreted in the literature within the "network liquid model" typically applied to molten alkali chlorides, whereby corner-sharing tetrahedral units leads to ordering of cation centers, and the alkali halide provides stabilization for "structural modification" leading to increasingly isolated oligomers and fewer bridging halides [140], [141]. Our studies confirm the presence of extended network formation in LiF-BeF_2 [29] mixtures, increasing with the fraction of BeF_2 (see Table 2.8). Together the bond angle distributions (Figure 2.18) and partial PDFs from EPSR and NNMD (Figure 2.12 and Figure 2.13) paint the picture of the 33.3BeF_2 and 50BeF_2 mixtures having more trF and higher, more distorted Li coordination, further supported by high values for AV in the low-BeF_2 region (Figure 2.19). In the mixtures with 83.2-91.3BeF_2, results show that Li exists in more regular, lower CN environments (Figure 2.21) with F tied up in the fluoroberyllate network. Our analysis applies the theory of the network liquid model with structural modification to a molten fluoride system (see Sections 2.4.1 and 2.4.2), describing the balance between BeF_2 network formation and Li^+ charge screening. In this balance, described in detail in Section 2.4.2, a larger fraction of BeF_2 means that more F- can interact with Be^{2+}, leading to a higher degree of polarization of F^-, but at the same time, when Li^+ are present, they are able to screen the electric field of trF.

From neutron scattering data from room temperature to melting point, the change in Be-F and F-F bond lengths (identified via their prominence in the total g(r) (Figure 2.11) and known positions in the partial PDFs) with temperature is quantified and discussed in Section 2.4.3. The Be-F bond length decreases with increasing temperature (summarized in Table 2.10) in the liquid only when Li is present so as to stabilize monomers (stabilize trF). In the 33.3BeF_2, 50BeF_2, and 75BeF_2, the inter-tetrahedral F-F distance increases with temperature, implying that F-Be-F bond bending dominates over bond stretching since the Be-F distance shortens. The second F-F peak, attributed to Fs on adjoining Be, within the same oligomer, or within adjacent oligomers (visualized in Figure 2.17), shortens with temperature for 33.3BeF_2, 50BeF_2, and 75BeF_2, providing further evidence of loss of medium-range structure supported by the stabilizing charge-screening of Li.

We find that the EPSR and NNMD models differ most significantly in their calculations of the Be-F-Be bond angle distributions, where NNMD reports a distribution of angles around 125° with an extended tail in the 70°-100° region, whereas EPSR peaks near 180° (Figure 2.30). It was found that for all compositions, both EPSR and NNMD failed to capture the complete features of the experimentally observed negative peak in the g(r) which is caused by Li-F scattering. It is possible that this might be due to under-constrained systems which inherently diminish Li contributions (particularly in the case of EPSR) given their weak weighting due to Li's small scattering length. Error in the NNMD simulations may be due to inaccurate melt density inputs, but further investigation is needed to establish the cause of these discrepancies.

For further analysis of excess bridging and CNCs, next areas of study might include calculating the fraction of edge-sharing tetrahedra quantitatively using the Be-Be CN calculated by EPSR (Figure 2.21). The role of Li's screening on modifying local Be-F geometry and trF versus brF as a function of composition might be further investigated by differentiating the F-F shoulder in the g(r) around 3 Å into the contributions from Li tetrahedra and the Be network. In addition, further analysis is needed to comprehensively extract structural information presented by the

complementary features of neutron and X-ray scattering data.

2.6 Acknowledgement

This chapter contains results from two manuscripts both supported by the U.S. Department of Energy (DOE), Office of Nuclear Energy (NE), under Award No. 21-24563.

"Liquid structure of $LiF\text{-}BeF_2$ molten salts via neutron and X-ray scattering and neural-network based molecular dynamics, and structural evolution with temperature" in preparation.

H.W. and D.N.G. designed and prepared the neutron samples. D.N.G prepared the X-ray samples along with Michael Borrello (UC Berkeley), with support from Tony Zheng (MIT). S.F., D.N.G., and J.C.N. collected the neutron measurements. D.S. and D.O. collected the X-ray measurements. S.F. and J.C.N. performed primary analysis of the neutron measurements. S.F., and S.F., D.S., J.C.N, and D.O. performed primary analysis of the X-ray measurements. B.Ka. performed and analyzed the EPSR. S.B. and S.L. developed, conducted, and analyzed results from the simulations. A.H., S.S., and M.A. developed oligomer distribution analysis. H.W. and D.N.G performed formal analysis of neutron, X-ray, and EPSR results. M.A., S.L., R.O.S., and B.Kh. conceptualized the project. S.L., R.O.S., and B.Kh. acquired funding. H.W., D.N.G., B.Ka., S.F., wrote and edited the manuscript. All authors discussed the results and reviewed the manuscript.

"Complex Structure of Molten FLiBe ($2LiF\text{-}BeF_2$) Examined by Experimental Neutron Scattering, X-Ray Scattering, and Deep-Neural-Network Based Molecular Dynamics" Sean Fayfar, Rajni Chahal, Haley Williams, D. Nathanael Gardner, Guiqiu Zheng, David Sprouster, Jörg C. Neuefeind, Dan Olds, Andrea Hwang, Joanna Mcfarlane, Ryan C. Gallagher, Mark Asta, Stephen Lam, Raluca O. Scarlat, and Boris Khaykovich

D.N.G., H.W., J.M., and R.C.G designed and prepared the neutron samples. G.Z., D.S., and B.K. designed and prepared the x-ray samples. S.F., D.N.G., and J.C.N. collected the neutron measurements. D.S. and D.O. collected the x-ray measurements. S.F. and J.C.N. analyzed the neutron measurements. S.F., D.S., J.C.N, and D.O. analyzed the x-ray measurements. R.C. and S.L. developed, conducted, and analyzed the results from the simulations. J.M., R.C.G., M.A., S.L., R.O.S., and B.K. conceptualized the project. S.L., R.O.S, and B.K. acquired funding. S.F., R.C., H.W., S.L, and B.K. wrote and edited the manuscript. All authors discussed the results and reviewed the manuscript.

3 FLUOROACIDITY STUDIES WITH CHROMIUM SOLUTES

Of the primary structural metals expected to be present in molten fluoride systems (Fe, Ni, Mo, Cr), chromium has the lowest oxidation potential, meaning it will be more readily oxidized in a molten fluoride salt in the presence of an oxidant such as H_2O [142]. The corrosivity of a melt is characterized by its *redox potential*, which is an indicator of its oxidizing power. Corrosivity, however, is also related to the solubility and speciation of the oxidized metal. Drivers for corrosion include thermodynamic drivers (redox), temperature gradients, and activity gradients (dissimilar materials) [143]. In this chapter, I study the speciation of chromium solutes in molten salts of different fluoroacidities, examining connections between acidity and corrosivity and addressing the question:

- Do acidic solvent species necessarily compete with chromium solutes for dissociated F^- (dsF)?

3.1 Background

Fluoroacidity is a solvoacidity metric which describes the degree of association or dissociation of a molten fluoride salt. Following from the Lux-Flood interpretation of Lewis acid-base theory [144], it describes the *chemical activity of* F^- (an electron pair donor, or a base) in a fluoride solvent (Eqn. B and C in Figure 3.1). The acidic species (or electron pair acceptors) would be those which can accept F^-. This includes ions which can accommodate a higher coordination number (such as BeF_3^-) or ions which share an F coordinate (i.e., brF).

Redox potential is a descriptor of the equilibrium of oxidation states in a molten salt (Figure 3.1). Redox potential describes the ratio between the high and low valence states of every ion in the melt, in equilibrium with all other redox couples in the melt. For the case when redox potential is defined relative to the $F_{2(g)}/F^-$ redox couple, redox potential would describe if the salt is more or less oxidizing than the $F_{2(g)}/F^-$ reference couple.

Figure 3.1 illustrates fluoroacidity and redox potential using the example of FLiBe (simulated salt snapshot from [19]) with redox control via beryllium metal [69]. The example equation related to fluoroacidity is the association/dissociation reaction of a fluoroberyllate complex from a Be-F CN of 3 to a CN of 4. The activity of the dsF which is complexed and de-complexed in this equation defines the fluoroacidity of the system (Eqn. A). The redox potential is shown to be referenced to the ratio of F_2 gas in equilibrium with the melt (oxidation state of 0) to total F^- in the melt (oxidation state of -1) (Eqn. D). The example shows that this manner of referencing redox potential, more specifically called the fluorine potential, is quantified by the partial molar Gibbs free energy of F_2 gas (Eqn. F). This chemical potential may also be expressed as an electrochemical potential, E (Eqn. F). Typical methods for controlling the redox potential of FLiBe include setting the potential by controlling the ratio of H^0 to H^+ via H_2/HF sparging or by controlling the ratio of Be^0 to Be^{2+} via Be metal additions [60], [69], [145]. In the MSRE, the ratio of U^{3+}/U^{4+} was considered for redox measurements and was controlled via Be additions [53], [146]. Figure 3.1 shows how the Be/Be^{2+} couple (Eqn. E) might be in equilibrium with the F^0/F^- couple (Eqn. D). In this example, the redox potential would be described by Eqn. G, in terms of the activity of BeF_2 (Be^{2+}) in FLiBe, since pF_2 is related to $a_{(BeF2)}$ and ΔG^o_{BeF2} via the law of mass action:

$$K = \frac{[a_{prod3}]^{stoic3}[a_{prod4}]^{stoic4}}{[a_{react1}]^{stoic1}[a_{react2}]^{stoic2}} = e^{-\Delta G°/RT} \quad \text{(Eqn. 3.1)}$$

where K is the equilibrium constant, *a* is the activity of each product or reactant, raised to the power of its stoichiometric coefficient at equilibrium, ΔG° is the standard Gibbs free energy of the reaction, R is the ideal gas constant, and T is the temperature.

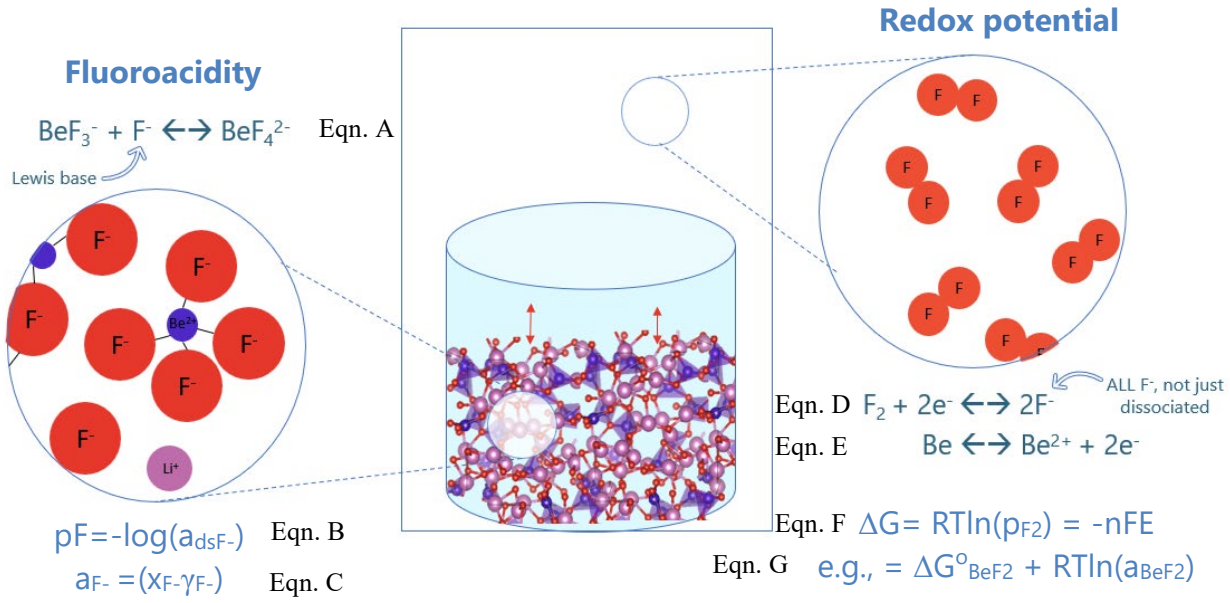

Figure 3.1. Defining fluoroacidity and redox potential for the example of molten FLiBe with redox control with Be metal. Fluoroacidity (left) is the chemical activity of dsF in the melt. Redox potential (right) is quantified with respect to a given redox couple, e.g. vs $F_{2(g)}/F^-$, and provides the chemical potential redox couples present in the salt.

Fluoroacidity has been characterized on a relative scale using electrochemical, chemical equilibrium, and mass transfer -based techniques, summarized in Table 3.1. Other studies have systematically measured redox potential (and thus activity) in molten fluorides to suggest the relative availability of F- [58], [92] or quantified the degree of electronic donation of fluoride anion on different probe cations (optical basicity) [147], but the examples in Table 3.1 are selected for further analysis due to their explicit framing of the *thermodynamic activity* of *dissociated fluoride* (not of LiF or BeF_2, or of F's polarizability) as fluoroacidity.

Jaskierowicz et al.'s method uses electrochemically measured activities of NiF_2 and F^- in each melt as an indicator of fluoroacidity relative to that of FLiNaK. Since the activity coefficient of NiF_2 is lumped with $a(F^-)$ as an indicator of fluoroacidity, they point out that their technique is indirect in addition to being relative to the acidity of FLiNaK, the reference solvent. Dewing's method is also relies on electrochemical measurements of activity (as well as measurements of vapor pressure), calculating the change in activity of the components of the solvent salt (3NaF-AlF_3) upon additions of fluorides. Dewing then ranks substances by their change in the activity of AlF_3 relative to the mole fraction of the added fluoride, explaining that positive $\delta a_{AlF3}/\delta x_{additive}$ indicate that the additive is acidic, and $\delta a_{AlF3}/\delta x_{additive} < -1$ indicate that the additive is basic [148].

Bieber et al.'s method estimates fluoroacidity by measuring the ratio over time of dissolved complex fluorosilicates to calculate the rate constant of silicon tetrafluoride gas evolution. The Si^{4+} concentration is measured electrochemically using a calibration curve relating peak current to solute concentration measured by Inductively Coupled Plasma-Atomic Emission Spectroscopy (ICP-AES). The change in Si^{4+} concentration over time is used to determine the rate constant of $SiF_{4(g)}$ release, which is then correlated to the fluoroacidity of the solvent, with the understanding that a basic solvent (with a higher dsF activity) is better able to stabilize Si^{4+} leading to less gas evolution.

Similar to Bieber et al., Kergoat et al.'s method relies on a kinetic rather than thermodynamic value, the dimensionless Schmidt number, to compare how momentum and mass diffuse through the molten fluoride. The Schmidt number, Sc, is defined as the ratio of solvent kinematic viscosity (the ratio of the dynamic viscosity and the fluid density) to solute diffusivity, as written in Table 3.1. With the assumption that viscosity *increases* with acidity and diffusivity *decreases*, the Schmidt number is postulated by Kergoat et al. to be more sensitive to differences in pF with temperature and composition compared to D or ν alone. The Schmidt number, however, depends on the solute identity; Kergoat et al. calculate Sc using both silicon and boron solutes and state that the ranking of fluoroacidity using either solute is the same as that by Bieber et al. [149].

Table 3.1. Existing methods used to indicate fluoroacidity.

Method	Description	Limitations & Challenges
Jaskierowicz et al., 2010 (electrochemical) [150]	The electrical potential of the Ni^{2+}/Ni couple in two different solvents (FLiNaK which is considered purely basic and another salt of interest) is measured. The electrical potential between these two systems is a function of the activities of NiF_2 and F^-.	Purity of solvent and therefore materials compatibility of the setup with fluorides is important for accurate measurements, e.g., to avoid effects of oxoacidity. ([150] used quartz containers, which would introduce oxide.) pF is quantified relative to a reference salt. Activity coefficients of NiF_2 and solubility of NiF_2 are needed for isolation of the activity of dsF.
Dewing, 1989 (differential activity) [148]	The change in the activity of AlF_3 and NaF are measured electrochemically (or by vapor pressure changes) when a salt of interest is added to the $3NaF\text{-}AlF_3$ solvent. The magnitude and direction of the change in activity relative to the mole fraction of the added salt is used as an indicator of acidity.	Additions to the solvent causes a shift in the ratio of NaF to AlF_3 shifts; the composition must be known or measured in order to correct for unintentional shifts in activity which may supercede the intented change [148]. Activity changes may be affected by composition-specific ionic interactions.

Bieber et al., 2011 (chemical equilibrium) [149]	The stability of SiF_{4+x}^{x} ions in melt relative to gas in equilibrium (shown in the chemical equation below) is measured electrochemically. $SiF_{4+x}^{x-} = SiF_{4(g)} + xF^-$ Considering that a melt with a high concentration of dsF can stabilize the Si ions, a low rate constant for gas evolution means the Si is staying in the melt, indicating relative basicity among different melts, and allowing for creation of an ordered list of solvents based on their basicity relative to each other.	Particularity of the solute to the solvent of interest. The authors point out that the solute must be (1) in equilibrium with a gaseous species, (2) nonreactive with solvent, (3) more fluoroacidic than the solvent. Gas evolution rate only provides a qualitative estimate of pF.
Kergoat et al., 2014 (mass transfer) [151]	Solute ion diffusion coefficient (D) (measured electrochemically) and solvent kinematic viscosity (ν) are used to find the Schmidt number, defined below, which is asserted to be an indicator of pF. $Sc = \nu / D$ The Schmidt number was validated against other techniques for estimating pF and found to increase with acidity of the solvent.	Diffusion coefficient is affected by solute ionic radius, temperature (equivalent comparison may be limited by solvent melting point). Electrochemical measurements of D require knowledge of the solute concentration, solubility, electrochemical reversibility, chemical compatibility, etc. Schmidt number provides an estimate of pF ranking since it is relative to the probe solute.

3.1.1 Discussion of fluoroacidity

As explained, fluoroacidity is a *thermodynamic* quantity and the Schmidt number and the rate constant of SiF_4 gas evolution are *kinetic* values. Thus, their relationship with pF is indirect and dependent on the system (composition and nature of ion interactions). Although Kergoat et al. found the pF ranking to be the same when using silicon versus boron as a probe solute (Table 3.3), Sc depends on the identity of the diffusing species and more accurately describes the coordination dynamics of the probe solute than the fluoride activity. Similarly, the rate of gas evolution of SiF_4 is related to the ability of the melt to stabilize the Si^{4+} solute, but this rate may also be affected by bulk transport in the melt, related to the Si^{4+} ion's speciation. Thus, it is true that the coordination dynamics represented by the kinetic parameters are, in fact, related to fluoroacidity, but it is necessary to unpack the relationship between these concepts and parameters to understand their strengths and limitations.

The relationship between solute diffusivity (a defining element of the Schmidt number) and solvent activity (specifically the activity of dissociated fluoride which is the fluoroacidity) is governed by chemical thermodynamics, transport theory, and local structure. A solute's diffusivity is related to:

- how it interacts with the solvent,
- the viscosity and structure of the solvent itself,
- the solute's identity (including charge density and ionic radius),
- and the temperature of the system.

If diffusion takes place by repeatedly coordinating and dissociating with dsF, a higher activity of F^- would mean that the solute can hop more freely. If, however, the solute moves through oligomeric structures, within the network of the melt rather than via exchange with bulk dsF, diffusion may not be so simply related to the activity of F^-. Thus, the impact of fluoroacidity on solute diffusivity *depends on the diffusion mechanism of the solute*, which is dictated by solute-solvent interactions and related to the bulleted aspects listed above.

Assuming a diffusing solute is spherical and moving independent of other solutes in Stokes flow (low Reynolds number), the solute's diffusivity may be estimated via the Stokes-Einstein (S-E) equation using the dynamic viscosity of the solvent:

$$D = \frac{kT}{6\pi\eta r} \qquad \text{(Eqn. 3.2)}$$

where D is the diffusion coefficient, k is the Boltzmann constant, T is the temperature in Kelvin, η is the dynamic viscosity (tabulated for FLiNaK in [152]), and *r* is the Stokes radius of the solute ion (a measure of the size of the solute interacting with the solvent). The coefficient '6' results from the assumption of a stick boundary condition; for a slip condition, the coefficient is 4 [153].

Table 3.3 presents the Schmidt number calculated for Si^{4+} and B^{3+} in molten FLiNaK at 50-degree increments from 700° to 900°C using D measured electrochemically by Kergoat et al. and calculated using the Stokes-Einstein equation. The first column of Sc presents the values provided by [151]. The second column, Sc_{recalc}, presents values recalculated using the ν tabulated by Kergoat et al. and the D measured by Kergoat et al. These values should be the same, but the discrepancy might be due to differences in the significant figures for the tabulated ν and D values. The third column, $Sc_{LaneKer}$, is calculated using ν from Lane et al. 1958 (which is the original source for the source cited by Kergoat et al.) and D from Kergoat et al. Despite being from presumably the same source, ν from Kergoat et al. and ν from Lane et al. differ by 14 to 20% (percent difference), with the percent difference increasing with temperature. This translates to the same percent difference (between 14 and 20%) between Sc_{recalc} and $Sc_{LaneKer}$. Given these discrepancies, we take the average Sc with two significant figures to be Sc_{avg}, with a standard deviation calculated from the values from the first three sources.

The Stokes-Einstein equation was used to calculate D using kinematic viscosities from Lane et al. and using ionic radii from Shannon 1976 (Table 3.2). Sc values with two significant figures which were calculated using these calculated diffusivities are listed in Table 3.3.

Table 3.2. Ionic radii of Si^{4+} and B^{3+} used to calculate D in Table 3.3. Slip and stick radii calculated from rearranged S-E equation with a coefficient of 4 or 6 depending on slip or stick boundary conditions using dynamic viscosity from Lane et al. and D_{Si4+} and D_{B3+} measured electrochemically by Kergoat et al.

Ion	Coordination Number	Ionic Radius (Å) [131]	Ionic Radius (m)	Slip Radius (Å) (700°C)	Stick Radius (Å) (700°C)
Si^{4+}	4	0.26	2.60E-11	8.18	5.45
	6	0.40	4.00E-11		
B^{3+}	3	0.01	1.00E-12	1.69	1.13
	4	0.11	1.10E-11		

The Schmidt numbers calculated using S-E diffusivity are approximately an order of magnitude less than those calculated using D measured electrochemically since the diffusivities calculated from these two methods differ by approximately an order of magnitude.

One challenge in the applicability of the Stokes-Einstein equation is approximating an accurate Stokes radius of the diffusing ion. Brookes et al. remark that Stokes' law does not hold for cations diffusing in molten salts if the crystallographic radius is used [153]. In their study of dilute additions of MCl_3 (2 mol%) to LiCl-KCl solvents, they calculated the hydrodynamic radii of M^{3+} solutes assuming slip or stick boundary conditions and found the calculated radii to be 3 to 5 times larger than the Shannon radii. Even if the radius of Si^{4+} (CN of 4) was 5 times larger than the Shannon value, the $Sc_{SE,CN4}$ for Si^{4+} would vary from 760 to 160 across the temperature range (700° to 900°C), still approximately an order of magnitude different from Sc_{avg} at 700°C.

Further, the hydrodynamic radii of Si^{4+} and B^{3+} for the Kergoat et al. system can be calculated assuming a slip or stick condition in FLiNaK at 700°C, by rearrangement of the S-E equation using dynamic viscosity tabulated by Lane et al. and D measured by Kergoat et al. (Table 3.2). The slip condition implies that there is solely a radial force from the spherical diffusing particle (seen by Brookes et al. to be relevant for the larger ions of oxidation state +1 or -1). The stick condition considers that there is also a tangential force, caused by a *textured* diffusing particle which interacts more with the solvent. Estimation of the radii from diffusivities gives radii which are 14x to 30x larger than the Shannon radii for Si^{4+} and which are 10x to 170x larger than the Shannon radii for B^{3+}. This large deviation of the experimentally-derived (hydrodynamic) radii from the crystal ionic radii points to the possible formation of diffusing complexes.

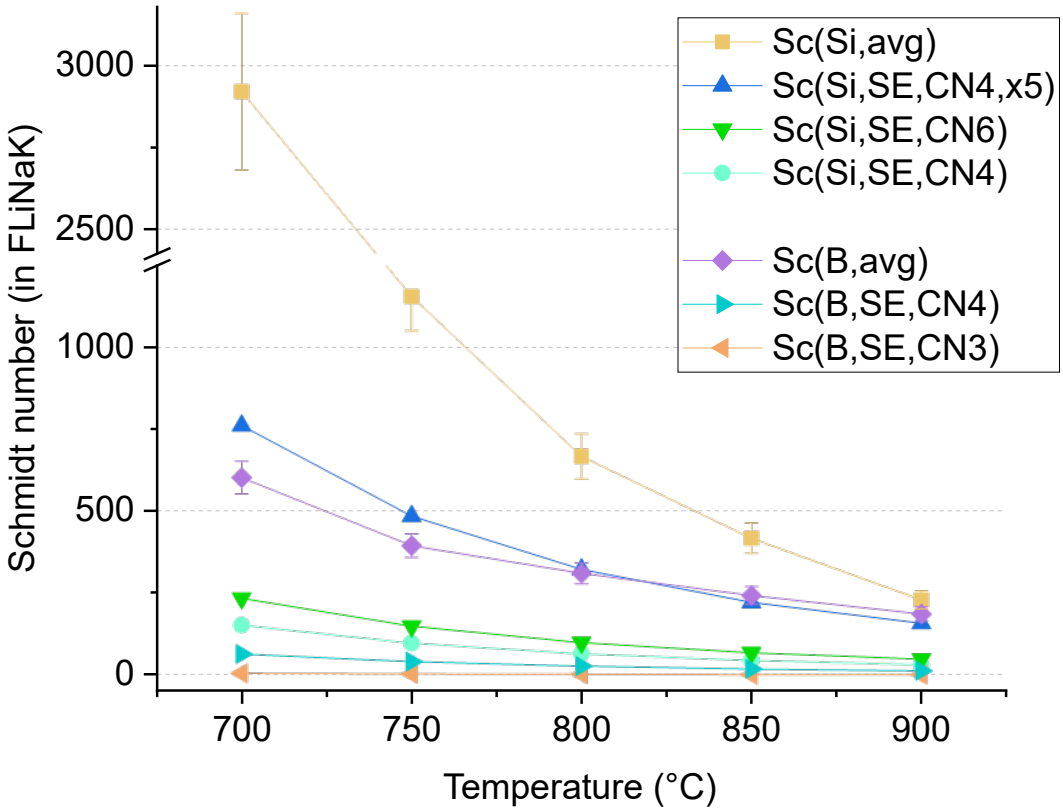

Figure 3.2. Schmidt number across temperature for Si^{4+} and B^{3+} in FLiNaK. Values tabulated in Table 3.3, with "avg" values calculated from Kergoat et al. diffusivity and "SE" values calculated from Stokes-Einstein diffusivity. The x5 value for Si^{4+} is calculated using an ionic radius which is five times the Shannon value.

The observed deviation from S-E indicates that the assumption of free spherical motion without strong interactions with the solvent may be invalid for both Si^{4+} and B^{3+} solutes. Additionally, the higher Sc values for Si^{4+} compared to B^{3+} indicates that Si^{4+} has lower ion mobility relative to the viscosity of the melt, suggesting a stronger or more stable degree of complexation. Even when a higher CN (meaning larger) ionic radius is used or when the radius is estimated to be 5 times larger than the Shannon ionic radius, S-E still underpredicts the diffusivity and thus the Schmidt number. This underprediction could be due to complexation with fluorides (indicating a high Lewis acidity of the solute) or dynamic association with oligomers in the melt (indicating a high Lewis (fluoro) acidity of the solvent). To assess this, we can look at the difference between the Si^{4+} and B^{3+} solutes, since their Lewis acidity is reflected in how they respond to the same solvent. Si^{4+} has a much higher Sc and stronger deviation from SE than B^{3+}, which diffuses more quickly. The difference in deviation from SE between the two solutes suggests that the deviation of Si^{4+} from SE is more likely due to its own acidity and complexation in the fluoride, since the common denominator of the FLiNaK solvent does not seem to affect B^{3+} diffusion to the same extent. To summarize, rather than purely indicating the fluoroacidity of the solvent, Sc also indicates the Lewis acidity of the solute. We conclude that Kergoat et al.'s study indicates that Si^{4+} is more acidic than B^{3+} and that deviation of Sc from SE primarily reflects the solute's Lewis acidity rather than the fluoroacidity of the solvent. In order to fully determine the applicability of Sc to pF in subsequent studies, analysis of solute coordination is necessary to understand if diffusion occurs among or within complexes.

Table 3.3. Schmidt number (v/D) of Si^{4+} (top) and B^{3+} (bottom) in FLiNaK, from Kergoat et al. 2014 and calculated using the Stokes-Einstein equation (rigid sphere diffusion) assuming ionic radii of Si^{4+} (CN = 4 and 6) and of B^{3+} (CN = 3 and 4) from [131].

Temperature (°C)	From Kergoat et al. 2014 [151] (cited [154] for viscosity which cites [152])		From Lane et al. 1958 [152]	Stokes-Einstein (using η from [152] and r from [131])		Schmidt number of Si^{4+} in FLiNaK					
	$\nu_{FLiNaK,2014}$ (m^2/s)	D_{Si4+} (m^2/s)	$\nu_{FLiNaK,1958}$ (m^2/s)	$D_{Si4+,CN4}$ (m^2/s)	$D_{Si4+,CN6}$ (m^2/s)	**Sc** [151]	Sc_{recalc}	$Sc_{LaneKer}$	Sc_{avg}	$Sc_{SE,CN4}$	$Sc_{SE,CN6}$
700	1.25E-06	4.50E-10	1.44E-06	9.44E-09	6.14E-09	2786	2778	3197	**2900 ±200**	150	230
750	1.02E-06	9.30E-10	1.19E-06	1.22E-08	7.95E-09	1094	1097	1278	**1200 ±100**	100	150
800	8.40E-07	1.34E-09	1.00E-06	1.55E-08	1.01E-08	629	627	747	**670± 70**	70	100
850	7.10E-07	1.82E-09	8.58E-07	1.93E-08	1.26E-08	391	390	472	**420± 50**	40	70
900	6.10E-07	2.85E-09	7.47E-07	2.36E-08	1.54E-08	214	214	262	**230± 30**	30	50

Temperature (°C)	From Kergoat et al. 2014 [151] (cited [154] for viscosity which cites [152])		From Lane et al. 1958 [152]	Stokes-Einstein (using η from [152] and r from [131])		Schmidt number of B^{3+} in FLiNaK					
	$\nu_{FLiNaK,2014}$ (m^2/s)	D_{B3+} (m^2/s)	$\nu_{FLiNaK,1958}$ (m^2/s)	$D_{B3+,CN3}$ (m^2/s)	$D_{B3+,CN4}$ (m^2/s)	**Sc** [151]	Sc_{recalc}	$Sc_{LaneKer}$	Sc_{avg}	$Sc_{SE,CN3}$	$Sc_{SE,CN4}$
700	1.25E-06	2.18E-09	1.44E-06	2.45E-07	2.23E-08	575	573	660	**600± 50**	6	60
750	1.02E-06	2.72E-09	1.19E-06	3.18E-07	2.89E-08	374	375	437	**400± 40**	4	40

78

800	8.40E-07	2.88E-09	1.00E-06	4.03E-07	3.67E-08	293	292	348	**310± 30**	2	30
850	7.10E-07	3.13E-09	8.58E-07	5.02E-07	4.56E-08	228	227	274	**240± 30**	2	20
900	6.10E-07	3.52E-09	7.47E-07	6.14E-07	5.58E-08	174	173	212	**190± 20**	1	10

3.1.2 Fluoroacidity and chromium

Fluoroacidity has been attributed to be the cause of the disproportionation of chromium in molten fluorides. That is, the concept of fluoroacidity has been used to explain why chromium exists in its multiple possible oxidation states (at a given redox potential) in various molten fluoride solvents (referred to as disproportionation). For chromium, this disproportionation is described by the equilibrium of Eqn. 3.3:

$$3CrF_2 = 2CrF_3 + Cr \quad \text{(Eqn. 3.3)}$$

$$K = (CrF_3)^2 / (CrF_2)^3 \quad \text{(Eqn. 3.4)}$$

where the 2+ oxidation state of chromium disproportionates to 2/3 of the 3+ oxidation state and 1/3 of the 0 oxidation state. A summary of studies quantifying the disproportionation of chromium in molten fluorides is provided in Table 3.4.

In the MSRE, the disproportionation of Cr^{2+} to Cr^{3+} and Cr^0 was found to depend on the concentration of ZrF_4 in a LiF-NaF-ZrF_4 melt (NaF-LiF, 40-60 mol%, 800°C) [155]. In melts with a larger concentration of ZrF_4, less dissolved chromium was present as Cr^{3+}, which was said to be indicative of the competition between acidic Zr^{4+} and Cr^{3+} for fluoride ions causing decreased stability of Cr^{3+} and thus a greater extent of Eqn. 3.3 proceeding to the left. Studies were performed in which CrF_3 and Cr^0 were added and allowed to equilibrate for 5 hours and in which CrF_2 was added, to check the reversibility of disproportionation. The same trends with ZrF_4 additions were observed, but the Cr^{3+}/Cr^{2+} ratios varied because of the activity of the deposited Cr metal was less than 1.

Similar tests were performed with LiF-BeF_2 (48–52 mol%) and LiF-BeF_2-ThF_4 (67–23-10 mol%) solvents to investigate the differences of melts with BeF_2 which the authors presumed to be less fluoroacidic than ZrF_4 (claimed as such "since [BeF_2] is a better fluoride donor for furnishing fluorides for complexing", without substantiation). Redman and co-workers concluded from their disproportionation studies that BeF_2-containing melts are more fluorobasic than their corresponding ZrF_4 mixtures (confirming their assumption) based on the finding that the degree of disproportionation in the melt with 52 mol% BeF_2 was approximately the same as in the melt with 35 mol% ZrF_4. They attribute disproportionation to fluoroacidity with the understanding that a higher ratio of Cr^{3+}/Cr^{2+} is indicative of a more fluorobasic mixture. Similar results are shown in [156], where the authors demonstrate, by Raman studies, that addition of fluorobasic LiF to FLiBe leads to Cr^{2+} disproportionation to Cr^{3+}. Qiu et al. studied the speciation of Cr corrosion products in molten FLiNaK using X-ray Absorption Near-Edge Structure spectroscopy (after quenching) and found the spectrum to approximately match that of CrF_3 [157]. Agreeing with the explanations of [158], Qiu et al. contend that, because of the fluorobasicity of FLiNaK, the higher valence Cr^{3+} can be stabilized by complexation with the available F^-, decreasing its chemical activity and consequently increasing the observed concentration of Cr^{3+} in the melt.

Redman and Weaver analyzed the filtrates of CrF_2 and CrF_3 additions to FLiNaK, 53NaF-47ZrF_4, 22NaF-55LiF-23ZrF_4 at 600°C and 800°C and concluded that "CrF_2 is not entirely stable in […] these solvents, although, when CrF_2 is the added constituent, the concentration of Cr^{2+} is generally higher than the concentration of Cr^{3+}" (see Additional data referenced in Chapter 3) [159]. The methods by which they identified the concentration of Cr^{2+} and $Cr_{(total)}$ are not stated. They observed an effect of the container material used (Ni versus Inconel (containing

14-17 wt% Cr)), stating that Cr^0 and possibly Fe^0 in the Inconel reacted with CrF_3, whereas the nickel container remained unoxidized.

Studies which indicate the disproportionation of chromium also give information about the solubility of chromium species in molten fluorides. Blood sought to directly measure CrF_2 solubility (equilibrium concentrations) in 62LiF-38BeF_2 in the temperature range from 750° to 850°C but equilibration was not reached after over three weeks. To make a measurement, the redox was fixed by H_2/HF to make an estimation of K for the reaction $CrF_2 + H_2 = Cr + 2HF$ [160]. Differences in the solvating ability of fluoride solvents has also been related to their fluoroacidity, with the understanding that fluorobasic melts are better able to solvate chromium (in any oxidation state) [158]. For example, Redman found that the solubility of CrF_2 at 600°C in 59NaF-41ZrF_4 was higher than the solubility in 53NaF-ZrF_4 [161], where NaF is fluorobasic and ZrF_4 is fluoroacidic [162].

As discussed in the previous section, the coordination environment of chromium is relevant to the interpretation of the impact of fluoroacidity on its diffusivity, as well as its speciation. Tetrahedral coordination has been observed for Cr^{2+} in molten alkali chlorides and octahedral coordination has been observed for Cr^{3+} [163], [164]. Rollet and Salanne and point out that in fluorides, however, steric hindrances prevent trivalent cations from fitting in the octahedral site, according to Raman spectra analysis [165]. Corradini et al. claim that, “It has been known for many years that when trivalent metal cations are dissolved in halide melts they are surrounded by a tightly coordinated shell of anions”, although the applicability of this statement to fluorides in addition to chlorides is unsupported [27]. If, for example, Cr^{3+} transport typically takes place by ligand-exchange (or hopping among fluorides with a strong degree of coordination), this would imply that the activity of dsF is more relevant to its diffusivity. If Cr cations diffuse as fluoro-complexes, fully solvated by fluorides, the activity of dsF is less relevant. The coordination environment of Cr^{2+} and Cr^{3+} in molten fluorides was studied via AIMD by Winner et al. and will be discussed in detail in the following section (3.2).

To summarize, fluoroacidity is related to chromium speciation and solubility:

- By the possibility that mixtures with a higher activity of dsF (more fluorobasic) can better stabilize Cr^{3+} (the higher oxidation state of Cr) than mixtures with low a_{dsF}
- By the relationship between solvent (F^-) activity and the ability to solvate chromium solutes of varied oxidation states (which is not necessarily directly proportional; note that incorporation of solutes may modify solvent activity).

Table 3.4. Disproportionation of chromium in molten fluorides in the literature. N/A means not available. Data listed as provided in each source.

Reference	Solvent (mole percent)	Added solute and quantity	Method (for distinguishing Cr^{2+} vs Cr^{3+}, determining total Cr in the melt)	Redox potential	Temperature (°C)	Ratio of Cr^{2+}/Cr^{3+}	Assumed coordination of Cr^{2+}	Assumed coordination of Cr^{3+}
Peng 2015 [47]	FLiNaK	600 to 1300 ppm CrF_2	Estimated concentration of Cr^{3+} using electrochemical calibration curve (from SWV current density of Cr^{3+}/Cr^{2+} reduction peak) and calculated Cr^{2+} concentration using disproportionation reaction (assumed speciation/coordination of the Cr^{2+} and $^{3+}$?); found Cr metal deposited in the bottom of the crucible using SEM-EDS and XRD.	N/A	600	Conversion ratio of Cr^{2+} to Cr^{3+}: 86.71% to 88.23%	N/A	N/A
Chan et al. 2022 [166]	FLiNaK	0.11 wt% CrF_3	Ratio of peak current densities from CV for Cr/Cr^{2+} and Cr^{2+}/Cr^{3+} used with diffusivities of Cr^{2+} and Cr^{3+} from [167] to calculate concentration ratio of Cr^{2+} and Cr^{3+} via the Randles-Sevcik equation.	N/A	600	1.99%	CrF^{3-} (postulated from $NaCrF_3$ and $KCrF_3$ in quenched sample, measured by XRD)	CrF_6^{3-} (postulated from K_3CrF_6, K_2NaCrF_6, Li_2NaCrF_6 in quenched sample, measured by XRD)_

82

Chan et al. 2022 [166]	FLiNaK	0.14 wt% CrF_3	" "	N/A	600	4.76%	CrF^{3-} " "	CrF_6^{3-} " "
Chan et al. 2022 [166]	FLiNaK	0.18 wt% CrF_3	" "	N/A	600	5.51%	CrF^{3-} " "	CrF_6^{3-} " "
Chan et al. 2022 [166]	FLiNaK	0.27 wt% CrF_3	" "	N/A	600	7.39%	CrF^{3-} " "	CrF_6^{3-} " "
Chan et al. 2022 [166]	FLiNaK	0.42 wt% CrF_3	" " ; Above saturation (solubility limit approximately 0.3wt% according to [168])	N/A	600	7.71% of CrF_3 converted to CrF_2	CrF^{3-} " "	CrF_6^{3-} " "
Redman and Weaver Sept 1955 (ORNL-1947) [159]	FLiNaK	4.8 wt% Cr (added as CrF_3)	12 hours equilibration, nickel container. 79±42ppm Ni total. Four replicates, with data shown as average ± standard deviation.	N/A	600	13±12 ppm Cr^{2+}, 0.27±0.06 wt% Cr total	N/A	N/A
Redman and Weaver Sept 1955 (ORNL-1947) [159]	FLiNaK	4.8 wt% Cr (added as CrF_3)	12 hours equilibration, nickel container. 58±22ppm Ni total. Four replicates, with data shown as average ± standard deviation.	N/A	800	18±17 ppm Cr^{2+}, 3.01±0.24 wt% Cr total	N/A	N/A
Redman and Weaver Sept 1955 (ORNL-1947) [159]	FLiNaK	3.8 wt% Cr (added as CrF_3)	5 hours equilibration, Inconel container. 88±81ppm Ni total. Duplicate data shown as average ± standard deviation.	N/A	800	800±280 ppm Cr^{2+}, 3.75±0.35 wt% Cr total	N/A	N/A
Redman Oct 1958 (ORNL-2626) [155]	48LiF-52BeF_2	2 wt% CrF_3, excess Cr metal	"chemical analyses [] of equilibrated samples contained in nickel filtration apparatus"; equilibration period of 5 hr at temperature; ensured below solubility limit; similar results at lower dilutions and temperatures.	N/A	800	CrF_3/CrF_2 = 0.15	CrF_2	CrF_3

83

Liu et al. 2020 [156]	FLiBe	0.20 wt% CrF_3, excess Cr metal	900 min equilibration; UV-Vis absorption with calibration curve based on the Beer-Lambert law.	N/A	600	~90%	N/A	CrF_6^{3-} (assumed, based on [48])
Redman Oct 1958 (ORNL-2626) [155]	67LiF-23BeF_2-10ThF_4	2 wt% CrF_3, excess Cr metal	5 hr equilibration, nickel apparatus.	N/A	800	CrF_3/CrF_2 = 0.4	CrF_2	CrF_3
Redman 1958	60LiF-40NaF	2 wt% CrF_3, excess Cr metal	5 hr equilibration, nickel apparatus.	N/A	800	1.32 wt% Cr^{2+}, 1.29 wt% Cr^{3+}	CrF_2	CrF_3
Redman Oct 1958 (ORNL-2626) [155]	60LiF-40NaF with 15 mol% ZrF_4	2 wt% CrF_3, excess Cr metal	5 hr equilibration, nickel apparatus.	N/A	800	wt% Cr^{2+}: 2.16 wt% Cr^{3+}: 0.66	CrF_2	CrF_3
Redman Oct 1958 (ORNL-2626) [155]	60LiF-40NaF with 25 mol% ZrF_4	2 wt% CrF_3, excess Cr metal	5 hr equilibration, nickel apparatus.	N/A	800	wt% Cr^{2+}: 2.28 wt% Cr^{3+}: 0.50	CrF_2	CrF_3
Redman Oct 1958 (ORNL-2626) [155]	60LiF-40NaF with 35 mol% ZrF_4	2 wt% CrF_3, excess Cr metal	5 hr equilibration, nickel apparatus.	N/A	800	wt% Cr^{2+}: 2.32 wt% Cr^{3+}: 0.46	CrF_2	CrF_3
Redman Oct 1958 (ORNL-2626) [155]	60LiF-40NaF with 47 mol% ZrF_4	2 wt% CrF_3, excess Cr metal	5 hr equilibration, nickel apparatus.	N/A	800	wt% Cr^{2+}: 2.54 wt% Cr^{3+}: 0.22	CrF_2	CrF_3
Redman Oct 1958 (ORNL-2626) [155]	60LiF-40NaF with 55 mol% ZrF_4	2 wt% CrF_3, excess Cr metal	5 hr equilibration, nickel apparatus.	N/A	800	wt% Cr^{2+}: 2.66 wt% Cr^{3+}: 0.18	CrF_2	CrF_3

84

Redman June 1956 (ORNL-2106) [169]	53NaF-47ZrF_4	9.6 wt% Cr (added as CrF2)	Starting molar ratio of Zr/Cr = 2.1. In filtrate, Zr/Na = 0.69±0.01. Duplicate data shown as average ± standard deviation.	N/A	600	5.35±0.49 wt% Cr^{2+}, 5.55±0.49 wt% Cr total	N/A	N/A
Redman June 1956 (ORNL-2106) [169]	53NaF-47ZrF_4	6.4 wt% Cr (added as CrF_2)	Starting molar ratio of Zr/Cr = 3.4. In filtrate, Zr/Na = 0.71±0.01. Duplicate data shown as average ± standard deviation.	N/A	600	3.45±0.07 wt% Cr^{2+}, 3.55±0.07 wt% Cr total	N/A	N/A
Redman June 1956 (ORNL-2106) [169]	53NaF-47ZrF_4	4.0 wt% Cr (added as CrF_2)	Starting molar ratio of Zr/Cr = 5.8. In filtrate, Zr/Na = 0.79±0.01. Duplicate data shown as average ± standard deviation.	N/A	600	2.05±0.07 wt% Cr^{2+}, 1.9 wt% Cr total	N/A	N/A
Redman June 1956 (ORNL-2106) [169]	53NaF-47ZrF_4	1.4 wt% Cr (added as CrF_2)	Starting molar ratio of Zr/Cr = 17. In filtrate, Zr/Na = 0.79±0.01. Duplicate data shown as average ± standard deviation.	N/A	600	0.66±0.01 wt% Cr^{2+}, 0.78±0.07 wt% Cr total	N/A	N/A
Redman & Weaver Sept 1955 (ORNL-1947) [159]	53NaF-47ZrF_4	1.0 wt% Cr (added as CrF_2)	50 ppm Ni total. 5 hours equilibration in nickel container. Chemical analysis (technique not specified) of filtrate.	N/A	600	0.40 ppm Cr^{2+}, 0.60 wt% Cr total	N/A	N/A

85

Redman & Weaver Sept 1955 (ORNL-1947) [159]	53NaF-47ZrF_4	0.1 wt% Cr (added as CrF_3)	70 ppm Ni total. 5 hours equilibration in nickel container. Chemical analysis (technique not specified) of filtrate. Duplicate data shown as average ± standard deviation.	N/A	600	0.07±0.02 ppm Cr^{2+}, 0.08 wt% Cr total	N/A	N/A
Redman & Weaver Sept 1955 (ORNL-1947) [159]	53NaF-47ZrF_4	0.88 wt% Cr (added as CrF_2)	53±18ppm Ni in filtrate. 5 hours equilibration in nickel container. Chemical analysis (technique not specified) of filtrate. Duplicate data shown as average ± standard deviation.	N/A	800	0.44±0.20 ppm Cr^{2+}, 0.81±0.08wt % Cr total	N/A	N/A
Redman & Weaver Sept 1955 (ORNL-1947) [159]	53NaF-47ZrF_4	12.0 wt% Cr (added as CrF_2)	288±25 ppm Ni total. 5 hours equilibration in nickel container. Chemical analysis (technique not specified) of filtrate. Duplicate data shown as average ± standard deviation.	N/A	800	9.2±0.1 ppm Cr^{2+}, 11.7±0.1 wt% Cr total	N/A	N/A
Redman & Weaver Sept 1955 (ORNL-1947) [159]	53NaF-47ZrF_4	4.0 wt% Cr (added as CrF_3)	280 ppm Ni total. 5 hours equilibration in nickel container. Chemical analysis (technique not specified) of filtrate. Duplicate data shown as average ± standard deviation.	N/A	800	1.6±0.1 ppm Cr^{2+}, 3.6 wt% Cr total	N/A	N/A

Redman & Weaver Sept 1955 (ORNL-1947) [159]	22NaF-55LiF-23ZrF_4	1.0 wt% Cr (added as CrF_2)	1 ppm Ni total. 5 hours equilibration in nickel container. Chemical analysis (technique not specified) of filtrate. Duplicate data shown as average ± standard deviation.	N/A	600	0.60±0.01 wt% Cr^{3+}, 0.86±0.11 wt% Cr total	N/A	N/A
Redman & Weaver Sept 1955 (ORNL-1947) [159]	22NaF-55LiF-23ZrF_4	1.0 wt% Cr (added as CrF_2)	15 ppm Ni total. 5 hours equilibration in nickel container. Chemical analysis (technique not specified) of filtrate.	N/A	800	0.65 wt% Cr^{3+}, 0.95 wt% Cr total	N/A	N/A
Redman & Weaver Sept 1955 (ORNL-1947) [159]	22NaF-55LiF-23ZrF_4	1.0 wt% Cr (added as CrF_3)	200 ppm Ni total. 5 hours equilibration in nickel container. Chemical analysis (technique not specified) of filtrate.	N/A	800	0.37 wt% Cr^{3+}, 1.05 wt% Cr total	N/A	N/A
Redman & Weaver Sept 1955 (ORNL-1947) [159]	22NaF-55LiF-23ZrF_4	2.0 wt% Cr (added as CrF_2)	93±88 ppm Ni total. 5 hours equilibration in nickel container. Chemical analysis (technique not specified) of filtrate. Duplicate data shown as average ± standard deviation.	N/A	600	1.00±0.01 wt% Cr^{3+}, 2.03±0.17 wt% Cr total	N/A	N/A

87

Redman & Weaver Sept 1955 (ORNL-1947) [159]	22NaF-55LiF-23ZrF_4	5.0 wt% Cr (added as CrF_2)	33±11 ppm Ni total. 5 hours equilibration in nickel container. Chemical analysis (technique not specified) of filtrate. Duplicate data shown as average ± standard deviation.	N/A	800	3.2±0.1 wt% Cr^{3+}, 4.6±0.1 wt% Cr total	N/A	N/A
Redman & Weaver Sept 1955 (ORNL-1947) [159]	22NaF-55LiF-23ZrF_4	4.0 wt% Cr (added as CrF_3)	160 ppm Ni total. 5 hours equilibration in nickel container. Chemical analysis (technique not specified) of filtrate.	N/A	800	1.2 wt% Cr^{3+}, 4.2 wt% Cr total	N/A	N/A
Redman Sept 1956 (ORNL-2157) [161]	52LiF-48ZrF_4	2.5 wt% Cr (added as CrF_2)	Starting molar ratio of Zr/Cr = 10. In filtrate, Zr/Li = 0.82±0.01 (nominal 0.92). Duplicate data shown as average ± standard deviation.	N/A	600	1.28±0.04 wt% Cr^{2+}, 1.57±0.04 wt% Cr total	N/A	N/A
Redman Sept 1956 (ORNL-2157) [161]	52LiF-48ZrF_4	5.0 wt% Cr (added as CrF_2)	Starting molar ratio of Zr/Cr = 4.9. In filtrate, Zr/Li = 0.76 (nominal 0.92). Duplicate data shown as average ± standard deviation.	N/A	600	2.2±0.3 wt% Cr^{2+}, 2.5±0.2 wt% Cr total	N/A	N/A
Redman Sept 1956 (ORNL-2157) [161]	52LiF-48ZrF_4	10.0 wt% Cr (added as CrF_2)	Starting molar ratio of Zr/Cr = 2.2. In filtrate, Zr/Li = 0.72±0.01 (nominal 0.92). Triplicate data shown as average ± standard deviation.	N/A	600	4.7±0.2 wt% Cr^{2+}, 5.8±0.1 wt% Cr total	N/A	N/A

88

Redman Sept 1956 (ORNL-2157) [161]	52LiF-48ZrF_4	10.0 wt% Cr (added as CrF_2)	Starting molar ratio of Zr/Cr = 2.2. In filtrate, Zr/Li = 0.87±0.03 (nominal 0.92). Duplicate data shown as average ± standard deviation.	N/A	800	6.3±0.2 wt% Cr^{2+}, 9.5 wt% Cr total	N/A	N/A
Redman Sept 1956 (ORNL-2157) [161]	52LiF-48ZrF_4	20 wt% Cr (added as CrF_2)	Starting molar ratio of Zr/Cr = 0.9. In filtrate, Zr/Li = 0.85±0.14 (nominal 0.92). Duplicate data shown as average ± standard deviation.	N/A	800	13.5±0.9 wt% Cr^{2+}, 19.1±0.1 wt% Cr total	N/A	N/A
Redman Sept 1956 (ORNL-2157) [161]	59NaF-41ZrF_4	1.5 wt% Cr (added as CrF_2)	Starting molar ratio of Zr/Cr = 15. In filtrate, Zr/Na = 0.69 (nominal 0.70). Duplicate data shown as average ± standard deviation.	N/A	600	1.1±0.1 wt% Cr^{2+}, 1.3±0.01 wt% Cr total	N/A	N/A
Redman Sept 1956 (ORNL-2157) [161]	59NaF-41ZrF_4	6.0 wt% Cr (added as CrF_2)	Starting molar ratio of Zr/Cr = 3.5. In filtrate, Zr/Na = 0.68±0.02 (nominal 0.70). Duplicate data shown as average ± standard deviation.	N/A	600	4.7±0.1 wt% Cr^{2+}, 5.4 wt% Cr total	N/A	N/A
Redman Sept 1956 (ORNL-2157) [161]	59NaF-41ZrF_4	10.0 wt% Cr (added as CrF_2)	Starting molar ratio of Zr/Cr = 2.0. In filtrate, Zr/Na = 0.70±0.01 (nominal 0.70). Duplicate data shown as average ± standard deviation.	N/A	600	8.1±0.1 wt% Cr^{2+}, 8.5±0.6 wt% Cr total	N/A	N/A
Redman Sept 1956 (ORNL-2157) [161]	59NaF-41ZrF_4	12.0 wt% Cr (added as CrF_2)	Starting molar ratio of Zr/Cr = 1.5. In filtrate, Zr/Na = 0.68±0.01 (nominal 0.70). Duplicate data shown as average ± standard deviation.	N/A	800	9.1±0.4 wt% Cr^{2+}, 10.8±0.7 wt% Cr total	N/A	N/A

Redman Sept 1956 (ORNL-2157) [161]	59NaF-41ZrF_4	20 wt% Cr (added as CrF_2)	Starting molar ratio of Zr/Cr = 0.8. In filtrate, Zr/Na = 0.69±0.01 (nominal 0.70). Duplicate data shown as average ± standard deviation.	N/A	800	17.5 wt% Cr^{2+}, 19.3 wt% Cr total	N/A	N/A
Redman Sept 1956 (ORNL-2157) [161]	52KF-48ZrF_4	5.0 wt% Cr (added as CrF_2)	Starting molar ratio of Zr/Cr = 4.2. In filtrate, Zr/K = 0.89±0.01 (nominal 0.92). Duplicate data shown as average ± standard deviation.	N/A	600	4.6±0.4 wt% Cr^{2+}, 4.8 wt% Cr total	N/A	N/A
Redman Sept 1956 (ORNL-2157) [161]	52KF-48ZrF_4	10 wt% Cr (added as CrF_2)	Starting molar ratio of Zr/Cr = 1.9. In filtrate, Zr/K = 0.92±0.01 (nominal 0.92). Duplicate data shown as average ± standard deviation.	N/A	600	7.0±0.1 wt% Cr^{2+}, 6.9±0.1 wt% Cr total	N/A	N/A
Redman Sept 1956 (ORNL-2157) [161]	52KF-48ZrF_4	10 wt% Cr (added as CrF_2)	Starting molar ratio of Zr/Cr = 1.9. In filtrate, Zr/K = 0.93±0.02 (nominal 0.92). Duplicate data shown as average ± standard deviation.	N/A	800	4.8±6.5wt% Cr^{2+}, 9.7 wt% Cr total	N/A	N/A
Redman Sept 1956 (ORNL-2157) [161]	52KF-48ZrF_4	20 wt% Cr (added as CrF_2)	Starting molar ratio of Zr/Cr = 0.8. In filtrate, Zr/K = 0.86±0.03 (nominal 0.92). Duplicate data shown as average ± standard deviation.	N/A	800	16.7±1.2 wt% Cr^{2+}, 19.5±0.1 wt% Cr total	N/A	N/A

Redman Dec 1956 (ORNL-2221) [170]	60RbF-40ZrF_4	1 wt % Cr (added as CrF_2)	5 hours equilibration (noted as possibly too slow for reduction to be complete). 98±18 ppm Ni total. Duplicate data shown as average ± standard deviation.	N/A	600	0.65±0.12 wt% Cr^{2+}, 1.00±0.03 wt% Cr total	N/A	N/A
Redman Dec 1956 (ORNL-2221) [170]	60RbF-40ZrF_4	5 wt % Cr (added as CrF_2)	“”,75±7 ppm Ni total. Duplicate data shown as average ± standard deviation.	N/A	600	1.4±0.1 wt% Cr^{2+}, 1.8±0.1 wt% Cr total	N/A	N/A
Redman Dec 1956 (ORNL-2221) [170]	60RbF-40ZrF_4	5 wt % Cr (added as CrF_2)	“”,65 ppm Ni total. Duplicate data shown as average ± standard deviation.	N/A	800	4.1±0.1 wt% Cr^{2+}, 5.1±0.1 wt% Cr total	N/A	N/A
Redman Dec 1956 (ORNL-2221) [170]	60RbF-40ZrF_4	10 wt % Cr (added as CrF_2)	“”, Ni total N/A. Duplicate data shown as average ± standard deviation.	N/A	800	8.8±0.2 wt% Cr^{2+}, 9.4±0.1 wt% Cr total	N/A	N/A
Redman Dec 1956 (ORNL-2221) [170]	60RbF-40ZrF_4	1 wt % Cr (added as CrF_3)	Reduction of Cr^{3+} to Cr^{2+} by the nickel container. 150±70 ppm Ni total. Duplicate data shown as average ± standard deviation.	N/A	600	0.40±0.03 wt% Cr^{2+}, 0.67±0.03 wt% Cr total	N/A	N/A
Redman Dec 1956 (ORNL-2221) [170]	60RbF-40ZrF_4	5 wt % Cr (added as CrF_3)	“”,170±20 ppm Ni total. Duplicate data shown as average ± standard deviation.	N/A	600	0.36±0.03 wt% Cr^{2+}, 0.62±0.04 wt% Cr total	N/A	N/A
Redman Dec 1956 (ORNL-2221) [170]	60RbF-40ZrF_4	5 wt % Cr (added as CrF_3)	“”,530±160 ppm Ni total. Duplicate data shown as average ± standard deviation.	N/A	800	0.65±0.01 wt% Cr^{2+}, 3.1 wt% Cr total	N/A	N/A
Redman Dec 1956 (ORNL-2221) [170]	60RbF-40ZrF_4	10 wt % Cr (added as CrF_3)	“”,1070±220 ppm Ni total. Duplicate data shown as average ± standard deviation.	N/A	800	0.80±0.07 wt% Cr^{2+}, 2.2±0.3 wt% Cr total	N/A	N/A

91

3.1.3 Studies of chromium electrochemical behavior in molten fluorides

Multiple studies have investigated the electrochemical behavior of chromium in molten FLiNaK. Table 3.5 presents a summary of the existing electrochemical studies of chromium in FLiNaK and FLiBe. A snapshot of a CV from each study is included for a qualitative comparison of the data. All studies attribute the two pairs of peaks to the Cr^0/Cr^{2+} and Cr^{2+}/Cr^{3+} redox couples. Results of the analyses of these peaks are summarized below. The electrochemical signature of Cr in FLiNaK from these studies serves as a benchmark for the novel data presented in this chapter.

Cr^0 ←→ Cr^{2+} in FLiNaK

- **Reversibility and reactant/product solubility:** Quasi-reversible [48], [171], insoluble-soluble
  - Slow at higher temperatures [48]
- **Rate limited by:** Diffusion [47], [48], [171], [172], [173] (linear dependence of peak current on (scan rate)$^{1/2}$)
- **Speciation:** $Cr + 3F^- \leftrightarrow CrF_3^- + 2e^-$
  - Wu et al. does not specify the intermediate valence state but calculates n = 0.8 from the peak separation in the CV with consecutive redox peaks and infers it to be Cr^{2+} [171]
  - Wu et al. observed an asymmetric reduction peak with the Cr reduction peak, which they attributed to nucleation effects upon deposition [171]
- Peng et al. used a quasi-reference electrode (QRE) but observed the Cr^0/Cr^{2+} redox peak around 1.15 V vs K/K^+ (308 ppm Cr^{3+} in FLiNaK at 600°C, scan rate = 200 mV/s) [47]
- Wu et al. observed that the anodic peak potential shifted in the oxidizing direction with an increase in the scan rate [171]. In contradiction, Yoko and Bailey observed that both the oxidation and reduction peaks shifted in the oxidizing direction with decreasing scan rate, decreasing temperature, and increasing concentration of Cr^{3+} [48].

Cr^{2+} ←→ Cr^{3+} in FLiNaK

- **Reversibility and reactant/product solubility:** Reversible according to [47], [167], [171], quasi-reversible according to [48] (suggested some complications from chemical reactions), soluble-soluble
  - Yoko and Bailey found the reduction product to be soluble at 983°C and insoluble but still electroactive below 893°C
- **Rate limited by:** Diffusion [47], [171], [172] (linear dependence of peak current on (scan rate)$^{1/2}$)
- **Speciation:** $CrF_3^- + 3F^- \leftrightarrow CrF_6^{3-} + e^-$ [167]
- Sharp peak when scan is wide (attributed to overlap with the other Cr peak), but broad, rounded peak when the peak redox potential is scanned in isolation [167]
- Reduction peak was found to not change with scan rate [47]. Reduction peak was observed to be only distinct at higher scan rates and higher temperatures (otherwise it appeared to be more of a plateau) [48].

The studies varied in their materials, temperatures, and methods. Limitations of, challenges, and differences interpretation of the existing studies include:

- **The use of quasi-reference electrodes.** Most studies report CVs and oxidation/reduction potentials vs Pt QREs. The thermodynamically predicted oxidation potentials of chromium

are typically not referenced. Oxidation/reduction peaks in CVs in the literature are attributed to chromium species because of their appearance after chromium additions, not because of their appearance at calculated thermodynamic redox potentials.

- **The electrochemical correlations used for analysis of D, such as the Randles-Ševčík and Berzins-Delahay equations.** The Randles-Ševčík equation is relevant for reversible, soluble oxidized species, soluble reduced species electrochemical system. It is additionally based on the assumption that there is only one species (oxidized *or* reduced) initially present. Chromium is divalent in some molten fluorides including FLiNaK, limiting the applicability of the Randles-Ševčík equation. Wu et al. used the Randles-Ševčík equation to calculate $D(Cr^{3+})$ for Cr^{2+}/Cr^{3+} [171]. Wang and Zhang [167] adopted the theory of Keightley et al. [174] in which ratio of D(reduced species) to D(oxidized species) can be predicted by ΔE_p since the $CD^{1/2}/CD^{1/2}$ ratio is dependent only on the potential difference between the forward and reverse peaks. The Berzins-Delahay equation is used for soluble-insoluble systems, but it can only be applied to one-step charge transfer reactions. Wu et al. used the Berzins-Delahay equation to calculate $D(Cr^{2+})$ from Cr^{2+}/Cr^{0} [171]. Rappleye and Fuller discuss the applicability of various correlations for electrodeposition providing examples of molten chloride salts [175].
- **Differences in the peak separation for the consecutive charge transfer reactions for the 3+ and 2+ oxidation states of chromium.** As described above, all of the studies reviewed attribute the two pairs of peaks to the Cr^{0}/Cr^{2+} and Cr^{2+}/Cr^{3+} redox couples, but the peak separation between the redox couples varies across studies.
- **The different chromium species in FLiNaK.** Studies varied in what chromium (fluoride) species was added, how it was added, and how the chromium concentration was determined. In most cases, CrF_2 or CrF_3 were added to the melt or solid, with no further analysis of the dissolved chromium content. The concentration of chromium was assumed to be the concentration that was added. Yoko and Bailey added CrF_3 or K_3CrF_6 to different studies and observed no difference in the electrochemical behavior of Cr^{3+} given the different Cr^{3+} species [48]. They also found that the electrochemical behavior of a melt with CrF_2 was qualitatively the same as when Cr^{3+} was used. Zakharova et al. [172] added excess CrF_3 and quantified chromium after electrochemical studies. They did not specify the technique used for elemental analysis. They found the Cr concentration in saturated melt (after addition of CrF_3) at 530°C to be < 0.1 wt% (method not specified) [172].

As explained in Section 3.1.2, the disproportionation of Cr^{2+} to Cr^{3+} and Cr^{0} has been observed to occur particularly in mixtures with a high activity of dissociated fluorides, like FLiNaK. Yoko and Bailey believed the disproportionation reaction to be slow and undetected by the scan rates used for their electroanalytical studies (100-50,000 mV/s). All the previous studies of chromium in FLiNaK used scan rates in this range, with most from 100 to 200 mV/s (Table 3.5). In their study in which they added 8 wt% CrF_2 to FLiNaK, Yoko & Bailey observed that "small amounts of Cr metal deposited on the surface of the Ni container after a week's experiment" [48].

The diffusivities of Cr^{2+} and Cr^{3+} have been previously measured and modeled in FLiBe and FLiNaK and are plotted versus temperature in Figure 3.3. It is generally observed that Cr^{2+} diffuses greater than or equal to one order of magnitude faster than Cr^{3+}. This suggests that Cr^{3+}, with its higher charge density, forms stronger coordination complexes with larger hydrodynamic radii, which diffuse slower. Outliers in the diffusivity measurements include Wang et al.'s 2016 measurement [176] using electrochemical impedance spectroscopy (which is highly dependent on the cell model and was possibly affected by natural convection, contrary to the authors' assumptions) and Wang and Zhang's 2020 measurement using chronopotentiometry [167].

Table 3.5. Summary of electroanalytical studies of chromium in molten fluorides. "Major" peak refers to the left peak attributed to chromium (Cr^0/Cr^{2+}). "Minor" peak refers to the right peak attributed to chromium (Cr^{2+}/Cr^{3+}).

	Reference	Sample CV	Temp (°C)	Cr concentr (species added) (method of addition)	Scan rate shown (mV/s)	Major peak separation (V) ΔE_p	Minor peak separation (V) ΔE_p	WE/RE/CE
FLiNaK solvent	Wang and Zhang 2020 [167]	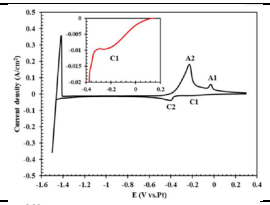	600	9.08E-5 mol/cm^3 (CrF_2) (added to solid)	100	0.229-0.246	~0.2	W/Pt/graphite
	Zakharova et al. 2020 [172]	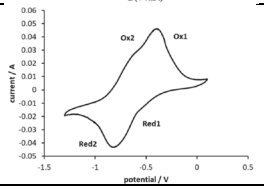	527	0.061+-0.003 wt% (CrF_3) (sampled after excess added, method of quantification not specified)	100	0.25	Convoluted	W/W/unknown
	Wu et al. 2018 [171]	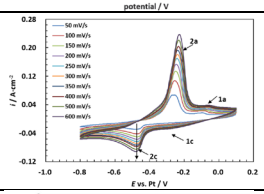	700	0.285 wt% (CrF_3) (added to solid)	100	0.24	~0.21	W/Pt/W
	Peng et al. 2015 [47]	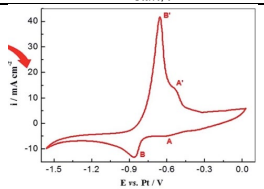	600	(308 ppm shown) [58 to 1500 ppm] (CrF_3) (added to melt)	200	0.21	0.11	Pt/Pt/graphite
	Peng et al. 2015 [47]	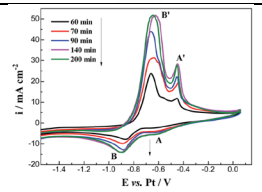 Different holding times.	600	(1300 ppm shown) [600-1300 ppm] (CrF_2) (added to melt)	100	0.21	0.11	Pt/Pt/graphite

94

FLiNaK solvent	Yoko and Bailey 1984 [48]	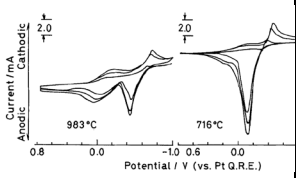	612-983 [983 (left) & 716 (right) shown here]	(0.10 mol/l) [0.07 to 0.13 mol/l] (CrF_3 or K_3CrF_6)	100, 500, 800	~0.31 (716°C)	~0.22 (716°C)	Pt/Pt plate/glassy carbon
FLiBe solvent	Doniger et al. 2019 [177]	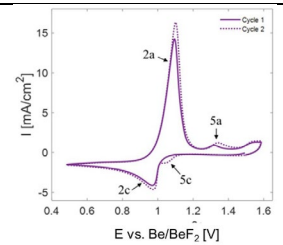	650	286 ppm Cr (CrF_2) ("added to the salt"; measured by ICP-OES, tested in triplicate, sampling method not provided)	80	~0.13	Convoluted (not reversible)	Mo/Mo/glassy carbon

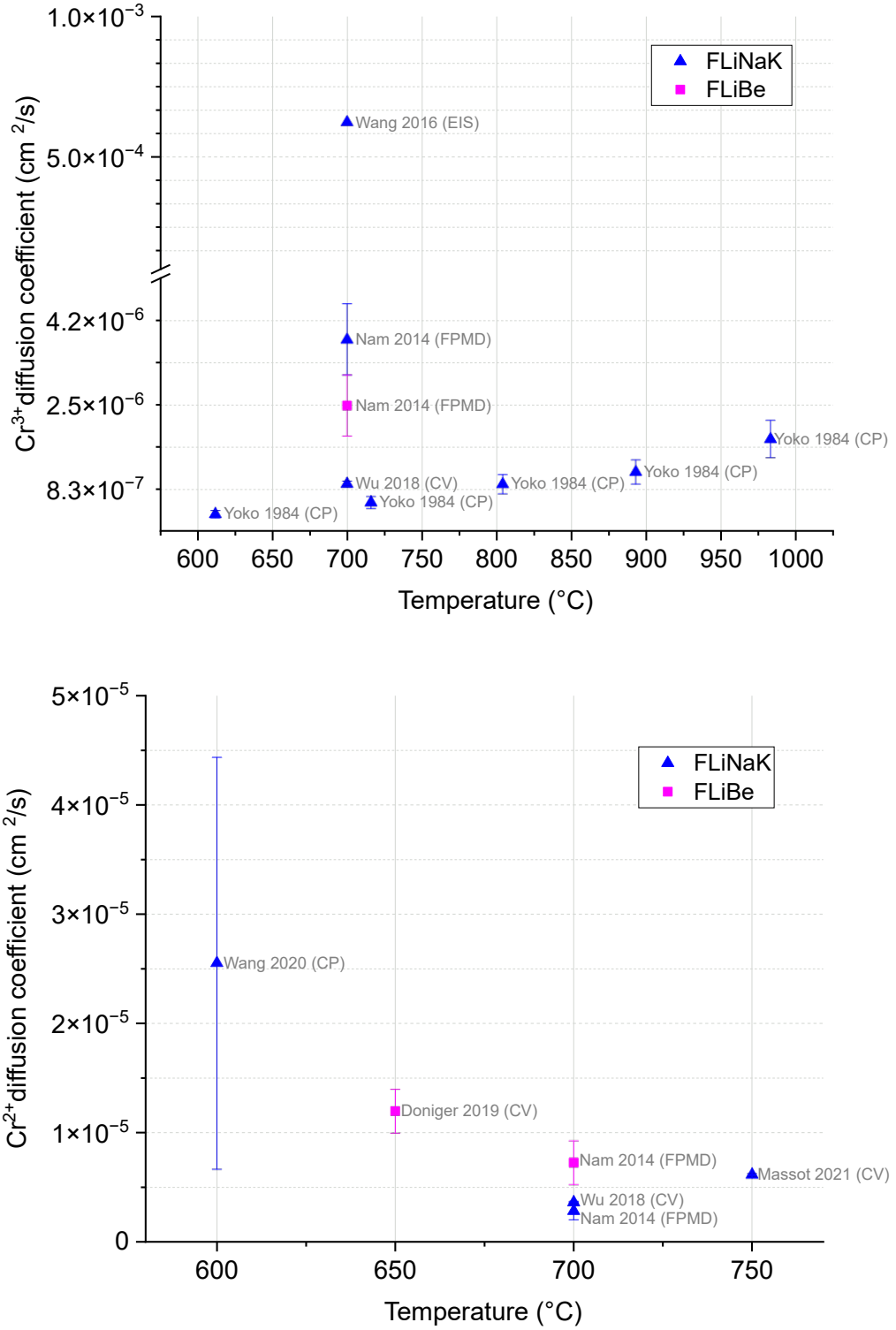

Figure 3.3. Diffusion coefficient of Cr^{3+} (top) and Cr^{2+} (bottom) in FLiNaK and FLiBe. CP = chronopotentiometry [48], [167], CV = cyclic voltammetry [171], [177], [178], EIS = electrochemical impedance spectroscopy [176], FPMD = first-principles molecular dynamics [102].

Yoko and Bailey comment that their calculated diffusion coefficients for Cr^{3+} in FLiNaK seem to be low considering the diffusion coefficients of nickel [179] and titanium [180] in molten FLiNaK [48]. They suggest that this might indicate the existence of larger complex anions such as CrF_6^{3-}, pointing out that Cr^{3+} has a maximum ligand field stabilization energy, meaning that among transition metal ions, Cr^{3+} has one of the most stabilizing electron arrangements since all three valence electrons exist in lower-energy d orbitals [48]. Because of this, Cr^{3+} forms stable complexes which are slow to exchange ligands. This is consistent with the slower diffusivities of Cr^{3+} compared to Cr^{2+}.

There exist few data in the literature on the diffusivity of chromium in FLiBe, but for the data shown in Figure 3.3, we see that the effect of the solvent on Cr diffusivity depends on the oxidation state of Cr. For Cr^{3+}, we can attribute the slower diffusion in FLiBe to FLiBe's higher viscosity and higher degree of acidity. For the lower-charge Cr^{2+}, the smaller chromium complexes affect diffusivity more than the solvent viscosity, and experiments show faster diffusion in FLiBe compared to FLiNaK.

3.2 AIMD simulation and interpretation

AIMD performed by Nicholas Winner served as a starting point for the experiments presented in Chapter 3. Interpretation of simulations of mixtures of 2KF-NaF, FLiBe, and 3LiF-AlF_3 with and without Cr^0, Cr^{2+}, and Cr^{3+} led to a more nuanced understanding of chromium solvation by oligomers in molten fluorides, described in this subsection after presentation of some simulation details which are relevant to their interpretation and to provide evidence of the validity of their interpretation.

3.2.1 Description of simulations from Winner et al. 2021

The fluorides modeled by AIMD (2KF-NaF, 3LiF-AlF_3, FLiBe) were chosen to represent a range of fluoroacidities, as well as to represent diversity in valency and coordination number. Stoichiometric ratios of the fluoride pairs were chosen such that Be^{2+} would be 4-fold coordinated and Al^{3+} would be 6-fold coordinated. In selecting the ratio for KF and NaF, it was considered that both cations are 4-fold coordinated but K^+ has a higher valence. Additionally, FLiBe was selected for its technological relevance, and 2KF-NaF and 3LiF-AlF_3 were selected as examples containing monovalent and trivalent cations, respectively.

Classical force fields were used to attain the initial structure of the mixtures, which then were input to the AIMD simulations. Simulations lasted between 38 and 51 ps, with an equilibration time of 5 ps and a 2 fs timestep. All three mixtures were modeled at 700°C, which is below the melting point of 2KF-NaF and 3LiF-AlF_3. Since nucleation of the solids takes longer than the timescale of the model, it is possible to model the salts as liquids below their melting point. To confirm that chromium remained in its prescribed oxidation state, the magnetic moment of the system was tracked. Charge neutrality upon chromium cation addition was maintained by removing weakly complexing cations, with the understanding that our goal was to examine possible competition for F^- between cations, so the ratio of fluorides to cations was kept constant. Each simulation cell consisted of approximately 100 atoms to ensure the cell was large enough to avoid periodic boundary conditions; this was checked by ensuring that the radial distribution function reached a value close to 1 within half the largest periodic length.

3.2.2 Fluoroacidities and buffering capacities of the simulated salts

Whereas AlF_3 and BeF_2 contribute acidic behavior to their mixtures, the 2KF-NaF composition is strongly basic, meaning that it forms only weak associates. Winner et al. give evidence for this by calculating the cation-anion cage-correlation times (τ) for each ion pair. The cage correlation time is the exponential decay constant which represents the time in which ~63% of the ion pair complexes change their state. As such, longer cage correlation times indicate greater stability of the complex. In 2KF-NaF, both Na-F and K-F have $\tau < 1$ ps. In FLiBe, Be-F was calculated to have $\tau = 24.6(8)$ ps, and in 3LiF-AlF_3, Al-F has $\tau = 13.3(8)$. For Li-F in both of the acidic mixtures, τ is approximately the same (around 0.4 ps). Given these differences, Be-F and Al-F are considered strong associates, whereas K-F, Na-F, and Li-F are said to be weak associates. Greater detail on the complexation and coordination environments of these basic cations is presented in a work by Frandsen et al. who studied the liquid structure of FLiNaK using AIMD and neutron scattering [30]. They found that the strongest ionic correlations were between Li and F, which had the shortest bond length, with a bond length that is approximately 0.2 Å shorter in the liquid than in the solid (consistent with a decrease in CN of Li by F in the liquid (CN =4) compared to the solid (CN = 6)) [30]. Most other peaks in the g(r) and partial g(r)s were broad, indicative of a low degree of ordering, consistent with the understanding of FLiNaK as a basic, dissociated melt.

Winner et al.'s study emphasized the importance of considering characteristics of acidic complexes in molten fluorides in addition to the quantity of basic dsF in order to fully characterize fluoroacidity. By definition, fluorobasicity depends on the quantity of dsF, whereas acidic behavior is lent by bridging fluorides (brF) and under-coordinated cation centers (ucC, or cations which can accommodate a higher coordination number). As seen in Figure 3.4, considering the fraction of F^- which are dissociated, 3LiF-AlF_3 is more basic than FLiBe. Considering the quantity of brF and ucC normalized to the number of cations in the simulation cell, 3LiF-AlF_3 is also more acidic than FLiBe. The balance of acidic and basic species existing in the same melt led to the definition of *acid-base buffering capacity* in molten fluorides. Functionally, buffering capacity describes the ability of a fluoride to produce dsF upon consumption of dsF (perhaps caused by dissolution of a solute) meaning that the system is able to maintain its fluoroacidity upon the addition of solutes. Physically, this means that there is some flexibility in the system, such as the ability to accommodate various coordination numbers, which allows for the coordination of cation centers to adapt to the addition of solutes. The ability to break and form bridges without a substantial energy change might also be an element of flexibility which contributes to a fluoride's acid-base buffering capacity. To summarize, acid-base buffering capacity refers to the melt's ability to stabilize its fluoroacidity via reversible complexation.

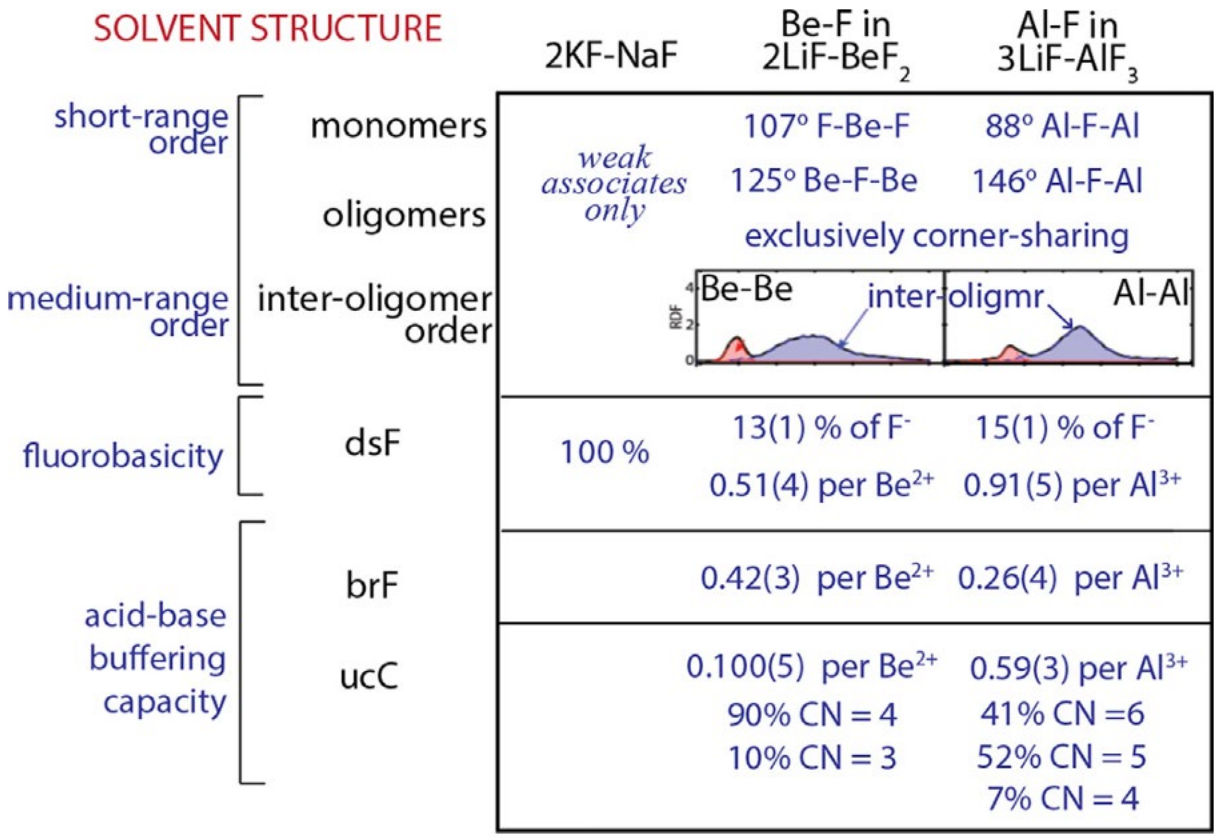

Figure 3.4. Graphical description of the structure of 2KF-NaF, FLiBe, and 3LiF-AlF_3 reproduced from Winner et al. 2021 [19].

Similarly, we might interpret the ordering between oligomers in light of acid-base buffering capacity. As seen in the snapshot in Figure 3.4 and enlarged in Figure 3.7, the second peak of the Be-Be RDF (which is representative of inter-oligomer ordering of beryllium, or beryllium ions which do not share a common neighbor) is more broad than the second peak of the Al-Al RDF. Be-Be inter-oligomer ordering then is more distributed across a broader range of distances (with most beryllium ions being 4 to 6 Å apart compared to most aluminum ions being 5 to 6 Å apart). The degree of oligomeric ordering in 3LiF-AlF_3 is higher than in FLiBe.

Al^{3+} has an ionic radius which is approximately twice that of Be^{2+} (Table 3.6). Since Al^{3+} is larger and more highly charged, it can accommodate more F^- coordinates since more and higher coordination numbers are geometrically and energetically accessible. Be^{2+} is smaller and more polarizing than Al^{3+} (Be^{2+} has a higher charge density), leading to the distortion of the F^- electron cloud and partial covalent character of Be-F bonds, according to Fajans' rules. The lower polarizing power of Al^{3+} means more diffuse electron interactions compared to the localized electron density overlap occurring in semi-covalent Be-F bonds. Further, the screening caused by other local ions causes the weakening of the effective electrostatic attraction within the ionic Al-F bond. As such, the greater ionic behavior of octahedral Al^{3+} complexes means that ligands are more easily exchanged without large energy costs.

Table 3.6. Characteristics of Be^{2+} and Al^{3+} relevant to their bonding in molten fluoride mixtures.

Cation	Charge	Ionic radius (Å) [131]	Charge density (z/r)	Electron config.	Bonding type with F^-	Coordination geometry	Observations from Winner et al.'s simulations
Be^{2+}	2+	0.27	7.41	[He] (empty 2s/2p)	Significantly covalent (directional and localized)	Tetrahedral (sp3-like)	Shorter, longer-lived Be-F bonds; less ordering between oligomers
Al^{3+}	3+	0.53	5.66	[Ne] (empty 3s/3p)	Mostly ionic	Octahedral (electrostatic packing)	Longer, shorter-lived Al-F bonds; more ordering between oligomers

These differences in acidic cation–F bonds give rise to a system ($3LiF\text{-}AlF_3$) which has longer and weaker cation–F bonds but more ordering between oligomers and a system (FLiBe) which has stronger, longer-lived cation–F bonds and less ordering between oligomers, where intra-oligomer ordering is evidenced by the secondary cation–cation peak in the RDF (see again Figure 3.4 and Figure 3.7). Since Al-F bonds are more flexible, it is possible for $Al_xF_{z-y}^{(z-y-3x)}$ units to adopt geometries that maximize favorable electrostatic interactions between oligomers. In contrast, BeF_4^{2-} tetrahedra are held rigidly by covalent character, making it more difficult to optimize oligomer packing and leading to a lesser degree of oligomeric ordering. Thus, where FLiBe forms covalent networks facilitated by sterics and hybridization, $3LiF\text{-}AlF_3$ favors maximizing electrostatic stabilization through charge balance and ionic packing.

Fluoroaluminates' ability to reorient and align is more fundamentally caused by their ionic, octahedral bonds (facilitated by the size, charge, and electron configuration of Al^{3+}) which give rise to multiple possible coordination numbers and more weakly maintained Al-F-Al bridges. Thus, we can relate the concept of acid-base buffering capacity to the nature of the acidic species in a melt. Building from the concept introduced by Winner et al., **I contend that the ionic or covalent nature of the acidic species influences how reversibly the cation binds fluoride and how effective it is as a buffer.** In an applied sense, I hypothesize that the more ionic and reversible the solvent cation bonding is, the more effective the solvent species are at buffering fluoride activity. Thus, the definition of acid-base buffering capacity might be refined to connect to the ionicity or covalency of the bonds formed by acidic species in the melt.

This concept of buffering capacity as the ionicity of acidic species is loosely related to (but not to be mistaken with) the concept of *ionicity* in ionic liquids, a *transport*-based concept which describes how closely the behavior of an ionic liquid matches that of an ideal ionic conductor. It

is generally understood that low ionicity, or deviation from ideality, means that ions behave as associates with greater molecular character or a higher degree of covalency. Ionicity is defined by Angell and Walden as the ratio of measured conductivity to that estimated by the Nernst-Einstein equation [181], [182]. Ionicity describes the fraction of ions available to participate in conduction, but it is limited in its relation to the chemical activity of ions, which MacFarlane et al. point out may depend more strongly on the degree of association of ions in the ionic liquid [182].

In addition to room temperature ionic liquids, comparison of the molar conductivities (related to ionicity) of high temperature molten salts have been performed [183]. Harris argues, however, that directly evaluating the ionicity of molten salts like alkali metal halides leads to conclusions which are incongruent with existing structural understandings from molecular dynamics. For example, complex-forming $ZnCl_2$ appears as an "ideal"[a] liquid and fully-dissociated NaCl appears as superionic in the Angell sense. Harris claims that Angell-Walden ionicity is only useful as a qualitative ranking of conductivity at a given viscosity [184].

Overall, a more nuanced understanding of acid-base behavior allows us to similarly avoid the pitfalls of a purely thermophysical understanding as in the transport-focused quantification of ionicity for ionic liquids. Whereas fluoroacidity has been simply understood as the activity of dsF and has been generally used to explain certain aspects of corrosion phenomena, interpretation of Winner et al. leads to the conclusion that examining also acidic contributions, particularly, we contend, the nature of acidic bonding, may be valuable in understanding the relevance of fluoroacidity to corrosion.

3.2.3 Chromium in the simulated salts

As introduced previously, prior to the study by Winner et al. it was generally understood that more fluorobasic salts were more corrosive than fluoroacidic salts due to their ability to accommodate corrosion products by dissolution via dsF. In addition to solvation by dsF, Winner et al. found that chromium was solvated by incorporation into the polymeric network of the associates of acidic melts. Figure 3.5 shows a snapshot of a $Be_3F_{11}Cr^{3-}$ oligomer in which the Cr^{2+} is solvated by brF, shared with Be^{2+} cations. The Cr^{2+} shares a brF with an under-coordinated Be^{2+}. In both FLiBe and 3LiF-AlF_3, chromium with an oxidation state of 0 was observed to bond directly with the acidic cation (Be^{2+} or Al^{3+}), as evidenced by the RDF in Figure 3.7.

[a] The ideal reference is defined by Angell and Walden as 1 mol/L aqueous KCl at 25°C, which has transport numbers and viscosity nearly independent of concentration (up to approximately 2.5 mol/L). This previously led to the understanding that K^+ and Cl^- had negligible effects on the structure of water. [184]

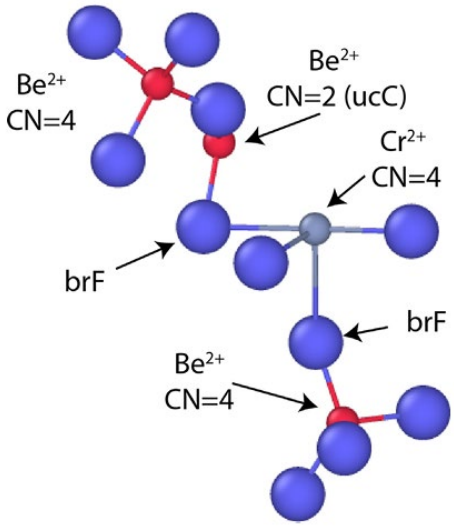

Figure 3.5. Oligomer present in simulation of FLiBe with Cr^{2+}. Be^{2+} are labeled as such, along with their coordination number. Cr^{2+} is labeled with its CN. F^- are purple and unlabeled, with the two visible bridging fluorides labeled as such. Reproduced from Winner et al. 2021.

The degree to which chromium was solvated by dsF or by oligomers was found to be dependent on the solvent fluoride composition (implying its fluoroacidity) and the oxidation state of chromium (redox potential). Figure 3.6 illustrates some trends and characteristics of chromium solvation in simulated solvents. The effects of solvation structure and oxidation state are stated, but there are also the considerations of network rigidity (related to the flexibility discussed as relevant to acid-base buffering capacity) as well as cation coordination behavior (looking at the chemical differences of Be^{2+} and Al^{3+} cations).

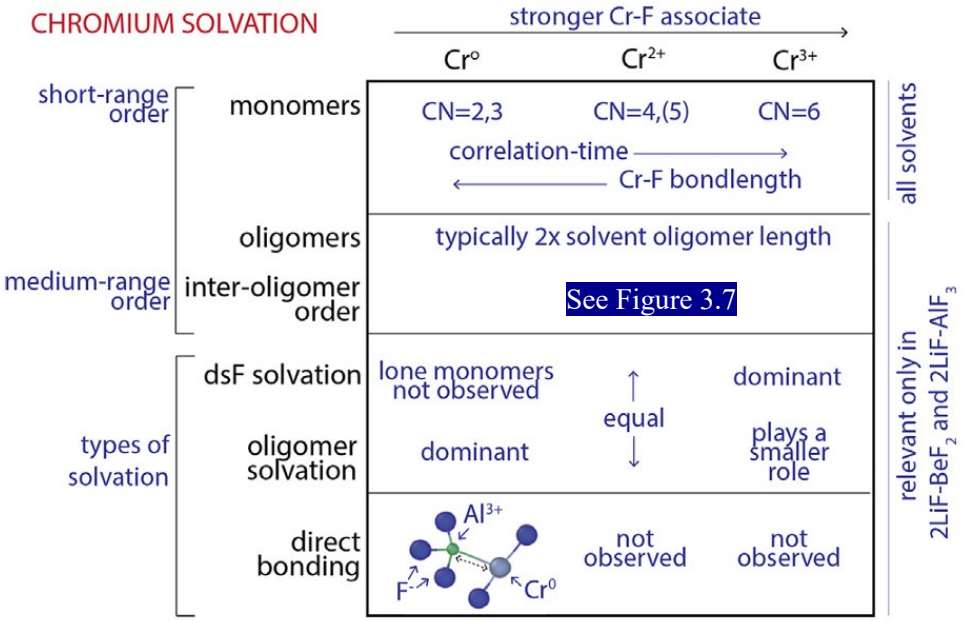

Figure 3.6. Graphical description of chromium solvation from Winner et al. 2021.

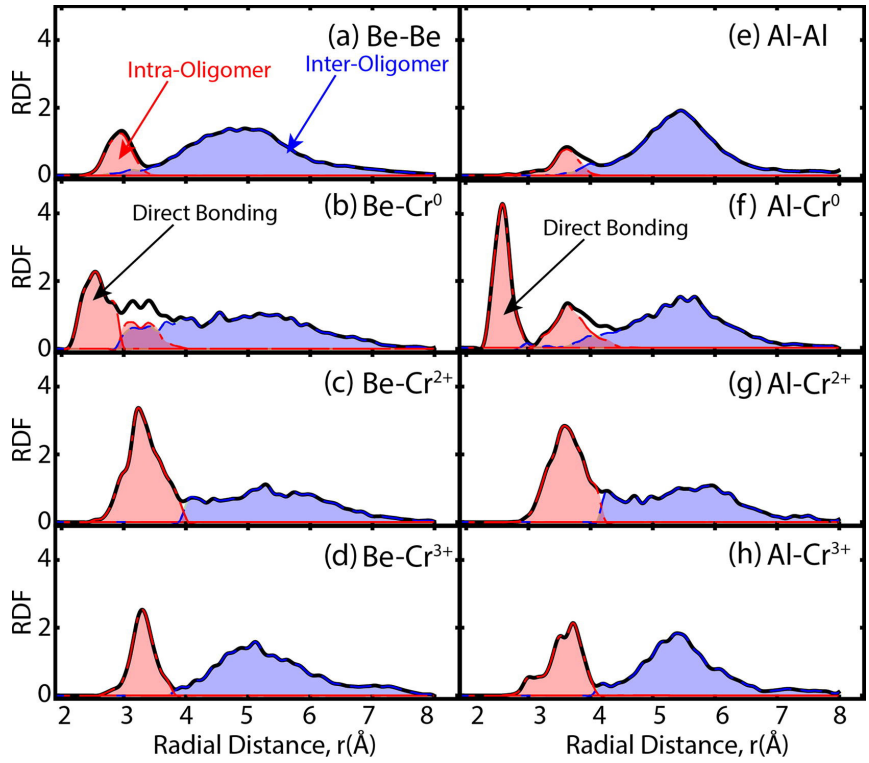

Figure 3.7. Radial distribution functions for cation pairs in FLiBe (a-d) and 3LiF-AlF_3 (e-h) with chromium of various oxidation states. Modeled at 700°C. Reproduced from Winner et al. 2021.

3.2.4 Oxyfluoride complex formation

Complexation in molten fluorides has been studied previously in the case of oxyfluoride complexes. Stefanidaki et al. performed neodymium oxide additions to NdF_3-LiF-KF-MgF_2 melts, quantifying oxide solubility as a function of solvent fluoride composition and identifying possible Nd-oxyfluoride complex ions present in the mixtures using Raman spectroscopy [185]. Elizarova added various quantities of gadolinium oxide to KCl-KF and applied a reducing potential, finding that the reduced species was an Fe-Gd alloy when an iron cathode was used and an oxyfluoride species (proposed to be GdOF based on X-ray diffraction of the cathode deposit) when a Mo or GC cathode was used [186]. Additionally, Chamelot et al. have identified and examined evidence of tantalum oxyfluoride formation in LiF-NaF [187] in their studies of electrodeposition of Ta from added K_2TaF_7. They attributed a pair of CV peaks to tantalum oxyfluoride, citing previous spectroscopic observations of $TaOF_6^{3-}$ in KCl-KF (Amosov 1965, unable to be accessed). Most relevant to our study of *chromium* in molten fluorides, Song et al. studied chromium oxyfluorides in FLiNaK and FLiBe with additions of ZrF_4 and LiF to alter the fluoroacidity [49]. They observed the solubility of Cr_2O_3 to increase with the increase in concentration of ZrF_4 in FLiNaK as well as with increasing concentration of basic LiF to acidic FLiBe-ZrF_4.

3.3 Methods

3.3.1 Salt preparation

2KF-NaF used was prepared from dried KF (Materion) and NaF (Materion). The constituent fluorides were measured on an analytical balance inside an inert argon glovebox with O_2 levels <1 ppm and H_2O levels <1 ppm. The constituent fluorides were then baked at 400±20°C for approximately 4 hours total in nickel and glassy carbon crucibles. When baked the KF sintered and became a solid powder agglomerate in the form of the crucible. After the 4 hours of baking the ~60 g mass of NaF had lost approximately 0.1 g of weight and the ~100 g mass of KF had lost approximately 1 g of weight. The KF was further dried for another 3.5 hours at 400°C (O_2: 0.4 ppm, H_2O: 0.0 ppm) until the mass change was <0.1 g. It continually formed a compressed powder clump and appeared grayish white. 2KF-NaF single phase liquid forms around 750°C [188]. 2KF-NaF is considered to be the most basic of the compositions, forming only weak associates. Simulated values for the fraction of dsF for each composition are in Figure 3.4.

FLiNaK was provided by ORNL. It originated from a commercial vendor and was likely purified via hydrofluorination. It was stored, handled, and melted in an inert argon glovebox. Its composition was characterized in a Round Robin study using Inductively Coupled Plasma – Mass Spectroscopy to verify its composition and inert gas fusion to measure oxygen content. FLiNaK (46.5LiF-11.5NaF-42KF) is considered to be highly basic with only weak associates. Lithium serves as a weaker base, however, and is slightly more acidic than K and Na.

3LiF-AlF_3 was prepared from constituent components (LiF, Materion; AlF_3, Materion). When AlF_3 was dried (in a nickel crucible) using the baking method detailed above (400°C for 2.5 hours), it turned darker gray. When AlF_3 was heated to 850°C, it remained powdered and appeared black. Dried salt was mixed to form 3LiF-AlF_3, but after heating to 1090°C, the salt had not melted. Fresh salt was mixed which had not been previously baked. The salt with un-baked AlF_3 melted around the expected melting point and was used for electroanalytical studies. 3LiF-AlF_3 single phase liquid forms around 800°C [189]. AlF_3 is considered to be more acidic than BeF_2 given differences in activity measured by [148].

FLiBe for the study with Cr_2O_3 additions was from the University of Wisconsin Heat & Mass Group (Jar B). FLiBe for the study with CrF_3 additions was prepared from constituent fluorides (LiF, Sigma Aldrich; BeF_2, Materion) which had not been previously baked. FLiBe experiments took place in a separate glovebox which was designated for experiments containing beryllium compounds. The beryllium gloveboxes are inert argon gloveboxes with O_2 levels operationally <10 ppm and H_2O levels <1 ppm which operate under negative pressure and are located in a designated workspace which maintains surface and airborne contamination levels below free-release, with quarterly monitoring. FLiBe is considered acidic due to the network formation of BeF_4^{2-} tetrahedra.

To introduce chromium to the fluorides, CrF_3 (99.98% metals basis, Fisher) and Cr_2O_3 (99.99% trace metals basis, anhydrous, Sigma-Aldrich) were added either while the salt was molten or after it had re-solidified after a baseline scan. The time allowed for the dissolution of chromium (or allowed equilibration time) ranged from a few minutes to a few hours, as time allowed, to test for changes in peak intensity as a function of time.

3.3.2 Apparatus and electrochemical cell design

3.3.2.1 Electrochemical cells

Separate electrochemical cells were used for experiments which used beryllium containing salts and those which did not. The non-Be cell was designed by Tony Consiglio [190] with design input and construction support from cell users Haley Williams and Lorenzo Vergari. All electrochemical cells were contained within inert argon gloveboxes. The non-Be electrochemical setup consisted of:

- Omega 115 V / 700 W ceramic cylindrical furnace
- Electrode probe located inserted in an ISO-K flange, with an adjustable compression-sealed feedthrough
- Probe includes eight copper wires for connecting electrodes of desired materials
- Stepper motor assembly for adjusting electrode probe position at the scale of 1 mm
- Type N thermocouples connected to LabView program for temperature monitoring and control (program developed at UW Madison)

The beryllium cell was similar to the non-Be, with modifications listed below. It was designed by Michael Borrello with design input and construction support from cell users Haley Williams and Timothy Pickarski.

- Lower-gauge copper wires within the electrode probe for increased durability
- Manual control of electrode probe height using screw
- Type K thermocouple connected to Omega PID controller
- Type N thermocouples connected to Omega TC reader for temperature monitoring

A Faraday cage was added to the later FLiBe experiment to minimize the interference effects of the furnace on electroanalytical measurements. Its efficacy in reducing noise in electrochemical measurements was not established.

Both the non-Be and Be electrochemical cells were primarily operated with an open-cell design, with the top flange suspended and held by the setup frame. In this mode of operation, the crucible is placed directly in the furnace (with a peripheral alumina crucible for secondary containment), allowing for visual access of the salt throughout the experiment. The bottom part of the stainless steel cell is unused, such that the crucible is open to the glovebox environment throughout the experiment. Unless otherwise stated, the temperature reported for all data is the temperature adjacent to the crucible (thermocouples were not placed in the molten salt).

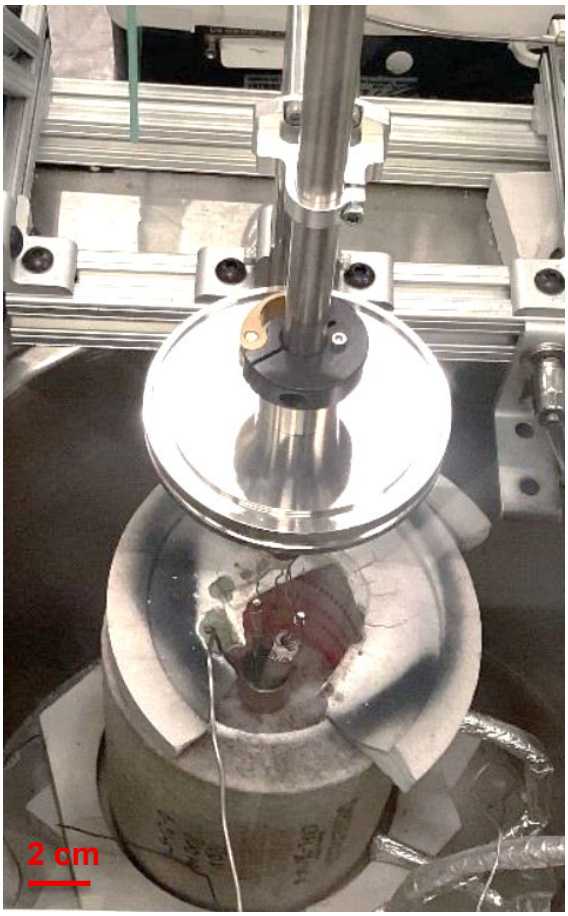

Figure 3.8. Electrochemical cell used for FLiNaK, 2KF-NaF, and 3LiF-AlF_3.

3.3.2.2 Containment

Salts were contained in glassy carbon and nickel crucibles. These crucibles were placed in a large alumina crucible for secondary containment, which fit snugly in the cylindrical furnace. Firebrick (calcium silicate) was used as insulation at the top of the open furnace/crucible. All ceramics were baked prior to use in experiments for off-gassing of oxygen and moisture. All salt preparation and experiments took place in custom-designed argon gloveboxes produced by LC Technology. Oxygen and moisture levels were recorded periodically for most of the studies and are reported in Table 3.7.

3.3.2.3 Electrodes

Electrodes were connected to the copper wires of the electrochemical cell using copper crimp connectors. For some of the experiments, copper might have been temporarily and occasionally submerged in the solvent in the event that the electrode connectors became submerged. Electrode surface areas were determined by photographing the electrodes frozen in the salt. Electrode submersion depth was adjusted using a stepper motor for the non-Be salts and manually for FLiBe studies. A summary of electrode materials is included in Table 3.7, but here we list descriptions of the electrode systems for each melt:

- For studies of FLiNaK and 2KF-NaF, gold was used as a working electrode, with platinum counter electrodes and platinum quasi-reference electrode. 3LiF-AlF_3 used a tungsten working electrode and platinum counter and quasi-reference electrodes.
- FLiBe experiments used both Au and Pt working electrodes, Pt counter and quasi-reference electrodes.
- The FLiBe sample with added Cr_2O_3 used a glassy carbon counter electrode for its larger surface area as well as a silver/silver fluoride thermodynamic reference electrode (TRE). This TRE, consisting of a Ag rod in pure AgF, contained within a BN sleeve with a LaF_3 membrane and hole similar to that in [59], was being tested for its stability [191]. Later studies confirmed that the AgF reacted with the BN to form fluoroborates and Ag metal, thus the listing of an Ag/AgF TRE is best described by an insulated Ag rod.

Because of the lack of TREs across all experiments, voltammograms were shifted after data collection to be referenced versus solvent metal deposition, or the reduction limit of the electrochemical window. For example, for studies of FLiBe, CVs were shifted so the potential of zero current for the Be deposition peak was located at 0 V. For smaller scans or those that did not reach the reduction potential for the solvent metal, full-window scans were performed periodically in order to identify major shifts or trends of shifts. Dynamic reference electrode techniques were not applied since the presence of chromium would affect the activity of the deposited metal and therefore its reduction potential. Although these shifts might be minor, the periodic full-window scans allow for a simple check of a shifting reference.

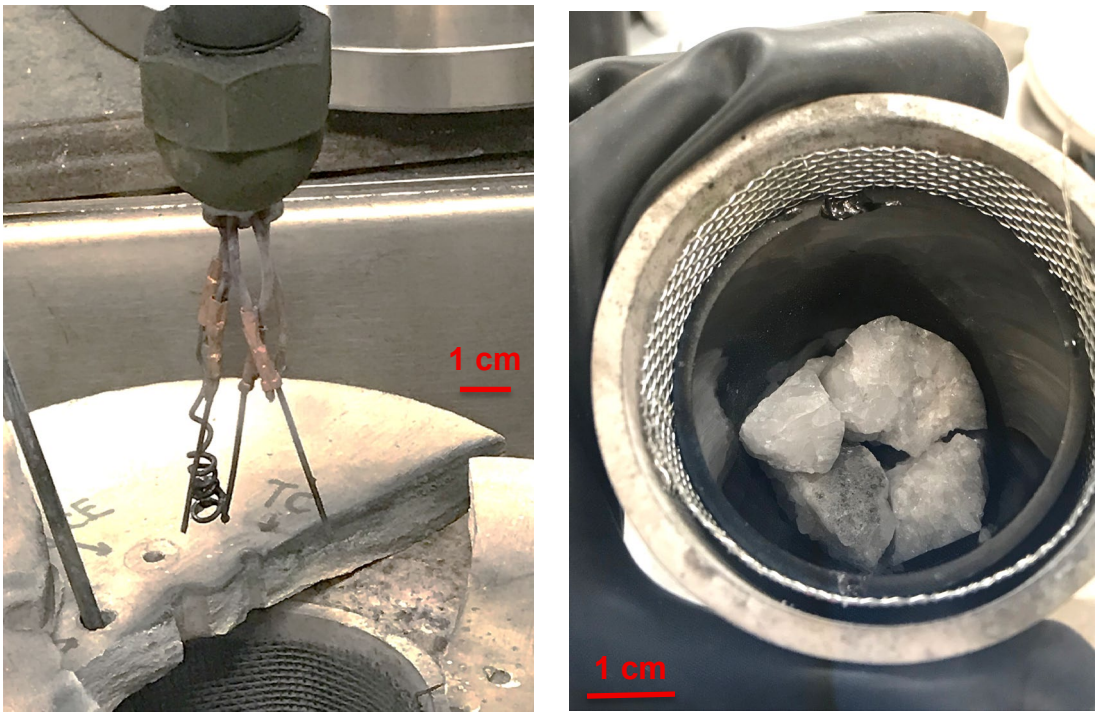

Figure 3.9. Left: Electrodes used for FLiBe + CrF_3 study (contrast edited for greater visibility of the electrodes and copper crimp connectors). Right: FLiBe in glassy carbon crucible, placed in alumina outer crucible for secondary containment with a Faraday cage insert constructed from stainless steel mesh.

3.3.3 Electroanalytical studies

Gamry Reference 600 and Interface 1000E potentiostats were used for measurements of the open circuit potential (OCP), cyclic voltammograms (CV), and square wave voltammograms (SWV). When CVs are presented, typically the second cycle is shown as that is when the system showed consistent behavior. If other cycles are shown, they are labeled as such. Unless otherwise stated, all CVs are scanned in the oxidizing direction first, then in the reducing direction. Estimation of the number of electrons transferred from characteristics of electroanalytical scans may be useful for identifying possible oxidation/reduction reactions. A derivation for the method of calculating number of electrons transferred from SWV is included in the Appendix Section 6.3.

3.4 Results & Analysis

Electroanalytical data from the experiments listed in Table 3.7 are presented in the following section. Cyclic voltammograms are presented, annotated with relevant thermodynamic data when appropriate.

Table 3.7. Summary of studies conducted on chromium in molten fluorides.

Solvent	Solute	Temp (°C)	WE/RE/CE	Electroanalytical studies	GB conditions
FLiNaK	None (blank)	460±20	Au/Pt/Pt	LSV, CV	0.3 ppm O_2 0.0 ppm H_2O
FLiNaK	0.3 wt% Cr^{3+} added as 0.0301 g CrF_3 to 4.3162 g FLiNaK	550 to 600	Au (0.16 cm^2)/Pt/Pt	CV, SWV	0.3 ppm O_2 0.0 ppm H_2O
2KF-NaF	None (blank)	780±5	Au/Pt/Pt (GC crucible)	CV, SWV	Unknown
2KF-NaF	0.3 wt% Cr^{3+} added as CrF_3 (0.0192 g CrF_3 added to frozen 2.9573 g 2KF-NaF)	780±5	Au/Pt/Pt (GC crucible, same sample)	CV, SWV	4 ppm O_2 12 ppm H_2O
FLiBe	None (blank)	650	Au/Pt/Pt	CV, CP (attempting DBRE)	Unknown
FLiBe	0.3 wt% Cr^{3+} added as 0.47 wt% Cr_2O_3	600 to 700	Pt (0.99 cm^2)/(Ag/AgF)/GC	CV, SWV (with conditioning)	10.6-39 ppm O_2 0-3.4 ppm H_2O
3LiF-AlF_3	None (blank)	860	W/Pt/Pt	CV	Unknown

3LiF-AlF_3	0.3 mol% Cr^{3+} added as CrF_3	860	W/Pt/Pt	CV, SWV	Unknown
FLiBe	None (blank)	600±15	W/Pt/Pt	CV, SWV	10-11.5 ppm O_2 0 ppm H_2O
FLiBe	0.0294 g CrF_3 added to 42.7361 g FLiBe (added to frozen salt then melted)	600±15	W/Pt/Pt	CV, SWV	8-25 ppm O_2 0 ppm H_2O

3.4.1 Basic melts

Cyclic voltammograms and square wave voltammograms were performed on FLiNaK and 2KF-NaF with and without chromium, added as CrF_3. FLiNaK's composition might be approximated as 4KF-NaF-5LiF to give a better sense of the difference in composition between the two melts. As a reference point, the order of basicity of the alkali fluorides has been characterized as [162]: KF, NaF, LiF (from most fluorobasic to most fluoroacidic).

3.4.1.1 FLiNaK

After the addition of CrF_3 to FLiNaK, the redox shifted approximately 0.8 V in the oxidizing direction (including drift in the QRE) according to the shift in the major reduction potential which is assumed to be attributed to the K/K^+ redox couple. The Nernst equation predicts that the addition of 0.3 wt% of CrF_3 (0.064 mol Cr^{3+}/kg FLiNaK) at 460°C would shift the potential approximately 0.2 V in the oxidizing direction, assuming the Cr^{3+}/Cr^{2+} is the dominant redox active pair and $[Cr^{2+}] << [Cr^{3+}]$. Figure 3.10 shows cyclic voltammograms before and directly after addition of CrF_3, referenced to the potential of zero current of the major reduction peak. The CV with CrF_3 shows a higher background current as well as peaks which appear around 0.35 V vs K/K^+, 1.2 V vs K/K^+. There also exists a peak at approximately 1.7 V vs K/K^+ which was not accessed during the blank scans.

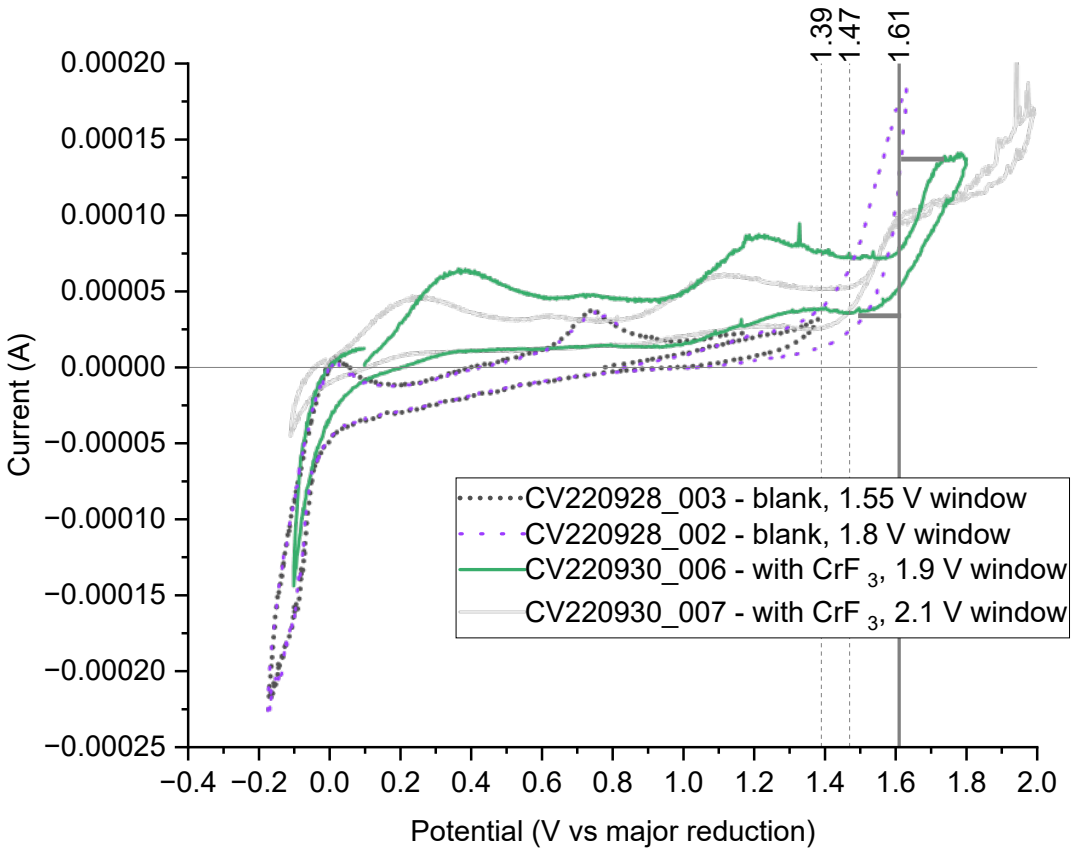

Figure 3.10. FLiNaK before and after CrF_3 addition. WE: Au, CE: Pt, QRE: Pt. Varied window limits. Scan rate: 30 mV/s. Referenced to major reduction peak (presumably K/K^+), which shifted the scans approximately 0.9 V in the oxidizing direction from the quasi-reference potential. 460±20°C.

From the ΔG tabulated in HSC, the standard reduction potentials for the Cr/Cr^{2+} and Cr^{2+}/Cr^{3+} couples were calculated (from data of pure components) and are listed in Table 3.8. The rightmost column provides the redox potentials for Cr/Cr^{2+} and Cr^{2+}/Cr^{3+} vs K/K^+ taking into account the molality of K^+ in FLiNaK and varied activities of Cr^{2+} and Cr^{3+}, estimated from the added concentration of chromium and from the Cr^{2+}/Cr^{3+} ratio observed in previous studies. Specifically, Redman and Weaver reported that the Cr^{2+}/Cr^{3+} ratio varied from 0.01 to 0.09 when 4.8 wt% Cr^{3+} was added to FLiNaK at 600°C, with varying concentrations of nickel present due to the nickel crucible **[192]**, so these ratios were used to calculated the shifted potential of the Cr^{2+}/Cr^{3+} couple, which would be 1.47 and 1.61 vs K/K^+ in FLiNaK, for each respective ratio.

Since Cr^{3+} was added to the melt, if it remained as Cr^{3+} we would expect the Cr^{3+}/Cr^{2+} peak to be predominantly a reduction peak. In Figure 3.10 we observe a peak which may be centered around 1.61 V vs K/K^+ in FLiNaK, as indicated by the reference line which is the equidistant centerline between the peaks in CV220930_006. We note that the blank CV220928_002 also shows oxidizing current in this region but with no reverse peak, such that it appears to be the limit of the electrochemical window. Further, the following scan of FLiNaK with CrF_3 (CV220930_007) shows a plateau or shelf in current in this region. Overall, with the background

current observed in the FLiNaK + CrF_3 CVs, it is challenging to distinguish redox peaks. If we assume all Cr^{3+} has been converted to Cr^{2+} and an activity of deposited Cr^0 is 0.5 to 1, the Cr^{2+}/Cr^0 redox peak would be predicted to occur around 1.37 to 1.39 V vs K/K^+ in FLiNaK. However, no peaks can be distinguished in this region, due to the background current.

Table 3.8. Standard reduction potentials calculated from ΔG from HSC 10.5.7.3. The rightmost column provides the Nernstian potential assuming the deviation from standard behavior provided in brackets.

Reaction	E^o(440°C)	E^o(460°C)	E^o(480°C)	E^o(600°C)	E^o(780°C)	E(460°C)
	V vs K/K^+					V vs K (a = 1) / K^+ (a ~ molality in FLiNaK, 10.2 mol/kg)
$CrF_2 = Cr + F_{2\,(g)}$	1.46	1.45	1.43	1.35	1.23	1.39 [total conversion of Cr^{3+} to Cr^{2+} → 0.3 wt% Cr^{2+}, $a_{Cr0} = 1$] 1.37 [0.3 wt% Cr^{2+}, $a_{Cr0} = 0.5$]
$CrF_3 = CrF_2 + 0.5F_{2\,(g)}$	1.91	1.91	1.90	1.90	1.89	1.47 [$Cr^{2+}/Cr^{3+} = 0.01$, see [192, p. 64]] 1.61 [$Cr^{2+}/Cr^{3+} = 0.09$, see [192, p. 64]]
$KF = K + 0.5F_{2\,(g)}$	0.00	0.00	0.00	0.00	0.00	0.00 (0.15 V vs standard state K/K+)
$NaF = Na + 0.5F_{2\,(g)}$	-0.08	-0.08	-0.08	-0.07	-0.07	---
$LiF = Li + 0.5F_{2\,(g)}$	-0.56	-0.56	-0.56	-0.56	-0.57	---

Since the CVs with CrF_3 presented in Figure 3.10 were collected shortly after CrF_3 addition and showed variation in consecutive scans, it is plausible that the system was not at equilibrium, meaning that the concentration of dissolved chromium species was not at equilibrium. Further evidence for this was the presence of a grayish scum-like phase on the surface of the melt. As such, the system was allowed to equilibrate at temperature (400 to 600°C) for several hours and subsequent scans were performed at higher scan rates, shown in Figure 3.11. Note that holding at

temperature was not fully continuous, and the FLiNaK + CrF_3 was frozen and re-melted several times.

The solubility of CrF_3 in FLiNaK has been thermodynamically predicted to be approximately 0.075 wt% at 800°C, which is an order of magnitude lower than the quantity added in this study [168]. However, the solubility was predicted to be about 0.3 wt% at 600°C when K_3CrF_6 is negligibly present in the liquid phase [168]. Data from Redman show the total chromium concentration to be on average 0.22 wt% at 600°C when CrF_3 was added to FLiNaK and equilibrated for 5 hours [193, p. 105]. Relative to Faradaic current, background current can become more dominant at low scan rates if the redox reaction is sluggish or mass-transport-limited.

Most authors of previous studies saw peaks attributed to chromium appear in the -0.4 to -0.1 V vs Pt QRE region or in the -0.9 to -0.4 V vs Pt QRE region (Table 3.5). We note that this is not a stable reference potential but rather gives some sense of the potential of the redox reaction of interest with respect to the overall redox condition of the melt. As such, if the redox potential of the melt is similar and the system is at equilibrium, we might expect the chromium peaks to appear at a roughly similar potential. In our study, the peaks that appeared upon CrF_3 addition and after several cycles of freezing and re-melting the salt (in an attempt to reach an equilibrium condition) were in the -0.4 to -0.1 V vs Pt QRE region, as shown in Figure 3.11. Note that this scan was started at 0 V vs OCP which approximately coincided with peak B. Thus, the peaks appeared in the order B, B', A', A for all of the following FLiNaK CVs. If shifted 0.9 V in the oxidizing direction, as was done in Figure 3.10 to reference the peaks vs K/K^+, peaks would appear at 0.5 to 0.8 V vs K/K^+, although this is a rough estimate which does not account for reference electrode drift. The predicted peak location would be 1.4 to 1.6 V vs K/K^+ in FLiNaK (Table 3.5).

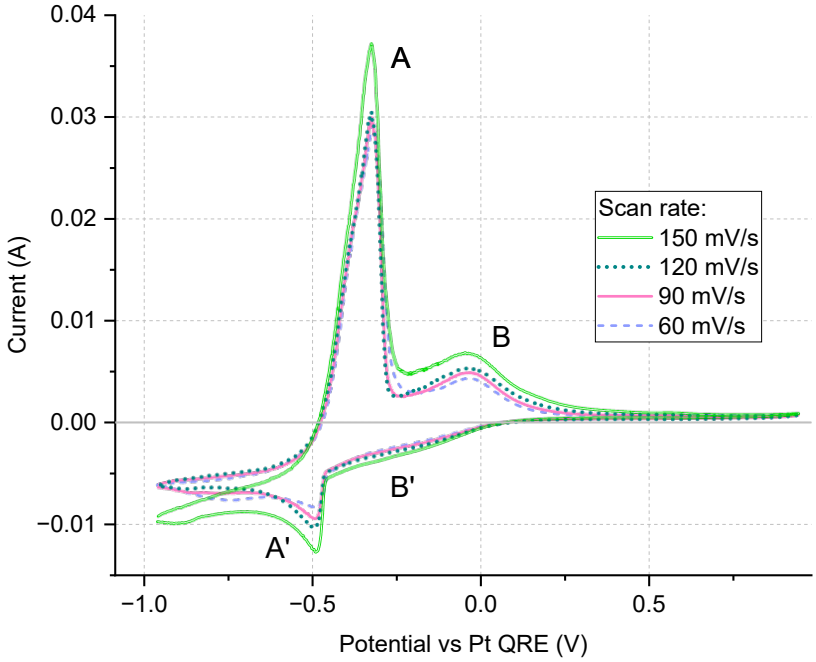

Figure 3.11. FLiNaK with 0.3 wt% Cr^{3+} added as CrF_3 with varied scan rate. WE: Au (0.16 cm^2)/, CE: Pt, QRE: Pt. 550±10°C, held at temperature for 4 hours.

The peaks labeled A, A', B, and B' in in Figure 3.11 are qualitatively similar to the cyclic voltammograms of chromium in FLiNaK summarized in Table 3.5, with the oxidation peaks of a higher intensity than the reduction peaks. Table 3.9 summarizes the peak-to-peak separation (ΔE_p) for the cathodic and anodic A/A' and B/B' couples along with their currents. ΔE_p(A/A') is consistently around 0.17 V, whereas the ΔE_p (B/B') is around 0.15 V. In the previous studies summarized in Table 3.5, the A/A' peak separation varied from 0.21 to 0.25 V for scan rates from 100 to 200 mV/s. The B/B' peak separation was generally lower, varying from 0.11 to 0.20 V. The consistency in peak separation across scan rates suggests electrochemical reversibility for both couples, yet the difference in peak current intensity for A/A' indicates some irreversibility. The sharp drop in current for the A' peak is characteristic of deposition at the electrode. In addition, the A' peak current is linear with the square root of the scan rate (Figure 3.12).

Table 3.9. Peak separation and current for CVs shown in Figure 3.11. Peak current with respect to drawn baselines.

Scan rate (mV/s)	ΔE_p A/A' (V)	ΔE_p B/B' (V)	I_p A (mA)	I_p A' (mA)	I_p B (mA)	I_p B' (mA)
60	0.167	0.148	32.63	3.26	3.18	1.98
90	0.170	0.150	33.37	4.77	3.75	1.88
120	0.172	0.138	31.94	5.36	4.22	2.24
150	0.164	0.152	39.26	6.97	4.82	2.47

Note that as seen in Figure 3.13, the A peak position drifts in the oxidizing direction over consecutive cycles. Peaks B, B', and A' are more consistent from cycle to cycle. Since peak A is hypothesized to indicate the oxidation of Cr^0 to Cr^{2+}, the higher potential required for each consecutive oxidation may be related to the evolving electrode surface as Cr is de-plated. Since this is hypothesized to be a soluble-insoluble reaction, with chromium deposition taking place on a dissimilar electrode, the Krulic equation can be used to estimate the diffusivity of Cr^{2+} knowing the step size is 2 mV and the peak reduction current from CV and assuming the concentration of Cr^{2+} and the density of the chromium deposit [175], [194]. When calculated using the Berzins-Delahay equation, the diffusivity of Cr^{2+} (using the A' peak current shown in Figure 3.11) ranges from 9.2E-07 cm^2/s to 2.4E-06 cm^2/s over all scan rates. This assumes a working electrode area of 0.16 cm2, a molar concentration of Cr^{2+} of 1.12E-04 mol/cm^3, 2 electrons transferred, and a temperature of 550°C. Note that this provides only an estimate of D_{Cr2+} since the Berzins-Delahay equation assumes electrochemical reversibility and the activity of the deposited metal is 1. If the number of electrons is calculated from the A/A' peak separation, we find an average of $n_{A/A'} = 0.96$. A more complete uncertainty and sensitivity analysis is needed.

Since the Cr^{2+}/Cr^{3+} couple is a quasi-reversible, soluble-soluble, non-stoichiometric (Cr^{2+}:Cr^{3+} ratio other than 1) reaction, to estimate the diffusivity of Cr^{3+} in FLiNaK from CV, a modified form of the Randles-Ševčík equation is required. If the Randles-Ševčík equation is used to approximate D_{Cr3+} from the B' peak current in Figure 3.11 (with the same assumptions stated in the previous paragraph), diffusivities range from 3.2E-08 cm^2/s to 7.68E-08 cm^2/s over the four scan rates. The number of electrons transferred calculated from the peak separation is on average 1.1. If these assumptions provide a reasonable estimate, we find that D_{Cr3+} is smaller than that of D_{Cr2+}, consistent with prior literature (Figure 3.3).

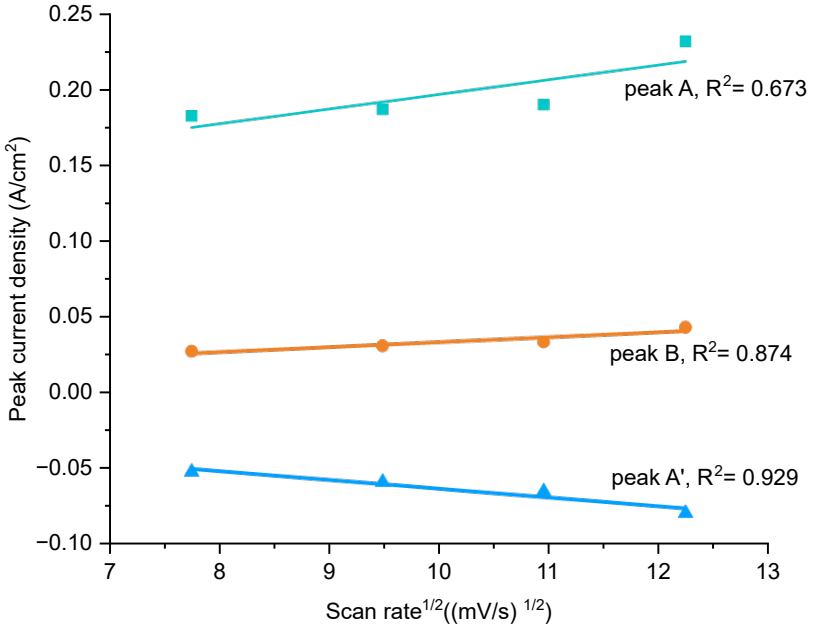

Figure 3.12. Dependence of peak current (i_p) on the square root of scan rate ($v^{1/2}$) for FLiNaK with 0.3 wt% Cr^{3+} added as CrF_3. Scan rates of 60, 90, 120, and 150 mV/s. B' not shown due to unclear peak position.

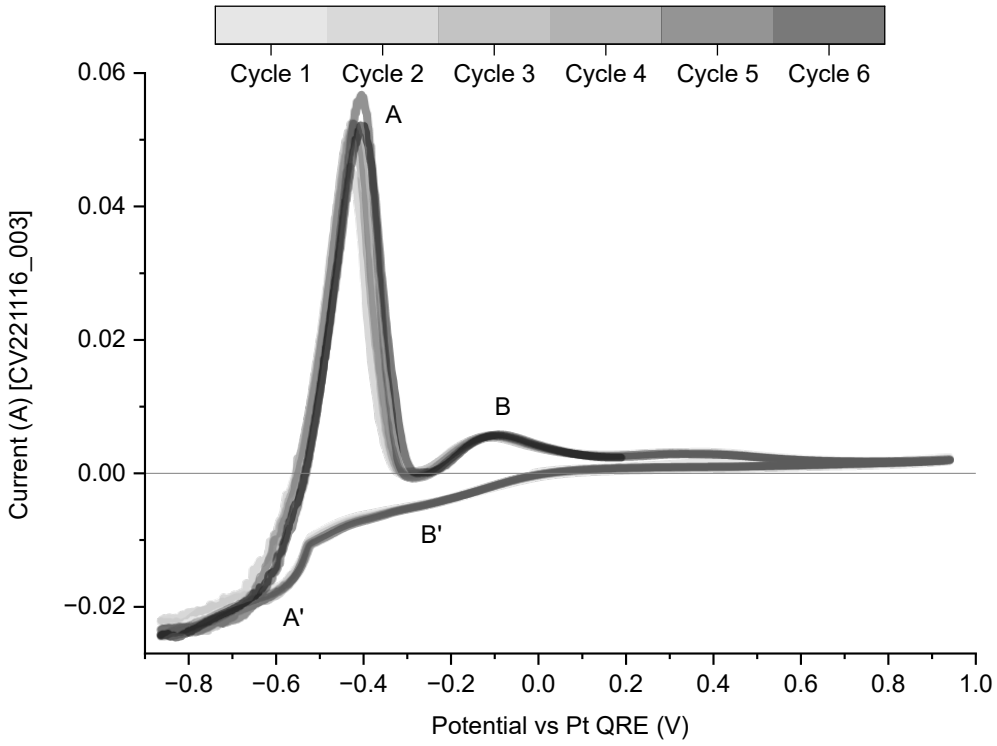

Figure 3.13. FLiNaK with 0.3 wt% Cr^{3+} added as CrF_3 over multiple scan cycles. WE: Au (0.16 cm^2)/, CE: Pt, QRE: Pt. Scan rate: 60 mV/s. 550±10°C, after temperature hold.

3.4.1.2 2KF-NaF

There were challenges collecting blank scans of the 2KF-NaF which required operation of the furnace at a higher temperature than previous use. This was hypothesized to be caused by interference between the furnace at high power and or issues with grounding the electrochemical cell. Additionally, the 2KF-NaF was prepared from constituent fluorides from the vendor and was not chemically purified. Figure 3.14 shows the dark phase that was observed at the bottom of the glassy carbon crucible after baseline scans of the 2KF-NaF with no chromium addition. Representative scans with and without chromium are shown in the Appendix Section 6.1.1 in Figure 6.9, indicating several peaks within a measured 3 V window. It was not possible to reference the blank or effectively measure working electrode surface area, so detailed analysis was not performed.

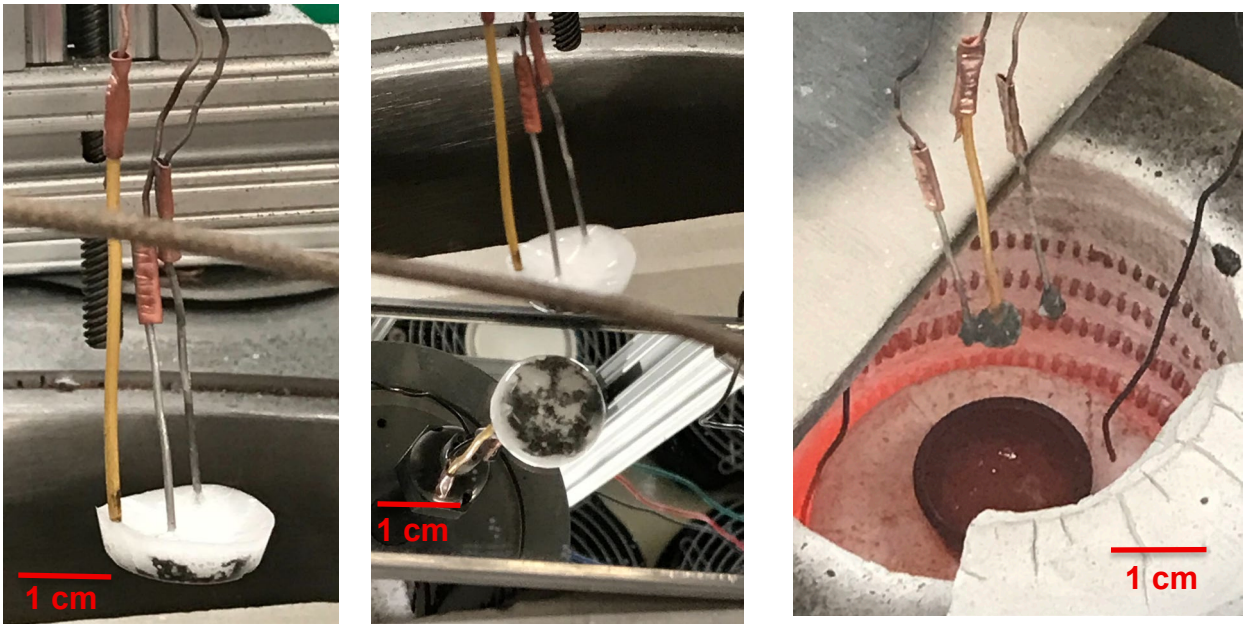

Figure 3.14. 2KF-NaF electrolyte and electrodes. Left: Electrodes were frozen in the salt to verify their immersion depth. Frozen salt shows a wetting behavior on the glassy carbon crucible. Center: View of the bottom of the solidified salt. Dark phase appeared before chromium fluoride addition, after cyclic voltammetry measurements. Right: Liquid salt with dark deposits on the WE, CE, and RE.

3.4.2 Acidic melts

Cyclic voltammograms and square wave voltammograms were performed on 3LiF-AlF_3 and FLiBe with and without chromium, added as CrF_3 and also as Cr_2O_3 to FLiBe.

3.4.2.1 3LiF-AlF_3

Cyclic voltammograms and square wave voltammograms were performed on 3LiF-AlF_3 with and without chromium, added as CrF_3. 3LiF-AlF_3 was non-wetting on the glassy carbon crucible and on the gold (working) electrode as seen in Figure 3.15. This non-wetting behavior introduced some challenges to positioning electrodes and establishing electrical contact.

The electrochemical window of the setup was shortened due to the use of a tungsten working electrode, which is fluorinated at approximately 1.8 V vs Al/Al^{3+}. This window is large enough to access the Cr/Cr^{2+} and Cr^{2+}/Cr^{3+} redox peaks according to thermodynamic data from HSC for pure mixtures. Note that the HSC data in Table 3.10 has not been adjusted for the fraction of Al^{3+} in 3LiF-AlF_3 or for the activity of chromium or tungsten.

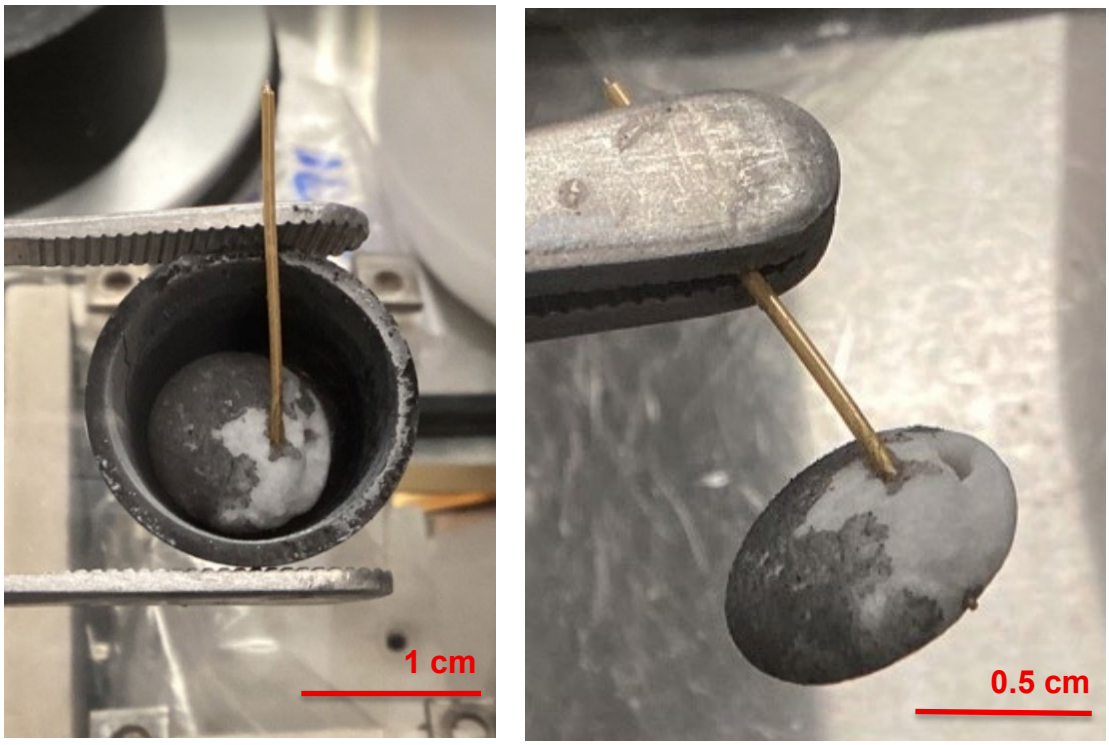

Figure 3.15. 3LiF-AlF_3 solidified after CrF_3 additions. (Left) In glassy carbon crucible, with gold rod frozen in the salt. (Right) Side view of the salt, showing that it was highly non-wetting on the glassy carbon crucible.

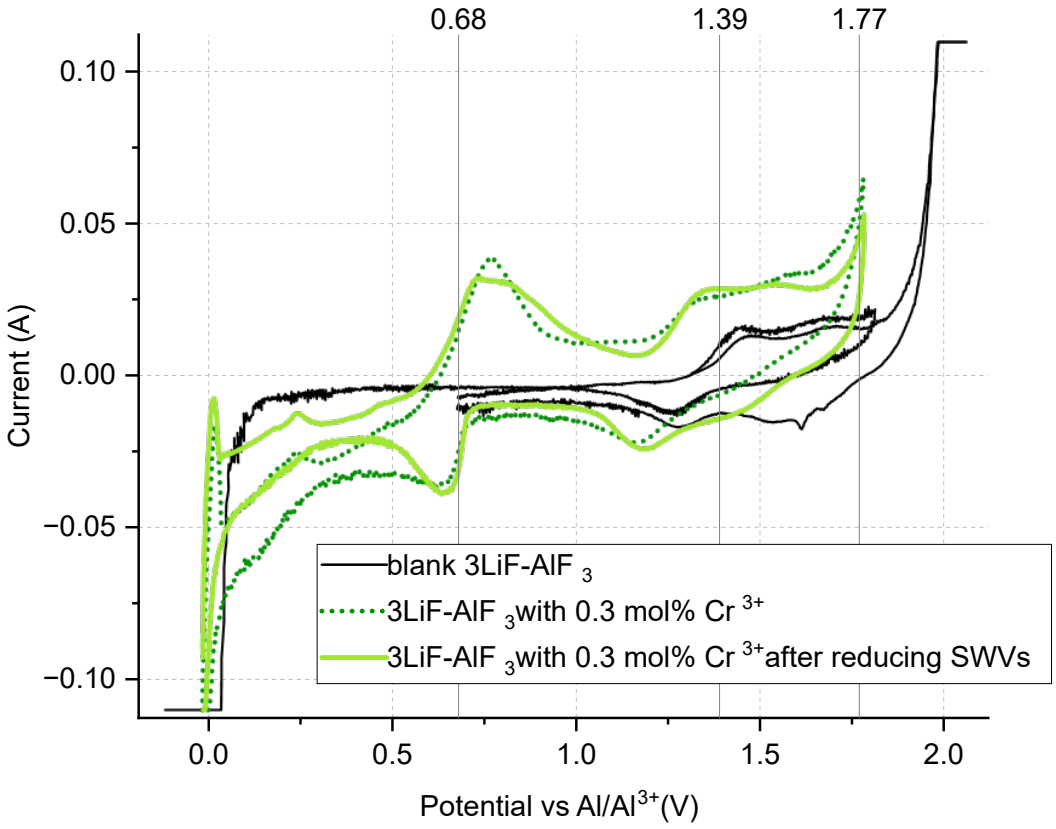

Figure 3.16. Cyclic voltammograms of 3LiF-AlF_3 + 0.3 wt% Cr^{3+} (added as CrF_3): 860°C, WE: W, CE: Pt, QRE: Pt, scan rate = 200 mV/s.

Table 3.10. Standard reduction potentials of Cr and W in fluoride vs Al from HSC 10.5.7.3.

Reaction	**E(860˚C) vs Al/Al^{3+}**
$CrF_2 = Cr + F_{2\,(g)}$	0.68
$CrF_3 = CrF_2 + 0.5F_{2\,(g)}$	1.39
$WF_4 = W + 2F_{2\,(g)}$	1.77

We observe the oxidizing limit of the electrochemical window to occur around 1.8-1.9 V vs Al/Al^{3+}, consistent with the expected fluorination of tungsten from HSC. Further, we observe peaks in the 0.68 V vs Al/Al^{3+} and 1.39 V vs Al/Al^{3+} regions, which are expected to be due to chromium. Most notably, the peak around 0.68 V vs Al/Al^{3+} features a sharp reduction which is characteristic of metal deposition at the electrode. Looking at the Cr^0/Cr^{2+} pair for the effect of scan rate on peak current, we observe variation in the peak position as seen in Figure 3.17. Figure 3.18 shows the trend of the peak current with the square root of scan rate, which is linear for scan rates from 50 to 200 mV/s (when 250 mV/s is excluded).

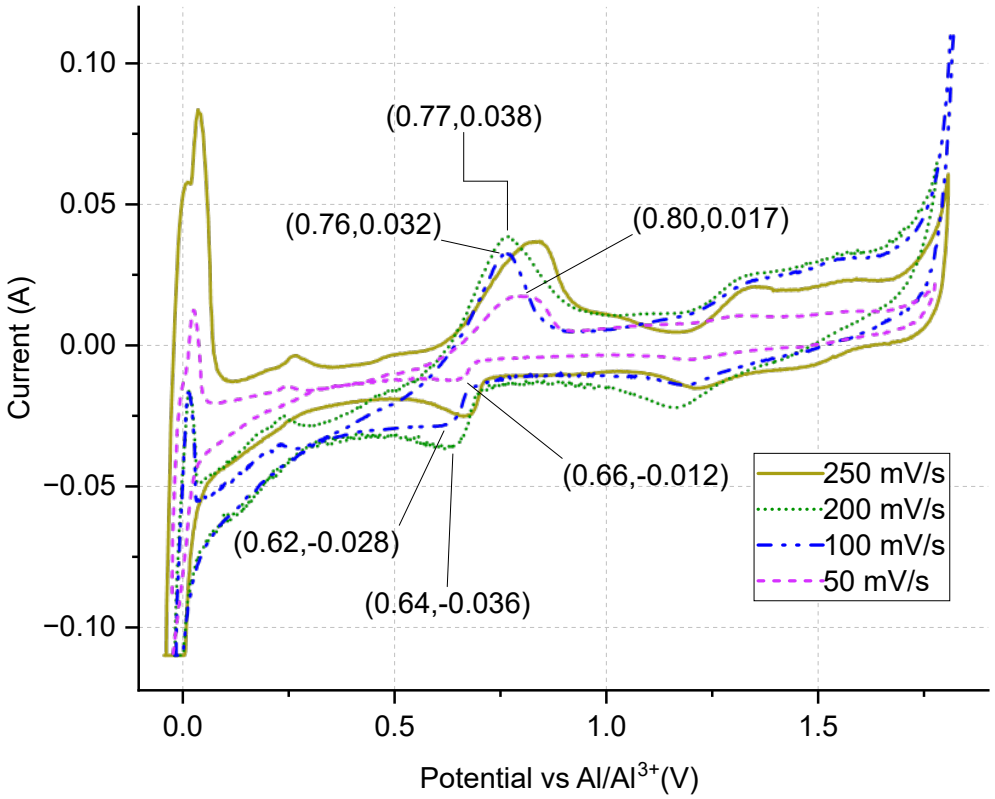

Figure 3.17. Cyclic voltammograms of 3LiF-AlF_3 + 0.3 wt% Cr^{3+} (added as CrF_3): 860°C, WE: W, CE: Pt, QRE: Pt, scan rate variable.

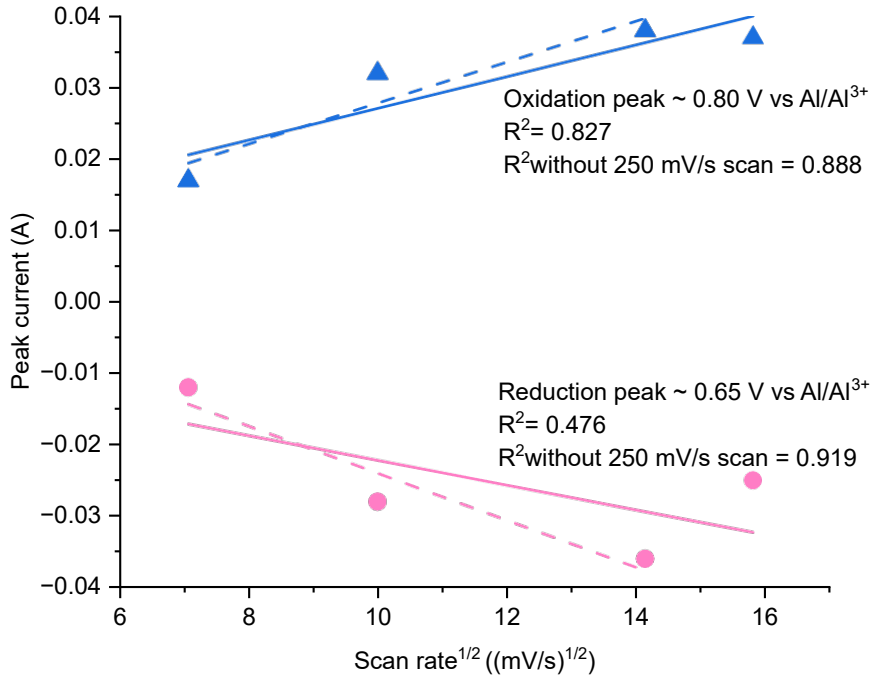

Figure 3.18**. Dependence of peak current with baseline of 0 on square root of scan rate for 3LiF-AlF_3 with 0.3 wt% Cr^{3+} added as CrF_3. Scan rates: 50, 100, 200, and 250 mV/s.**

3.4.2.2 FLiBe

Chromium was added to FLiBe in two separate studies, one in which Cr_2O_3 was added and one in which CrF_3 was added. For the sample with added Cr_2O_3, the green chromium oxide was found to collect around the perimeter of the FLiBe salt puck (Figure 3.19).

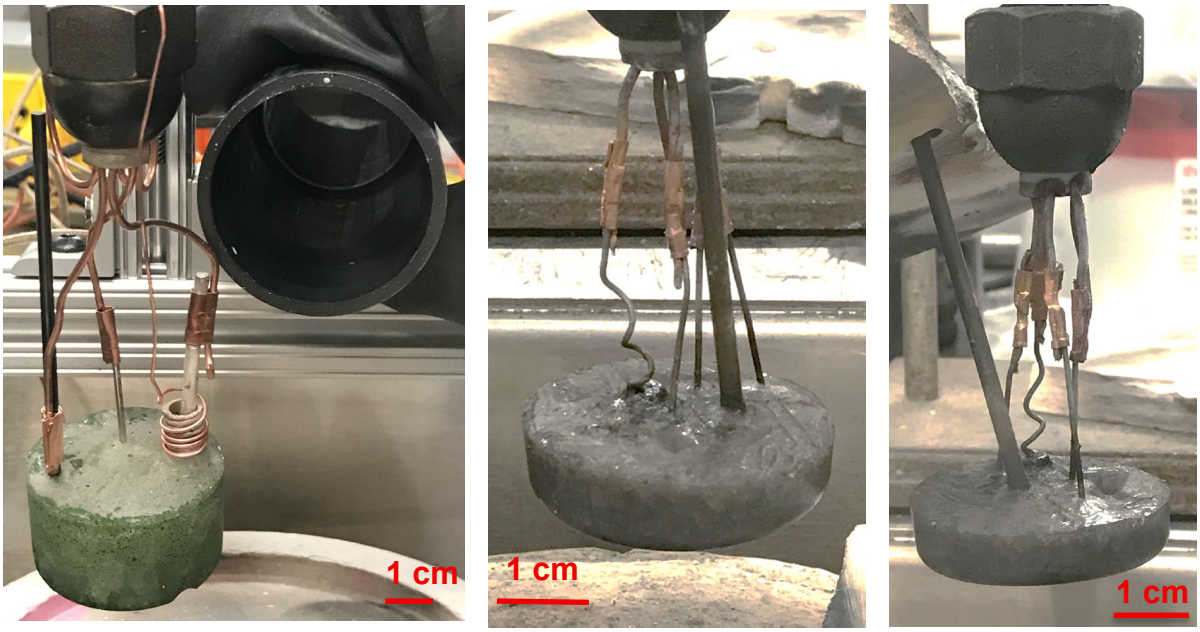

Figure 3.19. (Left) FLiBe with Cr_2O_3. (Center and Right) FLiBe with CrF_3.

Figure 3.20 shows CVs for FLiBe with and without Cr_2O_3, notably with different working electrodes. The FLiBe with added Cr_2O_3 shows a higher background current as well as a redox couple centered around approximately 0.67 V vs Be/Be^{2+} (reduction peak at 0.53 V and oxidation peak at 0.80 V). An additional oxidation peak appears around 1.5 V vs Be/Be^{2+}. Note that for the system with Cr the working electrode was platinum, whereas for the blank FLiBe the working electrode was gold. Figure 3.21 shows the square rate dependence of the peak current for the peak around 0.8 V vs Be/Be^{2+}, indicating linearity for scan rates less than 300 mV/s.

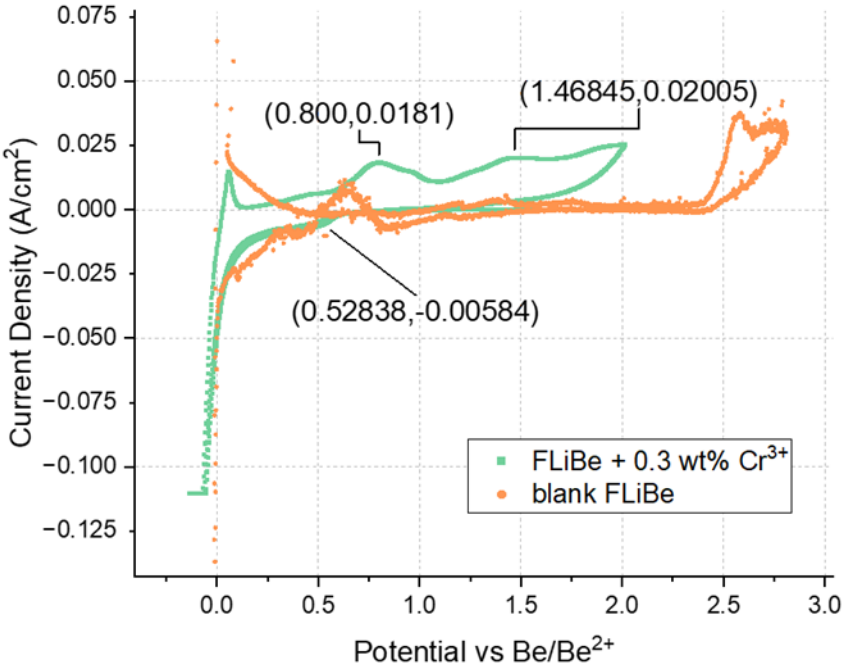

Figure 3.20. Cyclic voltammograms of FLiBe + 0.3 wt% Cr^{3+} (added as ~0.47 wt% Cr_2O_3): 600°C, WE: Pt, CE: GC, TRE: Ag/AgF, scan rate = 200 mV/s. FLiBe: 650°C, WE: Au, CE: Pt, QRE: Pt, scan rate = 200 mV/s. Note: different electrodes.

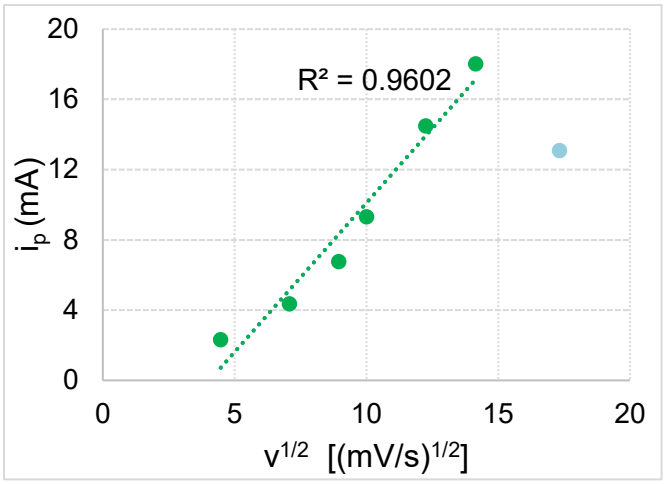

Figure 3.21. Peak position with the square root of scan rate for FLiBe + Cr_2O_3. 300 mV/s rate excluded from linear fit.

In order to compare a system in which no oxide was intentionally introduced, further studies were performed on FLiBe with added CrF_3. For the CVs shown in Figure 3.22, the same electrodes and setup were used for the blank and the CrF_3 addition, and the CVs are referenced with respect to the major reduction peak, assumed to be Be reduction.

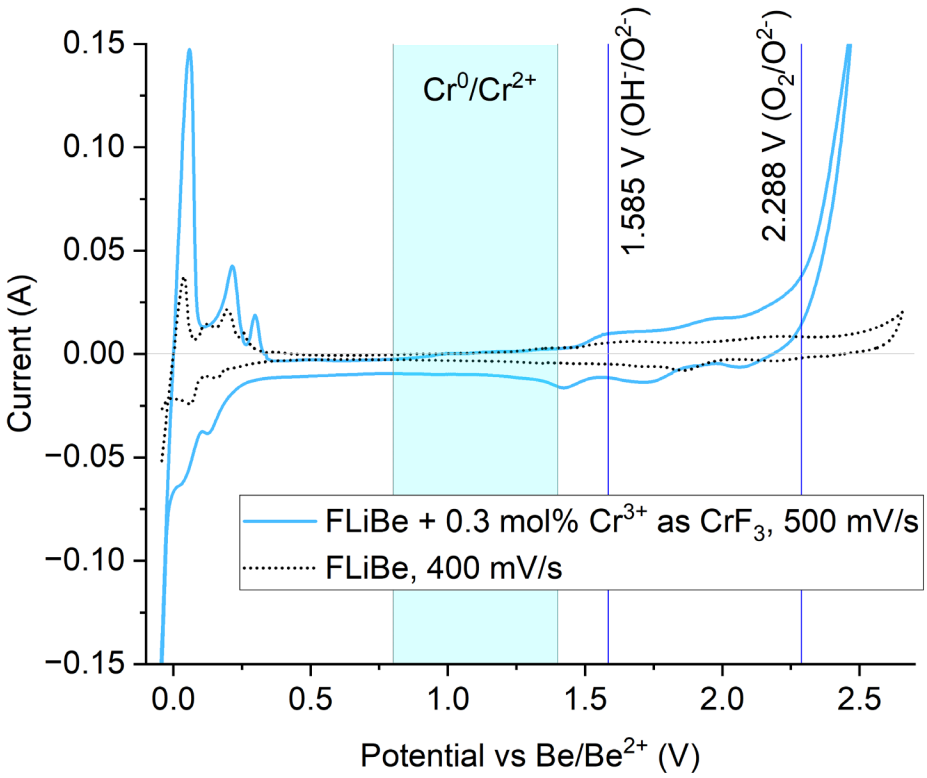

Figure 3.22. CV of FLiBe and FLiBe with 0.03 mol% Cr^{3+} added as CrF_3. WE: W, CE: Pt, QRE: Pt. Temp: 600±15°C. Window highlighted in blue is from 0.880 to 1.400 V vs Be/Be^{2+} which is the range of the expected Cr/Cr^{2+} redox couple at the range of temperatures and activities listed in Table 3.12.

In the thermodynamic data tabulated by Baes, the only species which have an oxidation potential within approximately 0.5 V of Be/Be^{2+} are Pu/Pu^{3+}, U/U^{3+}, U/U^{4+}, and Zr/Zr^{4+}, although several redox peaks appear near Be reduction in Figure 3.22 [58]. If Cr^0 was to nucleate on the working electrode, the reduction peak might be split into a potential for Cr adsorption on the electrode surface and one for bulk deposition. Figure 6.11 in the Appendix shows the scan rate dependence of the unknown peaks from 0 to 0.5 V vs Be/Be^{2+}. Shifts of the QRE led to an approximation of reference potential.

Reference lines in Figure 3.22 at 1.585 V vs Be/Be^{2+} and 2.288 V vs Be/Be^{2+} indicate the redox potentials of OH^-/O^{2-} and O_2/O^{2-}, respectively, assuming the activities listed in Table 3.11. Activity estimates are based on the solubility of H_2 in FLiBe [195], [196] and the known oxygen concentration in the glovebox during the experiment (Table 3.7). Peaks in these regions appear upon addition of CrF_3 to FLiBe, not just when Cr_2O_3 is added (Figure 3.20).

Table 3.11. Reduction potentials for half cell reactions in FLiBe tabulated in Baes 1969 [58]. E^0 assumes standard state is mol frac = 1 for each solute in FLiBe (for BeF_2 solvent composition is standard state, meaning $a_{Be2+} = 1$).

Half Cell Reaction	E^0(600˚C) vs Be^{2+}/Be	E^0(620˚C) vs Be^{2+}/Be	E^0(580˚C) vs Be^{2+}/Be	Assuming: activity(ox) activity(red)	E(600˚C) vs Be^{2+}/Be from Nernst for [red/ox]
$Be^{2+} + 2e^- = Be_{(solid)}$	0.000	0.000	0.000	$a(Be^{2+})$=0.33 a(Be)=0.8	-0.033
$0.5Cr_2O_{3(solid)} + 1.5Be^{2+} + 3e^- = Cr + 1.5BeO_{(solid)}$	1.854	1.840	1.868	$a(Cr_2O_3)$=0.003 $a(Be^{2+})$=0.33 a(Cr)=0.8 a(BeO)=1 (all based on mole fracs)	1.745
$H_2O_{(g)} + 1e^- = 0.5H_{2(g)} + OH^-$	1.260	1.242	1.278	$a(H_2O)$= 1000000 (unity for ppm) $a(H_2)$= 0.05 (ppm solubility in FLiBe) $a(OH^-)$= 100 (ppm)	2.066
$H_2O_{(g)} + 2e^- = H_{2(g)} + O^{2-}$	1.367	1.361	1.373	$a(H_2O)$= 1000000 (unity for ppm) $a(H_2)$= 0.05 (ppm solubility in FLiBe) $a(O^{2-})$= 100 (ppm)	1.826
$Cr^{2+} + 2e^- = Cr$	1.400	1.396	1.403	$a(Cr^{2+})$=0.003 a(Cr)=0.8	1.190
$OH^- + 1e^- = 0.5H_2(g) + O^{2-}$	1.472	1.478	1.466	$a(H_2)$= 0.05 (ppm solubility in FLiBe) $a(OH^-)$= 100 (ppm) $a(O^{2-})$= 100 (ppm)	1.585
$Fe^{2+} + 2e^- = Fe$	1.778	1.774	1.781	$a(Fe^{2+})$=0.001 a(Fe)=0.8	1.526
$Ni^{2+} + 2e^- = Ni$	2.042	2.045	2.039	$a(Ni^{2+})$=0.001 a(Ni)=0.8	1.790
$0.5O_{2(g)} + 2e- = O^{2-}$	2.400	2.389	2.412	$a(O_2)$=25 (ppm in GB) $a(O^{2-})$=100 (ppm)	2.288

$H^+ + 1e^- = 0.5H_{2(g)}$	2.489	2.495	2.482	$a(H^+)$= 110 (ppm solubility HF in FLiBe) $a(H_2)$= 0.05 (ppm)	2.955
$0.5F_{2(g)} + 1e- = F^-$	4.719	4.707	4.733	--	--

Cr_3Pt observed to deposit in FLiNaK by Chan et al. [166], suggesting a Cr activity of 0.75. The concentration estimate of 0.000001 would be equivalent to 1 wppm of Cr^{2+}.

Table 3.12. Reduction potential of $Cr^{2+} + 2e^- = Cr$ in FLiBe, adjusted from standard potential [58] using the Nernst equation.

Temperature (°C)	Activity Cr^{2+}	Activity Cr	E vs Be/Be^{2+} in FLiBe
600	1	1	1.400
600	0.003	0.8	1.190
600	0.003	1	1.181
600	0.003	0.75	1.192
700	0.003	0.75	1.150
750	0.003	0.75	1.128
580	0.003	0.75	1.200
550	0.003	0.75	1.213
600	0.0015	0.75	1.166
600	0.0001	0.75	1.064
600	0.0001	1	1.053
600	0.00001	1	0.967
600	0.000001	1	0.880
700	0.000001	1	0.802
600	0.006	1	1.207
600	0.006	0.75	1.218
550	0.006	0.75	1.238

3.5 Discussion

Although peaks similar to A/A' and B/B' in FLiNaK (Figure 3.11) have been previously attributed to Cr^0/Cr^{2+} and Cr^{2+}/Cr^{3+} (Table 3.7), it is possible that these peaks indicate other electrochemical species or oxidation states of chromium. As stated, previous studies attribute the peaks to chromium due to their appearance after chromium addition or by analysis of the species reduced on the electrode surface, however, peak characteristics have not been consistently representative of the proposed species. For the previous studies which did reference the Cr peaks with respect to the reduction edge of the electrochemical window (presumably K reduction), the

Cr^0/Cr^{2+} peaks were located around 1.15 V vs K/K^+ in FLiNaK at 600°C [47], [167]. The reference potential is inconsistent in this work, as well, so it is challenging to estimate the redox potential vs a standard reference. Regardless, the Cr^0/Cr^{2+} peak is thermodynamically estimated to occur at approximately 1.4 V vs K/K^+ in FLiNaK at the temperature studied (460°C) and at 1.3 V vs K/K^+ at 600°C (Table 3.8). Future work would benefit from consistent peak referencing techniques, elemental analysis of the salt and electrode deposits throughout electroanalytical studies, and/or spectroscopic studies of the in-situ oxidation states of chromium.

From the electroanalytical studies of the mixtures presented, we observe:

- The qualitative replicability in comparison to literature of peaks A/A' and B/B' upon addition of CrF_3 to FLiNaK (Figure 3.11).
    - These peaks are likely to be attributed to chromium species, but elemental analysis to confirm solubility and the presence of other species would aid in their interpretation given their redox potentials differ from those predicted by thermodynamics.
    - Further studies might: confirm the speciation of chromium via complementary spectroscopic or analytical methods. Quantify the diffusion coefficients of the diffusing species and perform an analysis of diffusion regimes, incorporating discussion of the Schmidt number following from the discussion in Section 3.1.1.
- A higher background current in FLiBe with CrF_3 compared to the blank.
    - This suggests capacitive charging at the electrode surface. In addition, apparent redox peaks seem to indicate the presence of oxygen-containing species, suggesting that chromium oxyfluoride species might be present in the melt.
    - The presence of oxygen is expected to facilitate the solubility of chromium. The formation of charge-transfer complexes has been seen to lead to a cathodic shift in peak position, with peaks shifting cathodically as degree of complexation increases [197]. However, the kinetic shift may be due to uncompensated resistance of the setup. Indeed, we note several challenges during experimentation related to possible feedback from the furnace and resistive effects of the electrochemical cell.
- Greater reversibility in the peaks attributed to chromium in 3LiF-AlF_3 compared to the peaks attributed to chromium in FLiNaK. (Attribution of peaks to chromium was not clear in the FLiBe systems.)
    - In FLiNaK, the oxidation peaks are of a higher amplitude than the reduction peaks (up to an 11:1 ratio, see Figure 3.11 and Table 3.9). In 3LiF-AlF_3, they are closer to 1:1 (Figure 3.17). Both systems have peak currents linear with the square root of scan rates for scan rates up to 150-200 mV/s.
    - This could suggest less of an energetic demand or lower kinetic barriers for the solvation of Cr^{2+} and Cr^{3+} in 3LiF-AlF_3 compared to FLiNaK (which would contradict the classic understanding of the fluoroacidity of the mixtures) or differences in the speciation of the oxidized/reduced species in each mixture. Further confirmation of the peak attribution and calculation of the diffusivity of Cr^{2+} and Cr^{3+} would aid in clarifying this interpretation.

In addition to differences in electrochemical behavior and melting point among the fluoride mixtures, we observed qualitative differences in the wetting behavior of the salts, most evident in the case of 3LiF-AlF_3 and 2KF-NaF in glassy carbon (seen in Figure 3.23). The wetting behavior of liquids is related to their surface tension within the liquid and the surface energy of the crucible. The difference in wetting for these salts on the same glassy carbon container indicates differences in the cohesive forces within the liquid, related to the dynamics of their liquid structure.

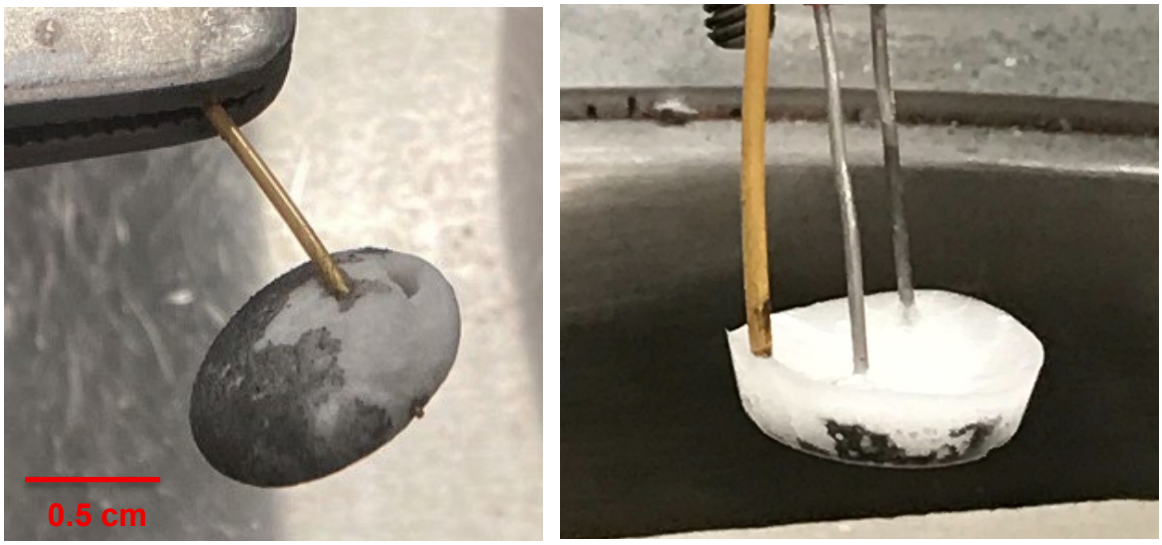

Figure 3.23. Left: 3LiF-AlF_3, previously frozen in a glassy carbon crucible. Right: 2KF-NaF with electrodes, previously frozen in a glassy carbon crucible.

A summary of wetting behavior and visual observations of the solvent salts and the dissolution of the added solutes is provided in Table 3.13.

Table 3.13. Summary of wetting behavior and visual observations of each of the solvent salts with and without solutes, all in glassy carbon crucibles.

Solvent salt	Description
FLiNaK	Uniform, opaque, white solid salt. Liquid salt appeared cloudy (slightly opaque streaks) upon freezing and re-melting. Pale green mixture after CrF_3 addition at temperature.
2KF-NaF	Spreading of liquid and wetting up the walls of the crucible when frozen. Upon melting (prior to Cr additions), a dark phase appeared at the bottom of the crucible. Uniform, opaque, white solid salt.
3LiF-AlF_3	Rounded droplet (beaded) shape. No sticking to the crucible, but Au electrode froze in place. Minimal spreading when liquid. Products from added CrF_3 stuck to the surface of the droplet and remained poorly dispersed. Grayish, splotchy, and uneven solid salt surface.

FLiBe	Somewhat rounded surface in the liquid and solid phases (poor wetting). Semi-opaque, gray-white solid salt with a blue-green tint. Cr_2O_3 additions collected around the perimeter of the salt, at the interface of the salt with the crucible. Whitish-gray film appeared on the surface of the liquid after Cr_2O_3 additions. CrF_3 additions led to a slightly darker gray mixture when solidified.

We now revisit our initial research question (if acidic solvent species necessarily compete with chromium solutes for dissociated F^-) in a conceptual manner. Shahbazi et al. summarized that most cation additions to molten fluorides result in negative deviations from ideality, which have increasing stability due to Coulombic interactions enhanced by the difference in the Z/r ratio [198]. Shahbazi et al. expand from the work of Blander, who noted that the extent of the deviation from ideality, quantified by the activity coefficient, is greater in mixtures in which the Z/r difference is greater for the cations in the mixture. Since the Z/r ratio is a measure of the Coulombic force between ions, this indicates that the electrostatic repulsion between cations is less when large and small cations alternate compared to the average repulsion between small cations and large cations with own kind [198]. Referencing this to the language of acid/base theory, an ARE report states that "the stronger the acid and the base that are combined, the stronger they complex each other on mixing, or stated in thermodynamic terms, the greater are the negative deviations from ideal solution behavior shown by the mixture" [193], [198]. As such, when chromium is added to molten fluorides, its stability is dictated by its difference in Z/r ratio compared to the solvent cations, or the existing acidic species in the solvent. It has been explained that in an ideal dilute solution, the addition of cations with an oxidation state of 3+ might result in a configuration in which "the cation could be regarded as having competed more strongly for the anions than the alkali cations [in order to] complete its ideal coordination structure" [27]. However, the authors of this work describe that this understanding is only valid for an *ideal* and *dilute* mixture, and thus, the added cation can either become under-coordinated or share anions, leading to network structure. As such, I conclude that the competition for fluorides among chromium and other solvent cations must be understood within the context of salt structure and that fluoroacidity should be understood only as a thermodynamic indicator of networked structure (and cannot be isolated from our developed understanding of buffering capacity and the ionic or covalent nature of the acidic species, discussed in Section 3.2 of this chapter).

3.6 Conclusion

In this chapter, I develop fundamental theory relating Winner et al.'s concept of acid-base buffering capacity to the nature of the acidic species in a melt as well as present electroanalytical data of chromium in FLiNaK, FLiBe, and 3LiF-AlF_3 to introduce how electrochemistry might be used to explore questions related to fluoroacidity. By reasoning about the differences in bond formation in structure in acidic and basic melts, I explain how the ionic or covalent nature of the acidic species influences how reversibly the cation binds fluoride and how effective it is as a buffer, with the understanding that the more ionic and flexible the bonding is, the more effective the species is at buffering fluoride activity. In a sense, fluoroacidity is a specific expression of

ionicity which focuses on the basic fluoride anion. A more nuanced understanding of acid-base behavior allows one to similarly avoid the pitfalls of a purely thermophysical understanding, similar to the transport-focused quantification of ionicity for ionic liquids. Whereas fluoroacidity has been simply understood as the activity of dsF and has been generally used to explain certain aspects of corrosion phenomena, interpretation of Winner et al. leads to the conclusion that examining also acidic contributions and the nature of acidic bonding may be valuable in understanding the relevance of fluoroacidity to corrosion.
Electrochemical studies of chromium in FLiBe, FLiNaK, 3LiF-AlF_3, and 2KF-NaF presented and discussed in this chapter show differing behavior in their CV signals in their reversibility (Cr in 3LiF-AlF_3 (Figure 3.16) vs in FLiNaK (Figure 3.11)) and in their background current. FLiBe with CrF_3 showed a higher background current relative to the blank (Figure 3.22), suggesting capacitive charging at the electrode surface with electrochemical signals which seem to indicate the presence of oxide species both when oxide was and was not added (Figure 3.20). The 3LiF-AlF_3 and 2KF-NaF mixtures are observed to demonstrate notable differences in wetting behavior on glassy carbon; 3LiF-AlF_3 is non-wetting, and 2KF-NaF is wetting (Figure 3.23). Future work includes estimating the diffusivities of chromium species in each of these solvents along with a complete sensitivity analysis and uncertainty quantification, along with analysis of SWV data for estimating the number of electrons transferred to aid in identifying chromium speciation.

Broadly, this work develops understanding of the electrochemical behavior of molten fluoride solvents of various compositions and fluoroacidities, presenting electrochemical data of chromium additions and discussing and developing the concept of fluoroacidity as it relates to solute speciation and activity. These fundamental studies of the evolution of salt chemistry upon addition of chromium, an expected corrosion product in engineered molten salt systems, support the development of chemistry control systems and electrochemical sensors for molten fluoride salts.

3.7 Acknowledgements

AIMD models and interpretation are published in “Ab-initio simulation studies of chromium solvation in molten fluoride salts” J. Mol. Liq., 2021. [19] This research was supported as part of FUTURE (Fundamental Understanding of Transport Under Reactor Extremes), an Energy Frontier Research Center funded by the U.S. Department of Energy (DOE), Office of Science, Basic Energy Sciences (BES).

NW, RS, and MA conceptualized the project. NW performed AIMD calculations with feedback from MA. NW analyzed the AIMD with feedback from both RS and MA. RS provided the chemical interpretation of the AIMD results. HW provided the literature background on fluoroacidity and chromium solvation. RS and HW developed the fluoroacidity discussion. All authors worked on writing the manuscript together.

Electrochemical experiments (salt preparation, baseline scans, and CrF_3 additions) were performed with Ruben Cho. FLiBe with Cr_2O_3 data was collected by Lorenzo Vergari. Discussion on interpretation of FLiBe with Cr_2O_3 data was developed partially with Dr. Sander Ratso.

4 KNOWING AND BEING AS A NUCLEAR ENGINEER

In this chapter, I examine questions related to **what it means *to know* and *identify* as a nuclear engineer.** "Knowing as an engineer" concerns the epistemological frameworks, heuristics, and rationalities that structure engineering knowledge-making. "Being as a nuclear engineer" references the identity of engineers, professionally and conceptually, which informs their intrinsic and contextual roles and responsibilities.

Interest in these questions arose from my understanding of my own professionalization as an engineer, and I note that my analysis is inextricably connected to my conceptualization and experiences of my own engineering identity. This work responds to the critique of engineers' participation in and complacence with "technological somnambulism", whereby engineers sleepwalk through the creation of technologies which alter the fabric of society, shaping both human activity and the meaning of human activity [70]. With the ultimate aim to alertly and thoughtfully proceed in engineering practice, I look to the foundational elements which are definitive of engineering and present a working definition of the term. I suggest the relationship between engineering and philosophy of engineering and present questions of interest to the philosophy of nuclear engineering.

In this work, I wish to suggest that reflexive practices are naturally intrinsic to engineering practices, such that the dismissal of social contexts and foundational values is not in line with the values of the engineering profession and the foundational vision of engineering education. This notion rejects the distinction between "traditional" engineers (those who hold elitist and capitalistic worldviews [75]) and "reflexive" engineers (those who consider socio-technical systems and dynamics) and addresses the dialectic existing in the literature that engineering is both sensitive to contexts and depoliticized. I would claim that engineering in its fullest expression is that which is reflexive and participates in both affective and rational reflection on network actors, including the self. In light of this, I present an analysis of core nuclear engineering textbooks for their underlying value systems and implicit and explicit statements about the role and responsibilities of the nuclear engineer.

As a note on the distinction of philosophies of engineering, the work addressed in this chapter is notably not simply categorized by "engineering ethics", a label which has been used to generally classify reflection on social impacts of engineering practice. Rather, I emphasize other branches of philosophy, namely epistemology and ontology. Drawing from the fields of science, technology, and society (STS) and engineering studies (ES) and taking inspiration from the history of science, I present an introduction to epistemological and praxis-oriented inquiry in nuclear engineering and an analysis of core nuclear engineering textbooks for their underlying values systems.

4.1 Statement of context

I have received training as a chemical engineer (having received my Bachelor of Science in Chemical Engineering) and as a nuclear engineer, the content and formation of which have shaped the research questions addressed in this chapter. I emphatically identify as an engineer, meaning that I believe my training as an engineer and role as an engineer are exemplified

through my work, technical and otherwise. That is, there are ways in which I feel I "think like an engineer". My views of what engineering is and what it can do affect how I make sense of the data[b] analyzed in this chapter, therefore I wish to be explicit about my perception of the role of engineers and engineering practices in society.

I believe that engineering practices (including the methodologies for solving problems and the development of technologies) can add value to the world if sensitivities towards power differentials—in terms of societal impact, funding mechanisms, institutional settings, and policy frameworks—are thoughtfully incorporated. I embrace the limitations of engineering practices and believe they require dialogue with other approaches to problem-solving, sense-making, and ways of knowing. I also recognize that, historically and still in the present day, engineering practices have caused and sustained harm to communities and the environment knowingly and unknowingly, intentionally and unintentionally, and by the practice themselves and through the values embedded in the technologies they produce [199]. To summarize my perspective, I believe that engineers *can* and *ought to do good* (while recognizing the historical engineering pitfall of coupling what can be and what should be [200]), which requires awareness of and sensitivity to human and social values, thoughtful cultivation of virtue, and truthful and humble[c] recognition of responsibilities and past harms.

Through this work, my goals are 1) to be explicit about the contexts (historical and philosophical) of my research and 2) to make visible the epistemological norms that I encounter in facets of my field of study.

4.2 Background & Pre-discussion

This chapter presents specific philosophical inquiry into a specific engineering discipline—an engineering discipline which has been examined for its social and political impacts, but not necessarily (or explicitly) for its philosophical underpinnings. In addressing this topic, we find ourselves situated in the relatively young field of *philosophy of engineering*, more generally.

Discussion of the philosophy of engineering and of engineering education emerged in the 21st century focusing on distinctions between science, engineering, and technology and the relevance or non-relevance of distinct philosophies of each. Several authors on the topic have described the absence and marginalization of philosophy of engineering, contrasting it to the much more established philosophy of science [201] [202]. Pirtle attributes the lack of philosophy of *engineering* to the field of philosophy's historic bias toward abstract theoretical knowledge over practical knowledge [203]. Some authors make note also of engineers' indifference to the philosophical foundations of their work [70], [204], mentioning, however, the exception of engineering ethics [205]. Engineering and philosophy have been described as inherently at odds

[b] By "data" I mean the inputs to my analysis of the epistemology and practice of nuclear engineering: the history of nuclear engineering presented, the textbooks analyzed, and the experiences which are the subject of reflection.

[c] My use of "humble" is aligned with that of Augustine of Hippo, where humility is the understanding of one's right place in the world (and society), justly exercising one's free will (De Natura Et Gratia, Chapter XXXII-XXXIII).

due to their differing ends (of transformation and understanding, respectively [206]) and differing means (action versus contemplation, and different attitudes towards ambiguity [207]). At the same time, several authors, including both philosophers and engineers, have advocated for the integration of the two disciplines for their mutual benefit [205]. Goldberg has expressed that the call for the philosophy of engineering has arisen in the last two decades due to an emerging crisis in engineering due to the "unsettling" reaches of technology [207]. In their introduction to their Handbook of Philosophy of Engineering, Michelfelder and Doorn attribute the increasing interest in the topic (which they identify as occurring post-2010) to:

> the myriad of ways in which engineering innovations are directly responsible for transforming the social fabric and established institutions of everyday life [which] are a matter of simultaneous systemic shifts in agency, as decision-making is transferred from humans to algorithmic processes; in responsibility for these decisions; and in how individual artifacts are linked and networked together [208].

To thinkers on the topic of philosophy of engineering, the influence of engineering on all aspects of life is both abundantly obvious and staggeringly profound. The motivation for reflecting on the nature of engineering and engineering artifacts, then, is highly practical (to ensure thoughtful development of society) and academically appealing (put simply, there is just so much to examine given the rate of technological progress). Further, with the transformation of social fabrics and institutions, philosopher Carl Mitcham claims: "The meaning of modernity and engineering are intertwined" [209]. In this understanding, there exists an intrinsic connection between the engineer who contributes to the design and creation of modern society and the philosopher to seeks to understand what it all means.

Putting the connection between philosophy and engineering more directly, Mitcham proposes: "Why is philosophy important to engineering? Ultimately and most deeply it is because engineering is philosophy—and through philosophy engineering will become more itself" [210]. And to this, philosopher Li Bo-cong adds: "Why is engineering important to philosophy? Ultimately and most deeply it is because philosophy is engineering, and through engineering philosophy will become more itself" [211]. Engineering might be considered philosophy in its pursuit of practical wisdom. And philosophy might be considered engineering in the world-making of its frameworks. Further, the two might be equated through their iterative relationship of continually transforming society and continually seeking understanding of society; engineers and philosophers can be considered the two kicking feet in the waters of society, propelling us into deeper knowledge both concretely and abstractly. Wisnioski makes a similar point about the philosophical nature of engineering in a more grounded sense:

> [E]ven the most taciturn of engineers is an intellectual of a sort because engineering is an inherently normative practice. While engineers frequently collapse is into ought or deny that a sociological imagination shapes their designs, to engineer is to build a social vision into material reality [200].

The pragmatic engineer can be considered an intellectual because they must, to some extent, engage with the conceptual and moral dimensions of their work, making foundational and consequential value-laden decisions. And at the same time, the creative, sometimes expansive,

problem-solving that engineers do is not far removed from the everyday problem-solving that all people perform. In this way, engineers are philosophers, philosophers are engineers, and everyone is an engineer and philosopher. Pitt points out that engineers rely heavily on commonsense-type knowledge, which comes into play whenever a human, engineer or not, makes a decision [212]. As such, the trope of "engineering as problem solving" is not a distinctive description—all people are problem solvers. At the same time, these broad categorizations point to the more fundamental relationship between engineering and philosophy as profoundly human endeavors.

In the remainder of this Section (4.2), I present a brief summary of themes in the literature concerning epistemology of engineering (knowing, more broadly) and engineering identities (being, more broadly). I include questions which follow from my understanding of these topics which I hope will serve as starting points for further analysis and discussion elsewhere. In the final sub-section, I present a brief history of how the field of "nuclear engineering" came to be.

4.2.1 Defining engineering and philosophy of engineering

Beyond the distinction between philosophies of engineering and technology, scholarly discussion has centered on *the prior need* to *define engineering itself*. Several authors have sought to distill "engineering"—the activity, the profession, the identity—into a succinct understanding, emphasizing concepts such as application and design (which will be discussed briefly in the following paragraphs). However, philosopher Michael Davis describes the confounding reality that "there is no function that engineers, and only engineers, seem to perform (except, of course, engineering itself [)]" [213], or, put more simply, "engineers engineer" [214]. This circular definition implies an ostensive and contextual understanding of engineering—engineering is what engineers are known to perform. This definition, perhaps like engineering itself, is empirical. Even more simply, engineering practice is self-evident. In the professional domain, this definition is not embraced since there exist state-specific practices in the U.S. for accrediting and licensing practicing engineers [215]. By bounding engineering to the work of engineers, however, the distinction of "engineering" (versus applied science or technological practice, for example) is taken for granted as real, identifiable, and (ideally) useful, allowing for an observation-grounded discussion without equivocating who is truly an engineer and who is not. For the purposes of this work (which is largely reflexive and intuitive), I choose to work with an intuitive understanding of the definition of engineering, particularly acknowledging this work as filtered through my personal intuition of what I and others do as engineers and what we ought to do as engineers, and our learned (and taught) understanding of what engineers do. Given this working definition of engineering, we can ask *what is observed as essential to the practice of nuclear engineering*, and what understanding of knowledge and their professional and social role is implicitly and explicitly taught to nuclear engineers. Broadly, I am labeling these types of questions as studies of *being* and *knowing* as a nuclear engineer, and I define the contexts of these topics in their applications to engineering in the following sections.

To introduce discussion of how engineers *know* and *are*, it is helpful to describe some attributes of what engineers generally do. Two attributes considered to be quintessential to engineering are

1) the notion of engineering design and 2) the applied nature of engineering practice. We will examine how these hallmarks of engineering activities—design and application—are interwoven with the engineering identity.

4.2.1.1 Engineering design: engineering knowledge and engineering judgment

Engineering *knowledge* and *judgment* are generally claimed to be essential elements of engineering *design* [216], with a particular type of knowledge and judgment considered definitive of engineering practice. Engineering knowledge is described as largely practical; it consists primarily of knowledge-*how* in a manner that is rooted in theory [217]. Engineering judgement informs the application of that knowledge, and its application is a creative process in such a way that it amounts to the quintessential act of engineers: design. For Layton, the (American) engineer is a "practical scientist who is able to design" [218]. Not only do engineers design processes and products, but they design in a way that is practical in managing constraints, is theory-based and grounded in empirical understandings of systems, and that relies on heuristics or rules of thumb [219]. The engineering judgment which constitutes engineering design involves integration with the norms of the profession and development of expertise in identifying constraints and objectives. Bulleit et al. describe the process of developing engineering judgment by the following:

> Over time, engineers develop conscious and unconscious ways of decomposing and solving problems based on what has and what has not worked for them. These are not necessarily processes that the engineers can communicate in words; they have become integral to who they are and how they operate. Competence is achieved when an engineer is capable of focusing intuitively on what really matters and converging relatively quickly on a viable solution. [217]

In Bulleit et al.'s description of the activities of engineers, engineering knowledge, judgement, action, design, and problem-solving converge. Notably, their description is highly intuition- and experience-based. With this perspective, theory-based education in engineering would provide foundational understanding, but it is applied work experience that most truly 'makes' one an engineer. This opinion is not unique—disregarding the requirements of professional licensure, it is colloquially understood by established engineers that what 'makes' someone an engineer is not a degree, but enculturation into the practices of problem solving and design, but at the same time, engineering students tend to identify as engineers or engineering-type persons due to their incorporation into professional norms from the time they declare their major [220], [221]. These perspectives suggest that the formation of an acute sense of engineering judgement (and therefore the establishment of engineering identity) is most tangible in real engineering contexts, with real problems and real consequences.

For Bulleit et al., engineering problem solving (or similarly the creative essence of engineering, described also by engineering "practice" or engineering "design") becomes an integrated way of knowing and being for the engineer. This practice, which is both a disposition and ability to develop solutions and a primary design methodology rooted in a sharpened sense of judgment, is so integral to the identity of the engineer it is nearly incommunicable according to Bulleit et al. Most notably, engineering judgment is a learned instinct and a refined intuition, such that the act

of ‘doing engineering’ becomes a way of being. The activities of engineers, then—including design, problem-solving, and judgment-making—define not just their professional identities as engineers (consistent with Davis [213]), but possibly also their broader world view and approach to understanding and action.

In addition, Bulleit et al. describe the engineer’s approach to solving problems as “decomposing” problems—a problem is to be dismantled in some manner, broken down into its more fundamental parts. Engineering judgment, then, involves an ability to determine how to effectively (and safely) trim down problems to a manageable size, as well as an ability to address and resolve the diagnosis. Engineers calculate, but they estimate [222]. And in this estimation, they rely on their own accumulated knowledge and the existing knowledge of the field to make a fitting estimate. Further, the *disposition* to participate in this type of design or problem solving is a relevant marker of an engineer. This way of assessing and approaching the world is, in a way, an applied philosophy by which engineers constantly operate, similar to the inherent and intuitive elements of the engineering identity discussed in the previous paragraph.

Similar to Bulleit et al.’s assessment of how engineering judgment develops “over time”, it is generally understood in the literature that the skill of engineering judgment is continually acquired through experience. However, Davis argues that *good judgment* is so crucial to engineering that it must be taught, particularly through the instruction of engineering ethics [223]. Engineering judgment requires management of values, giving it a moral character. Engineering, then, is inherently normative. It is a formalized professionalization of systematically assessing and addressing problems, leading to the design of optimal solutions in value-laden contexts.

4.2.1.2 Application

Most generally, engineers know so as to apply their knowledge to concrete outcomes, such as processes, systems, or products. As previously mentioned, the distinction between engineering and science has generally been characterized by the applied nature of the former. Discussion of the nuances of engineering and technology vs science vs applied science are extensive, dating back to Aristotle’s distinction between epistêmê and technê as different types of knowledge [224], [225], [226], [227]. Given our functional definition of engineering, the definition and distinction of these terms are also taken to be what they may. What is important to note, however, is the frequent association of engineering with *application*, *practicality*, and *utility*—values which are engrained in the epistemological and ethical identity of engineering.

Several authors emphasize the applicability, practicality, and the utility of engineering practices in different ways. Some examples include the following:

- “As an engineer, we do not want to get better and deeper knowledge, but better ends” [224].
- “Engineering is the art of utilizing the forces of nature for the use and convenience of man” [226].
- “In engineering the solutions of the technologists are applied to particular cases” [228].
- “In engineering, where practical application is paramount, […] knowledge finds its main and defining use in a separate institution [from where it is generated] – the industrial design office” [227].

- "The urgencies of the engineer's task impose the necessity to compromise the ideal with reality and successful compromise demands a feel or intuitive insight for the practical" [226].

From these quotations, written by both philosophers and engineers moonlighting as philosophers, we see that engineering is understood as being about *what* you build. The product is of greater importance than understanding or knowledge itself. There exists a particular end to which engineering knowledge is directed, and as this end is a product, there is often an orientation of engineering practice toward *industry*. Engineering knowledge is practically acquired, practically held, and practically applied. The practicality of the engineer's work is also linked to engineering design and judgment, as suggested in the final bulleted quote. As Poser notes, engineers do not seek true laws or theories, but rather "sufficient ones with respect to ends" [224].

Following the outlined understanding of engineering practice and design, engineering knowledge is distinctly creative and constructive. Aeronautical engineer Walter Vincenti notes that "by employing knowledge in design as well as in generating more knowledge – that is, for two uses instead of one – activity in engineering is distinctively asymmetric from activity in science" [227]. At the same time, according to Vincenti, engineering knowledge contains "a great deal more" than scientific knowledge applied to design. He explains this by giving an example of an aerospace engineering decision which involved math, science, and input from airplane pilots operating the engineered machines:

> "The […] tradeoff between conflicting requirements […] came into being because of the practical needs and limitations of the human pilot. The balance therefore could not have been achieved on purely intellectual grounds and without extensive flight experience. [The outcome] summarized a practical design judgment (based in this case on subjective opinion) of a sort that cannot be avoided in engineering. Achieving such judgment […] involved elements that can properly be regarded as science (e.g., the analysis of dynamic response by applied mathematicians). Predominantly, however, it called for a great deal more than simply the application of scientific knowledge and principles. It required a complex interaction of intellectual and experiential elements reacting to and going on within a context of practical design demands. This "great deal more" provides evidence […] of the epistemological difference [of] engineering." [229, p. 107]

According to Vincenti, engineering knowledge is more than applied science since it involves knowledge of the interactions between humans and machines. That is, the engineer integrates the engineered solution with its application, requiring both a broad and deep understanding of the technical, contextual, and experiential elements relevant to challenge at hand. In this way, the two key characteristics of engineering, design and application, are intrinsically linked.

Central to the societal value of engineers are the technological outcomes of engineering practice. From its conception as a term in the late 19th century used to describe the practical arts, "technology" has been linked with the notion of *progress* [230]. This is to say that, in some manner—be it only perceived or authentic—engineers offer society not just products and tools for the "use and convenience of man" but also the opportunity for development and social progress. Although it may be a dangerous generalization, if societal flourishing follows and is

truly linked to technological development in any way, then engineers perform a great service to society and carry responsibility for global well-being. Emphasizing that it is not obvious nor straightforward how technological development supports progress and authentic (human and ecological) flourishing, it is possible to say that the applied nature of engineering practice is central to the social value of engineers. This profound role and responsibility further enforce the understanding of the engineering identity and their obligation to produce influential outcomes. Further, if the social identity of engineers is substantially linked to the technological products and impacts of their work, we might ask if challenging technology implies a challenge to the essence of what it means to be an engineer. Wisnioski suggests this is the case for the engineer Samuel C. Florman, based on his writings about *The Existential Pleasures of Engineering* [200]. For Florman, the engineer is both the originator of modern successes and the scapegoat for the demise of humanity. In this way, the engineering identity is socially linked to both the benefits and ills of technology.

4.2.2 Identifying a tension in the framing of engineering

Engineers have been critiqued for being uninterested in the source and status of their knowledge, tending to carry the "engineering" attitude of "good enough" [204]. In Vincenti's 1990 work titled "What Engineers Know and How They Know It", the flagship work on applied engineering epistemology, Vincenti himself claims that "engineers tend not to be introspective" [229]. Although we may not be known for meaningful reflection, emerging from my brief introduction of engineering design and application is that there exist specific understandings of what it means to be an engineer, both in regard to their ways of knowing and their personal and social lived identities. Additionally, from examining the defining elements of the work of engineers, I suggested that engineering design and application are intrinsically linked. This understanding suggests a sense of integration of the essential elements of engineering. However, in this section I discuss a broader tension between the contextual and non-contextual elements of engineering.

According to engineering professor and scholar of philosophy of engineering Byron Newberry, dialectics in engineering, or tensions within engineering or perceptions of it, are abundant, particularly in considering engineering identity and purpose [231]. According to Newberry, engineering is omnipresent but obscure, is a unified profession but of widely diverse disciplines, and is scientific but business-oriented. More abstractly, Newberry claims that engineering is idealized in its benevolence but is rarely critically evaluated in its practice. In addition to these dialectics, I identify a broader tension in the overall framing of engineering. Specifically, from my reading, I have observed that engineering as a practice is either framed as *contextual* or is assessed as *non-self-critical*. A contextual framing of engineering includes descriptions of engineering as contingent, particular, pluralistic, subject to change, decentered, and boundary-crossing. What I am calling a non-critical framing of engineering includes descriptions of engineering as asocial, apolitical, objective, purely technical, non-emotional, and de-worlding.

This dialectic seems to be inherent to our understanding of engineering, meaning that from different perspectives, engineering is both contingent and objective. At the same time, this dialectic is most often unacknowledged; scholarly assessments of engineering tend to take either a contextual or non-critical approach. Some examples of what I classify as contextual versus

non-self-critical framings of engineering are presented in Table 4.1. Following from this tension, we can ask: A) What does this dialectic say about engineering? and B) How might both framings be true, and what can we learn from them?

Table 4.1. Examples of contradictory framings or assessments of engineering classified as either contextual (left) or non-critical (right).

Framed as contextual	Assessed as non-self-critical
"Engineering is paradigmatic of what is undervalued in Western 'high' culture. […] Engineering is contingent, constrained by dictated value judgements and highly particular. Its problem solutions are context sensitive, pluralistic, subject to uncertainty, subject to change over time and action directed." "The rationality of engineering can be described as being different from the rationality of science in exactly the same way that the rationality of contingency based philosophy is distinct from the rationality of necessity based philosophy." Goldman 2004 [201]	"The first important ideology within the culture of engineering is the notion that engineering is a purely 'technical' domain, and thus asocial and apolitical. Because science and mathematics knowledge is understood to be the basis of engineering expertise, engineering work is assumed to be carried out objectively and without bias. […] Connected to the understanding that engineering work can be separated from the social is the ideological belief that it *should* be separated from the social. I call this the ideology of depoliticization—the belief that engineering work, by definition, should disconnect itself from social and cultural realms because such realms taint otherwise pure engineering design methodologies. […] Today, most engineers continue to conceptualize and portray their work as generally above emotional, social or political messiness. […] The majority of students take on the dominant depoliticized worldview that is core to the professional culture into which they are being socialized." Cech 2013 [232]
"The engineering design process embodies and exhibits precisely the kind of contingent, decentered, boundary crossing, and emergent ordering processes that postmodernity analyzes, explores, and celebrates. Engineers live but do not speak postmodernism. Engineers are the unacknowledged philosophers of the postmodern world." Mitcham 1998 [210]	"Efficiency, productivity, objectivity, and precision are quintessential technical measures, even though different branches of engineering might interpret these measures differently." Moriarty 2008 [233] "Modern engineering employs what might be called a scientifically informed heuristic procedure applied to a collection of activities, including design, testing, production, manufacturing, marketing, maintenance, and control. All these activities are at first contextually situated and constrained, but once the method swings into gear, it seeks to elude its contextual constraints. If the methods of the modern engineering enterprise are truly de-worlded, then their unfoldings proceed in a straightforward and unencumbered fashion. That is the way, for the most part, that engineering is taught in engineering schools." Moriarty 2008 [233]

"The bottom line is that engineering is not deterministic; it routinely requires setting priorities and selecting the best way forward from among multiple options when there is no one *right* answer." "By contrast [to science] engineering is characterized by contingency, probability, particularity, and concreteness. Engineers rely on subjective *knowledge-how* and opinions that are derived from personal and historical experience, with the goal of willful action and use." Bulleit et al. 2015 [217]	

4.2.2.1 What does this dialectic say about engineering?

The contextual/non-critical dialectic has been implicitly suggested by electrical engineering professor and philosopher of technology Gene Moriarty in his 2008 book by the title "The Engineering Project". Moriarty describes engineering as both a contextualized and colonizing project. He asserts that it "takes acting in the service of the Good to retain and maintain [the balance between the forces of colonization and contextualization]", where the Good is defined as the foundation of existence which is the basis of all that is worth having [233]. To Moriarty, this dialectic is a true tension which must be balanced by the notion of the Good. Similarly, Karwat has described a difference between old and newer conceptualizations of engineering, referred to as "traditional engineering" and "reflexive engineering" [234]. For Karwat, these are two distinct "types" or phases of engineering, which are the result of historical understandings of the moral role of the engineer. However, the contextual/non-critical dialectic I pose here does not suggest an inherent tension, but rather a tension in certain understandings of engineering. That is, engineering practice is not at odds with itself but rather would benefit from an exploratory analysis of how both (and multiple) aspects of the dialectic might be true.

4.2.2.2 How might both framings be true?

As a human practice, engineering is contextual and scientific, and it is emotional and rational. In line with this, engineering is both affective and rational. Engineering deconstructs in multiple senses and constructs in multiple senses. In the understanding that engineering is philosophy and philosophy is engineering, it does not make sense to differentiate between "types" of engineering as context-sensitive or not. The tension within engineering is not necessarily a fracture of the discipline but a feature of this human practice.

A key aspect of the distinction between the ends of the engineering dialectic is the engineer's self awareness and understanding of their place. In this way, these end seem to describe two different manifestations the same profession, simply differing in their degree of humility, or right understanding of their place. Mitcham highlights the primacy of self-knowledge for engineers and the opportunity for engineers to learn through the philosophy of engineering. Reflexive practices involve thinking about our work, our thinking, our role, our identities as engineers—

and not only reflecting, but reflecting with a capacity and willingness to adapt our methodologies and questions to better integrate with our understanding of the results of our reflections. In this sense reflexive acts (the action-based outcomes of reflection) are to engineering as reflective acts are to philosophy. Furthermore, reflexivity in its creative capacity and response to contexts might be considered quintessential to engineering itself, such that through reflexivity, the balancing of this tension subsides, and the work of engineers is more fully oriented toward the Good.

4.2.3 Historical development of "nuclear engineering"

The term "nuclear engineer" was applied to the scientists and engineers who sought to deploy the power of nuclear physics and chemistry in the 20th century. In addition to developing as a novel technical domain, nuclear engineering developed within a new organizational context [235]. Previously, scientists practiced their research within university science departments and industrial laboratories, with relatively few of them employed by the government, but with the development of wartime research efforts, such as the Manhattan Project, many scientists and engineers found themselves employed by government and military-funded research initiatives. Post-WWII, these government research efforts continued via the establishment of national laboratories. The first national laboratory, Argonne National Laboratory, cites its establishment in 1946 as having the goal to perform "cooperative research in nucleonics", another term used to describe the field of 'nuclear engineering' or 'atomic energy' [236]. This time period was marked by specific understandings of the role of technology [230]. During the war, there was a remarkable sense of urgency in technological development. In his memoir, Lieutenant General Leslie Groves Jr., director of the Manhattan Project, describes how technological development had to be driven forward even before scientific understanding. Without scientific confirmation of how the enrichment of uranium would take place, he ordered that the technological infrastructure be built, with the belief that if understanding came before action, it would be too late for the war effort [237]. In the years and decades following the war, disillusionment with the failed promises of technology surfaced [238]. The birth of nuclear engineering, therefore, coincided with, developed out of, and contributed to shaping a time of transitions: from academic research to centralized war efforts, from the brand-new field of quantum mechanics to urgently demanded technologies, and from modernist views of boundless technological advances to subsequent pessimism. Nuclear engineers—those who investigated the possible uses of nuclear physics and nuclear chemistry—were the leaders of a domain which was entangled with military applications both in essence and in practice. The atoms carried within themselves the energy to cause unfathomable damage, and even peaceful applications of nuclear energy were plagued by potential misuse since reactors used for production of electricity could be employed, with modifications, also for the production of weapons-grade fissile material [239], [240]. Moreover, civilian nuclear energy was developed in and continually situated within the legacy of weapons research, particularly at the national laboratories [241]. These contexts—the social, political, and technological—along with the intrinsic properties of the atom and its accumulating legacy shaped what we understand as the academic discipline and practice of nuclear engineering today.

4.3 Methods: Textbook Analysis

Through this study, we address the question: What understandings of knowledge and the role of the engineer are embedded in core nuclear engineering textbooks? To analyze what constitutes "nuclear engineering knowledge", textbooks from a variety of nuclear engineering topics have been surveyed for evidence of epistemological and pedagogical claims and postures [242], [243], [244], [245], [246], [247], [248], [249], [250]. Textbooks were chosen as an indicator of core nuclear engineering knowledge because of their role as references — they provide a deep and broad presentation of core content for both students and practitioners of the field. As references, textbooks often seek to be comprehensive and authoritative. This authority is often claimed on the basis that the text presents a factual and essential view of the topic. Notably, the knowledge presented in a text intrinsically shows the choices of the author, for example, in their decisions on which topics should be considered as important (or which are excluded) and how topics should be organized. The dilemma of objectivity of references is detailed in the context of scientific images and atlases in the late 19th century by Daston and Galison [251]. Like atlases, textbooks serve to "drill the eye of the beginner and refresh the eye of the old hand" while capturing essential and impartial knowledge of a topic [251]. Defining what is essential and approaching impartiality requires value judgements which may reflect the values of the author and the values of the academic field.

Specifically, nuclear engineering textbooks were reviewed for how they define nuclear engineering and nuclear engineering knowledge both explicitly and implicitly, as outlined in Table 4.2. Explicit definitions include claims made about what constitutes an "engineering approach" or "engineering judgement". Explicit descriptions of the role of the nuclear engineer include broad outlines of the fields and topics relevant to nuclear engineering as well as claims of what the engineer "must know". When looking for implicit definitions, the texts were analyzed for underlying attitudes or assumptions. Indicators of this include phrasing of the author(s) perspectives (e.g. what is "expected" of the nuclear engineer, or what lessons have resulted from nuclear power plant accidents), anthropomorphisms, and normative claims. Specifically, the analysis consisted of recording notes on the goal of the text, applications of nuclear engineering (indicative of what nuclear engineering "is"), the impacts of nuclear engineering and technologies, the responsibilities of a nuclear engineer, the language used that indicates underlying attitudes and opinions about nuclear engineers' roles and responsibilities, and discussions of risk and public opinion. Narratives about risk and public opinion are specifically analyzed as topical categories because of the ways they reveal attitudes towards knowledge beliefs and priorities.

Table 4.2. Explicit and implicit definitions of nuclear engineering knowledge, with examples. Key phrases analyzed are shown in bold underline.

Explicit Statements which claim explicitly what engineering (or an objective related to engineering practice) or the author's goal is	**Implicit** Wording and examples which illustrate beliefs about or attitudes linked to engineering and engineering knowledge, without explicit claims
• Engineering approach or engineering judgement • What the engineer must know • Statements on the engineer's identity	• Underlying beliefs and assumptions • Anthropomorphisms • Normative claims • Attitudes

Example: "Our objective can often be achieved by applying the accumulated engineering experience in a manner that empirically relates macroscopic quantities, for example, the pressure drop and flow rate through a tube, without obtaining the detailed distribution of the fluid velocity or density in the tube. This **engineering approach** can be used whenever the flow characteristics fall within the range of previously established empiric relations" [242] (pg 439).	Example: "**Even if** the risks from low-level radiation were established quantitatively on a firm scientific basis the setting of limits would **still represent a social judgment** in deciding how great a risk **to allow**" [249] (pg 449).
Example: "The overall **objective of radiation protection** is to balance the risks and benefits from activities that involve radiation" [249] (pg 449).	Example: "This presentation is designed to **clearly illustrate** how this recompression cycle must be designed and analyzed, a subtlety which **otherwise easily confounds the inexperienced analyst**" [242] (pg xxii).

The surveyed texts were all published between the years 1975 and 2022, shown in Figure 4.1. Multiple editions of the same text were not reviewed, but the forewords of second or third editions often mentioned updates such as changes in the unit systems presented, as well as more substantial updates of the technical content to include discussion of advanced reactor concepts.

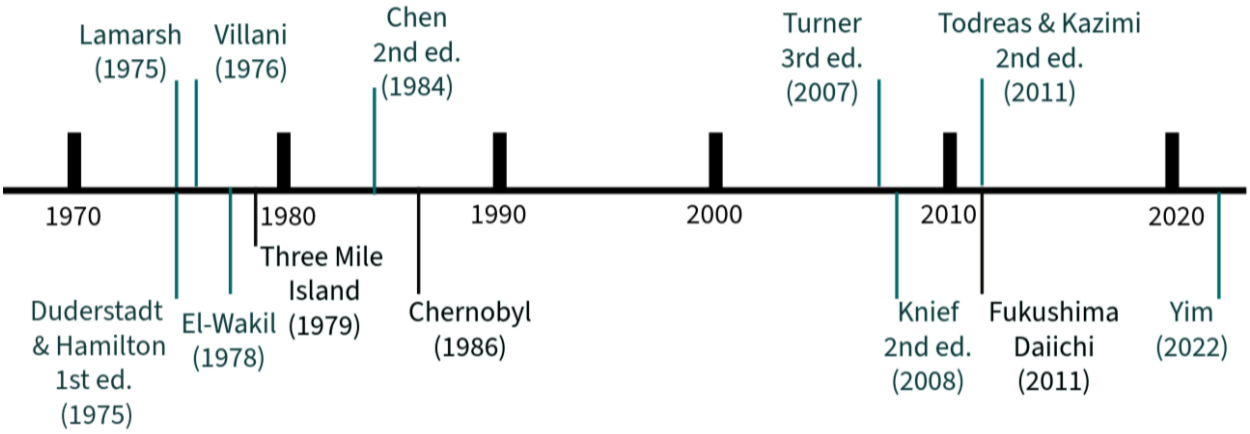

Figure 4.1. Timeline of the textbooks analyzed and historical events that are incorporated in some later editions of the textbooks as seminal case studies in nuclear engineering.

The aim was to analyze textbooks from a variety of topics within nuclear engineering, from neutronics and thermal hydraulics to radiation biophysics and nuclear waste management policy. We note that several textbooks were unintentionally not included in this analysis and should be included in further studies. These include [252], [253], [254]. When faculty teach courses, textbooks are not always available, thus a compilation of course notes and journal articles is created. Such compilations are sometimes the basis of new books that are written, thus out of the necessity of teaching courses and evolving the curriculum. Although there exists no primary

textbook or set of books that is exhaustive of nuclear engineering curricula, an analysis of some of the nuclear engineering textbooks that are available today offers a starting point for how knowledge is institutionally transferred throughout generations of engineering practitioners.

4.4 Analysis

Key themes about the identity of the nuclear engineer and of nuclear engineering knowledge found in the textbooks include 1) the authoritative nature of knowledge, 2) the relevance of multidisciplinarity in complex problem solving, and 3) the concept of the engineer as a problem-solver. These themes are detailed and discussed below.

4.4.1 Authoritative nature of knowledge

The social role of textbooks as references shapes their content and the way their content is presented. Several of the texts surveyed expressed in their prefaces the desire to serve as both an instructive resource for students and a reference for practitioners in the field. This is noted in the second row of Table 4.3, which offers the example of a textbook published by the American Nuclear Society, a primary professional society of the discipline in North America. The intended purpose of this text is not just to instruct students, but to serve as an authority, implying that knowledge claims require qualification. In claiming this purpose, the text makes implicit claims about the nature of knowledge and responsibilities of engineers. That is, the stated authoritative and universal nature of knowledge implies that *a truth*, which can be found in a textbook, largely remains valid across time, space, and across knowledge producers and consumers. This universalism, however, fails to acknowledge the ability of the field to adapt, grow, or change fundamentally. More abstractly, through the understanding that the authority of the field lies in its *factual truth* rather than in the hands of knowledge producers, a sense of the objectivity of the nuclear sciences is cultivated, shifting the responsibility away from individuals to the indisputable higher authority of facts.

Table 4.3. Some excerpts analyzed from the textbooks, our interpretation of the excerpt, and discussion on the implications of our reading of the text. These excerpts contribute to the theme of *the authoritative nature of knowledge*.

Text analyzed (emphasis added)	Our interpretation of the text's claims	Discussion of our interpretation
"published as one of a continuing series in [ANS]'s program for providing the nuclear community and related fields **authoritative** information in monograph form" [243] (pg iii).	• Textbooks must serve as an authority. • Engineers base their practice in truth, and truth is dictated by vetted references which summarize the foundational science and engineering designs. • The information presented is uncontestable.	The practice of engineering is colored by the understanding of science/engineering practice as universal. The textbook seeks to provide information which is true across time, space, and culture. This could limit the growth of the field. (See Section 4.4.1 below for further interpretation.)

"**everyone** has had the experience of a cigarette ash dropped innocuously on his hand" [248] (pg 7)	• This is an example to which every reader of the textbook can relate.	Although effective at explaining heat capacity, this statement confidently but falsely claims that this experience is universal. This might be considered an historical artifact, but statements like this (which persists in the 3rd edition published in 2016) can limit the present-day representation of the engineer to what it was in the 1980s.
"This presentation is designed to clearly illustrate how this recompression cycle must be designed and analyzed, **a subtlety which otherwise easily confounds the inexperienced analyst**" [17] (pg xxii)	• Textbooks help prevent pitfalls in learning. They should be used to help students learn the "correct" way to analyze. • Students and early-career engineers are easily confused by certain engineering topics.	This makes apparent the power difference between students and their instructors. Instructors (or textbook authors) in this mindset are authorities who have the right answers to help easily confused students. This, however, is only one way of viewing the dynamic between students and instructors.
"risk has been **unduly exaggerated** […] **In actual fact**, the risks from nuclear power are extremely low when compared with risks commonly accepted in other forms of human endeavor" [246] (pg 485)	• Risks are evaluated solely in a factual and rational manner. • Risks should be evaluated as relative and according to a standard that was constructed by engineering expertise. • Societal actors considered non-expert distort "true" risk when evaluating it. • The risks and safety of nuclear reactors are so well understood that this statement is universally true and should be taught to students of nuclear engineering.	See discussion in this Section for further interpretation. We note that this is only one text's view of risk.

"The remaining risk **must be acceptable** from the point of the people potentially affected by the presence of nuclear waste […] **Unfortunately**, the estimated risk does not determine whether the result is acceptable by the public. **The result does not dictate how people should feel about being safe**" [250] (pg 2)	• Feelings and emotions complicate risk management. • It is unfortunate that problems in risk management are not simply a matter of estimated risk; it is a problem or a bother that the public's opinion must be taken into account. • Some level of assumption of risk by the public is inevitable, and "acceptability" is the deciding factor for whether and how it is imposed.	We infer from this text that engineers prefer to solve problems in a way that focuses on estimation and quantification. The complications introduced by social factors and opinion are seen as undesirable, perhaps because of their subjectivity. No clarity on how what constitutes an "acceptable" risk and how it is determined—by or for affected people?—is offered. See further discussion of the related topic of rationality and quantification in Section 4.4.3.
"**It is evidently** not economically practical to reduce the emission of radioactivity from a nuclear power plant to zero, and **it is necessary**, therefore, to release to the environment, from time to time, small quantities of radionuclides" [246] (pg 563)	• It is *clearly true* that radioactive emissions cannot be zero for an economically attractive power plant. • Thus, since *economic practicality is a primary objective*, release of radionuclides is a *necessity*.	Rather than describing the contexts and conditions, this is prescriptive statement. It might have been said that release of radionuclides "is justifiable with stakeholder consent" under certain circumstances. The role of the engineer is asserted as an authoritative decision-maker who makes judgements based on what is evidently practical.

An explicit goal of several textbooks is to instruct the novice, and some texts reveal attitudes toward the novice and their competency. See, for example, Todreas and Kazimi's comments on students' mistakes in their text on thermal hydraulics, listed in the third row of Table 4.3. Some texts also seek to clear up misconceptions about nuclear technologies themselves. For example, Lamarsh addresses the conception of the risk of nuclear energy:

> All engineering structures and devices inherently present some element of risk to their owners or operators and to the public at large. Nuclear reactors are no exception in this regard. At times, however, this risk has been unduly exaggerated, in some measure because of the innate fear of nuclear radiation on the part of the public, and also by the memory of the awesome effects of the nuclear weapons employed in WWII. In actual fact, the risks from nuclear power are extremely low when compared with risks commonly accepted in other forms of human endeavor. Indeed, to date, the safety record of the nuclear power industry has been excellent. […] However, nuclear power plants do discharge small amounts of radioactivity to their environs. [246] (pg 485).

If the audience for this particular discussion are students and novices new to the field, then it is notable to observe that this clarification was considered foundational enough (i.e. that it would endure in importance as the field evolves over the years) to be introduced in a text that is to be considered a primary reference and foundational text.

In this example, "actual fact" is placed in opposition to the "unduly exaggerated" fears of the public. Note that Lamarsh's comments on the safety record of nuclear power industry were written in 1975 before the nuclear accidents at Three Mile Island or Chernobyl. The idea of dichotomizing fact and fear has persisted, however. For example, an article from ANS's blog (not expressing the views of ANS) titled *Can we repeat facts about Fukushima often enough to overcome fears?* asserts that "unlike people who have been trained in nuclear sciences and engineering, facts do not matter as much to nuclear activists" who "relish in stimulating […] fear" [255]. This juxtaposition of fear and facts is rooted in the association of fears with irrationality. A famous quotation by Maria Skłodowska-Curie eloquently implies this association: "Nothing in life is to be feared—it is only to be understood." In his 1968 essay imagining how nuclear technologies could reshape society for the better, nuclear pioneer Glenn Seaborg applies Curie's quote, declaring: "Now is the time to understand more—so that we may fear less" [256]. Introducing the concept that truth alone will dispel fear, Seaborg calls for a "human breakthrough" wishing "we could somehow convince our fellow men that we now live in an age when fear, mistrust, and blind passions based on and regenerated by past ignorance and error must give way to a new level of understanding and reason among men" [256]. Although we take these quotes from two great nuclear scientists in isolation, these examples point towards the greater trend in nuclear engineering and in perspectives towards technologies more broadly. Despite the pervasiveness of dichotomizing fact and fear among engineers and other technologists, sociologist William Freudenburg explains that doubling down on "actual fact" (meaning insisting on the value of quantitative risk estimates and eschewing public concerns) is indicative of "fundamental misunderstandings of the nature of technical societies" and perpetuates the decline in scientific (or engineering) credibility [257]. He points out that managing risk involves questions about values and blind spots—questions which quantitative risk assessment (or engineers) might not be able to best address. In addition, he emphasizes the risk of recreancy, or a failure to carry out one's duty or what is entrusted to them, causing a betrayal and erosion of trust [258]. This concept highlights a deeper issue at play; rather than the point of conflict being rationality/fact vs irrationality/fear, perhaps the conflict rather is rooted in distrust stemming from recreancy and an inadequate response to our role as stewards of the engineering profession. Further complicating this challenge is the experience that trust is easier lost than gained—and is perhaps even more challenging to restore.

Within the mindset expressed by Lamarsh, trained engineers hold an authority which is grounded in the *objectivity of the truth*. ANS's Principles of Professional Conduct lists this grounding in objectivity and truthfulness as a core principle: "We present all data and claims, with their bases, truthfully, and are honest and truthful in all aspects of our professional activities. We issue public statements and make presentations on professional matters in an objective and truthful manner" [259]. While we recognize these professional standards as noble and responsible in intent, the implication of these principles is that professional nuclear engineers speak solely in the language of facts, eschewing irrationality and subjectivity. This in turn reinforces the expert-lay divide by staking claims to who has the authority (or who does not) over determining what is "rational fact" and valued expertise (and what is not) [260]. If textbooks are to adhere to the principle of truthfulness, this requires recognition of the nuances of their objectivity and subjectivity.

The author or authority's voice and tone in the presentation of the text can also have an impact on the role of the nuclear engineer communicated in the text. Some texts emphasize the historical

contexts and growth of the nuclear sciences, such as [249]. Others offer a more personal commentary on this development. For example, Lamarsh weighs in unequivocally on the use of nuclear weapons, referring to the "bombs which were presumably instrumental in the sudden termination of WWII" [246]. When referring to the language commonly used in the field to describe advanced reactors as "inherently safe", Knief comments that this is a claim that is "probably inappropriate" [247]. Also apparent are sensitivities to the effects of nuclear technologies, particularly nuclear weapons. Turner describes the existing data on human exposures to radiation. He states, "With its enormous scope and scientific value, the studies of the Japanese atomic bomb survivors have certain drawbacks", namely, the poor statistics due to the fact that "the exposed populations [were] lacking in healthy males of military age" [249] (pg 413). The lack of data on the populations fighting the war is framed as a shortcoming rather than a benefit for the lives spared. It is inherent and valid that the author's voice is present in their text, as shown in these examples. However, this subjective voice contradicts the claimed or assumed objectivity and underlying rationality of the textbook. That these textbooks and the subjective narratives contained within have nevertheless become authoritative, incontestable references in the field only further highlights the need for the critical inquiry of this paper.

Other obstacles to the authority of knowledge claimed by textbooks are expressed, for example, in the assaults on the credibility of experts and institutions discussed in the 2022 text on nuclear waste management by Yim [250]. Yim describes the history of efforts to dispose of nuclear waste in the United States and the U.S. Department of Energy's subsequent loss of credibility by their inability to implement a solution. This case illustrates the complex nature of the social, political, and technical questions at play in nuclear technologies and demonstrates that the authority of knowledge of technical solutions is not sufficient for resolving the controversies surrounding nuclear technologies. In acknowledgement of this, Yim includes chapters on policy, regulations, and decision-making. By admitting and presenting the limits of technological expertise, perhaps the authority of knowledge is enhanced, in the sense that credibility is gained although the authority is less founded in the absolutism of knowledge.

In the nuclear engineering textbooks reviewed, we identify several key themes on the authoritative nature of knowledge. Namely, the textbooks often read as if they are books of universal facts which instruct both students and society by prescribing and defining factual knowledge. The textbooks are portrayed as objective and the authors are portrayed as primary and credible authorities, while simultaneously, the authors' personal perspectives are apparent in teach text. From our analysis, the textbooks analyzed offer a limited, specific, and subjective perspective on a scientific or engineering topic that reflect and reinforce what has been constructed to constitute valid nuclear engineering expertise. As such, the implicit as well as explicit values of the textbook authors are portrayed as authoritative knowledge, reinforcing the epistemic boundaries, logics, and underpinning values of the nuclear engineering discipline.

4.4.2 Relevance of multidisciplinarity in complex problem solving

Many of the texts emphasize how nuclear engineering is multidisciplinary. Following from its development from the varied fields of physics, chemical and mechanical engineering, and policy, among others, nuclear engineering includes a variety of topics despite being a relatively specialized field. By the same token, solving problems in nuclear engineering is complex and

requires knowledge of technical details, economics, policy, etc. Many authors, in training students to become practitioners of the discipline, warn of the limitations of categorization and siloing of knowledge inherent in the *engineering approach* to problem solving. This approach is introduced as a guide for students which outline how to break down problems and systematically acknowledge uncertainties, their tolerances, and relevant assumptions [242], [245]. Some authors clarify that prescriptive approaches for solving problems are not always advisable given the multidisciplinarity of the problems at hand. The limitation of narrow approaches is explicit in texts focusing on the design of reactor cores and nuclear power plant theory. Todreas and Kazimi caveat: "We do not attempt to present a procedure for thermal design because nuclear, thermal, and structural aspects are intertwined in a complicated, interactive process" [242] (pg 29). Similarly, Duderstadt and Hamilton explain that "understanding of core physics is not sufficient. […] [The engineer] must learn how to interface his specialized knowledge of nuclear reactor theory with the myriad of other engineering demands made upon a nuclear power reactor and with a variety of other disciplines" [245] (pg 7). Although a deconstructive approach to problem solving is presented as a tool for engineers, the authors warn of its limitations. Analysis of the theme of the limitations of narrow approaches is summarized below in Table 4.4.

Table 4.4. Some excerpts analyzed from the textbooks, our interpretation of the excerpt, and discussion on the implications of our reading of the text. These excerpts contribute to the theme of *the relevance of multidisciplinarity*.

Text analyzed (emphasis added)	Our interpretation of the text's claims	Discussion of our interpretation
"We do not attempt to present a procedure for thermal design because nuclear, thermal, and structural aspects are **intertwined in a complicated, interactive process**" [242] (pg 183)	• Nuclear engineering is complex, so there is no one way to solve thermal design problems.	Here, the textbook authors make it clear that they cannot be prescriptive in their design. It is helpful that they are clear about the limitations of what the textbook can offer, while introducing students to key design concepts.
"nuclear analysis of the core […] must **interact strongly** with […] thermal hydraulics analysis, structural analysis, economic performance" [245] (pg 447)	• Certain analyses cannot be taken in isolation since they are highly interactive with other aspects of the reactor design, operation, safety, and economics.	Similar to the text in the row above, nuclear core analysis is deeply intertwined with other aspects of the reactor. The textbook authors make it clear that a singular problem cannot be solved without consideration of its relationship with other aspects of the reactor.

"Different approaches can be taken to site selection. These approaches include the technical approach, the public participation approach, the market approach, and the distributive justice approach […] What is needed is **an integrative approach that combines the strengths** of different approaches **while compensating the weaknesses** of the respective approaches" [250] (pg 485-486)	• Site selection (for nuclear waste disposal) can be done in ways that emphasize the most technically apt location, the most financially lucrative option, the most publicly supported option, or in a way which is most just to the communities affected. • Integration (possibly meaning optimization) is the way to manage the multiple and different approaches to the selection of the site for nuclear waste disposal.	Rather than saying the optimal solution should be obtained by balancing/optimizing the various approaches to site selection, the author recommends that the various approaches be integrated. This language avoids emphasis on quantitative methods (see Section 4.4.3) and shifts focus to a natural blending of techniques to highlight the strengths of multiple viewpoints.
"**Of course** one desires to minimize electrical generation costs **but** must also ensure that the safety of the reactor is not compromised" [245] (pg 459)	• Minimizing costs is the primary goal—and this should be obvious to the reader. • However, safety must also be maintained.	This is an example of the most frequently cited example of "multidisciplinary" analysis in the nuclear engineering texts reviewed: safety/design and economics. (See Section 4.4.2 for further analysis.)
"Design criteria are frequently **contradictory in nature**, and hence require **optimization**" [245] (pg 97)	• Maybe related to the quote above—minimizing costs and maximizing safety might be "contradictory in nature". • Optimization is *the* way to manage competing criteria.	Although the criteria are not specified, if safety and cost-effectiveness are the inherently contradictory criteria (related to the example in the 5th row, above), this framing of safety has implications on design and the practice of engineering. In this case, safety is framed as a costly burden, whereas it could be otherwise—an integrated and primary criterion. If criteria are contradictory *in nature*, then design is a fundamental competition of values. We note that the way of framing design in the text is just one method, although it is presented as *the* method of engineering design.

"The subject of nuclear reactor safety is **exceedingly complex**, enmeshed in a labyrinth of complex technical, regulatory, political, philosophical, and **even emotional issues**" [245] (pg 459)	• Surprisingly, even emotion is relevant to nuclear reactor safety.	The authors might be highlighting that emotional issues are often ignored, or they might be expressing that it could be surprising that emotional issues are relevant to engineering. It is valuable that this lesser-discussed aspect of engineering problem solving is named. It would be beneficial, we believe, to elaborate on how emotion cannot be erased from what might be considered a purely rational method of problem solving. (See Section 4.4.3 for further discussion of rationality.)

The interdisciplinarity of nuclear engineers frequently refers to the analysis of both cost and performance of nuclear systems [242]. In describing the "very important constraints" of nuclear fuel management, Duderstadt and Hamilton explain: "Of course one desires to minimize electrical generation costs but must also ensure that the safety of the reactor is not compromised" [245] (pg 459). In interpreting the structure of this statement, we see that the goal of minimizing costs is subtly ranked of higher importance than the goal of safety. When there exists a hierarchy of goals, the "engineering approach" classically is to weigh the contributing factors and perform a cost/benefit analysis. In the texts, oftentimes the bridging of technical and economic analyses are what simply constitutes "multidisciplinarity", however some texts point out other aspects such as aesthetic, socioeconomic, and environmental analyses [250]. Almost exclusively, however, the texts describe that the engineer manages multiple options via optimization of multiple analyses. See the final three rows of Table 4.4 for a summary of further evidence and discussion.

To serve as references, many texts attempt to be broad, incorporating scientific foundations, technology-focused details, comments on economic and safety analyses, and (sometimes) regulatory frameworks. No textbook or set of textbooks claims to be or effectively serves as a sufficient summary of nuclear engineering. The practical limitations to how much can be included in a text are usually acknowledged, but nevertheless which topics are given priority reflects the authors' values and priorities. In Lamarsh's *Introduction to Nuclear Engineering*, he explains that "in order to meet a publication deadline, the discussion of environmental effects had to be confined to those associated with radioactive effluents" [246] (pg viii). The original goal was to include a separate chapter on all environmental effects of nuclear power, but this was relegated to a section in the chapter on licensing and safety. Perhaps a practical reason for shortening the discussion on environmental effects is legitimate, but we note which topics are not essential *enough* to receive full treatment in the introductory text. This decision offers some insight into the priorities and pressures within the field; thorough discussion of environmental effects was lower priority than reactor physics, or at least environmental effects come after reactor physics and then receive less attention. This, however, is only one way of rationalizing the design of a reactor. It is feasible to frame the problem with environmental effects as a starting

point, but the standard approach to nuclear engineering treats the environment as an addendum or final consideration.

We identify several elements of the key theme of the relevance of multidisciplinarity in the nuclear engineering textbooks analyzed. These patterns include comments that engineering is complex and involves the balancing of many demands. Most frequently, cost/benefit analysis or the combination of safety/design and economic analyses are cited. In the texts, optimization is the primary method for managing competing interests. From our interpretation, there is more to multidisciplinarity than economic and technical analyses; social and political aspects are also significant, and some texts make note of these. Even so, the multidisciplinarity acknowledged in these texts is limited in the sense that it generally fails to invite critical thought that may contest and expand the underpinning logics and assumptions of the nuclear engineering disciplines. Instead, the multiplicity of disciplines invited to engage with nuclear technology primarily encompass those that are instrumentally useful to reach an implicit normative goal of supporting societal progress through nuclear technology, with harmful impacts as discussed above an afterthought. We agree that no textbook can be fully comprehensive, and we believe that in generating a textbook, particular attention should be given to which topics are included and which are excluded. These decisions of what to highlight and dismiss sustain narratives of what is and should be essential to nuclear engineering.

4.4.3 Rationality and quantification in the pedagogy of problem solving in nuclear engineering

Complex problem solving, as it is taught in nuclear engineering texts, is often done by the deconstructive “engineering approach” as described in the previous section. Todreas and Kazimi are explicit in their definition of the engineering approach, which involves estimating via empirical correlations:

> Our objective can often be achieved by applying the accumulated engineering experience in a manner that empirically relates macroscopic quantities, for example, the pressure drop and flow rate through a tube, without obtaining the detailed distribution of the fluid velocity or density in the tube. This engineering approach can be used whenever the flow characteristics fall within the range of previously established empiric relations [242, p. 439].

According to this definition, engineers accumulate experience to have a working understanding of a topic, and they then apply that knowledge in a limited way to solve technical problems. They do not always need to have a detailed understanding of the more fundamental science at play. Some authors emphasize the benefit of understanding the underlying science to better understand engineering applications. Lamarsh describes the value of a "firm understanding of atomic and nuclear physics, since these subjects underlie much of the profession" [246]. But in how the engineering approach is described, there is an emphasis on practicality. The textbooks imply that fundamentals are only useful in that they serve the application. Todreas and Kazimi summarize the “basic question” of engineering practice as “how to predict the practically needed (and measurable) macroscopic behavior on the basis of whatever microscopic behavior may exist—and to the degree of accuracy required for the application” [242] (pg 183). Here, the

degree of accuracy required for the application is crucial. This requires a value judgement on what is considered appropriate or acceptable for a given system. This applies to the "engineering approach" more broadly, as well. The engineer must determine when and how much microscopic behavior is relevant to their application—or when the "engineering approach" applies to the problem at hand at all. In this way, the engineer must make subjective value judgements, and, if we interpret this in a manner consistent with the universalism and objectivity discussed in Section 4.4.1, the responsibility of the engineer is to do this in the most rational way possible, often by deconstructive and quantitative methods. In this singular approach to problem solving, there is some inflexibility. This approach does not necessarily provide solutions to questions like who has agency to make decisions on siting or in accident scenarios, for example, but these, too, are relevant to the operation of nuclear engineering technologies. Consistent with the dichotomization of fear and facts, rationality is elevated above other ways of knowing, such as emotion or imagination. This inflexibility, however, may be a barrier to more authentic exchange about issues in nuclear technologies such as safety and legacy.

Table 4.5. Some excerpts analyzed from the textbooks, our interpretation of the excerpt, and discussion on the implications of our reading of the text. These excerpts contribute to the theme of *rationality and quantification in the pedagogy of problem solving*.

Text analyzed (emphasis added)	**Our interpretation of the text's claims**	**Discussion of our interpretation**
" Hence what we should really look for is a **'fudged-up'** boundary condition which, although it may have little physical relevance at the boundary, **does in fact yield the correct neutron flux** deep within the reactor where diffusion theory is valid" [245] (pg 153)	• The "engineering approach" to problem solving involves estimation and empirical methods.	While rationality is emphasized in engineering and the sciences, rational decision-making is especially relevant to engineering.
"**Even if** the risks from low-level radiation were established quantitatively on a firm scientific basis the setting of limits would **still** represent a social judgment in deciding how great a risk to allow." [24] (pg 449)	• A social judgment is necessary for risk assessment. • The engineer might want to avoid subjective social judgments by their "firm" quantitative methods. But this cannot be avoided.	See detailed discussion in Section 4.4.3, below.

"While intervenors have acted **irresponsibly** in many NRC license hearings, and in some cases caused extensive delays in the construction of much-needed electrical generating capacity, the adversary proceedings of the public hearing have generally proved to be a sound method for **determining the truth in debatable issues** and for **providing a meaningful input from the public concerned**." [246] (pg 493)	• Public hearings have been largely helpful in finding solutions or the "truth" and allowing for public input. • At the same time, public hearings have led to unnecessary and harmful delays.	We note that the textbook authors describe that public hearings have effectively led to "determining the truth"—meaning that engineers and the concerned public were able to come to a shared understanding of the "facts". Rather than reaching consensus, this language implies that those involved were able to come to the "right" answer. See Section 4.4.1 for a related discussion on the authoritative nature of knowledge.

Risk management is discussed in the texts as one of the key problems that must be solved by engineers, as seen in the third row of Table 4.5. Like the value judgements necessary for applying the engineering approach to problem solving, value judgements are needed to manage risk in engineering applications. Turner explains:

> The overall objective of radiation protection is to balance the risks and benefits from activities that involve radiation. If the standards are too lax, the risks may be unacceptably large; if the standards are too stringent, the activities may be prohibitively expensive or impractical, to the overall detriment to society. The balancing of risks and benefits in radiation protection cannot be carried out in an exact manner. […] Even if the risks from low-level radiation were established quantitatively on a firm scientific basis the setting of limits would still represent a social judgment in deciding how great a risk to allow [249, p. 449].

As described in the example of radiation protection, managing risk is done in a manner analogous to design optimization, using the engineering approach. However, Turner points out the limits of quantitative risk management by explaining "even if" the engineer can establish a "scientific basis" for managing risk, value judgements on what risk is socially acceptable are necessary. In the tone in which we are interpreting the text, the language of "even if" is revealing of attitudes distinguishing a firm, factual understanding (what Turner might call the right answer) from a more subjective social judgement (what Turner might call a barrier to that factual answer). At face value, this quote shows commitment to a utilitarian understanding of risk, that is, weighing costs and benefits. More broadly, the implicit framing of risk as a problem (which may or may not be true in the case of Turner) highlights the epistemological attitude that the inability to be "exact", or perhaps purely quantitative, in solving a problem implies a weakening of the solution. In interpreting Turner, we read a sense of frustration with the inexactness of risk management—as if Turner is saying that it is annoying that one cannot get away from a social judgment, and since a social judgment is required, no exact answer can be construed. In this understanding, the engineer is profoundly committed to a singular method of problem solving. If the profession of engineering, as defined in nuclear engineering texts, is uncomfortable in managing inexactness or qualitative approaches to problem solving, this seems highly limiting to the effective development and implementation of technologies which are necessarily social in

nature. In this case, perhaps we engineers can learn from other disciplines on what are equally valid and useful ways of understanding and problem-solving, other than the "engineering approach".

Overall, rationality and quantification are predominant themes in the pedagogy of nuclear engineering, as revealed in the textbooks reviewed. Rationality and quantification are elements of the "engineering approach", which is a value judgement rooted in these principles which is often taught as the way that engineers solve problems. Several of the textbooks analyzed carried an undertone of frustration towards problems which cannot be solved in a straightforward manner via the "engineering approach", as it is defined in the texts. From our perspective, this points to the possibility that there are valid ways to solve or engage with problems beyond the engineering approach. We believe that engineers should learn from and collaborate with fellow problem-solvers who employ different methodologies or approaches, like social scientists or historians, who can offer critical and contextual frameworks that make visible the origins as well as impacts of the embedded values in and limitations of engineering disciplines.

4.4.4 Conclusion

By presenting an analysis of embedded value systems in nuclear engineering textbooks, we examine what is considered essential to being a nuclear engineer and explore how beliefs about knowledge and the role of the engineer shape how students train in the field and practice of nuclear engineering. We identify several key themes including the authoritative nature of knowledge, the relevance of (limited) multidisciplinarity, and the emphasis on rationality and quantification in pedagogy of engineering as problem solving. These themes, along with others, contribute to the historical narrative of what it means to be a nuclear engineer. In analyzing these themes, we identify a need for authors to acknowledge their subjectivities when portraying engineering information, that authors pay attention to what narratives are sustained by which topics are included and which are excluded from their texts, and that authors learn from and collaborate with researchers who solve problems via alternative and potentially critical methods to the "engineering approach".

4.5 Concluding discussion & a critical perspective

With the ultimate aim to alertly and thoughtfully proceed in engineering practice, I have looked to the foundational elements of engineering, namely engineering design (knowledge and judgment) and its applied nature, and presented an ostensive definition of engineering. In addressing the tension between engineering's management of context, I have presented the notion that reflexive practices are naturally intrinsic to engineering practices.

Designing chemistry control systems requires definitions of boundaries—of what compositions and flows are acceptable and unacceptable for the operation, maintenance, and safety of the system, for example. Further, building functional models of engineering systems, such as those of molten salts, may require elements of abstraction or simplification. From this work, it is apparent to me that engineers (and scientists) are responsible for rigorously defining systems, boundaries, and limits. That is, we must thoughtfully and intentionally make decisions while

holding risks, benefits, identities, and physical realities all in tension. Returning to Glissant (Section 1.5), these boundaries or borders necessarily invite exchange and encounter. They are created so as to *enable*, not limit, and any engineering decision or engineering boundary which does not enable is internally contradictory. I believe that as nuclear engineers, it is important to continually return to, reflect on, and engage with this aspect of engineering work with a reflexive attitude. And further, we can learn from the fields of philosophy and the social sciences to better understand both the human and social-technical aspects of this exchange and encounter.

4.6 Acknowledgements

The analysis of nuclear engineering textbooks was published in the transactions of the American Society for Engineering Education 2024 Annual Conference [261], supported by the Ron Gester Fellowship of the Department of Nuclear Engineering at the University of California – Berkeley.

Haley Williams: Conceptualization, Methodology, Investigation, Formal analysis, Writing – Original draft, Writing – Review and Editing **Denia Djokić:** Writing – Review and Editing, **Raluca O. Scarlat:** Conceptualization, Writing – Review and Editing, Supervision. We acknowledge generative engagements with STS concepts in nuclear engineering with Samuel Dotson (University of Illinois Urbana-Champaign).

5 CONCLUSION

To reiterate, molten salt *structure* refers to the dynamic ordering of ions over short- to intermediate-range length scales, while *speciation* refers to the identity, oxidation state, and (by relation) the chemical coordination environment of a component. Molten salt structure and speciation are relevant to advanced fission and fusion systems for their effects on thermophysical properties such as viscosity and conductivity. Structure and speciation are also tied to the salt's thermochemical behavior, such as the solubility of various species in the melt. In engineered molten salt systems such as loops, blankets, and reactor cores, it is imperative to understand salt chemistry to ensure cooling requirements are met, to sustain nuclear reactions, to maintain chemical compatibility and structural integrity, and to enable efficient heat transfer for energy production. This dissertation examines the structure of LiF-BeF_2 mixtures and the speciation of chromium in molten fluorides, providing analysis of the relation of structure and speciation for fundamental understanding of molten fluorides salts to enable chemistry control for a variety of applications.

In Chapter 2: Structural Studies of High Temperature LiF-BeF_2 mixtures, I present a structural interpretation of LiF-BeF_2 mixtures ranging from 33.3 to 100 mol% BeF_2 using neutron scattering data, EPSR models, and NNMD simulations. Our studies affirm the understanding of network formation in BeF2 mixtures and describe the balance between BeF_2 network formation and Li charge screening. Evidence of corner-sharing versus edge-sharing tetrahedra, the degree of distortion of tetrahedra with composition, temperature effects on Be-F and F-F bond lengths, and the role of lithium in the stabilization of terminal F are discussed. In addition, the differences between EPSR and NNMD models of the mixtures are addressed, with possible misattribution of Li features. Overall, these studies provide insight into the composition- and temperature-dependent structural features of LiF-BeF_2 mixtures which further provides foundational understanding for solute transport and solubility as well as momentum transfer and macroscopic thermophysical properties in molten fluoride salts.

In Chapter 3: Fluoroacidity Studies with Chromium Solutes, I present the results of electrochemical studies of chromium solutes in a variety of molten fluoride solvents. I examine thermodynamic and kinetic indicators of fluoroacidity as well as the electrochemical behavior of chromium solutes in each melt. I relate the concept of acid-base buffering capacity from Winner et al. to the nature of the acidic species in a melt, where the ionic or covalent nature of the acidic species influences how reversibly the cation binds fluoride and how effective it is as a buffer.

This work also emphasizes the reflexive practice of engineers by examining the nature of engineering knowledge and the engineering identity. In Chapter 4: Knowing and Being as a Nuclear Engineer, I open conversation about the field of philosophy of engineering and conclude with an analysis of core nuclear engineering textbooks. By attempting to integrate technical and philosophical topics, I hope to invite conversation on the foundational values, epistemologies, and priors of the field of nuclear engineering and the responsibility of engineers to engage in meaningful reflection on their work and identity.

The multidisciplinarity of nuclear engineering has always been an opportunity and challenge to the field. Dr. Philip Powers, founder of Purdue's nuclear engineering department, states in his history of nuclear engineering education, written in 1964:

> It is evident that engineering educators in all disciplines must find ways to work across departmental lines in order to deal with new and complex engineering systems, such as nuclear power, on earth, or in space. I believe, therefore, that as nuclear engineering educators we must face another important challenge. Not only must we gain research leadership, […], but we must also demonstrate how knowledge from several disciplines may be applied to engineering design problems. If we continue to pretend that we are a new engineering discipline, we are not only blinding ourselves to the true character of nuclear engineering, but we are missing an opportunity to demonstrate real leadership in the further improvement of engineering education in general. [262]

From its conception, the field nuclear engineering has blended the concepts and identities of several disciplines, and Powers points out that harking back to the roots of the field can only lead to growth, offering an example to emerging fields of many types. Further, multidisciplinarity is not only in our roots as nuclear engineers, but in our present identity, and, I believe, in our future. As I observe the emergence of new engineering majors such as those related to Artificial Intelligence [263], I wonder how a conceptualization of one's technical-professional identity rooted the breadth of social-technical practice might be beneficial to the emerging fields. I hope that this work might serve as a starting point for myself and others in discussing what it means to be a nuclear engineer, an AI engineer, or whatever type of engineer is yet to come.

6 APPENDICES

6.1 Data availability

6.1.1 Chapter 2: Structural Studies of High Temperature LiF:BeF_2 Mixtures

NOMAD 2022 and modeling data:

https://zenodo.org/records/7992414

NOMAD 2023, modeling, and EPSR:

Box, SALT_GROUP_FOLDERS, 99 – Personal Folders, Haley, Structure and speciation in molten fluoride salts – Dissertation data, Chapter 2 - Structure

Analysis, plots, and tables:

Box, SALT_GROUP_FOLDERS, 99 – Personal Folders, Haley, Structure and speciation in molten fluoride salts – Dissertation data, Chapter 2 - Structure

6.1.2 Chapter 3: Fluoroacidity Studies with Chromium Solutes

Box, SALT_GROUP_FOLDERS, 99 – Personal Folders, Haley, Structure and speciation in molten fluoride salts – Dissertation data, Chapter 3 – Chromium

6.2 Defining nuclear chemical engineering

In the United States, the field of nuclear engineering (NE) was, in part, reared by the field of chemical engineering (ChE). Those who came to be known as nuclear engineers (NEs) were trained physicists, chemists, and engineers with the objective of making useful the energy within the atom. With the urgent demand for nuclear weapons development during World War II, chemical engineers were enlisted to aid in the advancement and scaling-up of mining, ore refining, isotopic enrichment, chemical separations, and chemical processing and manufacturing [264]. Today, trained chemical engineers are involved with various aspects of the nuclear fuel cycle, including fuel production, waste processing, and other ChE-adjacent aspects of NE. However, even with the relevance of ChE processes to current NE practices, "nuclear chemical engineering" (which we will refer to as NuChE) remains rarely explicitly mentioned in NE academic training and has been called an "academic orphan" in this very journal in Axtmann (1975) [265]. To address this, Axtmann sought to define the nebulous field, or rather, topic, of NuChE, calling it "what chemical engineers do when faced by problems with a nuclear component" [265]. Axtmann explains that this definition is action-focused rather than education-focused because of how ChEs *participated in* NE; since the origins of the field of NE, ChEs were involved in nuclear technologies, but NuChE was never a distinct field of study. From our assessment, NuChE continues to be *practiced* but not described or defined as such. In light of the projected commercial development of advanced nuclear in the U.S. [266] and globally [267], we re-examine how NuChE might be *defined and studied* within academia. We argue that NuChE offers distinct, crucial, and substantial additions to the body of knowledge of the field of NE and contains topics that are critical to the formation of practicing nuclear engineers, i.e., that are essential to the development and operation of nuclear technologies. We propose a set of constituting concepts for the NuChE subdiscipline, and we make the case for the relevance of NuChE, given the present contexts of the growth of the NE industry [266] and further building on the historical development of the NE field that had at its roots NuChE as a necessary element.

To illustrate the value of incorporating NuChE concepts in NE curricula to better serve a growing need for a workforce that will help deploy and manage a new fleet of advanced reactors, **we use molten salt-employing reactors (fission and fusion concepts) to draw examples for the application of NuChE.** Axtmann (1975) points out that molten salt reactors are a central example where ChE is relevant to the "central device" of the reactor itself [265], [268], [269], [270]. Presently, many reactor designs are being developed which employ molten salts. Here, we refer to the fission and fusion systems which employ molten salts as *MSR+*, expanding the acronym for Molten Salt Reactors (MSR), which typically refers only to salt-fueled reactors or fission systems [268], [269], [270]. MSR+ includes salt-fueled reactors such as the molten chloride fast reactor (MCFR), salt-cooled reactors such as the fluoride salt-cooled high temperature reactor (FHR), and fusion systems with salt coolants and breeding blankets such as the ARC reactor [13], [271], [272][d]. While not within the scope of this work, examples for the

[d] An ANS Nuclear News article notes the status of several advanced nuclear companies and demonstration projects. Those which employ molten salts are the KP-FHR of Kairos Power, TerraPower's Natrium reactor which uses molten salt for thermal storage, the Molten Chloride Reactor Experiment which is a DOE project shared between Southern Company and TerraPower, and the molten salt research reactor to be built at Abilene Christian University

application of NuChE to the NE field can also be found within other emerging and growing areas of nuclear engineering—for example, other advanced reactor technologies, upstream and downstream aspects of the fuel cycle, nuclear security, fusion systems with other tritium production processes, medical isotope production, and other medical applications.

6.2.1 Background

Classically, "nuclear chemical engineering" has been defined by Benedict, Pigford, and Levi's 1981 text of the same name [274]. The topics in the textbook include isotope separation, separation of metals by solvent extraction, and large-scale separation and purification of radioactive materials, as well as fuel (re)processing and waste management. Of the 39 instances "nuclear chemical engineering" appears in the ANS Digital Nuclear Archive[e], 35 of the appearances are citations of Benedict's text. The others are:

- a list including NuChE as a specialized topic within waste management in a *Transactions* paper on the new adaptation of one university's fuel cycle/waste management curriculum (2011) [275],
- a list including "Introduction to Nuclear Chemical Engineering" as new, regularly offered, multidisciplinary course in a *Transactions* paper on developments within another university's NE training program (2013) [276],
- a reference to NuChE chemistry codes for liquid/liquid extraction in a *Transactions* paper on criticality safety for uranium extraction and purification using a multi-stage mixer-settler (2016) [277],
- and a mention of NuChE as a topic within a research consortium related to speciation, solubility, and radioisotope separations (2022) [278].

Within the decades of ANS digitized records (from 1959 to the present), there effectively exist just these four explicit mentions of NuChE, although chemical engineers are more regularly mentioned in earlier publications (Figure 1). To the best of our knowledge, no explicit descriptions of NuChE exist since Axtmann's 1975 paper and Benedict's 1981 textbook, and there exist very few mentions of the term as a distinct subtopic within the literature on nuclear technologies [265], [274]. In the literature on the history of ChE, there do exist some references to the contributions of ChEs to the nuclear industry, specifically in Canada and the United Kingdom [279], [280]. These discussions of NuChE are related to the heavy water production, coolant chemistry control, and irradiated fuel processing (for recovery of plutonium) for Canada's CANDU reactors and, in the UK, uranium processing and isotope separation. Overall, we observe that NuChE has rarely been explicitly referred to as a pertinent subdiscipline in NE. But NuChE is practiced and is relevant to fuel cycles, waste management, reactor operations, and

---

[273]. Commonwealth Fusion Systems exists to commercialize a fusion technology which uses molten salt as a tritium breeding blanket [13], along with other companies that seek to commercialize fusion systems that employ a salt blanket for tritium breeding and for capturing and transferring the produced heat to the power conversion system.

[e] The ANS Digital Nuclear Archive includes the complete Nuclear News (since 1959) and Radwaste Solutions (since 1994) archives, along with Transactions since 2004 and Proceedings since 2016.

other aspects of NE.

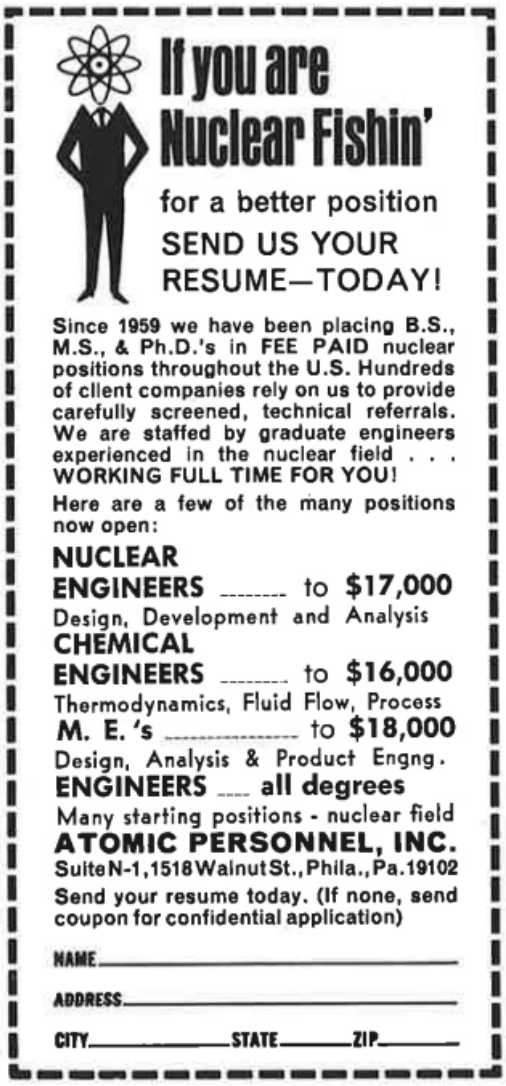

Figure 6.1 Advertisements in ANS's Nuclear News, such as this one from 1967, called for both ChEs and NEs to work in the nuclear industry. [21]

The relationship between the fields of ChE and NE is evident in the development of the fields' professional organizations. The oldest technical division of the American Institute of Chemical Engineering (AIChE) is the Nuclear Engineering Division (NED), chartered in 1954 [281]. It served as the first professional organization for the nuclear industry, inviting all nuclear workers, not just ChEs. As the desire for a new and independent professional organization for those working in nuclear energy was evidenced by a survey of Oak Ridge National Laboratory (ORNL) scientists and engineers, the American Nuclear Society (ANS) was established soon after in early 1955 [282]. A decade into the existence of ANS, nearly 20% of its members held degrees in ChE[f]. The NED of AIChE exists today, with an emphasis on the study of waste and fuel processing. Conversely, ANS does not include a distinct ChE division, but ChE topics are present in the ANS's Fuel Cycle & Waste Management Division. The history of the two professional organizations is telling, also, of the current relationship between NE and ChE. Since NE is more technologically specialized than ChE and since the field of ChE came first, NE can be considered a specialized offshoot of engineering and sciences, including ChE. Overall, NE exists as a distinct discipline with its own professional organization and with practitioners of a unique expertise, while maintaining elements of its parent disciplines, including ChE. Thus, NuChE is a subtopic within NE, both historically and practically; elements of ChE are found in NE because of the people who created the field, as well as due to the technical nature of the field. [283]

The existing present-day distinctions of the fields shape the practice of engineering, so we look to the historical motivations for the establishment of the field of NE to understand its definition. The establishment of NE as a specific undergraduate field of study, distinct from other engineering and sciences, was historically contentious. Considered as one type of "reactor" engineering, NE was, and, we concur, continues to be, more specialized than ChE, which has more varied applications such as biomedicine, petrochemicals, food, agriculture, and cosmetics. In the early days of the field, conversations took place regarding whether nuclear should be a specific type of engineering and whether NE should be

[f] From private communication with R. R. Quinn from Dec. 1974 cited in [265].

solely a graduate field of study. In his history of NE curricula, Murphy (1975) describes:

> One of the principal arguments that a field called nuclear engineering did exist and was not a mere subdivision of chemical engineering, mechanical engineering, electrical engineering, physics, or chemistry was the fact that it included [physics, radiochemistry, heat transfer, control theory, and many other related areas]. For a student to have adequate background in the fundamentals in all of these areas was not possible within the normal four-year program. Consequently the early philosophy was that an individual needed to have completed a BS program in an associated field before embarking upon the broader field of nuclear engineering. However, this view was not universally held[.] [284].

Murphy explains that some favored that NE remain a topic of graduate education only, stating the reasons for this as the *lack of nuclear industry* at the early stages of the field (thus, careers for graduates only existed in national laboratory research or faculty positions which required PhDs), as well as the breadth of knowledge and skills required, mentioned in the quote above. In addition, in the absence of a thriving nuclear industry, *research* on nuclear technologies has historically been supported *by federal grants* [285], [286]. Bachelor's programs did develop as the industry developed, however, and in the late 1950s, a committee was formed to define the essential topics of NE education [284], [287]. The report by this committee outlined several topics as key to the "substance" of an undergraduate NE program: mathematics, basic science (including physical chemistry[g]), engineering sciences, technology (analysis and design), technical electives, and liberal studies. They list "chemical processing" as a technical area for future nuclear activities, but they do not refer to the topics as chemical engineering. In this early definition of NE education, we see NuChE topics present in the guidelines for basic chemistry, engineering sciences, and technology studies. Since they have always been critical to nuclear technologies, ChE topics have been present from the beginning of formalized NE education. Further distinctions developed as the nuclear industry grew, and undergraduate education focused on the engineering topics relevant to the light water reactors of the time.

To summarize, nuclear chemical engineering has always existed as a subtopic within NE since ChEs were first enlisted to scale up separations and enrichment for weapons development. ChEs have worked in the nuclear industry, academia, and national laboratory research since the conception of the field of NE, both due to the relevance of ChE topics and the specialization of the field. The term "nuclear chemical engineering" has been used to describe what ChEs working in the industry do, but as the field has developed, NuChE has also come to describe *the chemical engineering that NEs do*, whether they realize it or not. The NuChE topics described in the literature fall under the following themes [288]:

- fuel conversion, manufacture, and reprocessing,
- isotope separation,
- release and transport of radionuclides in reactor accidents,
- and waste remediation.

---

[g] The Committee specifies that physical chemistry should include thermodynamics, chemical reaction kinetics, statistical mechanics, and kinetic theory [287].

ChE has always been relevant to NE, but it is not commonly part of the vocabulary of nuclear engineers. As the industry of advanced nuclear technology is growing, it is pertinent for undergraduate programs in nuclear engineering to formalize the training of these skills. By being explicit about the role of ChE in MSR+, i.e. explicitly describing NuChE in today's contexts, we hope to outline a legitimate field of study for nuclear engineers, thereby making connections between the fields of ChE and NE and generating more access points for ChEs to careers in the nuclear field.

6.2.2 Data

ABET lists the criteria for accreditation of ChE and NE programs as shown in Table 6.1. They clarify that they do not specify courses which should be offered, but rather they provide appropriate subjects which should be included. The criteria for NE are more specific than those for ChE—for NE, specific topics relevant to nuclear energy are listed, whereas for ChE, math, chemistry, and engineering are generally cited as requirements. No technological applications are listed for the ChE criteria, although the criteria are listed as applying to "chemical, biochemical, biomolecular and similarly named engineering programs" with a note that programs with bio-related modifiers "must also include biologically-based engineering applications in their curriculum as appropriate to the program's name and educational objectives" [289]. Notably, a few topics *are* listed explicitly for ChEs, including process control and process hazards. In the NE criteria, we would expect NuChE topics to be embedded in the "nuclear fuel cycles" and possibly the "nuclear or radiological systems and processes" topics. We note that chemistry is not listed as a relevant or required topic (whereas both chemistry and physics are listed for ChE, NE just requires atomic and nuclear physics, which may indirectly include physical chemistry).

Since ABET does not dictate which courses are required, just what topics should be included, curriculum is largely at the discretion of the department and takes shape based on the expertise and priorities of faculty. In this way, a ChE program might be more or less biology-focused, or might have an inclination toward petrochemicals, pharmaceuticals, or some other specific area. Similarly, the presence and strength of a department's teaching on nuclear waste management or fusion, for example, is influenced by the department's faculty.

Table 6.1. ABET subject area criteria (2023-2024) for ChE and NE undergraduate programs [289].

Chemical Engineering Curriculum Required Topics	Nuclear Engineering Curriculum Required Topics
"The curriculum must include: • Applications of mathematics, including differential equations and statistics to engineering problems. • College-level chemistry and physics courses, with some at an advanced level, as appropriate to the objectives of the program. • Engineering application of these sciences to the design, analysis, and control of processes, including the hazards associated with these processes."	"The program must include the following curricular topics in sufficient depth for engineering practice: • Mathematics, to support analyses of complex nuclear or radiological problems, • Atomic and nuclear physics, • Transport and interaction of radiation with matter, • Nuclear or radiological systems and processes, • Nuclear fuel cycles, • Nuclear radiation detection and measurement, • Nuclear or radiological system design."

Due to its specialization, it is understandable that fewer ABET accredited NE programs exist compared to ChE programs. The number of degrees awarded for each major, seen in Table 6.2,, also reflects this. ChE has approximately seven times the amount of ABET accredited undergraduate degree programs and graduates approximately 23 times more undergraduates (based on the number of degrees awarded in 2022), implying that ChE departments are much larger and host higher undergraduate enrollment than NE programs. The fraction of students who receive master's or doctoral degrees relative to the number of undergraduates in each field is approximately three times higher for NE than that for ChEs. This trend of a relatively higher number of graduate degrees for NE follows the historical perspective of NE education—that NE is more specialized and less industrial and hence lends itself more to graduate studies.

Table 6.2. Data comparing the higher education programming of chemical and nuclear engineering.

	Chemical Engineering	Nuclear Engineering
# of ABET accredited undergraduate degree programs, 2022 [290]	149[h]	20[i]
# of bachelor's degrees awarded in 2022 [291]	8,946	381
# of master's degrees awarded in 2022 [291]	1,531	217
# of doctoral degrees awarded in 2022 [291]	1,164	170
Ratio master's degrees to bachelor's	0.17	0.57
Ratio doctoral degrees to bachelor's	0.13	0.45

6.2.3 Concepts in Nuclear Chemical Engineering, and Corresponding MSR+ Examples

In Table 6.3, we present a set of constituting concepts for the NuChE subdiscipline, categorized in six unit topics: 1) equilibrium thermodynamics, 2) thermal hydraulics and mass transport, 3) process design and controls, 4) chemical process safety & environment, 5) fuel cycle & waste management, and 6) chemistry and kinetics. The relevance of nuclear engineers having proficiency in these concepts is then illustrated for MSR+ technologies. This organization and vocabulary (units, subtopics, concepts, motivation, and examples) is chosen to reflect what an undergraduate course in NuChE might include. The units are not equivalent in their breadth or in their depth of relevance, but we aim to be comprehensive in our assessment of NuChE topics relevant to MSR+. Table 3 is annotated to indicate which topics are typically included in NE curricula and which are typically included in ChE curricula (based on ABET criteria).

[h] Includes degrees titled "Chemical Engineering"—including all degree types (B.S., B.E., B.Ch.E., etc.). If variant ChE programs are included (e.g. Chemical and Biomolecular Engineering) this figure would be 167 programs.

[i] Includes degrees titled "Nuclear Engineering", "Nuclear and Radiological Engineering", "Nuclear Engineering and Radiological Science", "Nuclear Science and Engineering", and "Nuclear, Plasma, and Radiological Engineering". Note, the Nuclear Engineering Department Heads Organization lists 37 NE programs on their website: https://nedho.org/members.

Table 6.3. NuChE concepts and their relevance to the formation of nuclear engineers. Elements of NE or ChE curricula required by ABET accreditation (listed in Table 6.1) are indicated with superscripts. Application examples are provided for MSR+ technologies.

Unit topic	***Equilibrium thermodynamics***	***Fluid dynamics, heat, and mass transport***	***Process design and controls***	***Chemical process safety & environment***	***Fuel cycle & waste management***	***Chemistry and kinetics***
Sub-topics	—Chemical thermo[ChE] —Electrochemistry —Solution thermo	—Momentum transfer and fluid dynamics [ChE,NE] —Heat transfer[ChE,NE] —Mass transfer[ChE] —Mass balance[ChE] —Scaling analysis	—Process design[ChE] —Process control & instrumentation —Unit operations	—Chemical safety[ChE] —Environmental monitoring —Environmental decontamination	—Fuel cycle[NE] —Waste processing, storage, disposal [NE] —Lifecycle analysis	—Foundational chemistry: physical, analytical, inorganic chemistry [ChE] —Quantum mech [NE] —Radiochemistry —Kinetics and reactor engineering[ChE,NE]

164

Concepts	—Gibbs free energy, redox potential, derivation of the Nernst equation, activity coefficients and the connection to solvation structures and solvoacidity, Pourbaix diagrams, stability diagrams, equilibrium condition, chemical potential —Phase diagrams, free energy diagrams, solubility, concentration at chemical equilibrium, liquid/liquid separation, chemisorption, vapor pressure —Endothermic and exothermic reactions; energy balance —Chemistry control systems for source-term management and for corrosion control	—Radiative heat transfer with transparent and participating media —Species diffusion, concentration gradients —Diffusion and convection, with internal generation term —Residence time —Heat exchanger design —Turbomachinery design and specifications (pumps, valves, fans, turbines etc). —Specification of functional requirements and operational envelope for material properties —Fluid-structure interactions (thermal stresses, irradiation-induced stresses, thermal striping) —Scale-up and scale-down analysis	—Process design, definition of operational modes, functional requirements specification —Process energy integration —Scale-up and scale-down analysis —Piping and instrumentation diagrams —Material accountancy, safeguards by design —Plant layout —Controls hardware: sensors, transmitters, controllers, radiation-hardened sensors, testing, calibration, maintenance —Cybersecurity —Control system design —Control theory, feedback control, controller design and tuning —Frequency response analysis, system stability —Cost analysis	—Chemical risk assessment tools, hazards and safety protocols —Integration of chemical safety and radiation safety —Fundamentals of industrial hygiene —Emergency response planning —Fundamentals of human factors —Transport of radiochemicals in the environment —Regulatory limits for radiochemicals in effluents —Monitoring of environmental contamination	—Mining technology —Environmental impact assessment —Isotopic enrichment —Conversion —Synthesis of coolants and fuels —Separations: aqueous, pyroprocessing —Waste forms —Interim storage and long-term disposal —Lifecycle waste streams	—Chemical reaction kinetics —Irradiation effects on chemistry —Neutron activation effects on chemistry —Isotopic effects on chemistry —Radiolysis —Reaction progression variable —Actinide chemistry —Identification of oxidants and corrosion products, chemical and radiochemical reactions involved in environmental degradation of materials —Chemical speciation of radioisotopes in the environment —Chemical speciation of radioisotopes contributing to the source term in reactor severed accidents

165

Unit topic	***Equilibrium thermodynamics***	***Fluid dynamics, heat, and mass transport***	***Process design and controls***	***Chemical process safety & environment***	***Fuel cycle & waste management***	***Chemistry and kinetics***
Value of inclusion in NE curriculum	Fundamental understanding of liquid fuel reactors, fuel production and reprocessing, design of uranium extraction processes, source term prediction for molten salt fusion and fission systems, redox control for the purpose of corrosion control, redox control for the purpose of oxidation states of radioisotope and hence solubility and volatility of species that contribute to the source term.	Predictions for temperature, pressure, and species concentration vs time and space for containment barrier integrity and performance of functional confinement. Transport of source terms through fluid barriers and across phase interphases (liquid-solid, liquid-gas, liquid-liquid); of relevance to reactor design and transient analysis with advanced coolants and liquid fuels.	Identification of material diversion scenarios. Identification of potential source terms and rate of source terms leaking through containment boundaries during an accident scenario. Application of redundancy and diversity with a combination of active and passive safety sub-systems and the interplay between control systems and passive systems. Understanding of timescales of sub-system response and impact on response time required for operator action.	Background on chemical safety (in conjunction with radiation safety) is valuable for managing mixed plant hazards and avoiding safety strategies that are in contradiction (e.g., venting vs containment, dilution vs concentration and storage). Crosstalk between environmental monitoring and nuclear forensics/nuclear security/detection of diversion.	Relevant to development of new fuel cycles and new manufacturing supply chains.	Background in advanced chemistry such as analytical chemistry, physical chemistry, electrochemistry, or inorganic chemistry allows for crosstalk between the sciences and development of foundational knowledge of relevance to environmental transport and monitoring, fuel development, fuel cycle facility technologies, nuclear forensics, and design of reactor chemistry control systems.

Illustrative examples related to MSR+	Drivers for corrosion in a molten salt system: oxidants, dissimilar material effects, redox transients, temperature transients and gradients. Impact of redox potential on material diversion. Source term as a function of air ingress and oxide content (i.e., contaminant ingress). Definition of chemical operational envelope for specification of parts and components (e.g., pumps, valves, heat exchangers).	Use of sensors in non-well-mixed flows for temperature and composition. Verification of material inventories based on compositional measurements. Thermal striping in outlet plena. Design of heat exchangers and heat removal and heat addition systems for molten salts.	Avoiding system instabilities in passive (e.g., natural circulation loop) and active (feedback control) systems. Fueling and defueling planning for liquid fuel reactor, and implications on criticality safety. Design of reduced order tests (and characterization of their distortions from prototypical conditions) for testing of systems and components, such decay heat-removal system, and corrosion-irradiation testing.	Beryllium, HF, and F_2 safety instrumentation, safety strategy, and integration with radiological monitoring for tritium and other source terms that can present worker hazards during operation, inspection, maintenance and repairs.	Design of isotopic enrichment processes for light elements needed for MSR+: e.g., lithium, chlorine, boron.	Chemical consequences of neutron activation of salt coolants and of fission reactions (including corrosion). Solvoacidity, the connection to solvent structure, and the effect of radiation on solvoacidity in ionic melts. The impact of redox, oxoacidity, and solvoacidity on fuel inventory, source term, criticality safety, material accountability. Relevance of process testing with surrogate isotopes (e.g. D vs. T).

167

6.2.4 Discussion and Conclusion

Nuclear chemical engineering, as we have described it, is a blend of ChE topics applied to nuclear technologies and original concepts that arise from the synergy of the two disciplines. In this way, NuChE constitutes a unique subtopic within both NE and ChE. The value in NuChE lies in its relevance to the field of nuclear engineering, and thus, we believe that NuChE topics should be included within NE undergraduate curricula. We envision NuChE as the topic of one or several NE undergraduate courses, existing as a field of study alongside other classic educational and research topics such as thermal hydraulics, nuclear materials, or radiation detection. We suggest that NuChE should be *an option for specialization* for both undergraduate and graduate students. At the same time, we believe inclusion of NuChE topics in NE curricula would help other subdisciplines of NE bridge to NuChE topics and, furthermore, would provide an entry point for trained ChEs to the NE field. For example, inclusion of NuChE might be demonstrated through allowing the quantum mechanics prerequisite for NE degree programs to be met by either physical chemistry in the chemistry department or modern physics in the physics department. Additionally, NuChE-related courses such as advanced chemistry or process control could be explicitly listed as NE-relevant technical electives.

Based on the motivation to expand the nuclear workforce given projected buildout of nuclear within the U.S. [266] and globally [267], it is imperative to support pipelines to professions in the nuclear industry, which includes informing ChE of potential careers in nuclear. Other engineering disciplines such as ChE are large, well-established, and also have relevant elements of industrial application embedded in their curricula. Whereas the structure and content of NE education might not have historically emphasized preparation of students for careers in industry, we note that there is a need to make NE training “industrial” or at least to have the option of an “industrial” emphasis, particularly due to the need for a growing NE workforce to support advanced nuclear technologies. The inclusion of NuChE concepts in NE curricula is one step towards preparing students for careers in the nuclear industry.

In detailing the historical contexts of NuChE, we note that the initial involvement of ChEs in the development of nuclear technologies was for the purposes of nuclear weapons development during World War II. These fraught origins have contributed to our present understanding and definition of NuChE. As we envision of the development of NE curricula to better serve the goals of the field, we wish to emphasize the importance of thinking critically about our ethical and professional responsibilities in defining and pursuing the goals of nuclear technologies [292]. While the historical contexts of NuChE were acknowledged in the preparation of our definition of NuChE, future work could more thoroughly analyze underlying assumptions and social contexts.

In conclusion, we define six NuChE unit topics and their value in the formation of nuclear engineers and illustrate their relevance to MSR+: 1) equilibrium thermodynamics, 2) fluid dynamics, heat, and mass transport, 3) process design and controls, 4) chemical process safety & environment, 5) fuel cycle & waste management, and 6) chemistry and kinetics. Some of these topics exist already as embedded in NE curricula, however, some are typically ChE topics of study which we believe belong as foundational elements of the education of NE undergraduates, along with other traditional subfields such as thermal hydraulics, materials, and neutronics.

Overall, we believe that explicit inclusion of NuChE topics in NE curricula would create entry points for ChEs to the field of NE as well as provide for a more comprehensive NE education in light of the development and commercialization of fission reactors and fusion systems which employ new coolants, new fuels, and new fuel cycle technologies. Considering the historical contexts of "nuclear chemical engineering" as a topic and the development of NE and ChE higher education programs, we illustrate how nuclear chemical engineering would be implemented in the present-day NE curriculum in support of preparation of the workforce for innovation in, deployment, and management of advanced nuclear technologies.

6.2.5 Acknowledgements

This section includes work supported by Ron Gester Fellowship of the Department of Nuclear Engineering at the University of California – Berkeley. This material is based upon work supported by the Department of Energy National Nuclear Security Administration through the Nuclear Science and Security Consortium under Award Number(s) DE-NA0003996.

This work is included in the publication: Williams, H., & Scarlat, R. O. (2025). A Case for Nuclear Chemical Engineering in the Era of Fission and Fusion Reactors that Employ Molten Salts. *Nuclear Technology*, 1-12.

HW: Conceptualization, methodology, investigation, writing – original draft. RS: Conceptualization, methodology, writing – review & editing.

6.3 Additional data referenced in Chapter 2

6.3.1 Neutron scattering lengths, cross sections, & X-ray atomic form factors

Table 6.4. Neutron scattering lengths and cross sections for isotopes relevant to Chapter 2 studies, from NIST.

Isotope	Percent natural abundance	Coherent scattering length (fm)	Incoherent scattering length (fm)	Coherent scattering cross section (barn)	Incoherent scattering cross section (barn)	Total scattering cross section (barn)	Absorp. cross section for 2200 m/s neutrons (barn)
1H	99.985	-3.7406	25.274	1.7583	80.27	82.03	0.3326
6Li	7.5	2.00-0.261*i*	-1.89+0.26*i*	0.51	0.46	0.97	940±4
7Li	92.5	-2.22	-2.49	0.619	0.78	1.4	0.0454
Be	100	7.79	0.12	7.63	0.0018	7.63	0.0076
F	100	5.564	-0.082	4.017	0.0008	4.018	0.0096

Data in Table 6.4 were taken from the NIST NCNR website, which is a digital database for data from *Neutron News*, Vol. 3, No. 3, 1992, pp. 29-37.

X-ray atomic form factors are dependent on Q can be found in the International Tables for Crystallography (ITC) [293].

6.3.2 NOMAD Incident Analysis

Safety memo embedded in the following pages.

INCIDENT ANALYSIS FOR BERYLLIUM CONTAMINATION OF FURNACE AT NOMAD (JANUARY 2023)

Haley Williams and Nathanael Gardner

SCOPE

Review of sample preparation, decontamination, and discourse on safety for the NOMAD 2023 (IPTS-29309.1) experiment performed at ORNL.

SEQUENCE OF EVENTS

- Preparation and decon of samples

0. The approach to safety in the experiment proposal and in practice followed the practices used in the NOMAD 2022 experiment.
    - For the second experiment, measurement of mass loss of the canisters after beamtime was suggested but were said to be not necessary because the canisters were already verified to work according to ORNL.
    - Prior to the NOMAD 2022 experiment, a canister with FLiBe had been leak tested by Ryan Gallagher.
    - Leak testing results were below the free release limit, but there was an indication of a higher concentration of Be contamination after the sample that had been heated, possibly indicating minor leakage. Since this was below the free release limit, ORNL said it was possible to move forward with single containment. See Appendix A.
1. FLiBe and BeF2 were powderized and mixed in appropriate ratios for each sample. Samples were heated in a glassy carbon crucible within the furnace at 870 C to homogenize the salt mixtures.

Table 1. Sample can masses after preparation (filled with salt).

FLiBe	BeF2	90/10 BeF2/LiF	95/5 BeF2/LiF	75/25 BeF2/LiF	50/50 BeF2/LiF
8.8811 g	8.9672 g	8.8715	8.8707	8.8708	8.8702

2. The samples were sealed with a graphite gasket according to instructions provided by ORNL. Used high-temperature high-pressure Graphite Gasket Material 1/32” Thick from McMaster-Carr
3. The cans were wiped thoroughly with Ghost Wipes to decontaminate (while wearing clean nitrile gloves). This took place within the glovebox where the samples were prepared.
4. Swipe sampling was also done in Glovebox 2, where beryllium contamination was present. Clean gloves were worn, and the sample was passed between two people to avoid contamination of the gloves. Swipes were collected by wiping the entire surface area of the sample can.
5. Swiped samples were removed from the glovebox and shipped to ORNL. Sample swipes were sent for elemental analysis by ALS Environmental. Results in Appendix C.

- Decon of samples at ORNL
    1. Results from swipes indicated beryllium contamination (4-32 ug/sample) which was above the free release limit, so samples were further decontaminated at ORNL.
    2. Samples were then decontaminated at ORNL using a fume hood in a neighboring lab by Nathanael Gardner under the monitoring of Michelle Everett and Sean Fayfar. Participants wore SALT group standard PPE: a disposable lab coat, three pairs of gloves with the second layer taped to the lab coat to prevent dermal contact, and goggles. Decontamination was done by first placing a disposable cover on the bottom of the fume hood. Then one sample was brought out of the plastic bag and wiped 3 times with a ghost wipe and sprayed with water. After the third wipe, the sample was placed on the fume hood cover, and the exterior pair of gloves changed. The sample was then wiped 2 more times before being placed into a new ziploc bag for placement on the beam line. The exterior gloves were changed again. This process was then completed for the other 4 samples. All trash was loaded into a plastic bag and labeled beryllium trash. Also, the fume hood was thoroughly cleaned with ghost wipes, clorox wipes, and water after used and labeled potentially Beryllium contaminated
- Running of samples

    The samples were loaded onto and unloaded from the sample stick using the same level of PPE as cleaning. The sample stick was brought out from the oven and brought to the workbench. A sample can was then taken to the same fume hood used for cleaning, another cover placed down, and sprayed with boron nitride. This sample was then loaded onto the sample stick and the stick placed back into the oven. All sample handling was performed by Nathanael Gardner.

    During the measurement of BeF2, IPTS 29309, sample 86438 there was a large decrease in intensity. This anomaly led to the belief that the sample may have leaked through the gasket. However, Joerg Neuefeind has noted that this drop in intensity is possible due to an air bubble causing the sample to move around the can.

CONTAMINATION PATHWAY ANALYSIS AND RISK OF EXPOSURE

- If outer part of can was contaminated before experiment
    - Surface contamination of the sample would spread by surface contact
        - Workspaces, gloves, and furnace surface in contact with the sample would be potentially contaminated
            - Workspaces (fume hood) was swiped and determined clear of Be
            - Was the bench where samples were staged swiped?
            - Triple gloves were worn at all times when handling samples, with lab coat taped to gloves. Gloves were disposed of after use. The lab coat used was placed in a ziploc bag and disposed of.
- If sample can failed and Be-containing salt leaked into furnace

- Sample can likely would have leaked at high temperature. Experimental studies were run up to 800 °C.
  - At this temperature, FLiBe or BeF2 would be liquid. The vapor pressure of BeF2 would be higher than that of FLiBe and would be <0.01 atm (Cantor 1965, at 872.4°C). We might expect small amounts of Be-compounds as liquid or gas within the furnace.
  - The furnace was under vacuum at temperature. The gas was vented where. This line was sampled for Be contamination and was clean.
- The furnace was opened after sample cool-down to exchange samples
  - Any Be-compounds would be solid at that temperature. Particles could be airborne if there was a pressure difference, air flow through the furnace. There was no pressure difference.
  - Triple gloves and taped lab coats were worn when the furnace was opened and samples were exchanged.
- The can itself may have failed or the graphite gasket.
  - The sample was recovered after the experiment.
  - When a FLiNaK sample was tested in the sample can, it failed near the connection between the tube and bottom flange, not through the flange itself. This could be a weak point in the can.
  - The graphite gasket was cut following directions from ORNL.

QUESTIONS FOR ORNL

1. Could you provide analytical results for the Be swipes collected?
   a. When was the initial contamination found?
   b. What part of the furnace was swiped?
   c. How was the furnace decontaminated?
   d. What was the baseline Be contamination of the furnace before introduction of our samples? When was it last swiped before our experiment?
   e. When was the furnace swiped prior to decontamination?
   f. What other surfaces were surveyed?
2. Is air monitoring done in the vicinity or during decontamination of the furnace?
3. Are you able to follow up with visual inspection of the can and gasket?

APPENDIX A : EMAILS ABOUT SECONDARY CONTAINMENT FOR NOMAD 2022

NAMES REDACTED FOR PRIVACY WHEN IRRELEVANT

[redacted] Feb 17, 2022, 6:19 AM

Quick update,

I completed the heated tests of the LiF-BeF2 up to 750C for 12 hours in the vanadium PAC under vacuum (pulled to 6.3e-6 Torr and sealed prior to heating). Be samples were taken this morning and we will have the sampling results Tuesday or Wednesday. I did not see signs of oxidation like the previous LiF-NaF-KF heated tests, and the canister appears to be in good condition. I'll send some pictures out when I get the chance to check it out in a glovebox.

[redacted]
I'll be dropping of the PAC with LiF-NaF-KF this morning.

Thanks!
[redacted]

[redacted] Feb 22, 2022, 3:16 PM

Hi all,

The samples were shipped from UCB today and should arrive tomorrow. Tracking details attached.

We should have swipe results for the samples by Thursday. We thoroughly cleaned and swiped the vanadium cans and are having swipes analyzed both by ALS and our lab. Note that any inner plastic bags in the package have been kept clean to the best of our ability but have been inside a beryllium glovebox. Below I've pasted the details of the samples. Please let me know if you have any questions.

Best,
[redacted]

[redacted] Feb 23, 2022, 8:36 AM

The FLiBe pics look much improved over the FLiNaK pics. As long as the Be tests show no contamination we are good to run without a secondary containment.

[redacted] Feb 23, 2022, 1:17 PM

All

Thanks [redacted] for adding those samples!

The Be swipe results from heated testing are in, we remained below the DOE limit of 0.2 ug/100cm2 (though there was a slight increase the levels after the heating from <0.025 to 0.033 ug). See the attached email from [redacted] and the lab results.

Thanks!
[redacted]

Attached are the results as provided by the laboratory of wipe sampling conducted 2/8/22, 2/14/22 and 2/17/22 for beryllium on equipment in buildings 4500S, lab C147 and 4505, lab 26. All results were below the release limit (0.2 micrograms per 100 square centimeters), specifically <0.025 ug for all but the sample from the small capsule after heating. It is noteworthy that the result (0.033 ug) from the after heating was not the same as the before heating samples (<0.025 ug) … which indicates likelihood of some leakage during heating. The results for the small capsule normalized from 19 cm2 to 100 cm2 is 0.17 ug/100 cm2 … as compared to the occupational exposure limit of 0.2 ug/100 cm2. I don't know how sensitive SNS is to the potential contamination level.

I still need to complete input of the results and conclusions into our data system and generate a final report, but wanted to give you a heads-up ASAP.

Thank you.

[redacted]

OAK RIDGE National Laboratory

Analytical Report

Safety Services Division
Industrial Hygiene
Analytical Laboratory

[redacted]

Batch: 10031
Location: 4500S FIRST C147

Received Date: 2/17/2022
Analysis Date: 2/21/2022
Report Date: 2/23/2022

Sample ID	Analyte	Result	Units	Comments
SID15383-01	Beryllium, Whatman 541	<0.025	ug	
SID15383-02	Beryllium, Whatman 541	<0.025	ug	
SID15383-03	Beryllium, Whatman 541	<0.025	ug	
SID15383-04	Beryllium, Whatman 541	<0.025	ug	
SID15383-05	Beryllium, Whatman 541	<0.025	ug	
SID15383-06	Beryllium, Whatman 541	<0.025	ug	
SID15383-07	Beryllium, Whatman 541	<0.025	ug	
SID15383-08	Beryllium, Whatman 541	<0.025	ug	
SID15383-09	Beryllium, Whatman 541	<0.025	ug	
SID15383-10	Beryllium, Whatman 541	<0.025	ug	
SID15383-11	Beryllium, Whatman 541	<0.025	ug	
SID15383-12	Beryllium, Whatman 541	0.033	ug	
SID15383-13	Beryllium, Whatman 541	<0.025	ug	
SID15383-14	Beryllium, Whatman 541	<0.025	ug	

APPENDIX B: IMAGES FROM LEAK TESTING OF CANS

FLiNaK

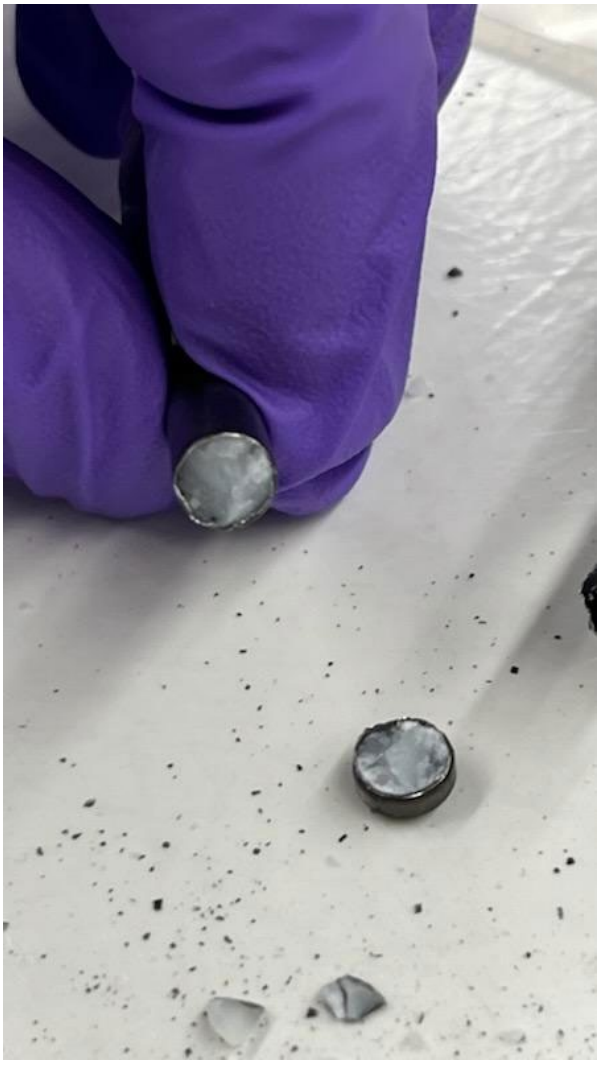

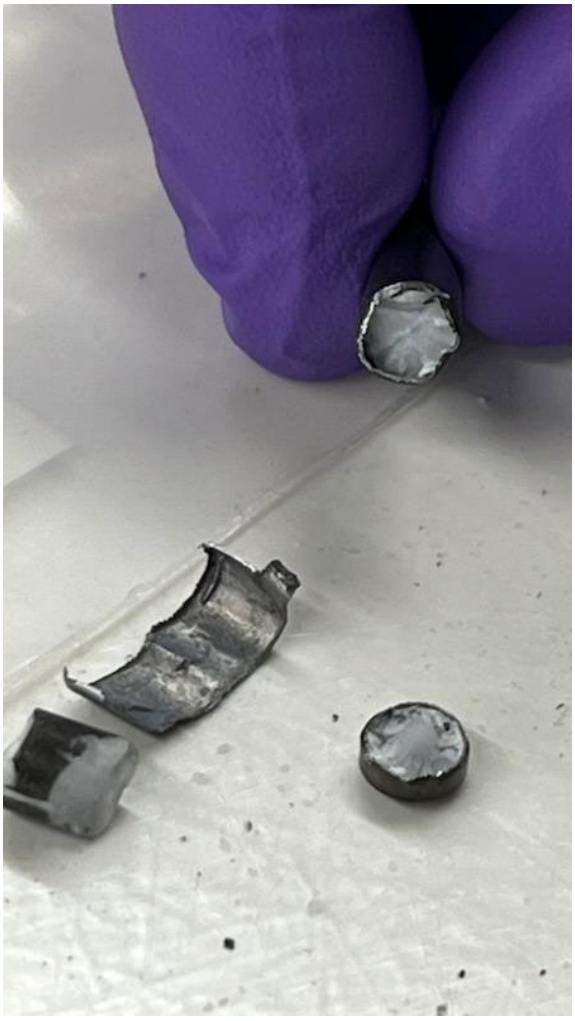


ruc.ble
ket

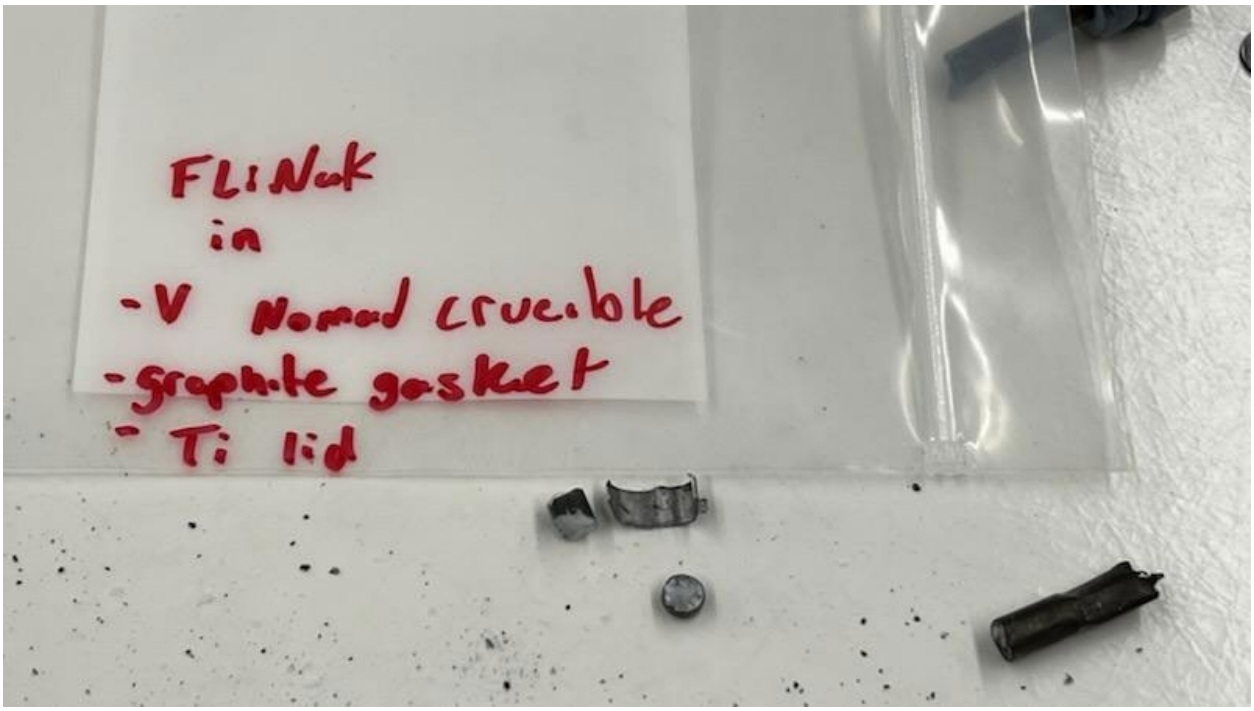
FLiNaK
in
-V Nomad crucible
-graphite gasket
-Ti lid

FLiBe


DANGE
CONTAMINA
WITH BERYLLIU
CAPSULE CONTAINS
DO NOT REMOVE DUST BY BLOWING OR
CANCER AND LUNG DISEASE HAZARD
CONTACT THE DSO FOR PROTOCOL FOR DIS
OF THIS ITEM.

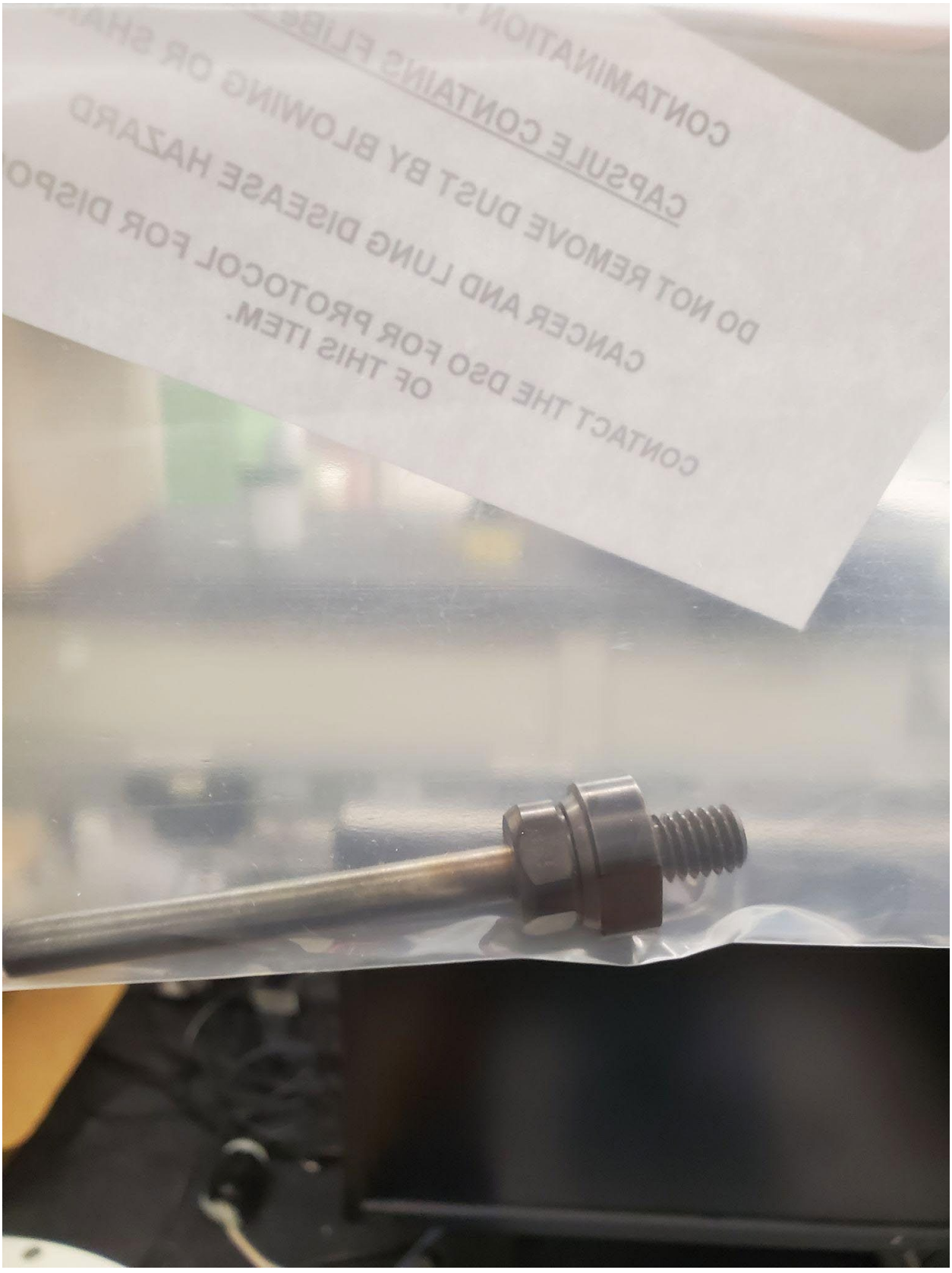
CONTAMINATION
CAPSULE CONTAINS
DO NOT REMOVE DUST BY BLOWING OR
CANCER AND LUNG DISEASE HAZARD
CONTACT THE DSO FOR PROTOCOL FOR
OF THIS ITEM.


CONTAMI
CAPSULE CONTAINS
DO NOT REMOVE DUST BY BLOWING
CANCER AND LUNG DISEASE HAZARD
CONTACT THE DSO FOR PROTOCOL FOR DISPOSING
OF THIS ITEM.

APPENDIX C: SAMPLE SWIPE RESULTS FROM ALS

ANALYTICAL REPORT

Report Date: January 26, 2023

[redacted]
U.C. Berkeley SALT Group
2521 Hearst Ave.
Etcheverry Hall 1110B
Berkeley, CA 94709

Phone: [redacted]

E-mail: [redacted]

Workorder: **34-2302506**
Client Project ID: UC Berkeley
Purchase Order: BB01563616
Project Manager: Stella Hanis

Analytical Results

Sample ID: **35-230124 Blank**
Lab ID: 2302506001
Sampling Location: UC Berkeley
Collected: 01/24/2023
Received: 01/25/2023

Method: NIOSH 7300, Be Oxide GW
Dilution: 1
Media: Ghost Wipe
Sampling Parameter: Area 100 cm²
Instrument: ICP13
Prepared: 01/25/2023 (302914)
Analyzed: 01/26/2023 (302957)

Analyte	Result (ug/sample)	Result (ug/100cm²)	RL (ug/sample)
Beryllium	**4.0**	**4.0**	0.0071

Sample ID: **35-230124 7 50/50 m**
Lab ID: 2302506002
Sampling Location: UC Berkeley
Collected: 01/24/2023
Received: 01/25/2023

Method: NIOSH 7300, Be Oxide GW
Dilution: 1
Media: Ghost Wipe
Sampling Parameter: Area 100 cm²
Instrument: ICP13
Prepared: 01/25/2023 (302914)
Analyzed: 01/26/2023 (302957)

Analyte	Result (ug/sample)	Result (ug/100cm²)	RL (ug/sample)
Beryllium	**32**	**32**	0.0071

Sample ID: **35-230124 6 75/25 mo**
Lab ID: 2302506003
Sampling Location: UC Berkeley
Collected: 01/24/2023
Received: 01/25/2023

Method: NIOSH 7300, Be Oxide GW
Dilution: 1
Media: Ghost Wipe
Sampling Parameter: Area 100 cm²
Instrument: ICP13
Prepared: 01/25/2023 (302914)
Analyzed: 01/26/2023 (302957)

Analyte	Result (ug/sample)	Result (ug/100cm²)	RL (ug/sample)
Beryllium	**30**	**30**	0.0071

Analytical Results

Sample ID: **35-230124 4 90/10 BeF2**			Collected: 01/24/2023
Lab ID: 2302506004	Sampling Location: UC Berkeley		Received: 01/25/2023
Method: NIOSH 7300, Be Oxide GW	**Media:** Ghost Wipe		**Instrument:** ICP13
Dilution: 1	**Sampling Parameter:** Area 100 cm²		**Prepared:** 01/25/2023 (302914)
			Analyzed: 01/26/2023 (302957)

Analyte	Result (ug/sample)	Result (ug/100cm²)	RL (ug/sample)
Beryllium	**7.1**	**7.1**	0.0071

Sample ID: **35-230124 3 95/5 BdF2**			Collected: 01/24/2023
Lab ID: 2302506005	Sampling Location: UC Berkeley		Received: 01/25/2023
Method: NIOSH 7300, Be Oxide GW	**Media:** Ghost Wipe		**Instrument:** ICP13
Dilution: 1	**Sampling Parameter:** Area 100 cm²		**Prepared:** 01/25/2023 (302914)
			Analyzed: 01/26/2023 (302957)

Analyte	Result (ug/sample)	Result (ug/100cm²)	RL (ug/sample)
Beryllium	**8.2**	**8.2**	0.0071

Sample ID: **35-230124 2 BeF2**			Collected: 01/24/2023
Lab ID: 2302506006	Sampling Location: UC Berkeley		Received: 01/25/2023
Method: NIOSH 7300, Be Oxide GW	**Media:** Ghost Wipe		**Instrument:** ICP13
Dilution: 1	**Sampling Parameter:** Area 100 cm²		**Prepared:** 01/25/2023 (302914)
			Analyzed: 01/26/2023 (302957)

Analyte	Result (ug/sample)	Result (ug/100cm²)	RL (ug/sample)
Beryllium	**4.4**	**4.4**	0.0071

Sample ID: **35-230124 1 F7LiBe**			Collected: 01/24/2023
Lab ID: 2302506007	Sampling Location: UC Berkeley		Received: 01/25/2023
Method: NIOSH 7300, Be Oxide GW	**Media:** Ghost Wipe		**Instrument:** ICP13
Dilution: 1	**Sampling Parameter:** Area 100 cm²		**Prepared:** 01/25/2023 (302914)
			Analyzed: 01/26/2023 (302957)

Analyte	Result (ug/sample)	Result (ug/100cm²)	RL (ug/sample)
Beryllium	**27**	**27**	0.0071

Comments

Quality Control: IH Metals, Be Oxide GW QC - (Batch: 302957)

NIOSH 7300 MOD: The samples were analyzed for beryllium by NIOSH Method 7300, and modified to accommodate the digestion beryllium fluoride collected on Ghost Wipes media. Accordingly, the samples were digested using a combination of concentrated sulfuric acid and hydrogen peroxide to maximize dissolution of the insoluble forms of beryllium fluoride.

Report Authorization (/S/ is an electronic signature that complies with 21 CFR Part 11)

Method (Analysis Batch)	Analyst	Peer Review
NIOSH 7300, Be Oxide GW (302957)	/S/ Ethan Hamilton 01/26/2023 12:28	/S/ Kristie F. Bitner 01/26/2023 12:59

Laboratory Contact Information

ALS Environmental
960 W Levoy Drive
Salt Lake City, Utah 84123

Phone: (801) 266-7700
Email: alslt.lab@ALSGlobal.com
Web: www.alsglobal.com/slt

General Lab Comments

The results provided in this report relate only to the items tested.
Samples were received in acceptable condition unless otherwise noted.
The following was provided by the client: Sample ID, Collection Date, Sampling Location, Media Type, Sampling Parameter.
Collection Date, Media Type, and Sampling Parameter can potentially affect the validity of the results.
Samples have not been blank corrected unless otherwise noted.

ALS provides professional analytical services for all samples submitted. ALS is not in a position to interpret the data and assumes no responsibility for the quality of the samples submitted.

All quality control samples processed with the samples in this report yielded acceptable results unless otherwise noted.

ALS is accredited for specific fields of testing (scopes) in the following testing sectors. The quality system implemented at ALS conforms to accreditation requirements and is applied to all analytical testing performed by ALS. The following table lists testing sector, accreditation body, accreditation number and website. Please contact these accrediting bodies or your ALS project manager for the current scope of accreditation that applies to your analytical testing.

Testing Sector	Accreditation Body (Standard)	Certificate Number	Website
Industrial Hygiene	AIHA (ISO 17025 & AIHA IHLAP)	101574	http://www.aihaaccreditedlabs.org
	DOECAP-AP	L22-62	http://www.pjlabs.com
	Washington	C596	https://ecology.wa.gov/Regulations-Permits/Permits-certifications/Laboratory-Accreditation
Dietary Supplements	PJLA (ISO 17025)	L22-61	http://www.pjlabs.com

Definitions

LOD = Limit of Detection = MDL = Method Detection Limit, A statistical estimate of method/media/instrument sensitivity.
LOQ = Limit of Quantitation = RL = Reporting Limit, A verified value of method/media/instrument sensitivity.
ND = Not Detected, Testing result not detected above the LOD or LOQ.
NA = Not Applicable.
** No result could be reported, see sample comments for details.
< Means this testing result is less than the numerical value.
( ) This testing result is between the LOD and LOQ and has higher analytical uncertainty than values at or above the LOQ.

DOCUMENT CONTROL

Version & Date of Issue	Authors of changes & Date	Description of Changes Made	Reviewers & Date of Review
UCBS02SF03RC004_NOMAD2023SafetyReview	Haley Williams & Nathanael Gardner 2023-05-11	o Document created o Document shared with ORNL	

6.3.3 Weighted structure factors from NNMD compared to neutron data

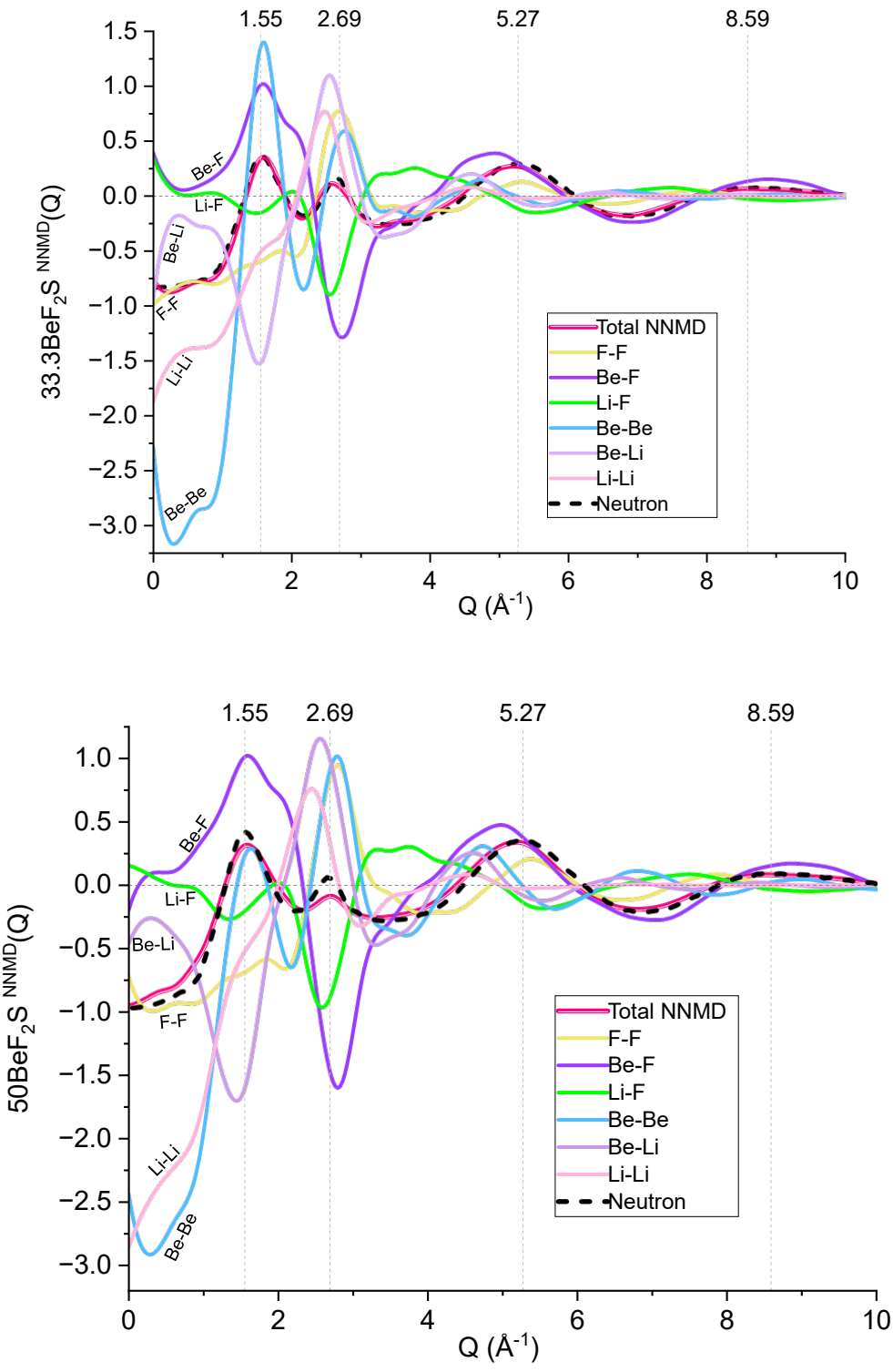

Figure 6.2. S(Q) from NNMD and neutron scattering at 700°C, with partial weighted S(Q) from NNMD. 33.3BeF_2 top, 50BeF_2 bottom.

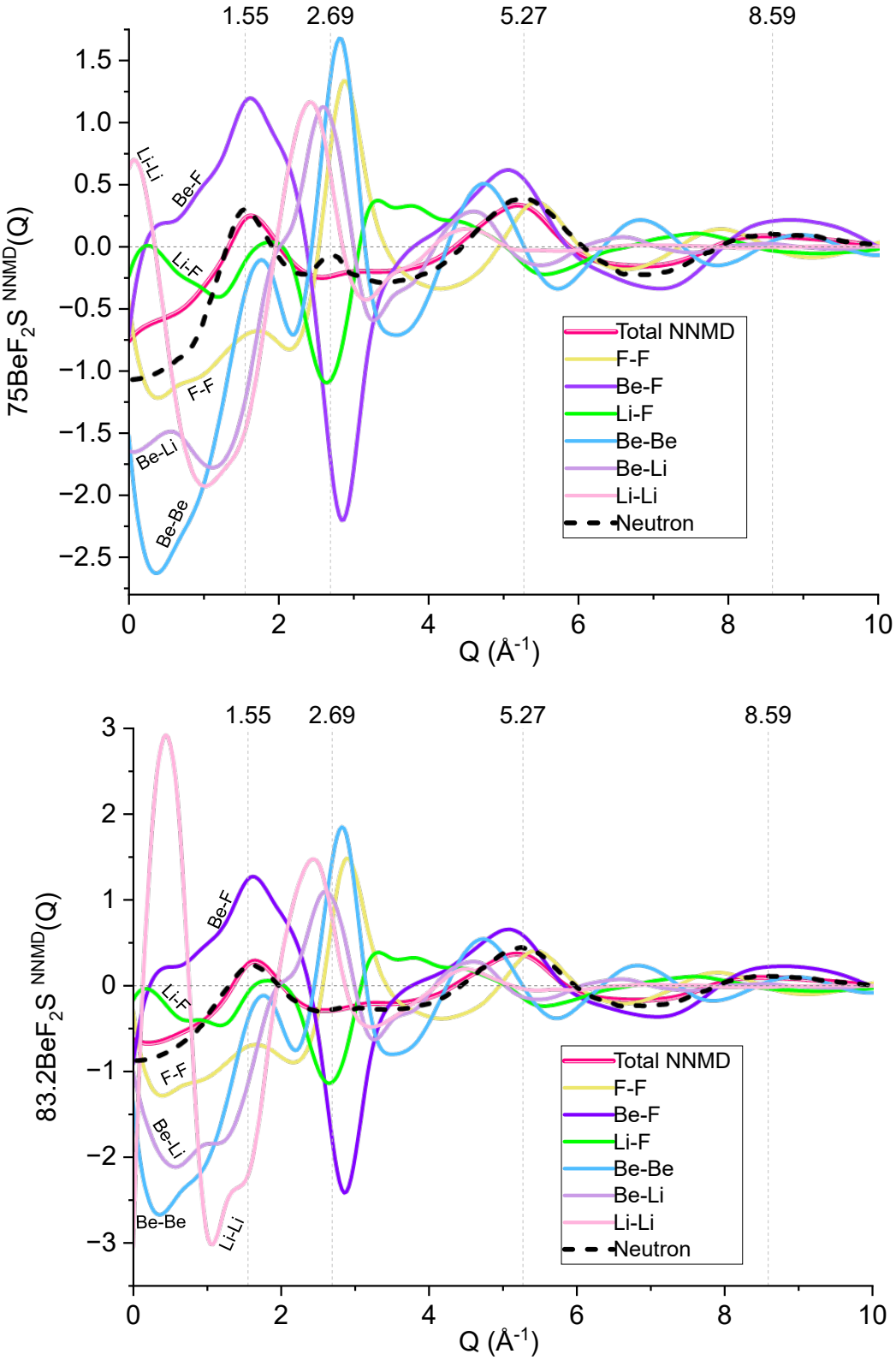

Figure 6.3. S(Q) from NNMD and neutron scattering at 700°C, with partial weighted S(Q) from NNMD. 75BeF_2 top, 83.2BeF_2 bottom.

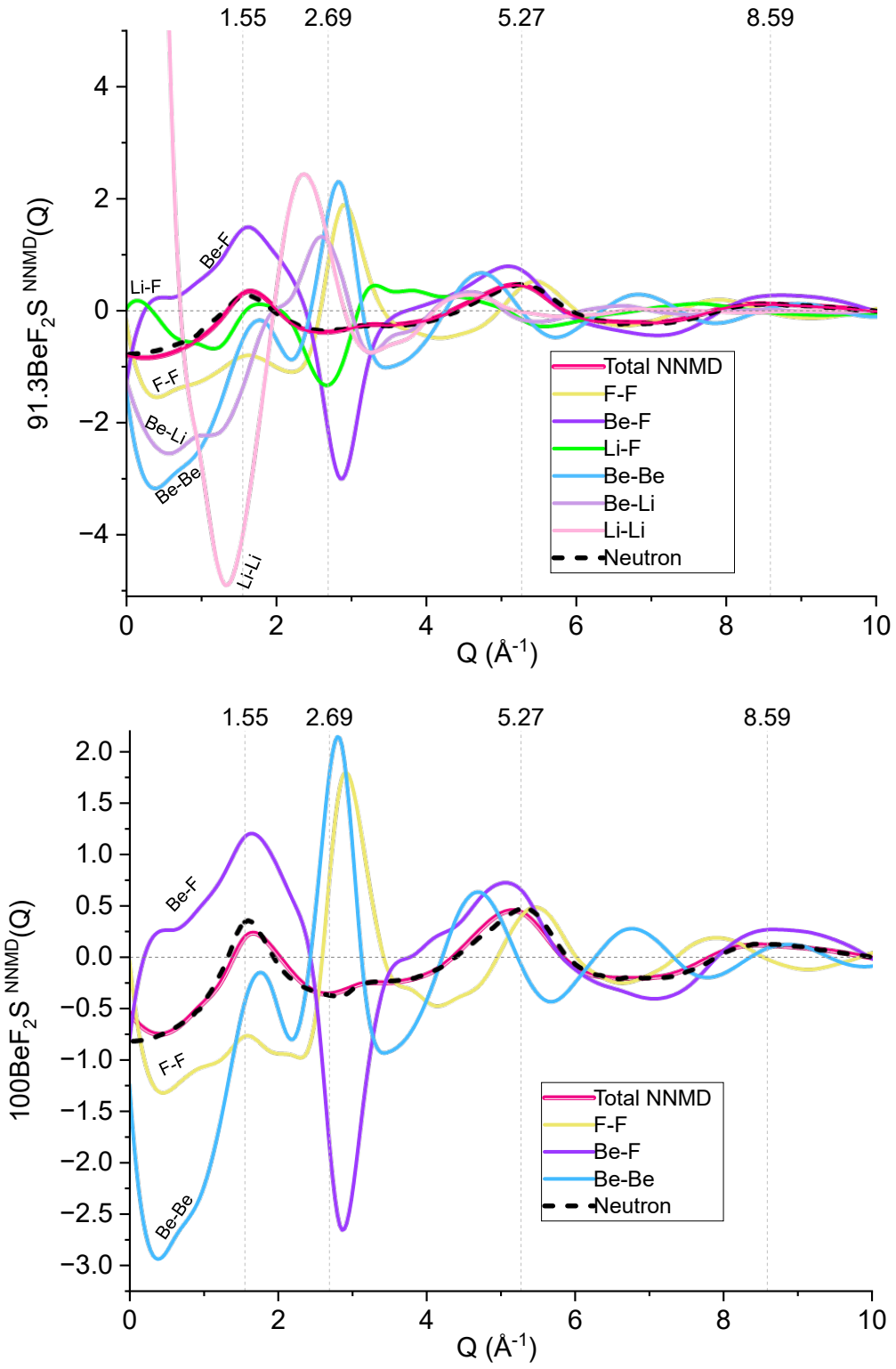

Figure 6.4. S(Q) from NNMD and neutron scattering at 700°C, with partial weighted S(Q) from NNMD. 91.3BeF_2 top, 100BeF_2 bottom.

6.3.4 Unweighted partial structure factors from EPSR for each ion pair

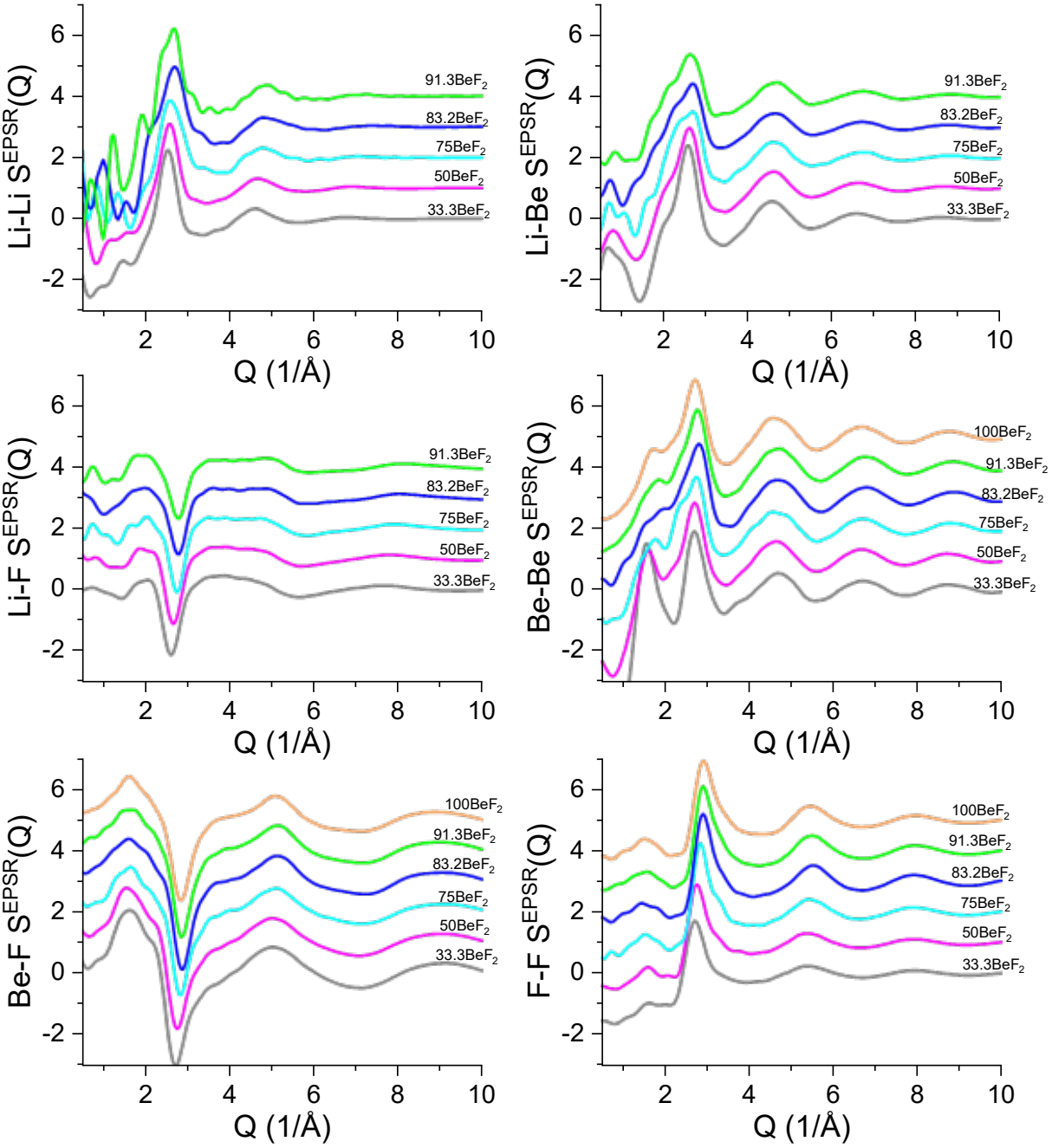

Figure 6.5. Unweighted S(Q) partials from EPSR at 700°C.

6.3.5 Unweighted partial structure factors from NNMD for each ion pair

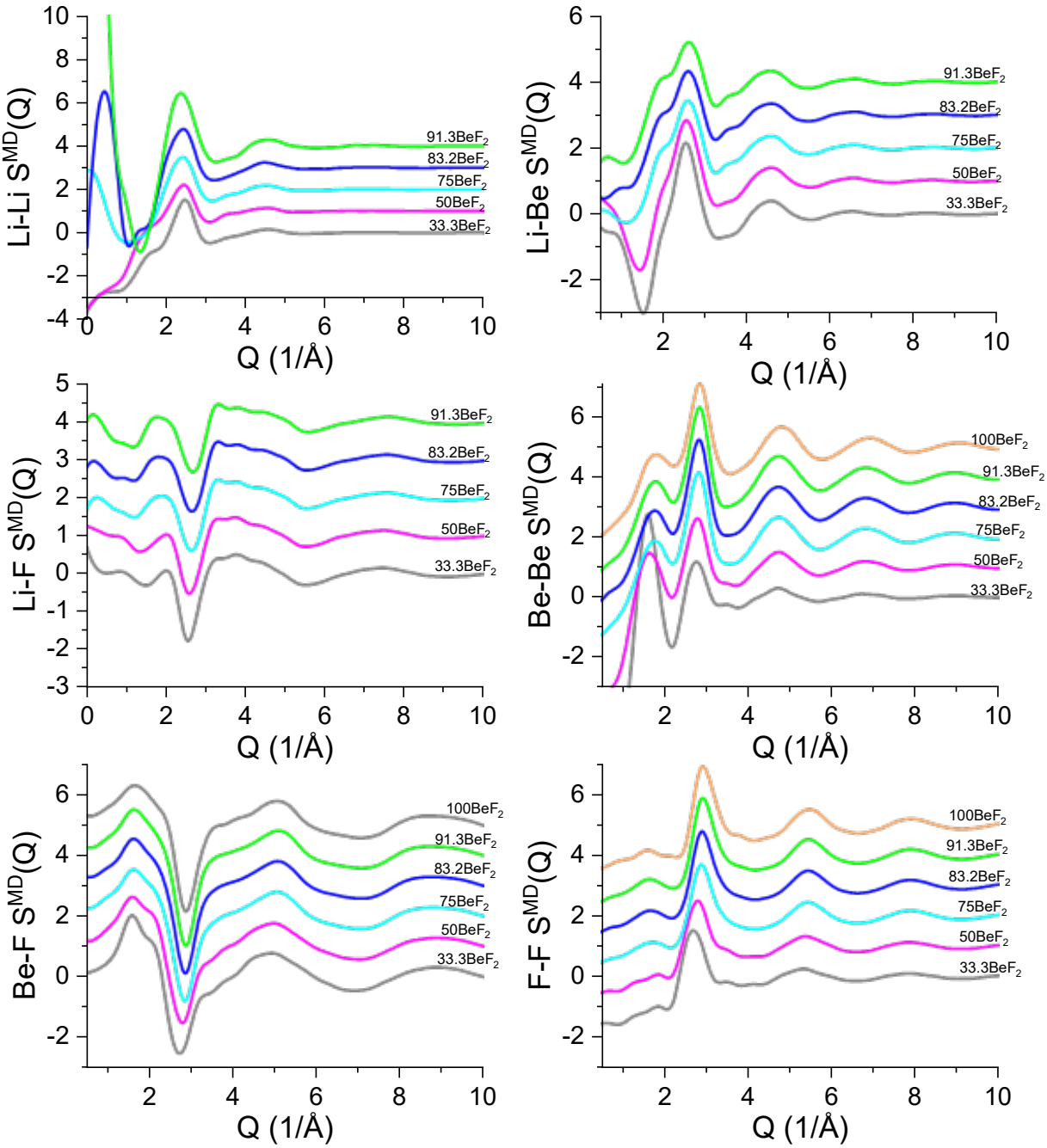

Figure 6.6. Unweighted S(Q) partials from NNMD at 700°C.

6.3.6 Be-F-F bond angle distribution skew

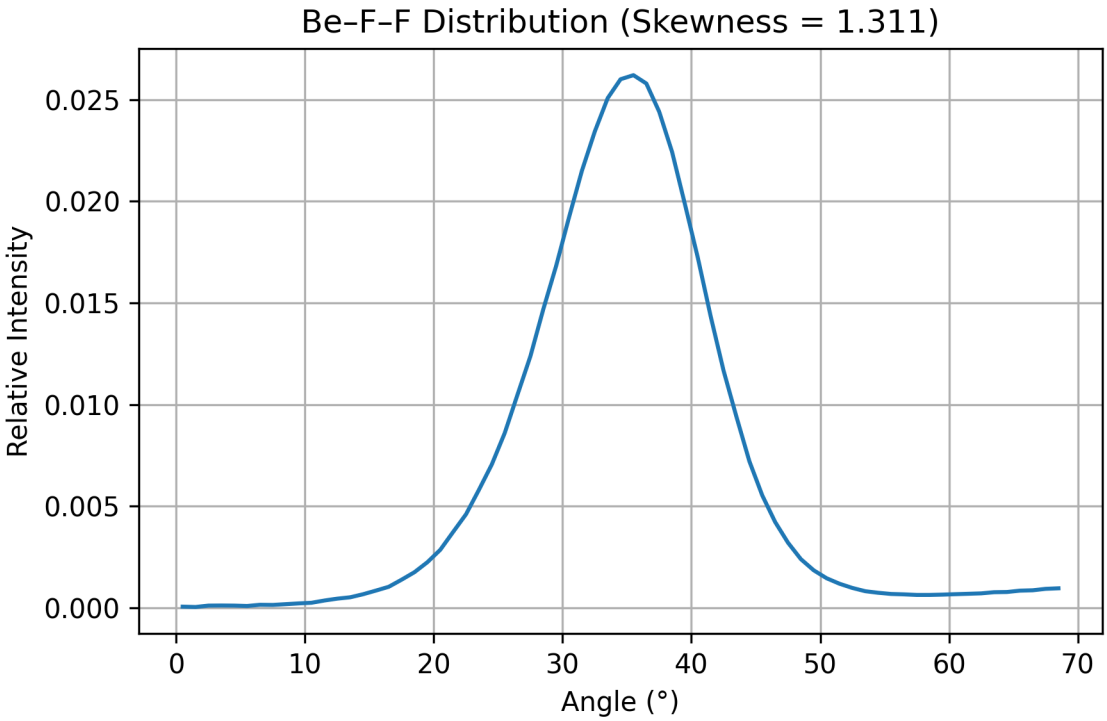

Figure 6.7. Be-F-F bond angle distribution skewness visualization using skew from scipy.stats. Code produced by ChatGPT 4.0. Skew = 1.3108078895220314

6.1 Additional data referenced in Chapter 3

6.1.1 FLiNaK

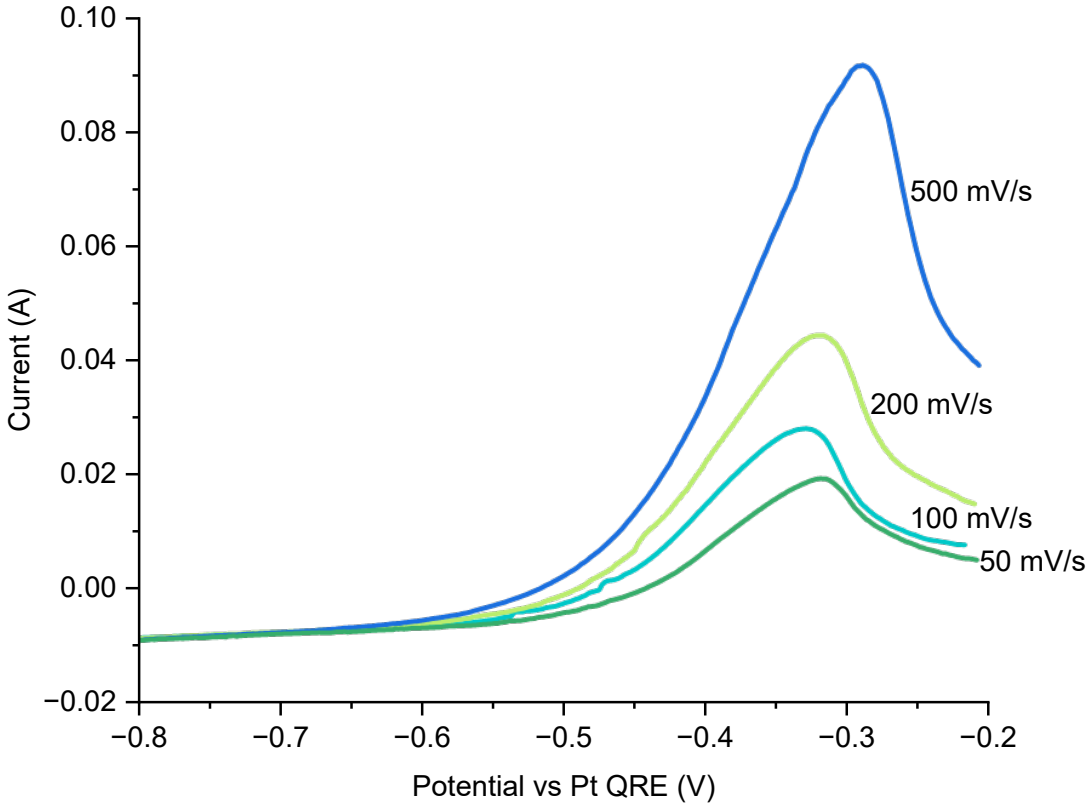

Figure 6.8. Linear sweep voltammograms of FLiNaK with 0.3 wt% Cr^{3+} added as CrF_3, labeled with sweep rate. WE: Au (0.16 cm^2)/, CE: Pt, QRE: Pt. 550±10°C, held at temperature for 4 hours. Step size: 2 mV. Data: LSV_22Nov16_002, LSV_22Nov16_003, LSV_22Nov16_004, LSV_22Nov16_005.

6.1.2 2KF-NaF

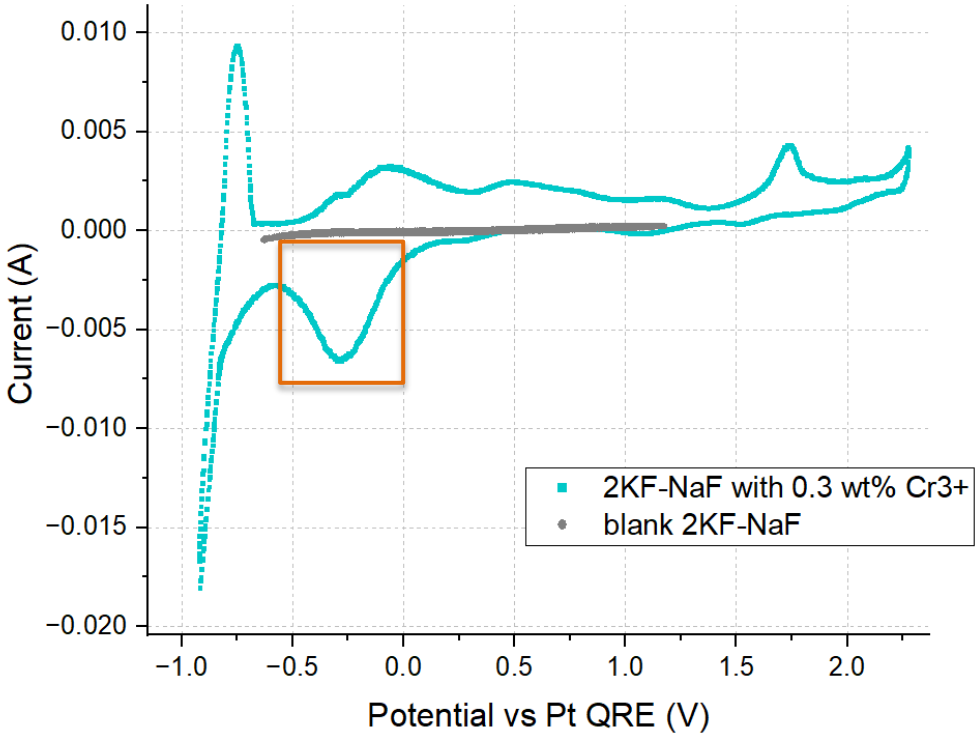

Figure 6.9. 2KF-NaF with and without 0.3 wt% Cr^{3+} added as CrF_3. Temperature: 780±5°C. Electrodes: Au WE, Pt QRE, Pt CE. Boxed peak referenced in SWV in Figure 6.10.

Note that although the current is unable to be scaled to surface area because of improper WE immersion depth measurements, the blank scan shows no distinguishable features when the current is amplified 100x. Note also that consistent referencing of the blank and 2KF-NaF with CrF_3 was not possible, so both scans are displayed vs Pt QRE, measured on different days after freezing and re-melting.

From SWV of the reduction peak around -0.25 V vs Pt QRE (seen in Figure 6.10) was calculated to have an n = 0.998, suggesting that it might be attributable to Cr^{2+}/Cr^{3+}. The predominance of the Cr^{2+}/Cr^{3+} peak over Cr^{0}/Cr^{2+} might suggest that disproportionation of Cr^{2+} in favor of Cr^{3+} could be stronger in the more basic 2KF-NaF than in FLiNaK.

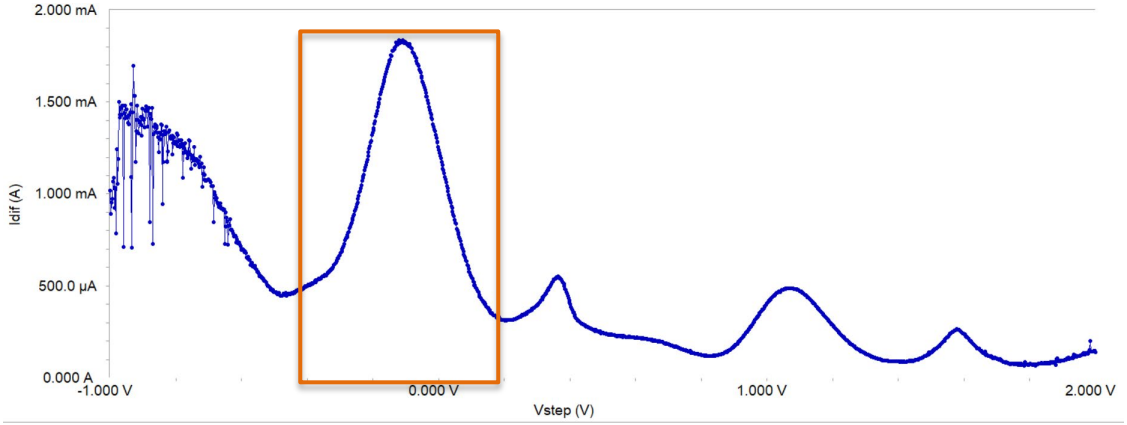

Figure 6.10. Reducing SWV of 2KF-NaF + 0.3 wt% Cr^{3+} at 780°C. WE: Au, CE: Pt, QRE: Pt, Frequency: 5 Hz, Pulse size: 20 mV.

6.1.3 FLiBe

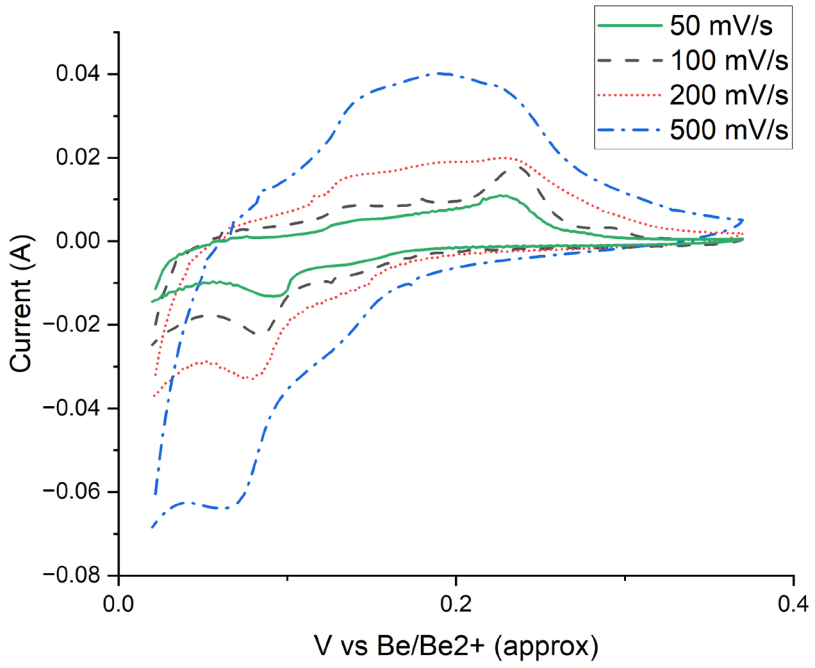

Figure 6.11. FLiBe with 0.03 mol% Cr^{3+} added as CrF_3. WE: W, CE: Pt, QRE: Pt. Temp: 600±15°C. Smaller scans of the unknown peaks near Be/Be^{2+}.

6.2 Oxyfluorides in FLiBe

Experiment details for additional studies with BeO. Data included in data repository (Other studies_Oxyfluoride studies).

Solvent	Solute	Temperature (°C)	WE/RE/CE	Electroanalytical studies	GB conditions
FLiBe (Sept 2024)	BeO • 0.0167 g BeO as 1st addition • 0.0457 g BeO (total after 2nd add) • 0.029 g BeO added as 3rd addition CrF_2 added: 0.048 g approx. CrF_2 added 2nd time: 0.1108 g added to 32.0014 g FLiBe	600±0.01	W/W/GC Au/Ag/W	CV, SWV	1.5-5.4 ppm O_2 0 ppm H_2O

6.3 Calculating n from SWV

A summary of the theory which estimates the number of electrons transferred in a redox reaction (n) to the full-width half-maximum (FWHM) of a square wave voltammogram peak.

The number of electrons transferred can be calculated by the equation:

$$W_{1/2} = 3.52 \cdot \frac{RT}{nF} \quad \text{(Eqn 6.3.1)}$$

where $W_{1/2}$ is the width of the current peak at half height, R is the ideal gas constant, T is the temperature, F is Faraday's constant, and n is the number of electrons transferred.

Parry and Osteryoung present a method for calculating this equation [294]. Given Equations A and B, one can solve for P at the condition where current is equal to its half maximum ($i = i_{max}/2$). From this P, one finds two values of E. The difference between these values gives $W_{1/2}$. The calculation is shown below.

Equation A:

$$\Delta i = \frac{n^2F^2}{RT} \cdot A \cdot C \cdot \Delta E \cdot \sqrt{\frac{D}{\pi t}} \cdot \frac{P}{(1+P)^2} \quad \text{(Eqn 6.3.2)}$$

Equation B:

$$\Delta i_{max} = \frac{n^2F^2}{4RT} \cdot A \cdot C \cdot \Delta E \cdot \sqrt{\frac{D}{\pi t}} \quad \text{(Eqn 6.3.3)}$$

A is the area of the electrode surface (typically an Hg drop) and C is the surface concentration. P is defined by Barker et al. [295] as the exponential term:

$$P = \exp\left(\frac{\left(E - E_{1/2}\right)nF}{RT}\right)$$

Equation A is given by Barker et al. [296] as Equation 24. It is only true when ΔE (the pulse amplitude of the square wave voltammogram) is smaller than RT/nF because it is a derivative approximated by a differential.

Equation B comes from maximizing current by taking the derivative and setting it to zero. At this maximum, P = 1.

Solve for P at $i = i_{max}/2$. The P value at the half maximum current is the width at current half-max on the voltammogram (FWHM).

$$\frac{n^2F^2}{RT} \cdot A \cdot C \cdot \Delta E \cdot \sqrt{\frac{D}{\pi t}} \cdot \frac{P}{(1+P)^2} = \frac{1}{2}\frac{n^2F^2}{4RT} \cdot A \cdot C \cdot \Delta E \cdot \sqrt{\frac{D}{\pi t}}$$

Canceling terms we find: $\frac{P}{(1+P)^2} = \frac{1}{8}$

Expanding this expression: $P^2 - 6P + 1 = 0$

Solving for P: $P = \frac{3 \pm 2\sqrt{2}}{4}$. Thus, P = 1.457 or 0.0429. Call these P_1 and P_2.

Knowing that $P = \exp\left(\frac{\left(E-E_{1/2}\right)nF}{RT}\right)$., we can obtain two values of E. The difference between these values gives the peak FWHM.

Solving the P identity expression for E: $E = E_{1/2} + \frac{RT}{nF}\ln(P)$.

$$E_1 - E_2 = \frac{RT}{nF}\ln(P_1 - P_2)$$

$$W_{1/2} = \frac{RT}{nF}\ln\left(\frac{P_1}{P_2}\right)$$

Plugging in P_1 and P_2 gives the equation $\boldsymbol{W_{1/2} = 3.52 \cdot \frac{RT}{nF}}$.

7 REFERENCES

[1] S. V. Volkov, "Chemical reactions in molten salts and their classification," *Chem. Soc. Rev.*, vol. 19, no. 1, p. 21, 1990, doi: 10.1039/cs9901900021.

[2] S. Zein El Abedin and F. Endres, "Ionic Liquids: The Link to High-Temperature Molten Salts?," *Acc. Chem. Res.*, vol. 40, no. 11, pp. 1106–1113, Nov. 2007, doi: 10.1021/ar700049w.

[3] B. Weyershausen, K. Hell, and U. Hesse, "Industrial application of ionic liquids as process aid," *Green Chem.*, vol. 7, no. 5, pp. 283–287, May 2005, doi: 10.1039/B408317B.

[4] W. H. Zachariasen, "The Atomic Arrangement in Glass," *J. Am. Chem. Soc.*, vol. 54, no. 10, pp. 3841–3851, Oct. 1932, doi: 10.1021/ja01349a006.

[5] "How aluminum changed the world: A metallurgical revolution through technological and cultural perspectives," *Technol. Forecast. Soc. Change*, vol. 143, pp. 101–113, June 2019, doi: 10.1016/j.techfore.2019.03.011.

[6] W. B. Cottrell, H. E. Hungerford, J. K. Leslie, and J. L. Meem, "Operation of the Aircraft Reactor Experiment," ORNL-1845(Del.), Sept. 1955. doi: 10.2172/4237975.

[7] H. G. MacPherson, "The Molten Salt Reactor Adventure," *Nucl. Sci. Eng.*, vol. 90, no. 4, pp. 374–380, Aug. 1985, doi: 10.13182/NSE90-374.

[8] M. Übeyli, "On the Tritium Breeding Capability of Flibe, Flinabe, and $Li_{20}Sn_{80}$ in a Fusion-Fission (Hybrid) Reactor," *J. Fusion Energy*, vol. 22, no. 1, pp. 51–57, Mar. 2003, doi: 10.1023/B:JOFE.0000021555.70423.f1.

[9] T. M. Besmann and J. Schorne-Pinto, "Developing Practical Models of Complex Salts for Molten Salt Reactors," *Thermo*, vol. 1, no. 2, pp. 168–178, July 2021, doi: 10.3390/thermo1020012.

[10] J. C. Ard *et al.*, "Development of the Molten Salt Thermal Properties Database − Thermochemical (MSTDB−TC), example applications, and LiCl−RbCl and UF3−UF4 system assessments," *J. Nucl. Mater.*, vol. 563, p. 153631, May 2022, doi: 10.1016/j.jnucmat.2022.153631.

[11] C. Andreades *et al.*, "Design Summary of the Mark-I Pebble-Bed, Fluoride Salt–Cooled, High-Temperature Reactor Commercial Power Plant," *Nucl. Technol.*, vol. 195, no. 3, pp. 223–238, Sept. 2016, doi: 10.13182/NT16-2.

[12] A. L. Qualls *et al.*, "Fluoride Salt-Cooled High-Temperature Demonstration Reactor Point Design," ORNL/TM-2016/85, 1245361, Feb. 2016. doi: 10.2172/1245361.

[13] B. N. Sorbom *et al.*, "ARC: A compact, high-field, fusion nuclear science facility and demonstration power plant with demountable magnets," *Fusion Eng. Des.*, vol. 100, pp. 378–405, Nov. 2015, doi: 10.1016/j.fusengdes.2015.07.008.

[14] A. Q. Kuang *et al.*, "Conceptual design study for heat exhaust management in the ARC fusion pilot plant," *Fusion Eng. Des.*, vol. 137, pp. 221–242, Dec. 2018, doi:

10.1016/j.fusengdes.2018.09.007.

[15] M. Rovere and M. P. Tosi, “Structure and dynamics of molten salts,” *Rep. Prog. Phys.*, vol. 49, no. 9, pp. 1001–1081, Sept. 1986, doi: 10.1088/0034-4885/49/9/002.

[16] W. Freyland, “Liquid Metals, Molten Salts, and Ionic Liquids: Some Basic Properties,” in *Coulombic Fluids: Bulk and Interfaces*, in Springer Series in Solid-State Sciences. , Springer Berlin Heidelberg, 2011.

[17] A. K. Soper, “GudrunN and GudrunX: programs for correcting raw neutron and X-ray diffraction data to differential scattering cross section,” Science & Technology Facilities Council, Oxford, UK, RAL-TR-2011-013, July 2011.

[18] R. L. McGreevy and L. Pusztai, “The Structure of Molten Salts,” *Proc. Math. Phys. Sci.*, vol. 430, no. 1878, pp. 241–261, July 1990.

[19] N. Winner, H. Williams, R. O. Scarlat, and M. Asta, “Ab-initio simulation studies of chromium solvation in molten fluoride salts,” *J. Mol. Liq.*, vol. 335, p. 116351, Aug. 2021, doi: 10.1016/j.molliq.2021.116351.

[20] M. Wilson, “The effects of topology on the structural, dynamic and mechanical properties of network-forming materials,” *J. Phys. Condens. Matter*, vol. 24, no. 28, p. 284114, June 2012, doi: 10.1088/0953-8984/24/28/284114.

[21] M. Wilson, “Model investigations of network-forming materials,” *Phys. Chem. Chem. Phys.*, vol. 14, no. 37, pp. 12701–12714, Aug. 2012, doi: 10.1039/C2CP41644A.

[22] R. S. Anaredy and S. K. Shaw, “Long-Range Ordering of Ionic Liquid Fluid Films,” *Langmuir*, vol. 32, no. 20, pp. 5147–5154, May 2016, doi: 10.1021/acs.langmuir.6b00304.

[23] B. L. Tremillon, “Acid-Base Effects in Molten Electrolytes,” in *Molten Salt Chemistry*, G. Mamantov and R. Marassi, Eds., Dordrecht: Springer Netherlands, 1987, pp. 279–303. doi: 10.1007/978-94-009-3863-2_14.

[24] C. Bessada, A. Rakhmatullin, A.-L. Rollet, and D. Zanghi, “High temperature NMR approach of mixtures of rare earth and alkali fluorides: An insight into the local structure,” *J. Fluor. Chem.*, vol. 130, no. 1, pp. 45–52, Jan. 2009, doi: 10.1016/j.jfluchem.2008.07.010.

[25] C. F. Baes, “A polymer model for BeF2 and SiO2 melts,” *J. Solid State Chem.*, vol. 1, no. 2, pp. 159–169, Jan. 1970, doi: 10.1016/0022-4596(70)90008-3.

[26] M. S. Emerson *et al.*, “Complete Description of the LaCl3 –NaCl Melt Structure and the Concept of a Spacer Salt That Causes Structural Heterogeneity,” *J. Am. Chem. Soc.*, vol. 144, no. 47, pp. 21751–21762, Nov. 2022, doi: 10.1021/jacs.2c09987.

[27] D. Corradini, P. A. Madden, and M. Salanne, “Coordination numbers and physical properties in molten salts and their mixtures,” *Faraday Discuss.*, vol. 190, no. 0, pp. 471–486, Aug. 2016, doi: 10.1039/C5FD00223K.

[28] F. Vaslow and A. H. Narten, “Diffraction pattern and structure of molten BeF_2 –LiF solutions,” *J. Chem. Phys.*, vol. 59, no. 9, pp. 4949–4954, Nov. 1973, doi:

10.1063/1.1680711.

[29] S. Fayfar *et al.*, “Complex Structure of Molten FLiBe (2 Li F – Be F 2) Examined by Experimental Neutron Scattering, X-Ray Scattering, and Deep-Neural-Network Based Molecular Dynamics,” *PRX Energy*, vol. 3, no. 1, p. 013001, Jan. 2024, doi: 10.1103/PRXEnergy.3.013001.

[30] B. A. Frandsen *et al.*, “The Structure of Molten FLiNaK,” *J. Nucl. Mater.*, vol. 537, p. 152219, Aug. 2020, doi: 10.1016/j.jnucmat.2020.152219.

[31] A.-L. Rollet *et al.*, “In situ high temperature NMR and EXAFS experiments in rare-earth fluoride molten salts,” *Comptes Rendus Chim.*, vol. 7, no. 12, pp. 1135–1140, Dec. 2004, doi: 10.1016/j.crci.2004.02.021.

[32] X. Fu *et al.*, “Probing the local structure of FLiBe melts and solidified salts by in situ high-temperature NMR,” *Phys. Chem. Chem. Phys.*, vol. 25, no. 29, pp. 19446–19452, 2023, doi: 10.1039/D3CP01096A.

[33] V. Sarou-Kanian, A.-L. Rollet, M. Salanne, C. Simon, C. Bessada, and P. A. Madden, “Diffusion coefficients and local structure in basic molten fluorides: in situ NMR measurements and molecular dynamics simulations,” *Phys. Chem. Chem. Phys.*, vol. 11, no. 48, p. 11501, 2009, doi: 10.1039/b912532a.

[34] A. S. Quist, J. B. Bates, and G. E. Boyd, “Raman spectra of tetrafluoroberyllate ion in molten sodium fluoride and lithium fluoride to 686.deg.,” *J. Phys. Chem.*, vol. 76, no. 1, pp. 78–83, Jan. 1972, doi: 10.1021/j100645a014.

[35] L. M. Toth, J. B. Bates, and G. E. Boyd, “Raman spectra of Be2F73- and higher polymers of beryllium fluorides in the crystalline and molten state,” *J. Phys. Chem.*, vol. 77, no. 2, pp. 216–221, Jan. 1973, doi: 10.1021/j100621a014.

[36] Y. Li, X. Liu, B. Wang, and C. Wang, “Raman and theoretical studies on structural evolution of Li2BeF4 and binary LiF-BeF2 melts,” *J. Mol. Liq.*, vol. 325, p. 115208, Mar. 2021, doi: 10.1016/j.molliq.2020.115208.

[37] K. B. Andersen, E. Christensen, R. W. Berg, N. J. Bjerrum, and J. H. von Barner, “Infrared and Raman Spectroscopic Investigations of the Nb(V) Fluoro and Oxofluoro Complexes in the LiF−NaF−KF Eutectic Melt with Development of a Diamond IR Cell,” *Inorg. Chem.*, vol. 39, no. 16, pp. 3449–3454, Aug. 2000, doi: 10.1021/ic991057t.

[38] J. K. Wilmshurst, “Infrared Spectra of Molten Salts.pdf,” *J Chem Phys*, vol. 39, pp. 2545–2548, 1963, doi: https://doi.org/10.1063/1.1734059.

[39] P. F. Peterson, D. Olds, M. T. McDonnell, and K. Page, “Illustrated formalisms for total scattering data: a guide for new practitioners,” *J. Appl. Crystallogr.*, vol. 54, no. 1, pp. 317–332, Feb. 2021, doi: 10.1107/s1600576720015630.

[40] M. Salanne, C. Simon, P. Turq, and P. A. Madden, “Conductivity−Viscosity−Structure: Unpicking the Relationship in an Ionic Liquid,” *J. Phys. Chem. B*, vol. 111, no. 18, pp. 4678–4684, May 2007, doi: 10.1021/jp067073a.

[41] S. Cantor, W. T. Ward, and C. T. Moynihan, “Viscosity and Density in Molten BeF2–LiF Solutions,” *J. Chem. Phys.*, vol. 50, no. 7, pp. 2874–2879, Apr. 1969, doi: 10.1063/1.1671478.

[42] B. S. Jabes and C. Chakravarty, “Relating composition, structural order, entropy and transport in multi-component molten salts,” *J. Chem. Phys.*, vol. 136, no. 14, p. 144507, Apr. 2012, doi: 10.1063/1.3702436.

[43] A. Birri, R. Gallagher, C. Agca, J. McMurray, and N. Dianne Bull Ezell, “Application of the Redlich-Kister expansion for estimating the density of molten fluoride psuedo-ternary salt systems of nuclear industry interest,” *Chem. Eng. Sci.*, vol. 260, p. 117954, Oct. 2022, doi: 10.1016/j.ces.2022.117954.

[44] B. Porter and R. E. Meaker, *Density and Molar Volumes of Binary Fluoride Mixtures*. U.S. Department of the Interior, Bureau of Mines, 1966.

[45] S. Roy *et al.*, “A Holistic Approach for Elucidating Local Structure, Dynamics, and Speciation in Molten Salts with High Structural Disorder,” *J. Am. Chem. Soc.*, vol. 143, no. 37, pp. 15298–15308, 2021, doi: 10.1021/jacs.1c06742.

[46] “Aircraft Nuclear Propulsion Project Quarterly Progress Report for Period Ending June 10, 1956,” Oak Ridge National Laboratory, ORNL-2106.

[47] H. Peng, M. Shen, C. Wang, T. Su, Y. Zuo, and L. Xie, “Electrochemical investigation of the stable chromium species in molten FLINAK,” *RSC Adv.*, vol. 5, no. 94, pp. 76689–76695, 2015, doi: 10.1039/C5RA09919F.

[48] T. Yoko and R. A. Bailey, “Electrochemical Studies of Chromium in Molten LiF - NaF - KF (FLINAK),” *J. Electrochem. Soc.*, vol. 131, no. 11, pp. 2590–2595, Nov. 1984, doi: 10.1149/1.2115363.

[49] Y. Song *et al.*, “Solubility of Cr_2O_3 in Molten Fluorides with Different ZrF_4 Contents and Fluoroacidities,” *J. Electrochem. Soc.*, vol. 167, no. 2, p. 023501, Jan. 2020, doi: 10.1149/1945-7111/ab6984.

[50] L. Massot, L. Cassayre, P. Chamelot, and P. Taxil, “On the use of electrochemical techniques to monitor free oxide content in molten fluoride media,” *J. Electroanal. Chem.*, vol. 606, no. 1, pp. 17–23, Aug. 2007, doi: 10.1016/j.jelechem.2007.04.005.

[51] M. Shen, H. Peng, M. Ge, Y. Zuo, and L. Xie, “Use of square wave voltammeter for online monitoring of O2− concentration in molten fluorides at 600°C,” *J. Electroanal. Chem.*, vol. 748, pp. 34–39, July 2015, doi: 10.1016/j.jelechem.2015.04.023.

[52] W. R. Grimes, “Molten-salt reactor chemistry,” *Nucl. Appl. Technol.*, vol. 8, no. 2, pp. 137–155, 1970.

[53] L. M. Toth, G. D. Del Cul, S. Dai, and D. H. Metcalf, “Molten fluoride fuel salt chemistry,” in *AIP Conference Proceedings*, Las Vegas, Nevada (USA): AIP, 1995, pp. 617–626. doi: 10.1063/1.49142.

[54] M. Blander, *Molten salt chemistry*. Interscience : John Wiley, 1964. Accessed: Apr. 17,

2025. [Online]. Available: https://cir.nii.ac.jp/crid/1130282271493875968

[55] J. Braunstein, G. Mamantov, and G. P. Smith, Eds., *Advances in Molten Salt Chemistry: Volume 1*. Boston, MA: Springer US, 1971. doi: 10.1007/978-1-4757-0504-1.

[56] G. Mamantov and R. Marassi, Eds., *Molten Salt Chemistry*. Dordrecht: Springer Netherlands, 1987. doi: 10.1007/978-94-009-3863-2.

[57] M. Gaune-Escard and G. M. Haarberg, *Molten Salts Chemistry and Technology*. John Wiley & Sons, Ltd, 2014. doi: 10.1002/9781118448847.index.

[58] C. F. Baes, "Chemistry and Thermodynamics of Molten Salt Reactor Fuels," *Nucl Met Met Soc AIME 15 617-441969*, Jan. 1969, [Online]. Available: https://www.osti.gov/biblio/4774915

[59] F. Carotti, H. Wu, and R. O. Scarlat, "Characterization of a Thermodynamic Reference Electrode for Molten LiF-BeF2 (FLiBe)," *J. Electrochem. Soc.*, vol. 164, no. 12, pp. 854–861, 2017, doi: 10.1149/2.1591712jes.

[60] J. Zhang *et al.*, "Redox potential control in molten salt systems for corrosion mitigation," *Corros. Sci.*, vol. 144, pp. 44–53, 2018, doi: 10.1016/j.corsci.2018.08.035.

[61] M. Hara, Y. Kawamura, and T. Tanabe, "Tritium Measurement I—Tritium in Gas, Liquid, and Solid," in *Tritium: Fuel of Fusion Reactors*, Springer, Tokyo, 2017, pp. 137–164. doi: 10.1007/978-4-431-56460-7_7.

[62] J. H. Shaffer, "Preparation and Handling of Salt Mixtures for the Molten Salt Reactor Experiment.," Oak Ridge National Lab. (ORNL), Oak Ridge, TN (United States), ORNL-4616, Jan. 1971. doi: 10.2172/4074869.

[63] Sylvie. Delpech, C. Cabet, C. Slim, and G. S. Picard, "Molten fluorides for nuclear applications," *Mater. Today*, vol. 13, no. 12, pp. 34–41, Dec. 2010, doi: 10.1016/S1369-7021(10)70222-4.

[64] S. Fukada *et al.*, "Reaction rate of beryllium with fluorine ion for Flibe redox control," *J. Nucl. Mater.*, vol. 367–370, pp. 1190–1196, Aug. 2007, doi: 10.1016/j.jnucmat.2007.03.218.

[65] P. Calderoni, P. Sharpe, M. Hara, and Y. Oya, "Measurement of tritium permeation in flibe (2LiF–BeF2)," *Fusion Eng. Des.*, vol. 83, no. 7, pp. 1331–1334, Dec. 2008, doi: 10.1016/j.fusengdes.2008.05.016.

[66] S. E. Ferry, K. B. Woller, E. E. Peterson, C. Sorensen, and D. G. Whyte, "The LIBRA Experiment: Investigating Robust Tritium Accountancy in Molten FLiBe Exposed to a D-T Fusion Neutron Spectrum," *Fusion Sci. Technol.*, vol. 79, no. 1, pp. 13–35, Jan. 2023, doi: 10.1080/15361055.2022.2078136.

[67] H. Li *et al.*, "Study on tritium transport characteristics in fluoride-salt-cooled high-temperature advanced reactor," *Int. J. Hydrog. Energy*, vol. 56, pp. 1101–1110, Feb. 2024, doi: 10.1016/j.ijhydene.2023.12.199.

[68] F. Carotti, E. Liu, D. D. Macdonald, and R. O. Scarlat, “An electrochemical study of hydrogen in molten 2LiF-BeF2 (FLiBe) with addition of LiH,” *Electrochimica Acta*, vol. 367, p. 137114, Jan. 2021, doi: 10.1016/j.electacta.2020.137114.

[69] D. Olander, “Redox condition in molten fluoride salts,” *J. Nucl. Mater.*, vol. 300, no. 2–3, pp. 270–272, Feb. 2002, doi: 10.1016/S0022-3115(01)00742-5.

[70] L. Winner, “Technologies as Forms of Life,” in *Ethics and Emerging Technologies*, R. L. Sandler, Ed., London: Palgrave Macmillan UK, 2014, pp. 48–60. doi: 10.1057/9781137349088_4.

[71] F. Kaplan, *The Wizards of Armageddon*. Stanford University Press, 1991.

[72] A. H. Kimura, *Radiation brain moms and citizen scientists: the gender politics of food contamination after Fukushima*. Durham: Duke University Press, 2016.

[73] M. W. Edwards, R. D. Schweitzer, J. Shakespeare-Finch, A. Byrne, and K. Gordon-King, “Living with nuclear energy: A systematic review of the psychological consequences of nuclear power,” *Energy Res. Soc. Sci.*, vol. 47, pp. 1–15, Jan. 2019, doi: 10.1016/j.erss.2018.08.016.

[74] L. Jolly and D. Radcliffe, “Reflexivity and hegemony: Changing engineers,” in *Proceedings of the 23rd HERDSA Annual Conference*, Toowoomba, Australia, 2000.

[75] P. T. Robbins, “The reflexive engineer: perceptions of integrated development,” *J. Int. Dev.*, vol. 19, no. 1, pp. 99–110, Jan. 2007, doi: 10.1002/jid.1351.

[76] E. Glissant, “Drawing lines in the sand,” Le Monde diplomatique. Accessed: July 23, 2025. [Online]. Available: https://mondediplo.com/2006/11/13frontiers

[77] S. Lam, S. Banerjee, and R. Chahal, “Uncertainty and Exploration of Deep Learning-based Atomistic Models for Screening Molten Salt Properties and Compositions,” in *Proceedings of ICAPP*, in 2023305. Gyeongju, Korea, Apr. 2023.

[78] A. K. Soper, “Partial structure factors from disordered materials diffraction data: An approach using empirical potential structure refinement,” *Phys. Rev. B*, vol. 72, no. 10, p. 104204, Sept. 2005, doi: 10.1103/PhysRevB.72.104204.

[79] R. Ya. Zakirov and V. V. Ignatiev, “Fuel Cycle of the LiF–BeF2 Molten Salt Actinide Burner Reactor,” *Phys. At. Nucl.*, vol. 86, no. 8, pp. 1894–1901, Dec. 2023, doi: 10.1134/S1063778823080276.

[80] C. Johnson, J. L. Slack, M. K. Sharma, C. K. Simpson, and J. L. Burnett, “Modeling of fission and activation products in molten salt reactors and their potential impact on the radionuclide monitoring stations of the International Monitoring System,” U.S. Department of Energy, Pacific Northwest National Laboratory, PNNL-30603, Aug. 2020.

[81] W. R. Grimes, F. F. Blankenship, G. W. Keilholtz, H. F. Poppendiek, and M. T. Robinson, “Chemical Aspects of Molten Fluoride Reactors,” Oak Ridge National Laboratory (ORNL), Oak Ridge, TN (United States), A/CONF.15/P/448, June 1958. doi: 10.2172/4305506.

[82] L. Vergari, R. O. Scarlat, R. D. Hayes, and M. Fratoni, "The corrosion effects of neutron activation of 2LiF-BeF2 (FLiBe)," *Nucl. Mater. Energy*, vol. 34, p. 101289, Mar. 2023, doi: 10.1016/j.nme.2022.101289.

[83] C. Forsberg, L. Hu, P. Peterson, and K. Sridharan, "Fluoride-Salt-Cooled High-Temperature Reactor (FHR) for Power and Process Heat," DOE/NEUP--11-3272, MIT-ANP-TR--157, 1183687, Jan. 2015. doi: 10.2172/1183687.

[84] A. L. Smith, E. Capelli, R. J. M. Konings, and A. E. Gheribi, "A new approach for coupled modelling of the structural and thermo-physical properties of molten salts. Case of a polymeric liquid LiF-BeF2," *J. Mol. Liq.*, vol. 299, p. 112165, Feb. 2020, doi: 10.1016/j.molliq.2019.112165.

[85] C. E. Vallet and J. Braunstein, "Thermodynamically Predicted Miscibility Gap in the System BeF2LiF," *J. Am. Ceram. Soc.*, vol. 60, no. 7–8, pp. 315–317, 1977, doi: 10.1111/j.1151-2916.1977.tb15549.x.

[86] A. Romero-Serrano, M. Hallen-Lopez, B. Zeifert, C. Gomez-Yañez, and A. Hernandez-Ramirez, "Thermodynamic analysis of LiF–BeF2 and KF–BeF2 melts by a structural model," *J. Fluor. Chem.*, vol. 130, no. 3, pp. 336–340, Mar. 2009, doi: 10.1016/j.jfluchem.2008.12.008.

[87] A. L. Smith, E. Capelli, R. J. M. Konings, and A. E. Gheribi, "A new approach for coupled modelling of the structural and thermo-physical properties of molten salts. Case of a polymeric liquid LiF-BeF2," *J. Mol. Liq.*, vol. 299, p. 112165, Feb. 2020, doi: 10.1016/j.molliq.2019.112165.

[88] D. M. Roy, R. Roy, and E. F. Osborn, "Phase Relations and Structural Phenomena in the Fluoride-Model Systems LiF-BeF2 and NaF-BeF2," *J. Am. Ceram. Soc.*, vol. 33, no. 3, pp. 85–90, 1950, doi: 10.1111/j.1151-2916.1950.tb12766.x.

[89] D. M. Roy, R. Roy, and E. F. Osborn, "Fluoride Model Systems: IV, The Systems LiF-BeF2 and PbF2-BeF2," *J. Am. Ceram. Soc.*, vol. 37, no. 7, pp. 300–305, 1954, doi: 10.1111/j.1151-2916.1954.tb14042.x.

[90] R. E. Thoma, H. Insley, H. A. Friedman, and G. M. Hebert, "Equilibrium Phase Diagram of the Lithium Fluoride-Beryllium Fluoridezirconium Fluoride System," *J. Nucl. Mater.*, vol. 27, no. 2, pp. 166–180, Aug. 1968, doi: 10.1016/0022-3115(68)90120-7.

[91] K. A. Romberger, J. Braustein, and R. E. Thoma, "New electrochemical measurements of the liquidus in the lithium fluoride-beryllium fluoride system. Congruency of lithium beryllium fluoride (Li2BeF4)," *J. Phys. Chem.*, vol. 76, no. 8, pp. 1154–1159, Apr. 1972, doi: 10.1021/j100652a012.

[92] B. F. Hitch and C. F. Baes, "An Electromotive Force Study of Molten Lithium Fluoride-Beryllium Fluoride Solutions," *Inorg. Chem.*, vol. 8, no. 2, 1969.

[93] B. E. Warren and C. F. Hill, "The Structure of Vitreous BeF2," *Z. Für Krist. - Cryst. Mater.*, vol. 89, no. 1–6, pp. 481–486, Dec. 1934, doi: 10.1524/zkri.1934.89.1.481.

[94] A. Rahman, R. H. Fowler, and A. H. Narten, "Structure and Motion in Liquid BeF_2, LiBeF

$_3$, and LiF from Molecular Dynamics Calculations," *J. Chem. Phys.*, vol. 57, no. 7, pp. 3010–3011, Oct. 1972, doi: 10.1063/1.1678700.

[95] S. Liu *et al.*, "Investigation on molecular structure of molten Li2BeF4 (FLiBe) salt by infrared absorption spectra and density functional theory (DFT)," *J. Mol. Liq.*, vol. 242, pp. 1052–1057, Sept. 2017, doi: 10.1016/j.molliq.2017.07.051.

[96] J. Sun, H. Huang, L. Han, X. Fu, H. Liu, and Y. Qian, "High-temperature and solid-state NMR investigation of the structural evolution and special phase transition in LiF–NaF–BeF_2 mixed salts," *Phys. Chem. Chem. Phys.*, vol. 27, no. 17, pp. 8903–8909, 2025, doi: 10.1039/D5CP00378D.

[97] J. Sun *et al.*, "HT-NMR Studies of the Be–F Coordination Structure in FNaBe and FLiBe Mixed Salts," *JACS Au*, vol. 4, no. 6, pp. 2211–2219, June 2024, doi: 10.1021/jacsau.4c00177.

[98] S. Attarian, D. Morgan, and I. Szlufarska, "Thermophysical properties of FLiBe using moment tensor potentials," *J. Mol. Liq.*, vol. 368, p. 120803, Dec. 2022, doi: 10.1016/j.molliq.2022.120803.

[99] K. Baral, S. San, R. Sakidja, A. Couet, K. Sridharan, and W.-Y. Ching, "Temperature-Dependent Properties of Molten Li2BeF4 Salt Using Ab Initio Molecular Dynamics," *ACS Omega*, 2021.

[100] A. Klix, A. Suzuki, and T. Terai, "Study of tritium migration in liquid Li2BeF4 with ab initio molecular dynamics," *Fusion Eng. Des.*, vol. 81, no. 1–7, pp. 713–717, Feb. 2006, doi: 10.1016/j.fusengdes.2005.09.034.

[101] S. T. Lam, Q.-J. Li, J. Mailoa, C. Forsberg, R. Ballinger, and J. Li, "The impact of hydrogen valence on its bonding and transport in molten fluoride salts," *J. Mater. Chem. A*, vol. 9, no. 3, pp. 1784–1794, 2021, doi: 10.1039/D0TA10576G.

[102] H. O. Nam, A. Bengtson, K. Vörtler, S. Saha, R. Sakidja, and D. Morgan, "First-principles molecular dynamics modeling of the molten fluoride salt with Cr solute," *J. Nucl. Mater.*, vol. 449, no. 1–3, pp. 148–157, June 2014, doi: 10.1016/j.jnucmat.2014.03.014.

[103] M. Salanne, C. Simon, P. Turq, R. J. Heaton, and P. A. Madden, "A First-Principles Description of Liquid BeF_2 and Its Mixtures with LiF: 2. Network Formation in LiF−BeF_2," *J. Phys. Chem. B*, vol. 110, no. 23, pp. 11461–11467, June 2006, doi: 10.1021/jp061002u.

[104] Seiler, Paul, "Estimation of Ionicity Coefficients in Li2BeF4 Crystals by X-ray Diffraction," *Acta Cryst*, vol. B49, pp. 223–235, 1993.

[105] D. S. Maltsev *et al.*, "Transient Covalency in Molten Uranium(III) Chloride," *J. Am. Chem. Soc.*, vol. 146, no. 31, pp. 21220–21224, Aug. 2024, doi: 10.1021/jacs.4c05765.

[106] M.-M. Walz and D. Van Der Spoel, "Molten alkali halides – temperature dependence of structure, dynamics and thermodynamics," *Phys. Chem. Chem. Phys.*, vol. 21, no. 34, pp. 18516–18524, 2019, doi: 10.1039/C9CP03603B.

[107] M. A. Howe, R. L. McGreevy, and W. S. Howells, “The analysis of liquid structure data from time-of-flight neutron diffractometry,” *J. Phys. Condens. Matter*, vol. 1, no. 22, pp. 3433–3451, June 1989, doi: 10.1088/0953-8984/1/22/005.

[108] H. Wang, B. Yue, L. Yan, T. Jiang, and S. Peng, “First-Principles Molecular Dynamics Study of the Behavior of Tritium in Molten LiF-BeF2 Eutectic,” *J. Mol. Liq.*, vol. 345, p. 117027, Jan. 2022, doi: 10.1016/j.molliq.2021.117027.

[109] R. Vidrio, S. Mastromarino, E. Still, L. Chapdelaine, and R. O. Scarlat, “Density and Thermal Expansivity of Molten 2LiF-BeF2 (FLiBe): Measurements and Uncertainty Quantification,” *J. Chem. Eng. Data*, Nov. 2022, doi: 10.1021/acs.jced.2c00212.

[110] B. C. Blanke, E. N. Bousquet, M. L. Curtis, and E. L. Murphy, “DENSITY AND VISCOSITY OF FUSED MIXTURES OF LITHIUM, BERYLLIUM, AND URANIUM FLUORIDES,” MLM–1086, 4274391, Dec. 1956. doi: 10.2172/4274391.

[111] J. D. Mackenzie, “Structure of Glass Forming Halides. I. Liquid Beryllium Fluoride,” *J. Chem. Phys.*, vol. 32, no. 4, pp. 1150–1152, Apr. 1960, doi: 10.1063/1.1730864.

[112] D. Sprouster *et al.*, “Molecular Structure and Phase Equilibria of Molten Fluoride Salt with and without Dissolved Cesium: FLiNaK–CsF (5 Mol %),” *ACS Appl. Energy Mater.*, June 2022, doi: 10.1021/acsaem.2c00544.

[113] M. T. McDonnell *et al.*, “ADDIE: ADvanced DIffraction Environment – a software environment for analyzing neutron diffraction data,” *Acta Crystallogr. Sect. Found. Adv.*, vol. 73, no. a1, pp. a377–a377, May 2017, doi: 10.1107/S0108767317096325.

[114] D. Olds, C. N. Saunders, M. Peters, T. Proffen, J. Neuefeind, and K. Page, “Precise implications for real-space pair distribution function modeling of effects intrinsic to modern time-of-flight neutron diffractometers,” *Acta Crystallogr. Sect. Found. Adv.*, vol. 74, no. 4, pp. 293–307, July 2018, doi: 10.1107/S2053273318003224.

[115] W. C. Morgan, “Thermal Expansion Coefficients of Graphite Crystals,” *Carbon*, vol. 10, no. 1, pp. 73–79, Feb. 1972, doi: 10.1016/0008-6223(72)90011-5.

[116] P. Juhás, T. Davis, C. L. Farrow, and S. J. L. Billinge, “PDFgetX3: A Rapid and Highly Automatable Program for Processing Powder Diffraction Data into Total Scattering Pair Distribution Functions,” *J. Appl. Crystallogr.*, vol. 46, no. 2, pp. 560–566, Apr. 2013, doi: 10.1107/S0021889813005190.

[117] A. Stukowski, “Visualization and analysis of atomistic simulation data with OVITO–the Open Visualization Tool,” *Model. Simul. Mater. Sci. Eng.*, vol. 18, no. 1, p. 015012, Jan. 2010, doi: 10.1088/0965-0393/18/1/015012.

[118] A. K. Soper, “The structure of molten ZnCl2: A new analysis of some old data,” *Pramana*, vol. 63, no. 1, pp. 41–50, July 2004, doi: 10.1007/BF02704049.

[119] E. T. Nienhuis *et al.*, “Structural characterization of ZnSO4-K2SO4-NaCl glasses,” *J. Non-Cryst. Solids*, vol. 524, p. 119639, Nov. 2019, doi: 10.1016/j.jnoncrysol.2019.119639.

[120] R. L. McGreevy and M. A. Howe, “The structure of molten LiCl,” *J. Phys. Condens.*

Matter, vol. 1, no. 49, pp. 9957–9962, Dec. 1989, doi: 10.1088/0953-8984/1/49/014.

[121] T. Corridoni, R. Mancinelli, M. A. Ricci, and F. Bruni, "Viscosity of Aqueous Solutions and Local Microscopic Structure," *J. Phys. Chem. B*, vol. 115, no. 48, pp. 14008–14013, Dec. 2011, doi: 10.1021/jp202755u.

[122] A. K. Soper, K. Page, and A. Llobet, "Empirical potential structure refinement of semi-crystalline polymer systems: polytetrafluoroethylene and polychlorotrifluoroethylene," *J. Phys. Condens. Matter*, vol. 25, no. 45, p. 454219, Nov. 2013, doi: 10.1088/0953-8984/25/45/454219.

[123] N. Termini, A. Birri, S. Henderson, and N. D. B. Ezell, "An Overview of the Molten Salt Thermal Properties Databas--Thermophysica, Version 2.1.1 (MSTDB-TP v.2.1.1)," ORNL/TM-2023-2955, July 2023.

[124] C. F. Macrae *et al.*, "Mercury 4.0: from visualization to analysis, design and prediction," *J. Appl. Crystallogr.*, vol. 53, no. 1, pp. 226–235, Feb. 2020, doi: 10.1107/S1600576719014092.

[125] K. Robinson, G. V. Gibbs, and P. H. Ribbe, "Quadratic Elongation: A Quantitative Measure of Distortion in Coordination Polyhedra," *Science*, vol. 172, no. 3983, pp. 567–570, May 1971, doi: 10.1126/science.172.3983.567.

[126] J. H. Burns and E. K. Gordon, "Refinement of the crystal structure of Li_2BeF_4," *Acta Crystallogr.*, vol. 20, no. 1, pp. 135–138, Jan. 1966, doi: 10.1107/S0365110X66000240.

[127] D. M. Collins, M. C. Mahar, and F. W. Whitehurst, "Bonding in lithium tetrafluoroberyllate(II)," *Acta Crystallogr. B*, vol. 39, no. 3, pp. 303–306, June 1983, doi: 10.1107/S010876818300244X.

[128] D. N. Gardner and et al, "Solid structure of Li BeF (FLiBe) from room temperature to melting studied by neutron and X-ray diffraction," *J Appl Cryst*, 2025, doi: https://doi.org/10.1107/S1600576725000548.

[129] W. R. Busing, "Interpretation of the Crystal Structure of Li2BeF4 in Terms of the Born-Mayer-Huggins Model," *J. Chem. Phys.*, vol. 57, no. 7, pp. 3008–3010, Oct. 1972, doi: 10.1063/1.1678699.

[130] J. L. Holm and O. J. Kleppa, "Enthalpies of mixing in liquid beryllium fluoride-alkali fluoride mixtures," *Inorg. Chem.*, vol. 8, no. 2, pp. 207–212, Feb. 1969, doi: 10.1021/ic50072a005.

[131] R. D. Shannon, "Revised effective ionic radii and systematic studies of interatomic distances in halides and chalcogenides," *Acta Crystallogr. A*, vol. 32, no. 5, pp. 751–767, Sept. 1976, doi: 10.1107/S0567739476001551.

[132] S. Alvarez, "A cartography of the van der Waals territories," *Dalton Trans.*, vol. 42, no. 24, pp. 8617–8636, May 2013, doi: 10.1039/C3DT50599E.

[133] S. T. Lam, Q.-J. Li, R. Ballinger, C. Forsberg, and J. Li, "Modeling LiF and FLiBe Molten Salts with Robust Neural Network Interatomic Potential," *ACS Appl. Mater.*

Interfaces, vol. 13, no. 21, pp. 24582–24592, June 2021, doi: 10.1021/acsami.1c00604.

[134] M. Salanne and P. A. and Madden, "Polarization effects in ionic solids and melts," *Mol. Phys.*, vol. 109, no. 19, pp. 2299–2315, Oct. 2011, doi: 10.1080/00268976.2011.617523.

[135] R. J. Heaton, R. Brookes, P. A. Madden, M. Salanne, C. Simon, and P. Turq, "A First-Principles Description of Liquid BeF_2 and Its Mixtures with LiF: 1. Potential Development and Pure BeF_2," *J. Phys. Chem. B*, vol. 110, no. 23, pp. 11454–11460, June 2006, doi: 10.1021/jp061000+.

[136] B. S. Jabes, M. Agarwal, and C. Chakravarty, "Structure and transport properties of LiF–BeF2 mixtures: Comparison of rigid and polarizable ion potentials," *J. Chem. Sci.*, vol. 124, no. 1, pp. 261–269, Jan. 2012, doi: 10.1007/s12039-012-0225-5.

[137] M. P. Tosi, "Structure of covalent liquids," *J. Phys. Condens. Matter*, vol. 6, no. 23A, pp. A13–A28, June 1994, doi: 10.1088/0953-8984/6/23A/003.

[138] T. Førland, "Thermodynamic Properties of Fused Salts," in *Fused Salts*, New York: McGraw-Hill, 1964.

[139] B. R. Sundheim, Ed., *Fused Salts*. McGraw-Hill, 1964.

[140] Y. S. Badyal and R. A. Howe, "Structural modification in molten metal chloride and alkali chloride mixtures," *J. Phys. Condens. Matter*, vol. 5, no. 39, pp. 7189–7202, Sept. 1993, doi: 10.1088/0953-8984/5/39/007.

[141] D. A. Allen, R. A. Howe, N. D. Wood, and W. S. Howells, "The structure of molten zinc chloride and potassium chloride mixtures," *J. Phys. Condens. Matter*, vol. 4, no. 6, pp. 1407–1418, Feb. 1992, doi: 10.1088/0953-8984/4/6/005.

[142] J. Zhang *et al.*, "Redox potential control in molten salt systems for corrosion mitigation," *Corros. Sci.*, vol. 144, pp. 44–53, 2018, doi: 10.1016/j.corsci.2018.08.035.

[143] K. Sridharan and T. R. Allen, "Corrosion in Molten Salts," in *Molten Salts Chemistry*, Elsevier, 2013, pp. 241–267. doi: 10.1016/B978-0-12-398538-5.00012-3.

[144] B. Trémillon, "Diagrammes d'équilibre potentiel-acidité (pO2-) dans les sels et hydroxydes alcalins fondus," *Pure Appl. Chem.*, vol. 25, no. 2, pp. 395–428, Jan. 1971, doi: 10.1351/pac197125020395.

[145] P. Calderoni, P. Sharpe, H. Nishimura, and T. Terai, "Control of Molten Salt Corrosion of Fusion Structural Materials by Metallic Beryllium," *J. Nucl. Mater.*, vol. 386–388, pp. 1102–1106, Apr. 2009, doi: 10.1016/j.jnucmat.2008.12.292.

[146] S. Delpech, "Molten Salts for Nuclear Applications," in *Molten Salts Chemistry*, Elsevier, 2013, pp. 497–520. doi: 10.1016/B978-0-12-398538-5.00024-X.

[147] J. A. Duffy, "A common optical basicity scale for oxide and fluoride glasses," *J. Non-Cryst. Solids*, vol. 109, no. 1, pp. 35–39, 1989, doi: 10.1016/0022-3093(89)90438-9.

[148] E. W. Dewing, "The effect of additives on activities in cryolite melts," *Metall. Trans. B*,

vol. 20, no. 5, pp. 675–677, Oct. 1989, doi: 10.1007/BF02655924.

[149] A. L. Bieber, L. Massot, M. Gibilaro, L. Cassayre, P. Chamelot, and P. Taxil, "Fluoroacidity evaluation in molten salts," *Electrochimica Acta*, vol. 56, no. 14, pp. 5022–5027, May 2011, doi: 10.1016/j.electacta.2011.03.099.

[150] S. Jaskierowicz, S. Delpech, C. Slim, and G. Picard, "Attempt to classify various molten fluoride mixtures according to their solvation powers regarding metal fluorides," presented at the First ACSEPT International Workshop, 2010.

[151] M. Kergoat, L. Massot, M. Gibilaro, and P. Chamelot, "Investigation on fluoroacidity of molten fluorides solutions in relation with mass transport," *Electrochimica Acta*, vol. 120, pp. 258–263, Feb. 2014, doi: 10.1016/j.electacta.2013.12.035.

[152] J. A. Lane, H. G. MacPherson, and F. Maslan, *Fluid Fuel Reactors*. Addison-Wesley Publishing Company, Inc., 1958.

[153] R. Brookes, A. Davies, G. Ketwaroo, and P. A. Madden, "Diffusion Coefficients in Ionic Liquids: Relationship to the Viscosity," *J. Phys. Chem. B*, vol. 109, no. 14, pp. 6485–6490, Apr. 2005, doi: 10.1021/jp046355c.

[154] G. J. Janz, "VISCOSITY," in *Molten Salts Handbook*, Elsevier, 1967, pp. 52–62. doi: 10.1016/B978-0-12-395642-2.50008-3.

[155] J. D. Redman, "Effect of Fuel Composition on the Equilibria 3CrF2 = 2CrF3 + Cr and 3FeF2 = 2FeF3 + Fe," ORNL-2626, Oct. 1958.

[156] Y. Liu *et al.*, "Corrosion of Cr in molten salts with different fluoroacidity in the presence of CrF3," *Corros. Sci.*, vol. 169, p. 108636, June 2020, doi: 10.1016/j.corsci.2020.108636.

[157] J. Qiu, Y. Zou, and G.-J. Yu, "Speciation study of chromium corrosion product in molten LiF-NaF-KF salt," *Nucl Sci Tech*, p. 4, 2015.

[158] D. F. Williams, "Assessment of Candidate Molten Salt Coolants for the Advanced High Temperature Reactor (AHTR)," ORNL/TM-2006/12, 885975, Mar. 2006. doi: 10.2172/885975.

[159] J. D. Redman and C. F. Weaver, "Stability of Chromium and Iron Fluorides in Various Molten Fluorides," ORNL-1947.

[160] C. M. Blood, "Solubility and Stability of Structural Metal Diflorides in Molten Fluoride Mixtures," Oak Ridge National Lab. (ORNL), Oak Ridge, TN (United States), ORNL-TM-760, Jan. 1964.

[161] J. D. Redman, "Solubility and Stability of Structural Metal Fluorides in Various Fluoride Mixtures," ORNL-2157, Sept. 1956.

[162] M. Kergoat, "Evaluation de la fluoroacidité en milieux de sels fondus," Doctoral, Université Toulouse 3 Paul Sabatier, 2014.

[163] M. Revere and M. P. Tosi, "Structure and dynamics of molten salts," *Rep. Prog. Phys.*,

vol. 49, no. 9, p. 1001, Sept. 1986, doi: 10.1088/0034-4885/49/9/002.

[164] D. M. Gruen and R. L. McBeth, “The coordination chemistry of 3d transition metal ions in fused salt solutions,” *Pure Appl. Chem.*, vol. 6, no. 1, pp. 23–48, Jan. 1963, doi: 10.1351/pac196306010023.

[165] A. L. Rollet and M. Salanne, “Studies of the local structures of molten metal halides,” *Annu. Rep. Prog. Chem. - Sect. C*, vol. 107, pp. 88–123, 2011, doi: 10.1039/c1pc90003j.

[166] H. L. Chan, E. Romanovskaia, J. Qiu, P. Hosemann, and J. R. Scully, “Insights on the corrosion thermodynamics of chromium in molten LiF-NaF-KF eutectic salts,” *Npj Mater. Degrad.*, vol. 6, no. 1, p. 46, Dec. 2022, doi: 10.1038/s41529-022-00251-3.

[167] Y. Wang and J. Zhang, “Electrochemical Properties of CrF_2 in FLiNaK Molten Salt and the New Analytical Methods for their Determination,” *J. Electrochem. Soc.*, vol. 167, no. 8, p. 086503, Apr. 2020, doi: 10.1149/1945-7111/ab8923.

[168] H. Yin *et al.*, “Thermodynamic modeling of LiF-NaF-KF-CrF3 system,” *J. Fluor. Chem.*, vol. 209, pp. 6–13, May 2018, doi: 10.1016/j.jfluchem.2018.02.005.

[169] J. D. Redman, “Solubility and Stability of Structural Metal Fluorides in Molten NaF-ZrF4,” ORNL-2106, June 1956.

[170] J. D. Redman, “Solubility and Stability of Structural Metal Fluorides in Various Fluoride Mixtures,” ORNL-2221, 1956.

[171] W. Wu, S. Guo, and J. Zhang, “Electrochemical Behaviors of Cr(III) in Molten LiF-NaF-KF Eutectic,” *Int. J. Electrochem. Sci.*, pp. 225–234, Jan. 2018, doi: 10.20964/2018.01.21.

[172] V. V. Zakharova, A. A. Ryzhov, and V. A. Volkovich, “Electrochemistry of iron, nickel and chromium in LiF–NaF–KF (FLiNaK) eutectic melt: A cyclic voltammetry study,” presented at the The 2nd International Conference on Physical Instrumentation and Advanced Materials, Surabaya, Indonesia, 2020, p. 050039. doi: 10.1063/5.0032424.

[173] D. Ludwig, L. Olson, K. Sridharan, M. Anderson, and T. Allen, “High temperature electrochemistry of molten fluoride salt for measurement of dissolved chromium,” *Corros. Eng. Sci. Technol.*, vol. 46, no. 4, pp. 360–364, June 2011, doi: 10.1179/147842209X12579401586645.

[174] A. M. Keightley, J. C. Myland, K. B. Oldham, and P. G. Symons, “Reversible cyclic voltammetry in the presence of product,” *J. Electroanal. Chem.*, vol. 322, no. 1–2, pp. 25–54, Jan. 1992, doi: 10.1016/0022-0728(92)80065-C.

[175] D. S. Rappleye and R. G. Fuller, “Bringing the Analysis of Electrodeposition Signals in Voltammetry Out of the Shadows,” *J. Electrochem. Soc.*, vol. 170, no. 6, p. 063505, June 2023, doi: 10.1149/1945-7111/acd879.

[176] Y. L. Wang, Q. Wang, H. J. Liu, and C. L. Zeng, “Effects of the oxidants H2O and CrF3 on the corrosion of pure metals in molten (Li,Na,K)F,” *Corros. Sci.*, vol. 103, pp. 268–282, Feb. 2016, doi: 10.1016/j.corsci.2015.11.032.

[177] W. H. Doniger and K. Sridharan, “Application of voltammetry for quantitative analysis of chromium in molten 2LiF-BeF2 (FLiBe) salt,” *J. Electroanal. Chem.*, vol. 838, pp. 73–81, Apr. 2019, doi: 10.1016/j.jelechem.2019.02.048.

[178] L. Massot, M. Gibilaro, D. Quaranta, and P. Chamelot, “Corrosion Products Electrochemical Behaviour into Molten LiF-NaF: Investigation of Cr(II) System,” *J. Electrochem. Soc.*, vol. 168, no. 2, p. 026510, Feb. 2021, doi: 10.1149/1945-7111/abe088.

[179] D. L. Manning, “Voltammetry of Nickel in Molten Lithium Fluoride-Sodium Fluoride-Potassium Fluoride,” *J. Electroanal. Chem.*, vol. 7, pp. 302–306, Jan. 1964.

[180] F. R. Clayton, G. Mamantov, and D. L. Manning, “Electrochemical Studies of Titanium in Molten Fluorides,” *J. Electrochem. Soc.*, vol. 120, no. 9, p. 1193, Sept. 1973, doi: 10.1149/1.2403659.

[181] K. Xu, W. Xu, and S. S. Zhang, “Austen Angell’s legacy in electrolyte research,” *J. Non-Cryst. Solids X*, vol. 14, p. 100088, June 2022, doi: 10.1016/j.nocx.2022.100088.

[182] D. R. MacFarlane, M. Forsyth, E. I. Izgorodina, A. P. Abbott, G. Annat, and K. Fraser, “On the concept of ionicity in ionic liquids,” *Phys. Chem. Chem. Phys.*, vol. 11, no. 25, p. 4962, 2009, doi: 10.1039/b900201d.

[183] G. Ciccotti, G. Jacucci, and I. R. McDonald, “Transport properties of molten alkali halides,” *Phys. Rev. A*, vol. 13, no. 1, pp. 426–436, Jan. 1976, doi: 10.1103/PhysRevA.13.426.

[184] K. R. Harris, “On the Use of the Angell–Walden Equation To Determine the ‘Ionicity’ of Molten Salts and Ionic Liquids,” *J. Phys. Chem. B*, vol. 123, no. 32, pp. 7014–7023, Aug. 2019, doi: 10.1021/acs.jpcb.9b04443.

[185] E. Stefanidaki, G. M. Photiadis, C. G. Kontoyannis, A. F. Vik, and T. Østvold, “Oxide solubility and Raman spectra of NdF3–LiF–KF–MgF2–Nd2O3 melts,” *J. Chem. Soc. Dalton Trans.*, no. 11, pp. 2302–2307, May 2002, doi: 10.1039/b111563b.

[186] I. R. Elizarova, “Electrode Processes in a Eutectic KCl–KF Melt Containing Gadolinium Oxide,” vol. 38, no. 7, 2002.

[187] P. Chamelot, P. Taxil, and B. Lafage, “Voltammetric studies of tantalum electrodeposition baths,” *Electrochimica Acta*, vol. 39, no. 17, pp. 2571–2575, Dec. 1994, doi: 10.1016/0013-4686(94)00262-2.

[188] M. Glazoff, I. Charit, and P. Sabharwall, “Computational Thermodynamic Modeling of Hot Corrosion of Alloys Haynes 242 and Hastelloy N for Molten Salt Service,” Idaho National Laboratory (INL), Idaho Falls, ID (United States), INL/JOU-13-30754, Sept. 2014.

[189] “FThall - FACT Hall Process Phase Diagrams.” Accessed: Sept. 26, 2025. [Online]. Available: http://www.factsage.cn/fact/documentation/FThall/FThall_Figs.htm

[190] A. Consiglio, “Electrochemical cell and microfabricated chip sensors for electroanalysis of molten salt,” University of California, Berkeley, 2020.

[191] T. R. Pickarski, H. Williams, R. O. Scarlat, and M. Borrello, “Evaluation of an Ag/AgF Reference Electrode for Electrochemical Measurements of Molten 2LiF-BeF2,” *ECS Meet. Abstr.*, vol. MA2024-02, no. 57, p. 3788, Nov. 2024, doi: 10.1149/MA2024-02573788mtgabs.

[192] W. H. Jordan and et al., “Aircraft Nuclear Propulsion Project Quarterly Progress Report for period ending Dec. 10, 1954, ORNL-1816.” Oak Ridge National Laboratory, 1954.

[193] W. H. Jordan and et al., “Aircraft Nuclear Propulsion Project Quarterly Progress Report for period ending Sept. 10, 1956, ORNL-2157.” Oak Ridge National Laboratory, 1956.

[194] D. Krulic, N. Fatouros, and D. Liu, “A complementary survey of staircase voltammetry with metal ion deposition on macroelectrodes,” *J. Electroanal. Chem.*, vol. 754, pp. 30–39, Oct. 2015, doi: 10.1016/j.jelechem.2015.06.012.

[195] P. Malinauskas and D. M. Richardson, “The Solubilities of Hydrogen, Deuterium, and Helium in Molten Li2BeF4,” *Ind Eng Chem*, vol. 13, no. 3, 1974.

[196] P. E. Field and J. H. Shaffer, “The solubilities of hydrogen fluoride and deuterium fluoride in molten fluorides,” *J. Phys. Chem.*, vol. 71, no. 10, pp. 3218–3222, Sept. 1967, doi: 10.1021/j100869a013.

[197] C. Sandford *et al.*, “A synthetic chemist’s guide to electroanalytical tools for studying reaction mechanisms,” *Chem. Sci.*, vol. 10, no. 26, pp. 6404–6422, 2019, doi: 10.1039/C9SC01545K.

[198] S. Shahbazi, M. Bucknor, S. Thomas, A. Merwin, and Q. Zhou, “Thermochemical Modeling in Molten Fluoride Salts for Radionuclide Speciation,” Argonne National Laboratory (ANL), Argonne, IL (United States), ANL/KP-21/1, Feb. 2021. doi: 10.2172/1812872.

[199] L. Winner, “Do Artifacts Have Politics?,” *Daedalus*, vol. 109, no. 1, pp. 121–136, 1980.

[200] M. H. Wisnioski, *Engineers for change: Competing visions of technology in 1960s America*. Mit Press, 2012.

[201] S. L. Goldman, “Why we need a philosophy of engineering: a work in progress,” *Interdiscip. Sci. Rev.*, vol. 29, no. 2, pp. 163–176, June 2004, doi: 10.1179/030801804225012572.

[202] I. van de Poel and D. Goldberg, Eds., *Philosophy and Engineering: An Emerging Agenda*, vol. 2. in Philosophy of Engineering and Technology, vol. 2. Dordrecht: Springer Netherlands, 2010. doi: 10.1007/978-90-481-2804-4.

[203] Z. Pirtle, “How the Models of Engineering Tell the Truth,” in *Philosophy and Engineering*, Springer, 2010.

[204] L. L. Bucciarelli, *Engineering philosophy*. Delft, The Netherlands: DUP Satellite, 2003.

[205] I. Van De Poel, “Philosophy and Engineering: Setting the Stage,” in *Philosophy and Engineering: An Emerging Agenda*, Springer Netherlands, 2010.

[206] P. Dias, “The Engineer’s Identity Crisis: Homo Faber or Homo Sapiens?,” in *Philosophy and Engineering: Reflections on Practice, Principles and Process*, vol. 15, D. P. Michelfelder, N. McCarthy, and D. E. Goldberg, Eds., in Philosophy of Engineering and Technology, vol. 15. , Dordrecht: Springer Netherlands, 2013, pp. 139–150. doi: 10.1007/978-94-007-7762-0_11.

[207] D. E. Goldberg, “Why Philosophy? Why Now? Engineering Responds to the Crisis of a Creative Era,” in *Philosophy and Engineering:*, vol. 2, I. Poel and D. Goldberg, Eds., in Philosophy of Engineering and Technology, vol. 2. , Dordrecht: Springer Netherlands, 2009, pp. 255–263. doi: 10.1007/978-90-481-2804-4_21.

[208] D. P. Michelfelder and N. Doorn, Eds., *The Routledge Handbook of the Philosophy of Engineering*, 1st ed. Routledge, 2020. doi: 10.4324/9781315276502.

[209] C. Mitcham, “What Is Engineering?,” in *The Routledge Handbook of the Philosophy of Engineering*, Routledge, 2020, pp. 11–24.

[210] C. Mitcham, “The Importance of Philosophy to Engineering,” *Teorema Rev. Int. Filos.*, vol. 17, no. 3, pp. 27–47, 1998.

[211] L. Bo-cong, “The Rise of Philosophy of Engineering in the East and the West,” in *Philosophy and Engineering:*, vol. 2, I. Poel and D. Goldberg, Eds., in Philosophy of Engineering and Technology, vol. 2. , Dordrecht: Springer Netherlands, 2009, pp. 31–40. doi: 10.1007/978-90-481-2804-4_3.

[212] J. C. Pitt, “Fitting Engineering into Philosophy,” in *Philosophy and Engineering: Reflections on Practice, Principles and Process*, vol. 15, D. P. Michelfelder, N. McCarthy, and D. E. Goldberg, Eds., in Philosophy of Engineering and Technology, vol. 15. , Dordrecht: Springer Netherlands, 2013, pp. 91–101. doi: 10.1007/978-94-007-7762-0_8.

[213] M. Davis, “Engineering as Profession: Some Methodological Problems in Its Study,” in *Engineering Identities, Epistemologies and Values*, vol. 21, S. H. Christensen, C. Didier, A. Jamison, M. Meganck, C. Mitcham, and B. Newberry, Eds., in Philosophy of Engineering and Technology, vol. 21. , Cham: Springer International Publishing, 2015, pp. 65–79. doi: 10.1007/978-3-319-16172-3_4.

[214] M. Davis, “Defining Engineering from Chicago to Shantou,” *Monist*, vol. 92, no. 3, pp. 325–338, 2009, doi: 10.5840/monist200992319.

[215] “NSPE Position Statement No. 10-58 Employment Practices – Use of Engineering Titles.” National Society of Professional Engineers, Jan. 2023.

[216] M. Davis, “Distinguishing architects from engineers: A pilot study in differences between engineers and other technologists,” in *Philosophy and Engineering*, Springer Netherlands, 2010.

[217] W. Bulleit, J. Schmidt, I. Alvi, E. Nelson, and T. Rodriguez-Nikl, “Philosophy of Engineering: What It Is and Why It Matters,” *J. Prof. Issues Eng. Educ. Pract.*, vol. 141, no. 3, p. 02514003, July 2015, doi: 10.1061/(ASCE)EI.1943-5541.0000205.

[218] E. T. Layton, “Technology as Knowledge”.

[219] J. A. Schmidt, “What Makes Engineering, Engineering?,” in *Structures Congress 2012*, Chicago, Illinois, United States: American Society of Civil Engineers, Mar. 2012, pp. 1160–1168. doi: 10.1061/9780784412367.104.

[220] C. A. Gray, R. E. Gray, M. M. Canipe, S. W. J. Armfield, and R. Tuchscherer, “Developing Engineering Identity in an Introductory Engineering Course: A Multi-Case Analysis,” *J. Res. Sci. Math. Technol. Educ.*, vol. 4, no. 3, pp. 153–177, Sept. 2021, doi: 10.31756/jrsmte.431.

[221] S. A. Claussen, J. Y. Tsai, K. Johnson, J. Blacklock, and J. A. Leydens, “‘Not an Engineer Yet’: Manifestations of Liminal Engineering Identities,” *Stud. Eng. Educ.*, vol. 4, no. 2, pp. 95–121, Nov. 2023, doi: 10.21061/see.89.

[222] B. M. Linder, “Understanding Estimation and its Relation to Engineering Education,” Massachusetts Institute of Technology, 1999.

[223] M. Davis, “A Plea for Judgment,” *Sci. Eng. Ethics*, vol. 18, no. 4, pp. 789–808, Dec. 2012, doi: 10.1007/s11948-011-9254-6.

[224] H. Poser, “On Structural Differences Between Science and Engineering,” *Soc. Philos. Technol. Q. Electron. J.*, vol. 4, no. 2, pp. 128–135, 1998, doi: 10.5840/techne1998426.

[225] M. Boon, “In Defense of Engineering Sciences: On the Epistemological Relations Between Science and Technology,” *Techné Res. Philos. Technol.*, vol. 15, no. 1, pp. 49–71, 2011, doi: 10.5840/techne20111515.

[226] H. F. Rase, *The philosophy and logic of chemical engineering*. Houston, TX: Gulf Pub. Co., 1961.

[227] W. G. Vincenti, “Engineering Knowledge, Type of Design, and Level of Hierarchy: Further Thoughts About What Engineers Know…,” in *Technological Development and Science in the Industrial Age*, vol. 144, P. Kroes and M. Bakker, Eds., in Boston Studies in the Philosophy of Science, vol. 144. , Dordrecht: Springer Netherlands, 1992, pp. 17–34. doi: 10.1007/978-94-015-8010-6_2.

[228] J. K. Feibleman, “Pure Science, Applied Science, Technology, Engineering: An Attempt at Definitions,” *Technol. Cult.*, vol. 2, no. 4, p. 305, 1961, doi: 10.2307/3100886.

[229] W. G. Vincenti, *What Engineers Know and How They Know It*, vol. 141. Baltimore: Johns Hopkins University Press, 1990.

[230] L. Marx, “The Idea of ‘Technology’ and Postmodern Pessimism,” in *Technology, Pessimism, and Postmodernism*, Y. Ezrahi, E. Mendelsohn, and H. Segal, Eds., Dordrecht: Springer Netherlands, 1994, pp. 11–28. doi: 10.1007/978-94-011-0876-8_2.

[231] B. Newberry, “The Dialectics of Engineering,” in *Engineering Identities, Epistemologies and Values*, vol. 21, S. H. Christensen, C. Didier, A. Jamison, M. Meganck, C. Mitcham, and B. Newberry, Eds., in Philosophy of Engineering and Technology, vol. 21. , Cham: Springer International Publishing, 2015, pp. 9–22. doi: 10.1007/978-3-319-16172-3_1.

[232] J. Lucena, Ed., *Engineering Education for Social Justice: Critical Explorations and*

Opportunities, vol. 10. in Philosophy of Engineering and Technology, vol. 10. Dordrecht: Springer Netherlands, 2013. doi: 10.1007/978-94-007-6350-0.

[233] G. Moriarty, *The Engineering Project: Its Nature, Ethics, and Promise*. University Park, Pa: The Pennsylvania State University Press, 2008.

[234] D. M. A. Karwat, "Self-reflection for Activist Engineering," *Sci. Eng. Ethics*, vol. 26, no. 3, pp. 1329–1352, June 2020, doi: 10.1007/s11948-019-00150-y.

[235] S. Johnston, *The Neutron's Children: Nuclear Engineers and the Shaping of Identity*. Oxford University Press, 2012.

[236] "Argonne National Laboratory: Our History." UChicago Argonne, LLC. [Online]. Available: https://www.anl.gov/our-history

[237] G. L. R. Groves, *Now It Can Be Told: The Story Of The Manhattan Project*. Hachette Books, 2009.

[238] U. K. Heise, "Science, Technology, and Postmodernism," in *The Cambridge companion to postmodernism*, S. Connor, Ed., Cambridge University Press, 2004, pp. 136–67.

[239] V. Gilinsky, "Breeder Reactors and the Spread of Plutonium," P-3483, Nov. 1966.

[240] "Safeguards for Reprocessing and Enrichment Plants," *IAEA Bull.*, vol. 19, no. 5, pp. 30–33.

[241] H. Gusterson, *Nuclear rites: A weapons laboratory at the end of the Cold War*. Univ of California Press, 1996.

[242] N. E. Todreas and M. S. Kazimi, *Nuclear Systems: Thermal Hydraulic Fundamentals*, 2nd ed. Taylor & Francis, 2011.

[243] S. Villani, *Isotope Separation*. in ANS Monographs. American Nuclear Society, 1976.

[244] M. M. El-Wakil, *Nuclear Heat Transport*. American Nuclear Society, 1978.

[245] J. J. Duderstadt and L. J. Hamilton, *Nuclear Reactor Analysis*. New York: Wiley, 1976.

[246] J. R. Lamarsh, *Introduction to Nuclear Engineering*. Reading, Mass: Addison-Wesley Pub. Co., 1975.

[247] R. A. Knief, *Nuclear Engineering : Theory and Technology of Commercial Nuclear Power*, 2nd ed. LaGrange Park, Ill: American Nuclear Society, 2008.

[248] F. F. Chen and F. F. Chen, *Introduction to plasma physics and controlled fusion / Francis F. Chen.*, 2nd ed. New York: Plenum Press, 1984.

[249] J. E. Turner, *Atoms, radiation, and radiation protection*, 3rd ed. in Physics textbook. Weinheim: Wiley-VCH, 2007.

[250] M. S. Yim, *Nuclear Waste Management: Science, Technology, and Policy*. in Lecture Notes in Energy. Springer Netherlands, 2021.

[251] L. Daston and P. Galison, “The Image of Objectivity,” *Representations*, vol. 40, pp. 81–128, Oct. 1992, doi: 10.2307/2928741.

[252] N. Tsoulfanidis, *The Nuclear Fuel Cycle*. American Nuclear Society, 2013.

[253] M. Benedict, T. H. Pigford, and H. W. Levi, *Nuclear chemical engineering*, 2d ed. in McGraw-Hill series in nuclear engineering. New York: McGraw-Hill, 1981.

[254] D. R. Olander and A. T. Motta, *Light Water Reactor Materials*. American Nuclear Society, 2017.

[255] R. Adams, “Can we repeat facts about Fukushima often enough to overcome fears?,” Nuclear Newswire. Accessed: Feb. 07, 2024. [Online]. Available: https://www.ans.org/news/article-958/fukushima-facts-to-overcome-fears/

[256] G. T. Seaborg, “Need We Fear Our Nuclear Future?,” *Bull. At. Sci.*, vol. 24, no. 1, pp. 36–42, Jan. 1968, doi: 10.1080/00963402.1968.11457616.

[257] W. R. Freudenburg, “Risky Thinking: Irrational Fears about Risk and Society,” *Ann. Am. Acad. Pol. Soc. Sci.*, vol. 545, no. 1, pp. 44–53, May 1996, doi: 10.1177/0002716296545001005.

[258] W. R. Freudenburg, “Risk and Recreancy: Weber, the Division of Labor, and the Rationality of Risk Perceptions,” *Soc. Forces*, vol. 71, no. 4, pp. 909–932, June 1993.

[259] “Code of Ethics,” American Nuclear Society. Accessed: Feb. 07, 2024. [Online]. Available: https://www.ans.org/about/coe/

[260] B. Wynne, “Misunderstood misunderstanding: social identities and public uptake of science,” *Public Underst. Sci.*, vol. 1, no. 3, pp. 281–304, July 1992, doi: 10.1088/0963-6625/1/3/004.

[261] H. Williams, D. Djokić, and R. O. Scarlat, “Curriculum-embedded Epistemological Foundations in Nuclear Engineering,” presented at the ASEE Annual Conference & Exposition, Portland, OR: ASEE, 2024.

[262] P. N. Powers, “The History of Nuclear Engineering Education,” *J. Eng. Educ.*, vol. 54, no. 10, p. 364, June 1964.

[263] “Artificial Intelligence and Decision Making (Course 6-4),” MIT Course Catalog 2025-2026. Accessed: Dec. 18, 2025. [Online]. Available: https://catalog.mit.edu/degree-charts/artifical-intelligence-decision-making-course-6-4/

[264] L. M. Groves, *Now It Can Be Told, The Story of the Manhattan Project*. Da Capo Press, 1983.

[265] R. C. Axtmann, “Nuclear Chemical Engineering,” *Nucl. Technol.*, vol. 27, no. 1, pp. 78–83, Sept. 1975, doi: 10.13182/NT75-A15939.

[266] J. Kozeracki *et al.*, “Pathways to Commercial Liftoff: Advanced Nuclear,” Department of Energy, Mar. 2023.

[267] "The Path to a New Era for Nuclear Energy," International Energy Agency, Jan. 2025.

[268] M. W. Rosenthal, P. R. Kasten, and R. B. Briggs, "Molten-Salt Reactors—History, Status, and Potential," *Nucl. Appl. Technol.*, vol. 8, no. 2, pp. 107–117, Feb. 1970, doi: 10.13182/NT70-A28619.

[269] J. Serp *et al.*, "The molten salt reactor (MSR) in generation IV: overview and perspectives," *Prog. Nucl. Energy*, vol. 77, pp. 308–319, 2014.

[270] V. V. Ignatiev *et al.*, "Molten-Salt Reactors: New Possibilities, Problems and Solutions," *At. Energy*, vol. 112, no. 3, pp. 157–165, July 2012, doi: 10.1007/s10512-012-9537-2.

[271] J. Krepel and K. J. Kramer, "TerraPower fast chloride reactor," in *Molten Salt Reactors and Thorium Energy*, Elsevier, 2024, pp. 953–972. doi: 10.1016/B978-0-323-99355-5.00020-3.

[272] C. Andreades *et al.*, *Technical Description of the "Mark 1" Pebble-Bed Fluoride-Salt-Cooled High-Temperature Reactor (PB-FHR) Power Plant*. 2014.

[273] M. Wald, "2024: The State of Advanced Reactors," *Nucl. News*, Jan. 2024, [Online]. Available: https://www.ans.org/news/article-5634/2024-the-state-of-advanced-reactors/

[274] M. Benedict, T. H. Pigford, and H. W. Levi, *Nuclear chemical Engineering*, 2. ed. in McGraw-Hill Series in nuclear engineering. New York: McGraw-Hill, 1981.

[275] G. Cerefice, "Adapting Waste Management Education at UNLV for an Evolving Fuel Cycle," *Trans. Am. Nucl. Soc.*, vol. 105, 2011.

[276] M. Nilsson, G. Miller, and A. J. Shaka, "The Nuclear Education and Training Program at University of California Irvine," *Trans. Am. Nucl. Soc.*, vol. 109, p. 218, Nov. 2013.

[277] T. Stover and S. Kessler, "A Chemistry Based Criticality Safety Evaluation of the HM-Process Mixer Settlers," *Trans. Am. Nucl. Soc.*, vol. 114, 2016.

[278] "UC Berkeley-led Nuclear Science and Security Consortium enters its eleventh year," *Nuclear News*, p. 58, June 2022.

[279] H. K. Rae, "Three Decades of Canadian Nuclear Chemical Engineering," in *History of Chemical Engineering*, W. F. Furter, Ed., Washington, D.C.: American Chemical Society, 1980, pp. 313–333.

[280] N. L. Franklin, J. C. Clarke, D. W. Clelland, K. D. B. Johnson, J. E. Littlechild, and B. F. Warner, "The Contribution of Chemical Engineering to the U.K. Nuclear Industry," in *History of Chemical Engineering*, vol. 190, W. F. Furter, Ed., in Advances in Chemistry, vol. 190. , WASHINGTON, D. C.: AMERICAN CHEMICAL SOCIETY, 1980. doi: 10.1021/ba-1980-0190.

[281] S. T. Arm and P. R. Westmoreland, "Chemical Engineers and a Nuclear Renaissance," *CEP*, p. 20, Apr. 2022.

[282] S. Gallier and E. Thro, "ANS: 50 years of accomplishment," *Nucl. News*, pp. 44–63, June

2004.

[283] "Nuclear News," *Nuclear News*, vol. 10, no. 9, Sept. 1967.

[284] G. Murphy, "History of Nuclear Engineering Curricula," *Nucl. Technol.*, vol. 27, no. 1, pp. 11–14, Sept. 1975, doi: 10.13182/NT75-A15930.

[285] "DOE Agency Financial Report Fiscal Year 2024," Department of Energy, DOE/CF-0211, 2024.

[286] "U.S. Department of Energy Surpasses $1 Billion in Support to U.S. Colleges and Universities to Advance Nuclear Science and Technology," Department of Energy, Office of Nuclear Energy. Accessed: Mar. 17, 2025. [Online]. Available: https://www.energy.gov/ne/articles/us-department-energy-surpasses-1-billion-support-us-colleges-and-universities-advance

[287] "Report on Objective Criteria in Nuclear Engineering Education," *J. Eng. Educ.*, vol. 54, no. 10, p. 371, June 1964.

[288] S. R. Hatcher, "The Chemical Engineer's Role in Nuclear-Power-Reactor Design, Development and Operation," in *AECL-3911*, Chalk River Nuclear Laboratories: Atomic Energy of Canada Ltd., 1971, pp. 41–45.

[289] "2023-2024 Criteria for Accrediting Engineering Programs," ABET, 2022.

[290] "Engineering Undergraduate Degree Programs, 2022," ASEE, By the Numbers, 2022. [Online]. Available: https://ira.asee.org/by-the-numbers/

[291] "Engineering & Engineering Technology By the Numbers," ASEE, Washington, D.C., 2022.

[292] A. Verma and D. Djokić, "Reimagining Nuclear Engineering," *Issues Sci. Technol.*, vol. 37, no. 3, pp. 64–69, Spring 2021.

[293] P. J. Brown, A. G. Fox, E. N. Maslen, M. A. O'Keefe, and B. T. M. Willis, "Intensity of diffracted intensities," *urn:isbn:*, vol. C, pp. 554–595, 2006, doi: 10.1107/97809553602060000600.

[294] E. P. Parry and R. A. Osteryoung, "Evaluation of Analytical Pulse Polarography," *Anal. Chem.*, vol. 37, no. 13, pp. 1634–1637, 1965, doi: 10.1021/ac60232a001.

[295] G. C. Barker, R. L. Faircloth, and A. W. Gardner, "SQUARE WAVE POLAROGRAPHY. PART IV. AN INTRODUCTION TO THE THEORETICAL ASPECTS OF SQUARE WAVE POLAROGRAPHY," Great Britain Atomic Energy Research Establishment, Harwell, Berks, England (United Kingdom), AERE-C/R-1786, Feb. 1956. Accessed: Oct. 03, 2024. [Online]. Available: https://www.osti.gov/biblio/4317989

[296] G. C. Barker, R. L. Faircloth, and A. W. Gardner, "Square Wave Polarogaphy Part IV, An Introduction to the Theoretical Aspects of Square Wave Polarography," *At. Energy Res. Establ.*, 1956.